NASA CR-835

ANALYSIS AND DESIGN OF SPACE VEHICLE FLIGHT CONTROL SYSTEMS

VOLUME XVI – ABORT

By Arthur L. Greensite

Issued by Originator as GDC-DDE 68-001

Prepared under Contract No. NAS 8-21383 by
GENERAL DYNAMICS CONVAIR
A DIVISION OF GENERAL DYNAMICS CORPORATION
San Diego, Calif.

for George C. Marshall Space Flight Center

NATIONAL AERONAUTICS AND SPACE ADMINISTRATION

For sale by the Clearinghouse for Federal Scientific and Technical Information
Springfield, Virginia 22151 – CFSTI price $3.00

FOREWORD

This report (Volume XVI) was prepared under Contract No. NAS 8-21383 and is one of a series intended to illustrate methods used for the design and analysis of space vehicle flight control systems. Previous volumes in the series were prepared under Contract No. NAS 8-11494. Below is a complete list of the reports in the series:

Volume I	Short Period Dynamics
Volume II	Trajectory Equations
Volume III	Linear Systems
Volume IV	Nonlinear Systems
Volume V	Sensitivity Theory
Volume VI	Stochastic Effects
Volume VII	Attitude Control During Launch
Volume VIII	Rendezvous and Docking
Volume IX	Optimization Methods
Volume X	Man in the Loop
Volume XI	Component Dynamics
Volume XII	Attitude Control in Space
Volume XIII	Adaptive Control
Volume XIV	Load Relief
Volume XV	Elastic Body Equations
Volume XVI	Abort

The work was conducted under the direction of Clyde D. Baker, Billy G. Davis and Fred W. Swift, Aero-Astro Dynamics Laboratory, George C. Marshall Space Flight Center. The General Dynamics Convair program was conducted under the direction of Arthur L. Greensite.

TABLE OF CONTENTS

Section			Page
1	STATEMENT OF THE PROBLEM.		1
2	STATE OF THE ART		3
3	RECOMMENDED PROCEDURES		5
	3.1 Abort Modes		5
	3.1.1	On-the-Pad Abort	7
	3.1.2	Atmospheric Abort	31
	3.1.3	Exoatmospheric Abort	44
		3.1.3.1 Determination of Abort Thrust Requirements	49
	3.1.4	Abort From Satellite in Orbit	76
		3.1.4.1 Abort Via Deorbiting	77
		3.1.4.2 Rescue Via Ground Based Facilities . .	79
		3.1.4.3 Rescue Via Satellite-Based Facilities . .	82
	3.1.5	Lunar Mission Abort	103
		3.1.5.1 Midcourse Region	104
		3.1.5.2 Lunar Region	114
	3.2 Gemini Abort System		118
	3.3 Apollo Abort System		127
	3.3.1	General	127
	3.3.2	Design Philosophy	136
	3.3.3	Operational Features	136
		3.3.3.1 Abort Parameters	136
		3.3.3.2 Abort Modes	140
		3.3.3.3 Aerodynamic Characteristics	141
	3.4 Emergency Escape Systems		142
	3.4.1	Satellite Life Jacket	145
	3.4.2	Satellite Life Raft	149
	3.4.3	Satellite Life Boat	154
	3.4.4	EGRESS	156
	3.4.5	Paracone	160
4	REFERENCES		165

TABLE OF CONTENTS, Contd

Appendix		Page
A	LIST OF SYMBOLS	A-1
B	ORBITAL MECHANICS	B-1
C	ENTRY DYNAMICS	C-1
D	AERODYNAMIC HEATING	D-1
E	GEOPHYSICAL CONSTANTS	E-1

LIST OF TABLES

Table		Page
I	Categories of Emergency	6
II	Boost Phase Emergencies	8
III	Summary of Design Considerations for Boost Phase Abort	9
IV	Liquid Propellant Explosive Equivalents	10
V	Spherical Charge of TNT, Standard Atmosphere at Sea Level Conditions, Yield One Ton	12
VI	Transmission Factors for the ARDC Model Atmosphere	15
VII	In-space Emergency	143
VIII	Escape Conditions During Boost	159

LIST OF ILLUSTRATIONS

Figure		Page
1	Typical Pressure-Time Curve for an Explosive Blast Wave	11
2	Explosion Characteristics of One Ton of TNT at Sea Level Conditions	13
3	Shock Wave Propagation for One Kiloton Explosion at Sea Level.	16
4	Recommended Maximum Tolerance Limits to Acceleration	17
5	Ballistic Body — Escape Capsule	20
6	Lifting Body — Escape Capsule	22
7	Five psi Overpressure Characteristics	24
8	Minimum Warn Time Required for 5 psi Maximum Overpressure	24
9	Effect of Thrust Magnitude and Direction on On-the-Pad Separation Distance; Ballistic Body	25
10	Effect of Rocket Burning Time on On-the-Pad Separation Distance; Ballistic Body	26
11	Effect of Rocket Burning Time on On-the-Pad Separation Distance; Ballistic Body	27
12	Effect of Thrust, Magnitude, and Direction on On-the-Pad Separation Distance; Lifting Body	28
13	Effect of Rocket Burning Time on On-the-Pad Separation Distance; Lifting Body	29
14	Effect of Rocket Burning Time on On-the-Pad Separation Distance; Lifting Body	30
15	Forces and Geometry at Abort Vehicle Separation	33
16	Effect of Dynamic Pressure and Drag Parameter on Separation Criteria	35
17	Effect of Lift-to-Drag Ratio on Separation Criteria	36
18	Effect of Angle of Attack on Separation Criteria	37
19	Effect of Flight Path Angle on Separation Criteria	38
20	Effect of Dynamic Pressure and Drag Parameter on Acceleration Criteria	39
21	Effect of Lift-to-Drag Ratio on Acceleration	40

Figure		Page
22	Effect of Drag Parameter on Acceleration Criteria	41
23	Deceleration Decay	43
24	Abort Thrust Requirement Versus Flight Time	44
25	10G Entry Trajectories	45
26	Escape Boundaries	46
27	Typical Ascent Trajectory for Lunar Mission	47
28	Evaluation of Typical Ascent Trajectory	47
29	Safe Ascent Corridor - Without Escape Rocket	48
30	Entry Deceleration, L/D = 0	50
31	Entry Deceleration, L/D = 0.50	51
32	Entry Deceleration, L/D = 1.0	52
33	Entry Deceleration, L/D = 2.0	53
34	Burnout Conditions at Supercircular Speed and Entry Conditions for the Overshoot Boundary - h_{bo} = 500,000 ft	55
35	Burnout Conditions at Supercircular Speed and Entry Conditions for the Overshoot Boundary - h_{bo} = 1,000,000 ft	56
36	Burnout Conditions at Supercircular Speed and Entry Conditions for the Overshoot Boundary - h_{bo} = 1,500,000 ft	57
37	Effect of $C_D S/W$ on Abort Velocity Requirement for Burnout at Escape Speed	58
38	Effect of L/D on Abort Velocity Requirement for Burnout at Escape Speed	59
39	Effect of Burnout Velocity on Abort Velocity Requirement	60
40	Effect of Burnout Flight-Path Angle on Abort Velocity Requirement for Burnout at Escape Speed	61
41	Entry Trajectory With No Abort Thrust	64
42	Optimal Direction of Abort Thrust - Subcircular Velocity	65
43	Variation of Peak Deceleration With Thrust Direction	66
44	Deceleration-Time Histories for Abort Thrust Applied at Various Points Along Trajectory	67

LIST OF ILLUSTRATIONS, Contd

Figure		Page
45	Maximum Decelerations on Entry After Thrust Initiation at Various Altitudes (or Dynamic Pressure) Along Trajectory	68
46	Relationship Between Abort Velocity and Ratio of Fuel Weight to Vehicle Weight	69
47	Influence of Propellant Mass Ratio on Supercircular Velocity Abort Trajectory	71
48	Influence of Abort Thrust Level on Supercircular Velocity Abort Trajectory	71
49	Propellant Weight Required to Return Vehicle to Earth for Aborts Initiated Along the Launch Trajectory	73
50	Abort Propellant Weight Required to Return Vehicle to Earth With the Time Delay From Abort Initiation to Thrust Initiation	74
51	Deorbing Parameters	78
52	Effects of Angle of Deorbiting Impulse on Reentry	78
53	Minimum Deorbiting-Velocity Impulse for Circular Orbits	79
54	Range From Orbit to Impact Using Nominal Deorbiting Impulse	79
55	Range Dispersion Due to Deorbiting-Velocity Variations	80
56	Maximum Reentry Deceleration Using Nominal Deorbiting Impulse	80
57	Schematic of Lifting Vehicle Reentry Trajectory	81
58	Maximum Deceleration During Lifting Reentry From Orbit	81
59	Rescue Via Earth-Based Vehicle	82
60	Coplanar Transfer Techniques	83
61	Inward Transfer in Circular Orbit	84
62	Outward Transfer in Circular Orbit	86
63	Total Velocity Increment for Cyclic Inward Transfer Between Satellites on the Same Circular Orbit	87
64	Total Velocity Increment for Cyclic Outward Transfer Between Satellites on Same Circular Orbit	88
65	Outward Hohmann Transfer	89
66	Velocity Increment for Hohmann Transfer	90

LIST OF ILLUSTRATIONS, Contd

Figure		Page
67	Velocity Increment for Hohmann Transfer	91
68	Phase Angles for Outward Hohmann Transfer	92
69	Inward Hohmann Transfer	93
70	Phase Angles for Inward Hohmann Transfer	94
71	Iso-Orbital Rendezvous Via Hyperbolic Transfer Orbit	95
72	Rendezvous Via Direct Hyperbolic Transfer Orbit	99
73	Total Velocity Increment Versus Minimum Time	102
74	Typical Trajectory for a Lunar Mission	103
75	Reentry Geometry	105
76	Velocity Hodograph for Perigee Radius of 6,450 km	107
77	Hodograph of Abort Trajectory	107
78	Perigee Miss Distance Due to Two-Body Guidance Law	108
79	Flight Time From Abort to Perigee; Outbound Leg	109
80	Flight Time From Abort to Perigee; Return Leg	109
81	Total Flight Time, Injection to Perigee	110
82	Trajectory Characteristics for Abort During Earth-Moon Transfer With One Lunar Stage	110
83	Abort Capabilities During Earth-Moon Transfer Using the Lunar Landing or Launch Stage (Velocity Increment = 10,000 fps)	111
84	Abort Capabilities During Earth-Moon Transfer Using Both Lunar Landing and Launch Stages Velocity Increment = 20,000 fps)	111
85	Abort Velocity Requirement and Flight Time for Parabolic Return From the Earth-Moon Transfer Trajectory	112
86	Typical Abort Hodograph Charts	113
87	Abort Chart for Way Station	114
88	Abort From Lunar Parking Orbit	115
89	Elapsed Time for Direct and Indirect Returns From 100-Nautical-Mile Circular Parking Orbit	117

LIST OF ILLUSTRATIONS, Contd

Figure		Page
90	Velocity Increment for Direct and Indirect Returns From 100-Nautical-Mile Circular Parking Orbit	118
91	Time Saved Versus Velocity Increment Penalty for Direct Return Abort From 100-Nautical-Mile Circular Parking Orbit	119
92	Cues for Astronaut Abort in Gemini	121
93	Gemini Malfunction Detection System (MDS)	122
94	Gemini Launch Parameters	123
95	Gemini Abort Sequences	124
96	Off the Pad Escape	124
97	Violent Controls Malfunction	126
98	Inadvertent Thrust Termination	126
99	The Saturn V Configuration	128
100	The Saturn Vehicles	129
101	Saturn IB Failure Modes	132
102	Saturn IB Critical Angle of Attack Versus Flight Time	133
103	Abort Warning Time Requirements for Saturn V Explosion	134
104	Command Module and Launch Vehicle Trajectories Following Abort	135
105	Crew Safety System (Saturn V)	137
106	Launch Escape Vehicle	141
107	Low-altitude Abort Mode	141
108	High-altitude Abort Mode	141
109	Types of Abort Vehicle Configuration	144
110	MOOSE Operation	145
111	Satellite Life Jacket, MOOSE	146
112	Satellite Life Jacket, MOOSE Profile	147
113	MOOSE Trajectories	147
114	Reentry Heat Flux, Stagnation Point, Space Life Jacket, MOOSE	148
115	MOOSE Reentry Total Heating	148

LIST OF ILLUSTRATIONS, Contd

Figure		Page
116	Satellite Life Jacket, MOOSE Ablation Shield	149
117	Satellite Life Raft	150
118	Satellite Life Raft Operation	150
119	Satellite Life Raft Trajectories	152
120	Reentry Heat Flux Stagnation Point Satellite Life Raft	152
121	Life Raft Reentry Total Heating	153
122	Satellite Life Raft Ablation Shield	153
123	Variation in Cross-Range Maneuver With Initial Velocity	154
124	Satellite Lifeboat	155
125	Satellite Lifeboat Operation	155
126	EGRESS Vehicle	156
127	Typical Boost Time History	158
128	Ballistic Reentry Phase	160
129	Ballistic Reentry Phase Time History	160
130	Paracone Concept	161
131	Paracone Configuration	162
132	Paracone Survival Pack	162
133	On-the-Pad Emergency Escape; Paracone	163

1. STATEMENT OF THE PROBLEM

Abort may be defined as the deliberate or unintentional termination of a manned space mission followed by a safe and expedient return of the crew to earth. It is a well defined policy of the Air Force and NASA that all crewmen should have a planned means of escape and reentry for all foreseeable emergency situations. Space flight since the days of Icarus has always involved some risk. Nevertheless, a concerted effort aimed at minimizing such risk and providing reasonable assurance of survival in the event of accidents is a prime obligation of the designer.

For each mission, therefore, every conceivable set of circumstances must be considered and evaluated to see if an abort of the mission is called for, and to determine what sequence of events should occur to bring the spacecraft and crew back to earth with the highest probability of success. One must take account of such factors as: (1) how to specify and sense an abort condition; (2) how much fuel should be allotted for abort purposes; (3) what size and type of engines are best suited for each mission; (4) what is the optimum time to fire the abort engines; (5) what should be the magnitude and direction of the induced velocity changes; (6) what role in the abort sequence is to be delegated to the crew; (7) what compromises are incurred due to other mission requirements; etc.

There are different levels of hazard to which a crew is exposed in the course of a typical mission. First, the situation on the launch pad at zero velocity places the crew in the immediate vicinity of tremendous quantities of highly explosive and inflammable materials. Thus provision must be made for essentially instantaneous clearance from the vehicle to a safe area in case of launch difficulty. The nature of the abort difficulties changes when the vehicle is in flight through the earth's atmosphere. Here, questions of acceleration and clearance from the boost vehicle assume a primary importance. The picture again changes when the vehicle is above the earth's atmosphere in a hostile environment (radiation belt) and at high velocity. Consequently, a variety of conceptual philosophies must be employed in initiating an abort sequence.

In this monograph, emphasis is placed on control system requirements for the abort problem. These requirements, however, cannot be completely divorced from hardware implementations, and the latter will be discussed in general terms where appropriate.

2. STATE OF THE ART

Space flight is still in its infancy and firm requirements for an abort system are not yet fully established. The abort techniques used on Mercury and Gemini were of a comparatively modest level in terms of complexity and energy management. Since these were for the most part suborbital missions, attention was focused on off-the-pad and atmospheric abort. For these conditions, the Mercury spacecraft used a set of tower-mounted solid rockets. This system went through an extensive series of tests early in the development program and was considered one of the most reliable components of the Mercury spacecraft. However, during certain phases of the mission, the abort procedure was known to be only marginally effective. For example, when the booster vehicle has attained a velocity of 2,000 to 3,000 ft/sec and an abort is required, the fuel supply to the booster engines is shut off, and the spacecraft is separated from the boost vehicle by firing the tower-mounted rockets. The initial separation velocity in this case is about 400 ft/sec. However, immediately following separation the spacecraft is subject to a dynamic pressure somewhat greater than that of the launch vehicle while the weight or inertia of the booster vehicle is about 100 times greater than that of the spacecraft. Even with a tumbling booster vehicle, this difference in inertia and dynamic pressure would be enough to cause the booster vehicle to overtake the spacecraft in 5 to 10 seconds. For this reason, the thrust line of the escape rockets does not pass through the center of gravity of the spacecraft, thereby producing a pitching moment which steers it away from the trajectory of the launch vehicle.

When the vehicle reaches the fringes of the atmosphere at velocities of 14,000 to 16,000 ft/sec, the deceleration factor is critical. Since the Mercury spacecraft has no lift capability, an abort at this time will induce as much as a 16 g reentry.

The abort system for the Gemini spacecraft is somewhat more sophisticated. This is reflected mainly in more extensive sensing of abort parameters, and in the provision for three separate abort modes which include the use of ejection seats. Also, the crew is given a greater degree of control in initiating and operating the abort sequence.

In any event, because of the limited nature of the Mercury and Gemini missions, the abort procedures did not require a complex guidance and control system. However, the abort systems for the next generation of manned spacecraft will make stringent demands in the way of onboard guidance, control, and computation. Orbital or translunar aborts, for example, will require highly accurate velocity changes, accurately timed. Related sensing and computational facilities (onboard) must be correspondingly accurate. In some cases, a certain degree of simplification may be achieved with stored programs. Systems of this type will employ the concept of "abort way-stations" or "abort corridors," and similar schemes whose fundamental

aim is to minimize onboard computations in emergency situations. On the other hand, for certain cases such as missions in the lunar vicinity a fairly sophisticated onboard guidance and control facility will be required in order to achieve a successful abort.

Most of these problems are presently under active investigation. One aspect of this effort is directed at formulating realistic guidance and energy management concepts insofar as they relate to abort and are consistent with other mission constraints. A parallel effort is aimed at devising suitable escape and recovery configurations consistent with the primary mission of the spacecraft. A discussion of some of the more promising of these methods forms the subject matter of this monograph.

3. RECOMMENDED PROCEDURES

It must be emphasized that at the present state of development of the manned space flight program, few definitive solutions of the abort problem are available. Most of the guide lines in this respect are derived from experience with the Mercury and Gemini programs. However, there is no operational data on the abort system since these flights were (fortunately) remarkably successful.

For present purposes therefore we will concentrate on defining the problem areas and indicating the trends of current research. It is generally agreed that a superorbital manned space mission can be divided into five regiors during which the abort methodology will differ: (1) on the pad, (2) atmospheric (especially the high q region), (3) exoatmospheric, (4) orbital, and (5) lunar. An abort in each of these regions poses its own unique problems. The guidance and control aspects of each of these abort modes is considered in Sec. 3.1. Unclassified details relating to the complete Gemini and Apollo abort systems are discussed in Secs. 3.2 and 3.3. Finally, in Sec. 3.4, some of the more sophisticated rescue and recovery systems are surveyed briefly. It should be clearly understood that these concepts are still in the exploratory stage, and represent possible rather than definitive solutions.

3.1 ABORT MODES

For any particular manned space mission, one can conceive of a multitude of possible emergency situations which can be assigned different hazard levels from the point of view of crew survival. Thus the nature of the abort sequence is directely related to the type of emergency that occurs. Miller and Bloom[1] have classified the types of emergency into seven categories, which are summarized in Table I. These categories are defined as follows:

Category A-1: Emergency conditions which require immediate action and which will result in a complete abort of the mission; e.g., explosion of the booster during launch.

Category A-2: Those emergency conditions which require immediate action which will result in a deviation from the planned mission objectives to a secondary objective; e.g., insufficient final stage boost which will allow deviation from a lunar mission to a secondary earth orbit mission.

Category B-1: Major emergencies and systems failures which will result in the complete abort of the mission. These differ from Category A-1 failures in that sufficient time is available to allow for an analysis of the emergency, by either crew members or ground monitors, and manual initiation of the abort procedure; e.g.,

Table I. Categories of Emergency

Category	Immediate Action Required	Result of Failure	Repairs or Replacement Possible
A-1	Yes	Abort	No
A-2	Yes	Abort, emergency return, or secondary mission	No
B-1	No	Abort or emergency return	No
B-2	No	Abort, emergency return, or secondary mission	No
C-1	Nc	Emergency return or secondary mission	Yes
C-2	No	No change	Yes
D	No	No change	Yes

power supply failure. The availability of redundant systems will not affect this category of emergency.

Category B-2: Major emergencies and systems failures which allow sufficient time for analysis of the problem and manual initiation of a procedure which will result in a change to a secondary mission objective; e.g., insufficient fuel remaining to make necessary trajectory correction and still complete lunar mission. The availability of redundant systems will not affect this category of emergency.

Category C-1: Equipment failure in a major system which is repairable or where a redundant system is available. If the failed component is not repairable or replaceable in flight, the Category C-1 failure will result in an emergency return or change to a secondary mission objective in order to shorten the mission time; e.g., loss of pressure in one tank of a multi-tank oxygen supply system.

Category C-2: Equipment failure, which although compromising the mission objectives somewhat, does not require a deviation from the planned profile. If a Category C-2 failure occurs in a major operating system, repair of the malfunctioning equipment must be possible; e.g., voice communications failure. If a Category C-2 failure occurs in a non-operating or minor system and is not repairable, the mission may still be completed with some degradation in expected results; e.g., partial failure of mission instrumentation equipment.

Category D: Equipment or system failure external to the flight vehicle. This may include range instrumentation, GSE, etc. During the prelaunch phase this will result in a countdown hold. At other times, the mission will not be affected as it is expected that redundant ground-based systems and sufficient spare parts will be available.

The emergency situations which could occur during boost phase are summarized in Table II. Some of those emergencies could also occur in the orbital or lunar phase, in which case the category of emergency might be different. For example, loss of thrust in some of the engines in exoatmospheric phase would constitute an A-2 emergency due to the possibility of changing from a lunar to earth orbital mission. On the other hand, loss of engine thrust during boost phase would be classified as an A-1 emergency.

The design of the abort system itself is subject to two fundamental constraints. First, it must maximize the probability of crew survival; and secondly, it must be compatible with the overall mission requirements.

The areas that command consideration in this respect are summarized in Table III. A detailed analysis of those condictions may be pursued once the main problem areas have been identified, and specific abort philosophies formulated. This will be done with respect to each of the mission phases in the following sections.

3.1.1 On-the-Pad Abort

When the spacecraft is positioned on top of the booster on the launch pad, it is in the immediate vicinity of a large quantity of highly volatile fuel. In the event of an explosion, the crew must be removed immediately from the danger area by applying some form of thrust to the escape capsule (which may be the spacecraft itself). To do this successfully requires a careful consideration of the following factors:

a. Acceleration imposed on the crew.

b. Overpressure imposed on escape capsule (or spacecraft) due to explosion shock waves.

c. Weight of abort propulsion system.

d. Altitude and range requirements to avoid local obstacles.

These in turn are directly influenced by the time-distance relations for the pressure waves generated by the explosion. For purposes of analyzing the detonation properties of typical booster fuels, the latter are usually considered in terms of an equivalent quantity of TNT. Some TNT equivalents for common booster fuels are given in Table IV, which is abstracted from Ref. 30. We see, for example, that one million pounds of a liquid hydrogen-liquid oxygen combination is equivalent to 600,000 pounds of TNT in explosion potential.

Table II. Boost Phase Emergencies

Emergency	Category	Abort/Emergency Return Initiation	Method of Abort/Emergency Return
Boost Explosion	A-1	Automatic	Eject using escape rockets, automatically activate recovery aids and emergency systems. If beyond 2nd stage burnout, utilize on-board propulsion to change trajectory.
Power Supply Failure	A-1		
Loss of Thrust/Insufficient Thrust	A-1*		
Booster Fails to Ignite	A-1**		
Stage Separation Failure	A-1		
Guidance System Failure	A-1		
Control Failure	A-1		
Major Structural Failure	A-1		
Fire in Mission Module	A-2		
Fire in Reentry Vehicle	A-1		
Telemetry Failure	A-2	Automatic (1)	Automatic reprogramming of guidance system to initiate earth orbit mission. Manual control after arriving in orbit.
Leaks	A-2	Automatic (1)	
Meteoroid Penetration	A-2***	Automatic (1)	
Human Failure-Physiological	B-1	Manual	Initiate preprogrammed change in guidance and booster control system to effect rapid return to earth.
Human Failure-Psychological	B-1	Manual	
Communications Failure	C-1	Manual	Change to earth orbit mission. Perform on-board maintenance. If not successful in repairing, initiate action to return to earth.
Tracking Beacon Failure	C-1	Manual	
Vehicle Instrumentation/Display Failure	C-1	Manual	
Cabin Gaseous Control Failure	C-1	Manual	
Cabin Thermal Control Failure	C-1	Manual	
Bio-instrumentation Failure	C-2	None	None. On-board maintenance.
Failure External to Vehicle	D	None	Ground maintenance.

* Category A-2 during 3rd stage boost

** Category B-1 during 1st stage boost

*** Not applicable during 1st stage boost

(1) Crew member action to repair/reduce leaks taken after earth orbit is established.

Table III. Summary of Design Considerations for Boost Phase Abort

Areas of Consideration	Functions of
Reliability	Reduced complexity Safety margins Part de-rating
Man's Tolerance	Acceleration Acceleration onset Direction of acceleration or onset Required tasks
Structural Response	Acceleration loads Overpressure loads Flight loads Recovery subsystem loads Safety margins
Separation, Booster-Abort Vehicle	Abort rocket - sizing - location - inclination Drag load Booster acceleration
Abort Vehicle Stability	Thrust vector location Thrust vector accuracy Abort vehicle c.g. Aerodynamics Required maneuvers
Recovery Subsystem	Altitude for safe operation Velocity for safe operation Tolerances on operational sequence Landing site selection - all abort cases Landing site limits - winds, fire on pad
Warning/Action Time	Booster type Abort rocket type
Detection/Warning Instrumentation	Possible failures - propulsion - guidance, control - staging - structure - electric power - fire - environmental control
Payload Penalty	Booster staging Abort rocket jettisoning Abort rocket packaging, location
Control of Abort	Location of maximum information Ease of initiation by crew
Compatibility	Equipment of nominal mission Multi-purpose design

Table IV. Liquid Propellant Explosive Equivalents

Propellant Combination	Static Test Stands	Range Launch Pads
LO_2 - LH_2	60%	60%
LO_2 - LH_2 + RP-1	Sum of (60% for LO_2-LH_2) (10% for LO_2-RP-1)	Sum of (60% for LO_2-LH_2) (20% for LO_2-RP-1)
LO_2 - RP-1 or LO_2 - NH_3	10%	20% up to 500,000 pounds plus 10% over 500,000 pounds
IRFNA - Aniline*	10%	10%
IRFNA - UDMH*	10%	10%
IRFNA - UDMH + JP-4*	10%	10%
N_2O_4 - UDMH + N_2H_4*	5%	10%
N_2O_4 - UDMH + N_2H_4 - Solid*	5% plus the explosive equivalent of the solid propellant	10% plus the explosive equivalent of the solid propellant
Tetranitromethane (alone or in combination)	100%	100%
Nitromethane (alone or in combination)	100%	100%

* These are hypergolic combinations.

Basis: Recommendations of ASESB Work Group on Explosive Equivalents for Liquid Propellants. Tetranitromethane and nitromethane are known to be detonable.

NOTES: 1. The percentage factors are used to determine the explosive equivalencies of propellant mixtures at launch pads and static test stands when such propellants are located aboveground and are unconfined except for their tankage. Any configurations other than stated above should be considered on an individual basis to determine the equivalencies.

2. The equivalencies of any non-nuclear explosives will be added to the above equivalencies.

The mathematical model used in analyzing a booster explosion involves a numerical solution of the partial differential equations of hydrodynamic motion for the case of a center denotated spherical change of TNT.[33] The pressure-time history of a typical blast wave as observed at a location removed from the center of explosion is shown in Fig. 1. At an arrival time of t_x seconds after the explosion, the pressure at this removed location suddenly jumps to a peak value of overpressure.

An object at this location is then subjected to an instantaneous force equal to the product of this overpressure and the projected area in the plane of the blast wave. The overpressure immediately begins to decay following a pressure-time relationship of the type shown in the figure which is quasi exponential in character.

The explosion characteristics for a spherical charge of one ton of TNT at sea level conditions is shown in Table V. This data is presented in graphical form in Fig. 2.

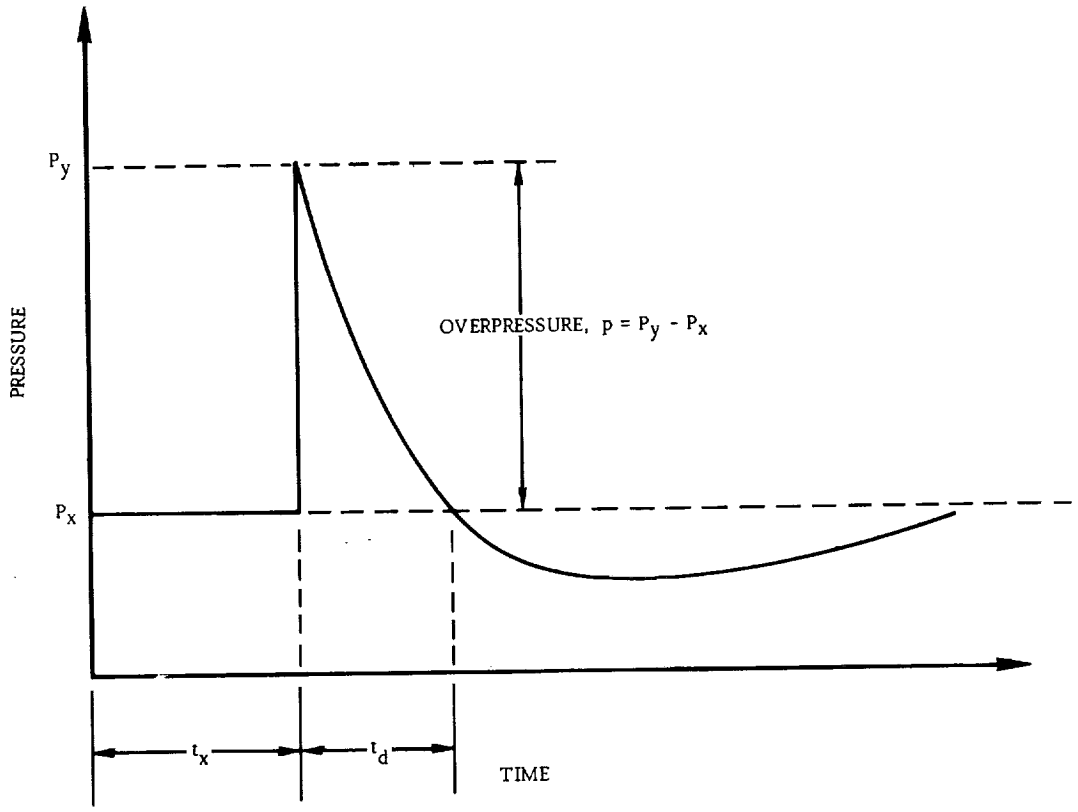

Figure 1. Typical Pressure-Time Curve for an Explosive Blast Wave

Table V. Reference Explosions

d Radial Distance (ft)	p/P_x Peak Overpressure Ratio	t_x Arrival Time (milli-sec)	t_d Duration (milli-sec)
5	192	0.28	2.5
10	76	0.70	1.5
15	35	1.29	0.6
20	21	2.22	1.9
25	14	3.34	5.6
30	9.3	4.7	6.0
35	6.8	6.2	6.5
40	4.9	8.1	7.4
45	3.6	10.1	8.3
50	2.7	12.3	9.3
55	2.10	14.7	10.2
60	1.65	17.3	11.1
65	1.32	20.1	12.0
70	1.10	23.3	12.9
75	0.95	26.6	13.8
80	0.85	29.9	14.6
85	0.76	33.3	15.3
90	0.68	36.8	16.0
95	0.62	40.3	16.7
100	0.57	43.9	17.3
105	0.52	47.6	17.9
110	0.48	51.3	18.4
115	0.44	55.1	18.7
120	0.41	58.9	19.0
125	0.38	62.8	19.3
130	0.35	66.7	19.6
135	0.33	70.6	19.8
140	0.31	74.5	20.1
145	0.292	78.4	20.4
150	0.276	82.3	20.6
155	0.262	86.3	20.9
160	0.250	90.3	21.2
165	0.238	94.3	21.5
170	0.227	98.3	21.8
175	0.217	102.4	22.0
180	0.208	107	22.3
185	0.200	111	22.6
190	0.193	115	22.9
195	0.186	119	23.2
200	0.181	123	23.4
205	0.174	127	23.6
210	0.168	131	23.8
215	0.162	135	23.9
220	0.156	138	24.1
225	0.151	144	24.2
230	0.146	148	24.3
235	0.141	152	24.4
240	0.136	156	24.4
245	0.133	160	24.5
250	0.129	165	24.6

Based on Mizner and Ripley, "The ARDC Model Atmosphere 1956," ASTIA document 110233 (1956).

† Abstracted from Ref. 34.

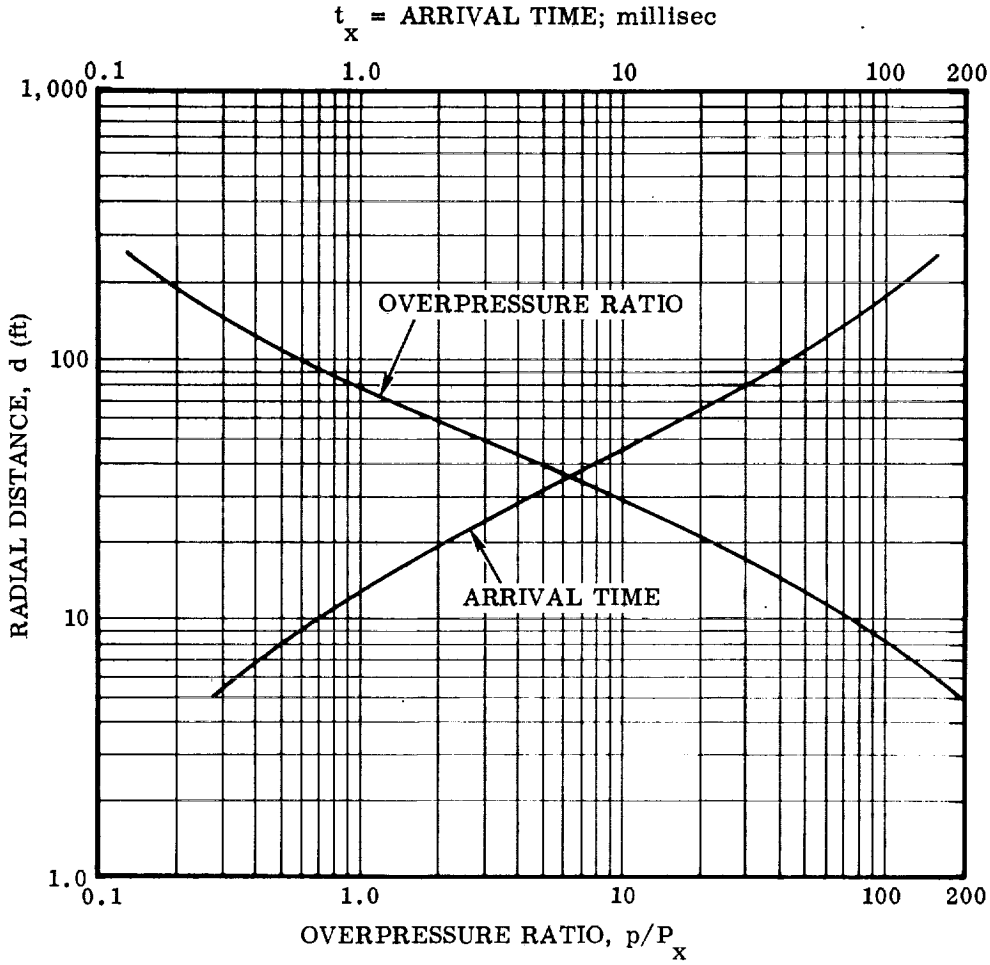

Figure 2. Explosion Characteristics of One Ton of TNT at Sea Level Conditions

To obtain the explosion characteristics for other weights of TNT at any given altitude, we use the fact that, "two explosions will give identical blast wave intensities at distances which are proportional to the cube root of the respective energy release." Application of this idea leads to the concept of a "scaled distance" which is used in the following way. Suppose that it is desired to obtain the explosion characteristics at a distance d from the center, for W_T tons of TNT exploded at an altitude h. This is derived from the data for a one ton explosion at sea level (Table V) by first calculating a scaled distance d′,

$$d' = d\left(\frac{1}{W_T}\right)^{1/3}\left(\frac{\rho}{\rho_{SL}}\right)^{1/3} \qquad (1)$$

where ρ and ρ_{SL} are the atmospheric densities at altitude h and at sea level respectively. The explosion characteristics at distance d due to W_T tons exploding at altitude h are precisely those values in Table V corresponding to the scaled distance d'. Let $(p/P_x)'$, t'_x, and t'_d denote the overpressure ratio, arrival time, and duration which correspond to d'. Then the actual arrival time and actual duration are given by

$$t_x = t'_x (W_T)^{1/3} \left(\frac{\rho_{SL}}{\rho}\right)^{1/3} \left(\frac{\sigma_{SL}}{\sigma}\right) \tag{2}$$

$$t_d = t'_d (W_T)^{1/3} \left(\frac{\rho_{SL}}{\rho}\right)^{1/3} \left(\frac{\sigma_{SL}}{\sigma}\right) \tag{3}$$

where σ and σ_{SL} are the speed of sound at altitude h and sea level respectively. The actual overpressure is

$$p = \left(\frac{p}{P_x}\right)' P_x \tag{4}$$

P_x = atmospheric pressure at altitude h - psia

For convenience in the use of Eqs. (2) and (3), the transmission factors for the ARDC Model Atmosphere are summarized in Table VI.

A graphic illustration of the shock wave propagation due to the explosion of one kiloton of TNT (at sea level) is shown in Fig. 3.

In order to use the above data effectively, one must know first, the overpressure capability of the spacecraft (or escape capsule), and secondly, the acceleration limitations of the human body. For the spacecraft currently in use, the overpressure capability is on the order of 5 to 10 psi. Human tolerance limits to acceleration are given in Fig. 4. This data, which represents a compilation of results from twelve sources, is taken from Ref. 31. The ordinate in Fig. 4 represents the maximum acceleration which can be endured for a given duration in each of the four directions of acceleration shown. It appears that a rate of onset of approximately 1000 g's per second is tolerable. From a design standpoint, this limitation presents no problem because of tolerances available in thrust buildup. However the durations of acceleration do impose definite design limitations on the abort propulsion system since durations of 2 to 3 seconds are required to restrict the overpressure level.

To examine the implication of the above ideas, consider a launch vehicle having a propellant (LO_2-RP1) weight of 5,000,000 lb. This is representative of a system required to place a space vehicle weighing 10,000 lb on a circumlunar trajectory. According to Table IV, the TNT equivalent is $W_T = 275$ tons. If the overpressure capability of the escape capsule is 10 psi, then the overpressure ratio (at sea level) is $p/P_x = 10/14.7 = 0.68$. For a one-ton explosion, we have from Table V: $d' = 90$ ft

Table VI. Transmission Factors for the ARDC Model Atmosphere

Altitude (ft)	Pressure (psia)	Temperature °C	Temperature °F	$\left(\frac{\rho}{\rho_{SL}}\right)^{1/3}$	$\frac{\sigma}{\sigma_{SL}}$
-2,500	16.07	20.0	67.9	1.0245	1.0086
0	14.6959	15.0	59.0	1.0000	1.0000
2,500	13.42	10.0	50.1	0.9755	0.9914
5,000	12.23	5.1	41.2	0.9516	0.9827
7,500	11.13	0.1	32.3	0.9276	0.9739
10,000	10.10	-4.8	23.3	0.9039	0.9650
12,500	9.16	-9.8	14.4	0.8893	0.9561
15,000	8.29	-14.7	5.5	0.8569	0.9470
17,500	7.49	-10.7	-3.4	0.8337	0.9379
20,000	6.75	-24.6	-12.3	0.8107	0.9287
22,500	6.08	-29.6	-21.3	0.7879	0.9195
25,000	5.45	-34.6	-30.2	0.7652	0.9100
27,500	4.88	-39.5	-39.1	0.7428	0.9005
30,000	4.36	-44.4	-50.0	0.7206	0.8909
32,500	3.89	-49.4	-56.9	0.6985	0.8812
35,000	3.46	-54.3	-65.8	0.6767	0.8714
37,500	3.07	-56.5	-69.7	0.6523	0.8671
40,000	2.72	-56.5	-69.7	0.6267	0.8671
42,500	2.41	-56.5	-69.7	0.6021	0.8671
45,000	2.14	-56.5	-69.7	0.5789	0.8671
47,500	1.90	-56.5	-69.7	0.5558	0.8671
50,000	1.68	-56.5	-69.7	0.5339	0.8671
52,500	1.49	-56.5	-69.7	0.5130	0.8671
55,000	1.32	-56.5	-69.7	0.4928	0.8671
57,500	1.17	-56.5	-69.7	0.4735	0.8671
60,000	1.04	-56.5	-69.7	0.4549	0.8671
70,000	0.64	-56.5	-69.7	0.3876	0.8671
80,000	0.40	-56.5	-69.7	0.3301	0.8671
90,000	0.25	-49.2	-57.2	0.2788	0.8809
100,000	0.16	-40.2	-40.9	0.2363	0.8994
110,000	0.101	-30.9	-23.6	0.2016	0.9169
120,000	0.066	-21.8	-7.2	0.1730	0.9329
130,000	0.044	-12.6	-9.3	0.1493	0.9509
140,000	0.030	-3.5	25.7	0.1295	0.9674
150,000	0.020	5.7	42.2	0.1128	0.9837
160,000	0.014	9.5	49.1	0.09928	0.9904
170,000	0.0097	9.5	49.1	0.08781	0.9904
180,000	0.0067	2.2	36.0	0.07826	0.9776
190,000	0.0046	-9.7	14.6	0.06982	0.9563
200,000	0.0031	-21.5	-6.8	0.06196	0.9344
210,000	0.00200	-33.4	-28.2	0.05467	0.9121
220,000	0.00128	-45.3	-49.6	0.04793	0.8892
230,000	0.00080	-57.2	-71.0	0.04241	0.8717
240,000	0.00049	-69.1	-92.4	0.03604	0.8415
250,000	0.00029	-76.3	-105.3	0.03064	0.8266
260,000	0.00017	-76.3	-105.3	0.02569	0.8266
270,000	0.00010	-76.3	-105.3	0.02153	0.8266
280,000	0.000059	-76.3	-105.3	0.01927	0.8266
290,000	0.000035	-76.3	-105.3	0.01513	0.8266
300,000	0.000026	-75.8	-104.5	0.01267	0.8267

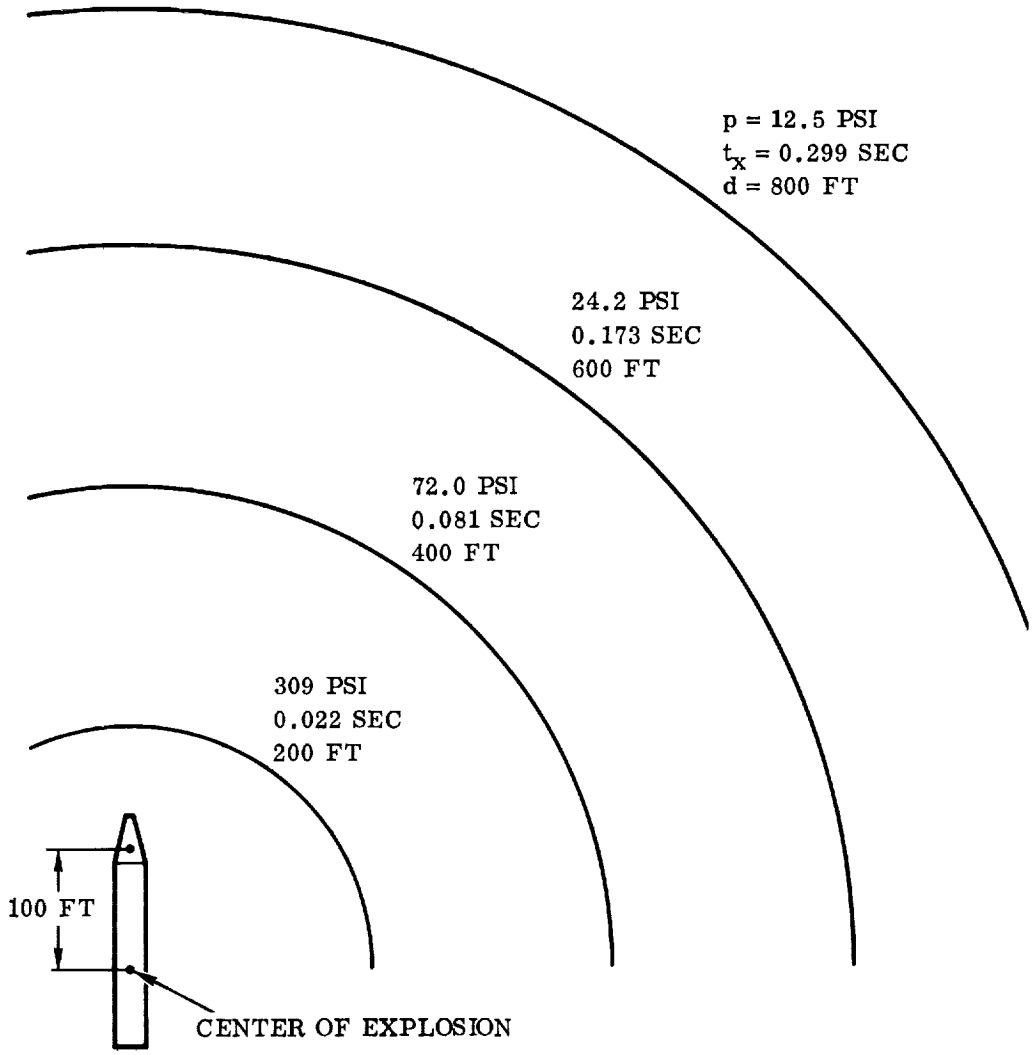

Figure 3. Shock Wave Propagation for One Kiloton Explosion at Sea Level

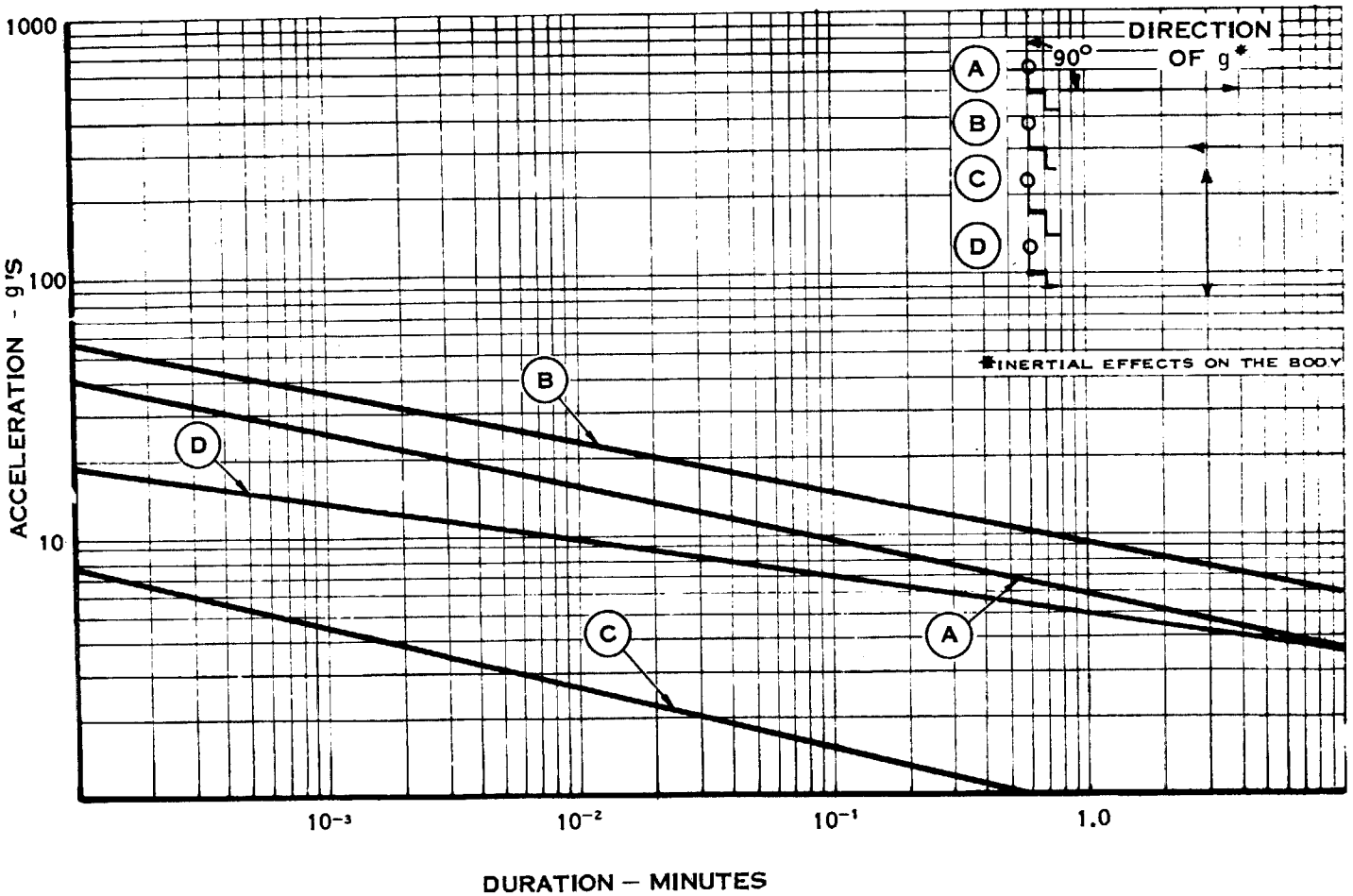

Figure 4. Recommended Maximum Tolerance Limits to Acceleration

and $t'_x = 0.0368$ sec. Consequently, for an explosion of 275 tons of TNT, a 10 psi overpressure occurs at

$$d = 90 \times 275^{1/3} = 585 \text{ ft}$$

with an arrival time

$$t_x = 0.0368 \times 275^{1/3} = 0.239 \text{ sec}$$

If the abort system is actuated simultaneously with the explosion, then it is required to move the capsule (assumed located 100 ft from the center of the explosion) a distance 585 - 100 = 485 ft in 0.239 sec. But this induces an acceleration in excess of 500g's on the vehicle and crew, which is a completely intolerable situation. It is therefore necessary that sufficient warning time be available prior to an explosion in order to abort safely without imposing intolerable accelerations on the crew or requiring excessive thrust capability in the abort engines.

Available information indicates that by sensing chamber pressure, one can obtain a 2 second warning time prior to an impending explosion. If 0.50 second is allowing for sensing, actuation of the abort mechanism, and thrust buildup in the abort rockets, then there is a warning time of 1.50 seconds available prior to an explosion. In this case, using the previous example, the escape capsule is required to move 485 feet in $1.5 + 0.239 \approx 1.74$ seconds. Under vacuum conditions, this implies a longitudinal acceleration of approximately 10 g's. This is an approximate figure and would be refined by a more detailed analysis. However, the above results suggest that an available warning time of about two seconds can bring the problem down to manageable proportions.

For any specific space mission, the general configuration of the escape capsule is dictated by the mission requirements. Thus the abort vehicle may be either the spacecraft itself or else a separate escape capsule. In either event, once this is established, a maximum overpressure criterion may be specified. It is then a question of conducting various parametric studies on the influence of abort system parameters on the time-separation distance relationships for an equivalent TNT explosion of the booster fuel weight. A quantitative study along these lines was conducted by Cohan,[30] from which some general qualitative trends may be inferred. The analysis was made for a ballistic and lifting type of escape capsule with the general form and basic properties shown in Figs. 5 and 6. For each capsule, the maximum allowable overpressure was 5 psi. The following three booster configurations were investigated:

Configuration	Gross Takeoff Weight (lb)	Propellant H_2-O_2 Weight (lb)
A	500,000	427,000
B	2,000,000	1,707,000
C	6,000,000	5,130,000

The 5 psi overpressure characteristics for an equivalent TNT explosion in each of the above cases is shown in Fig. 7. The corresponding minimum warning times (to limit vehicle accelerations to tolerable limits) required are shown in Fig. 8 as a function of

$\frac{T}{W} \equiv$ thrust loading $\equiv$ thrust to weight ratio of the abort (escape) capsule

and

$t_b \equiv$ burning time of abort rockets

It is apparent that adequate warning time becomes a critical factor for the larger gross takeoff weights.

The design of the abort propulsion system is governed by the time-separation distance requirements which in turn stem from the overpressure and acceleration constraints. To begin with, the abort rocket thrust vector must be at some angle with the vertical since both altitude and range separation is required; altitude is necessary for possible chute deployment, and range is necessary to clear local obstacles. Consequently, the basic abort propulsion parameters are

a. Thrust loading, $\frac{T}{W}$.

b. Thrust angle, δ.

c. Rocket burn time, t_b.

The manner in which these influence the time-separation distance relationships for both the ballistic and lifting type vehicles is shown in Figs. 9 to 14. As expected, higher thrust loading and increased burning time increase the separation distance. We note further that decreasing the thrust angle increases the separation distance. This is due to the fact that lower thrust angles yield lower initial angles of attack and therefore result in less drag. It appears from these figures that, in general, variations in the thrust parameters yield similar trends for both the ballistic and lifting type vehicles. Lower values of thrust loading were used for the lifting body than for the ballistic body since the ballistic body would have higher drag at the higher dynamic pressures necessitating higher separation forces.

In all of the above calculations, it was implicitly assumed that the warning time for an impending explosion was adequate. Actually, while crude estimates can be obtained using the methods described above, a more accurate evaluation of the ability of pressure sensors to detect impending explosions is required. Some of the current studies in this area are classified and cannot be reported here. Also, more detailed investigations of the explosion process are required before firm design

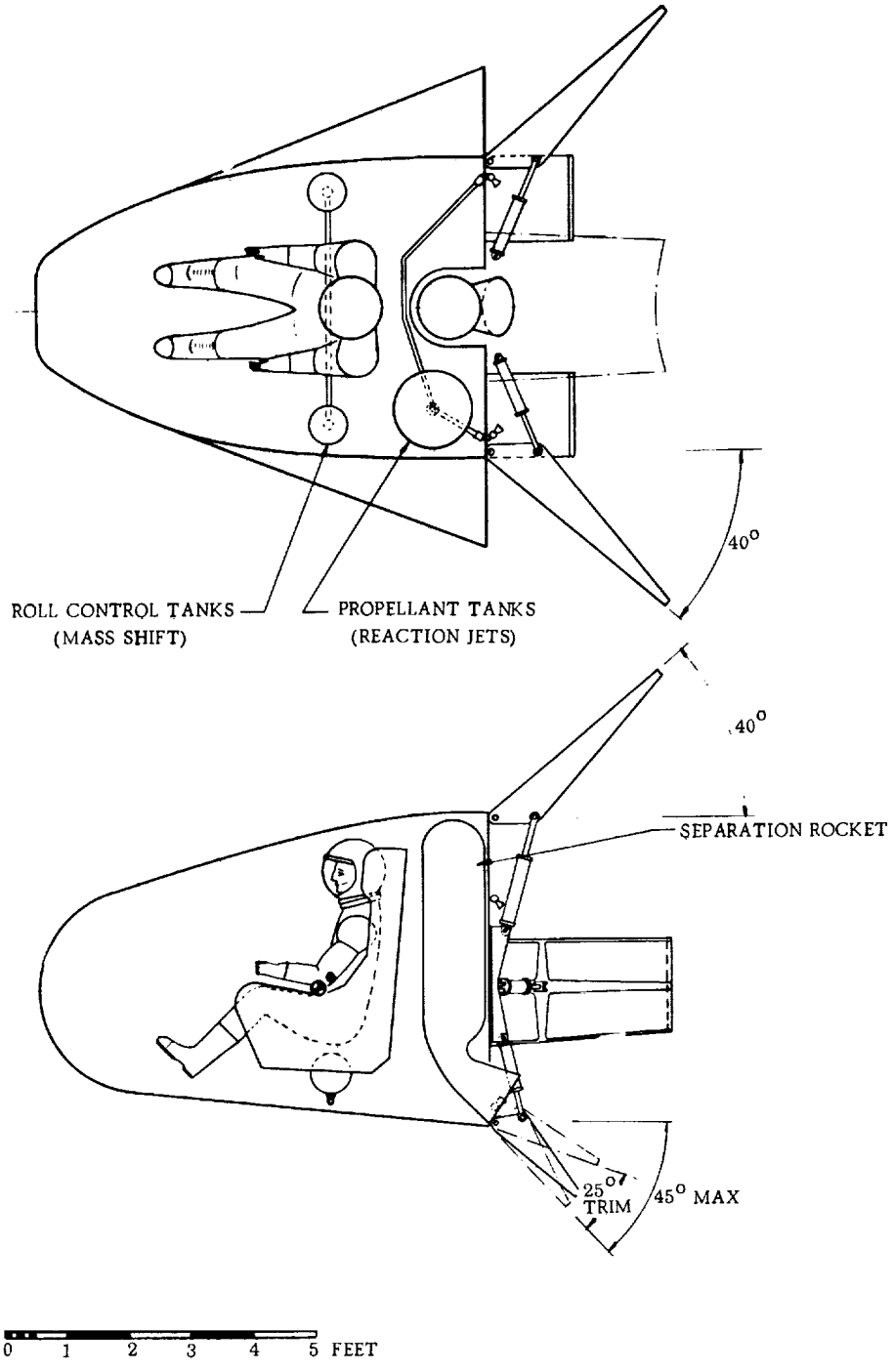

Figure 5. Ballistic

VEHICLE DATA	
REFERENCE AREA - PLANFORM	37 SQ FT
SIDE FLAP AREA - EACH	6.03 SQ FT
UPPER FLAP AREA	8.1 SQ FT .
LOWER FLAP AREA - TOTAL	4.9 SQ FT
REFERENCE LENGTH ALONG BODY $\mathbb{Q}$	7.25 FT
WEIGHT (PRIOR TO THRUSTING)	2,680 LB
WEIGHT (AFTER THRUSTING)	2,500 LB
I_{xx} (AFTER THRUSTING)	190 SLUG-FT^2
I_{yy} (AFTER THRUSTING)	541 SLUG-FT^2
I_{zz} (AFTER THRUSTING)	530 SLUG-FT^2
I_{zy} (AFTER THRUSTING)	+56.7 SLUG-FT^2

SEPARATION ROCKET DATA	
THRUST (NOM)	40,000 LB
TOTAL IMPULSE	40,000 LB-SEC
PROPELLANT	SOLID
SPECIFIC IMPULSE (S. L.)	220 LB/LB/SEC
THROAT AREA	5.8 SQ IN
EXPANSION AREA	3:1
CHAMBER PRESSURE	1,000 PSI

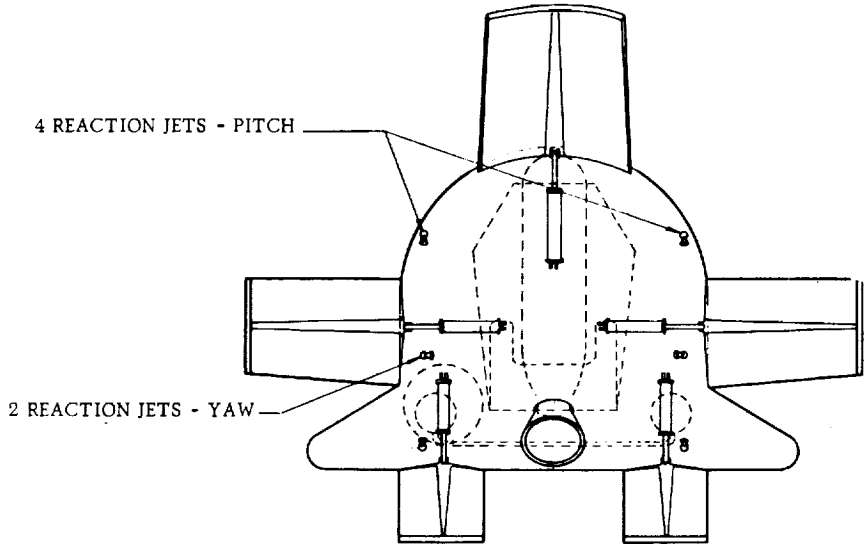

Body — Escape Capsule

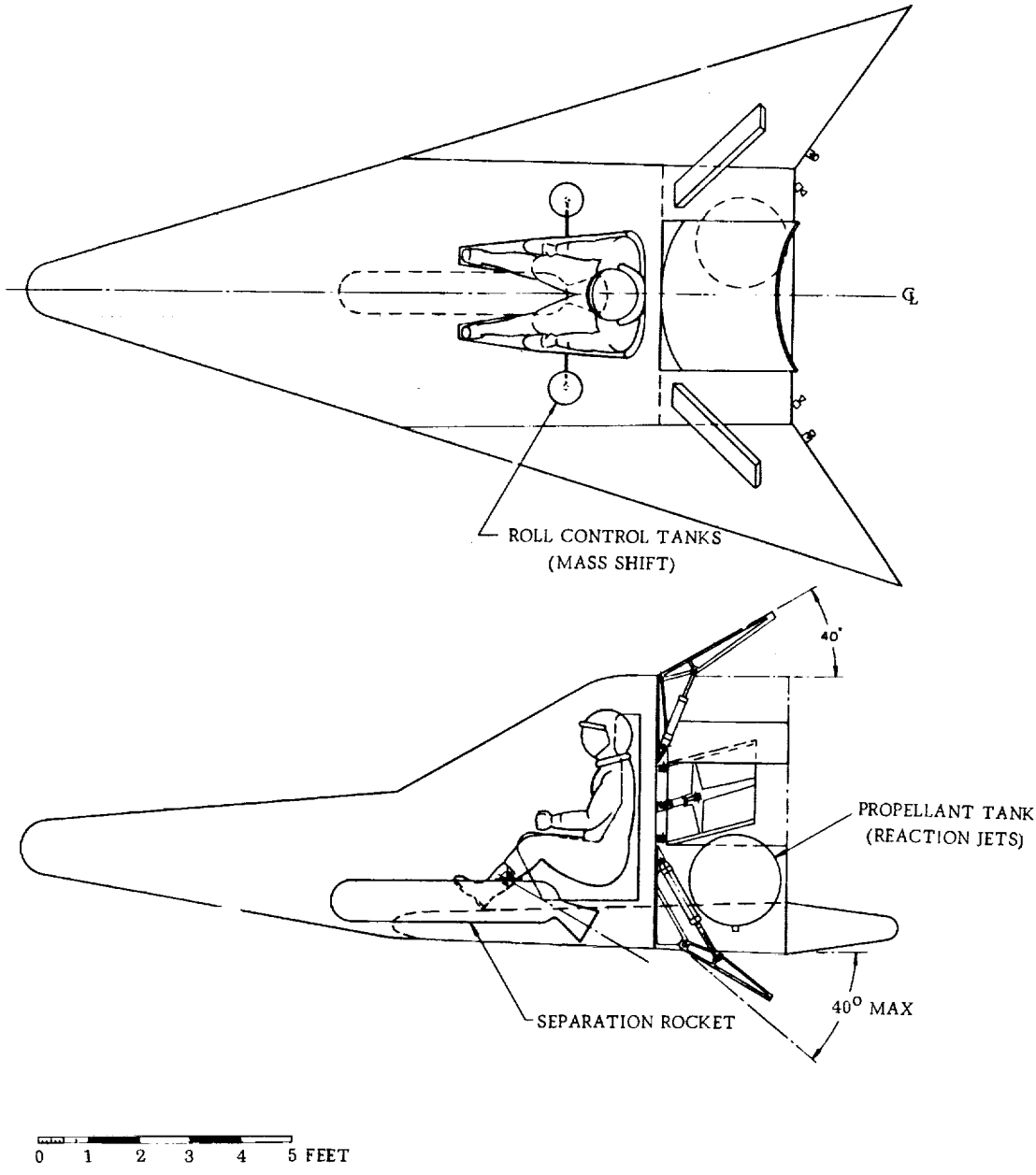

Figure 6. Lifting Body –

VEHICLE DATA	
REFERENCE AREA - PLANFORM	88 SQ FT
SIDE FLAP AREA - EACH	3.8 SQ FT
UPPER FLAP AREA	9.4 SQ FT
LOWER FLAP AREA - TOTAL	6.0 SQ FT
REFERENCE LENGTH ALONG BODY $\mathcal{L}$	15.1 FT
WEIGHT (PRIOR TO THRUSTING)	2,613 LB
WEIGHT (AFTER THRUSTING)	2,500 LB
I_{xx} (AFTER THRUSTING)	236 SLUG-FT^2
I_{yy} (AFTER THRUSTING)	971 SLUG-FT^2
I_{zz} (AFTER THRUSTING)	956 SLUG-FT^2
I_{zy} (AFTER THRUSTING)	-34 SLUG-FT^2

SEPARATION ROCKET DATA	
THRUST (NOMINAL)	25,000 LB
TOTAL IMPULSE	25,000 LB-SEC
PROPELLANT	SOLID
SPECIFIC IMPULSE (SL)	220 LB/LB/SEC
THROAT AREA	3.7 SQ IN.
EXPANSION RATIO	3:1
CHAMBER PRESSURE	1,000 PSI

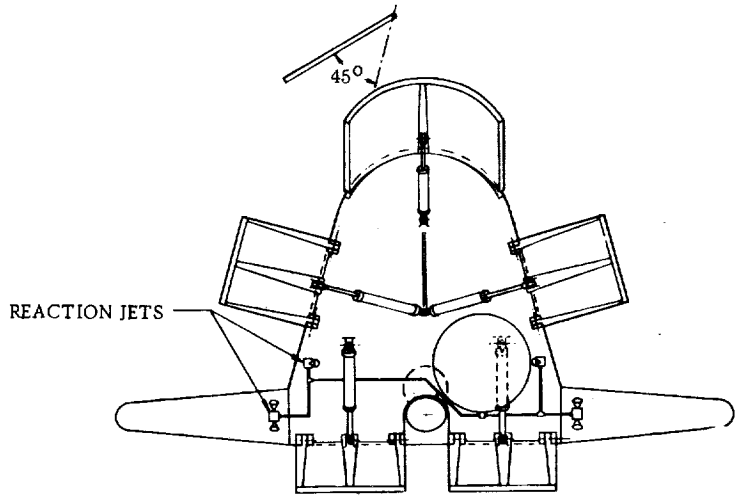

Escape Capsule

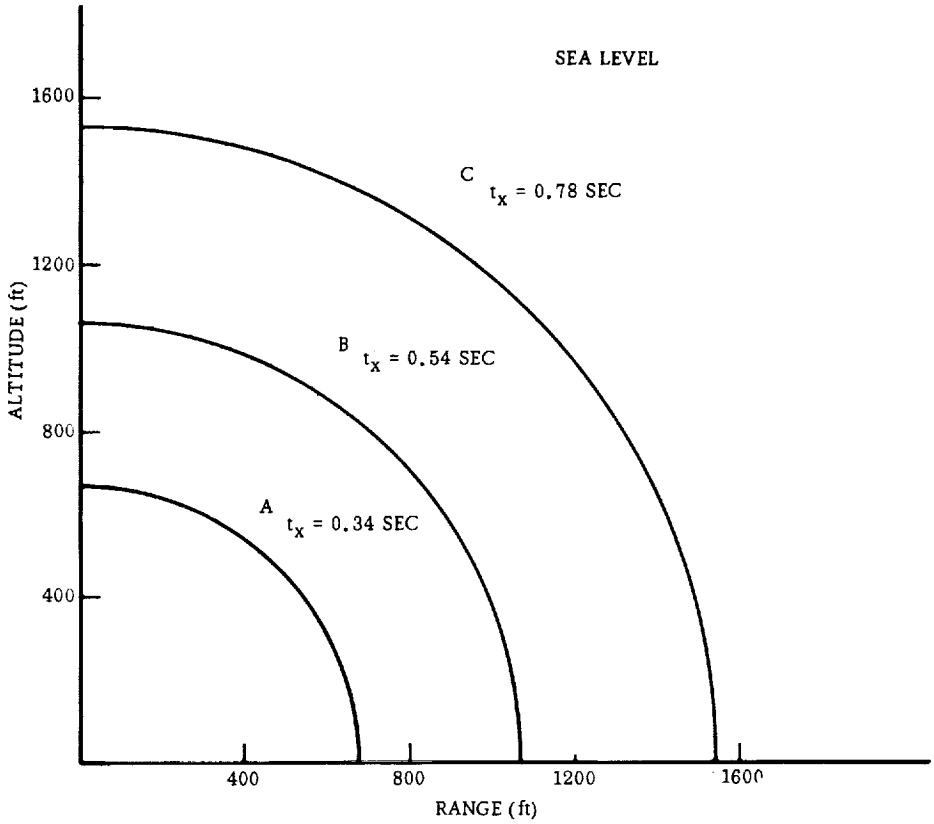

Figure 7. Five psi Overpressure Characteristics

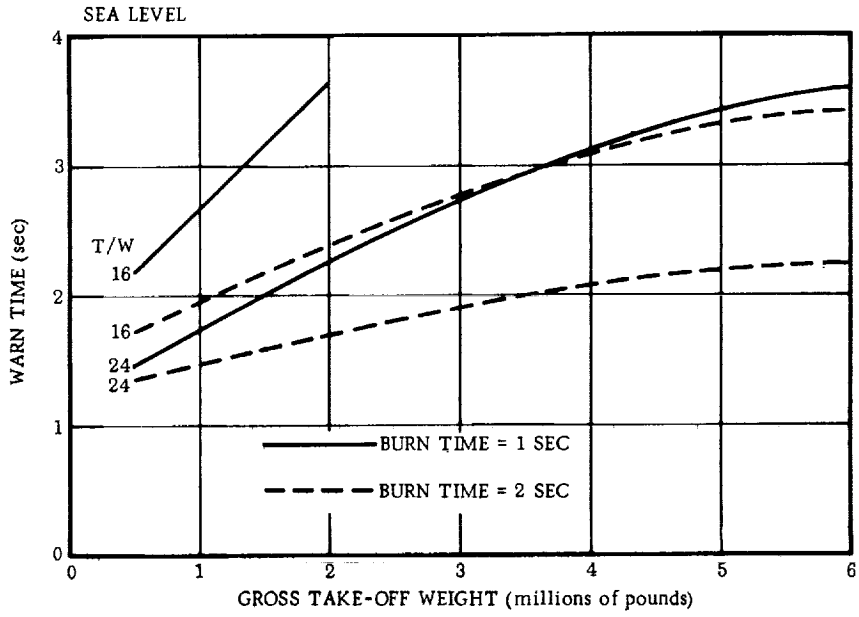

Figure 8. Minimum Warn Time Required for 5 psi Maximum Overpressure

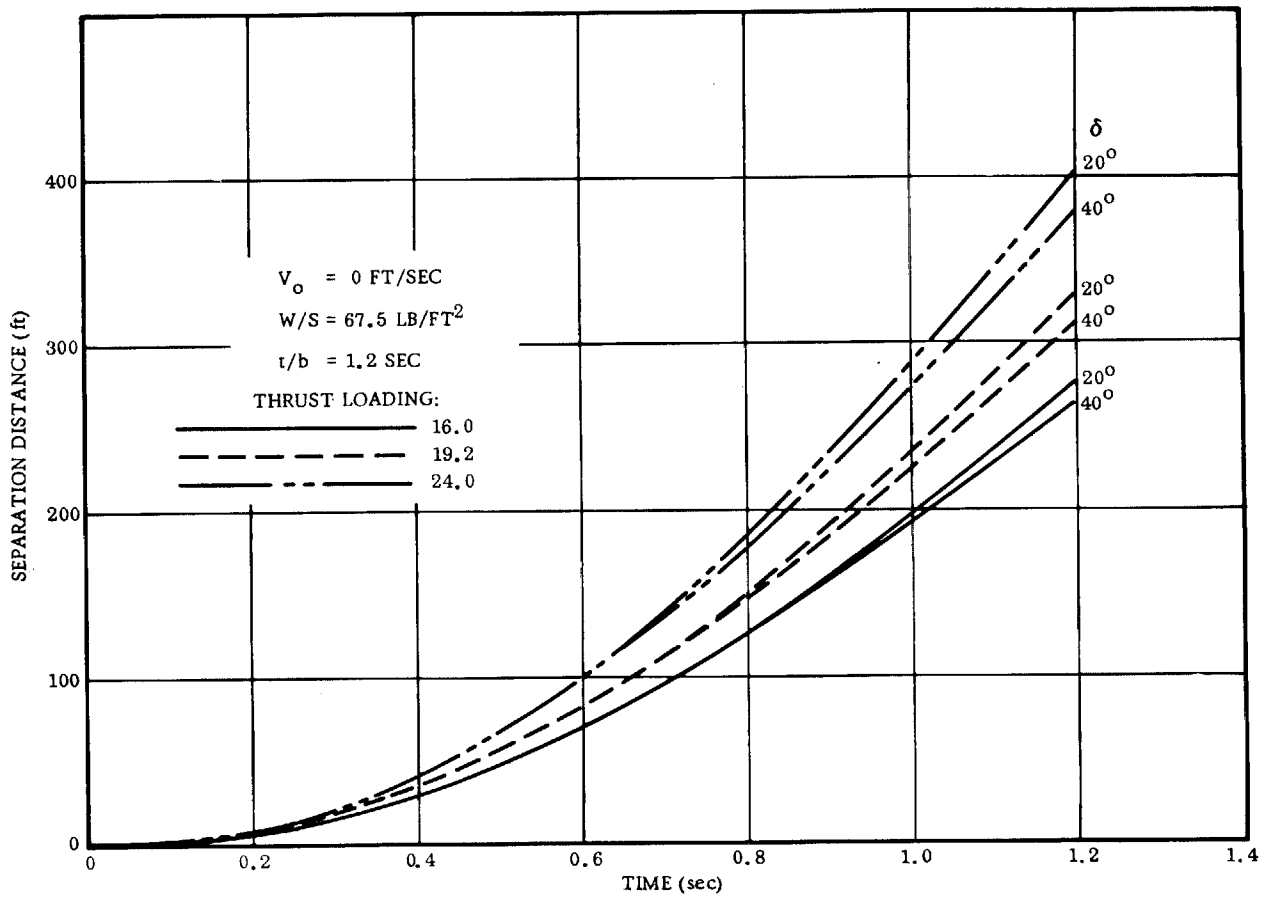

Figure 9. Effect of Thrust Magnitude and Direction on On-the-Pad Separation Distance; Ballistic Body

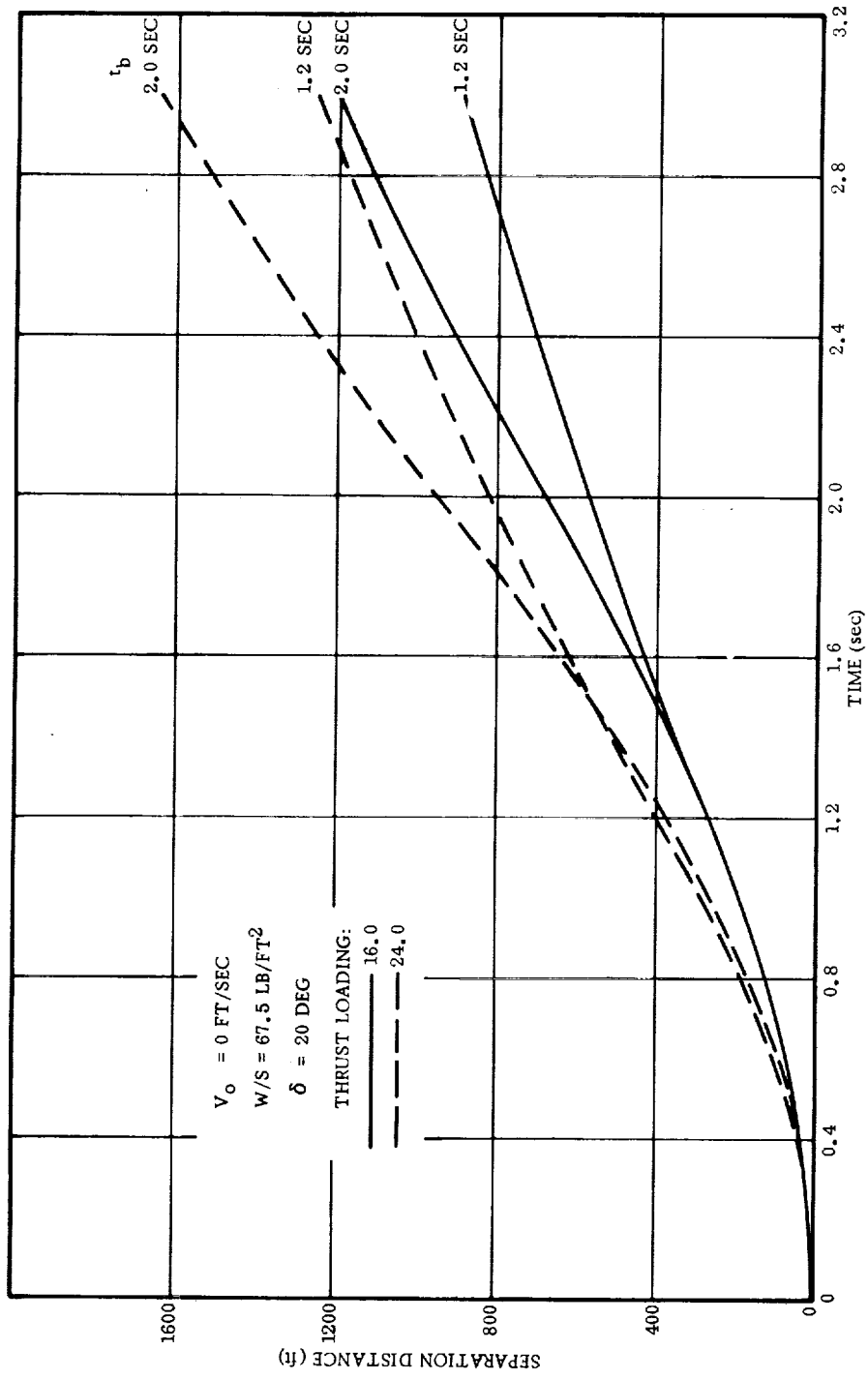

Figure 10. Effect of Rocket Burning Time on On-the-Pad Separation Distance; Ballistic Body

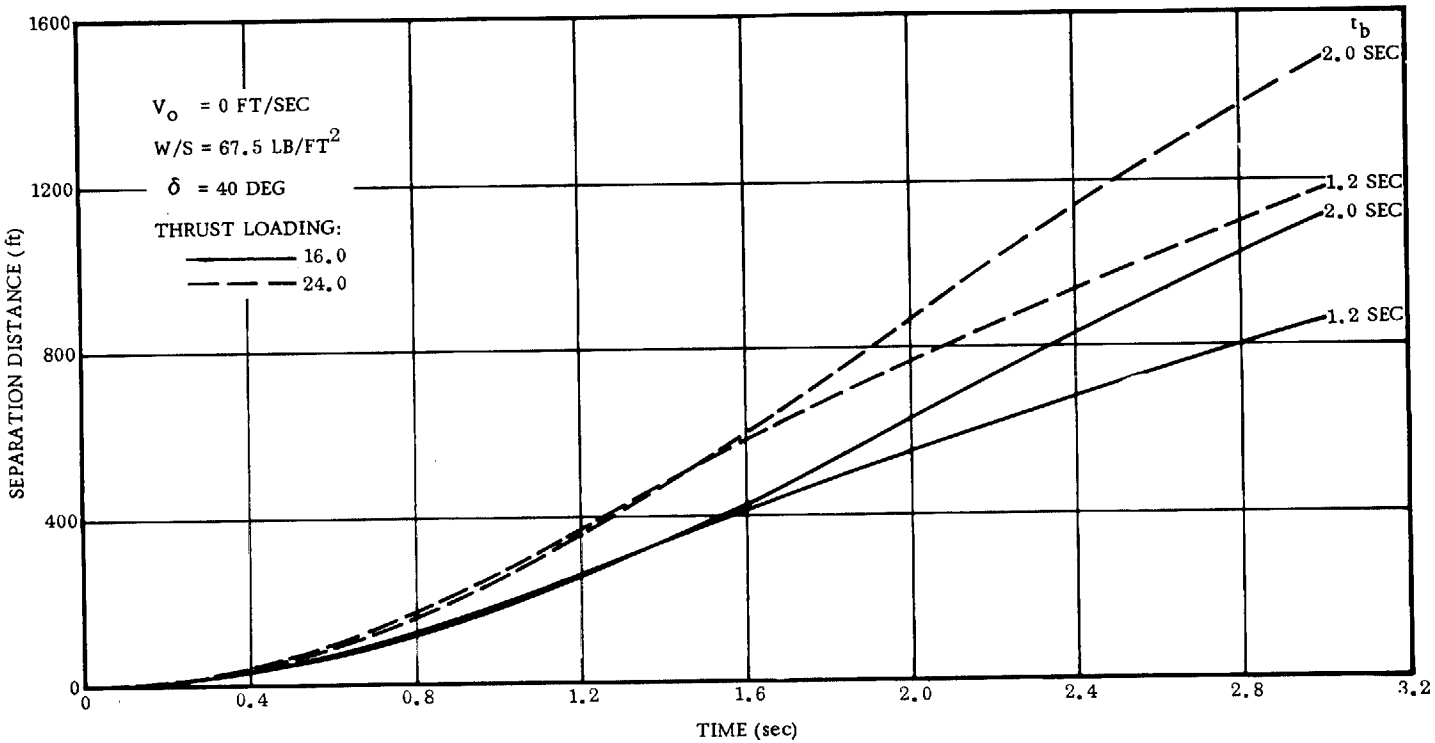

Figure 11. Effect of Rocket Burning Time on On-the-Pad Separation Distance; Ballistic Body

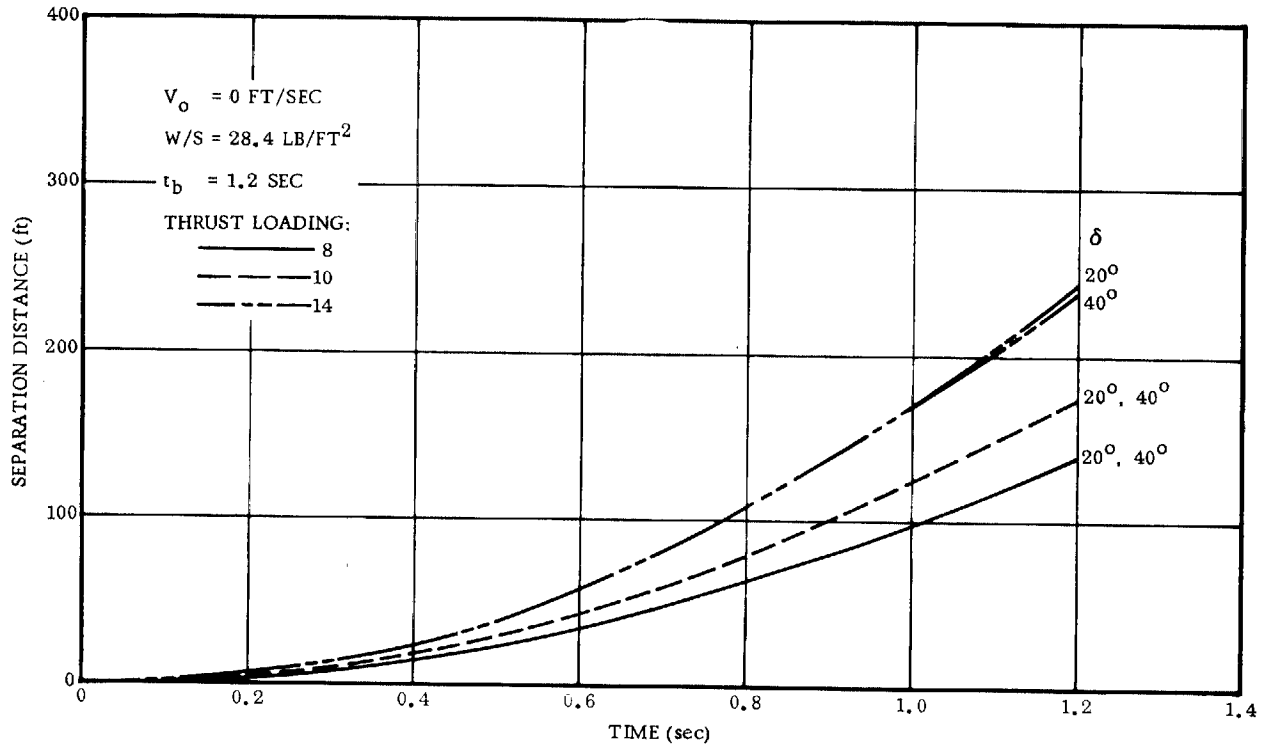

Figure 12. Effect of Thrust, Magnitude, and Direction on On-the-Pad Separation Distance; Lifting Body

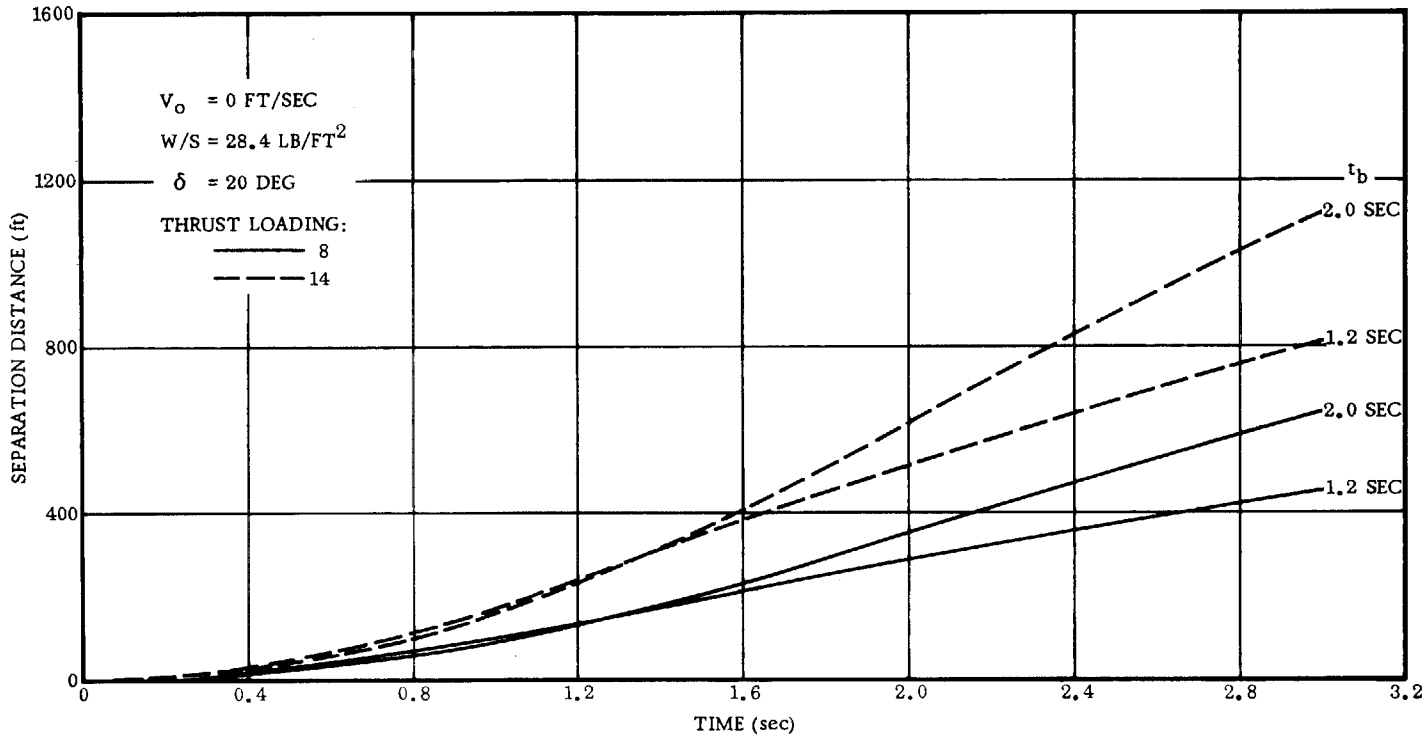

Figure 13. Effect of Rocket Burning Time on On-the-Pad Separation Distance; Lifting Body

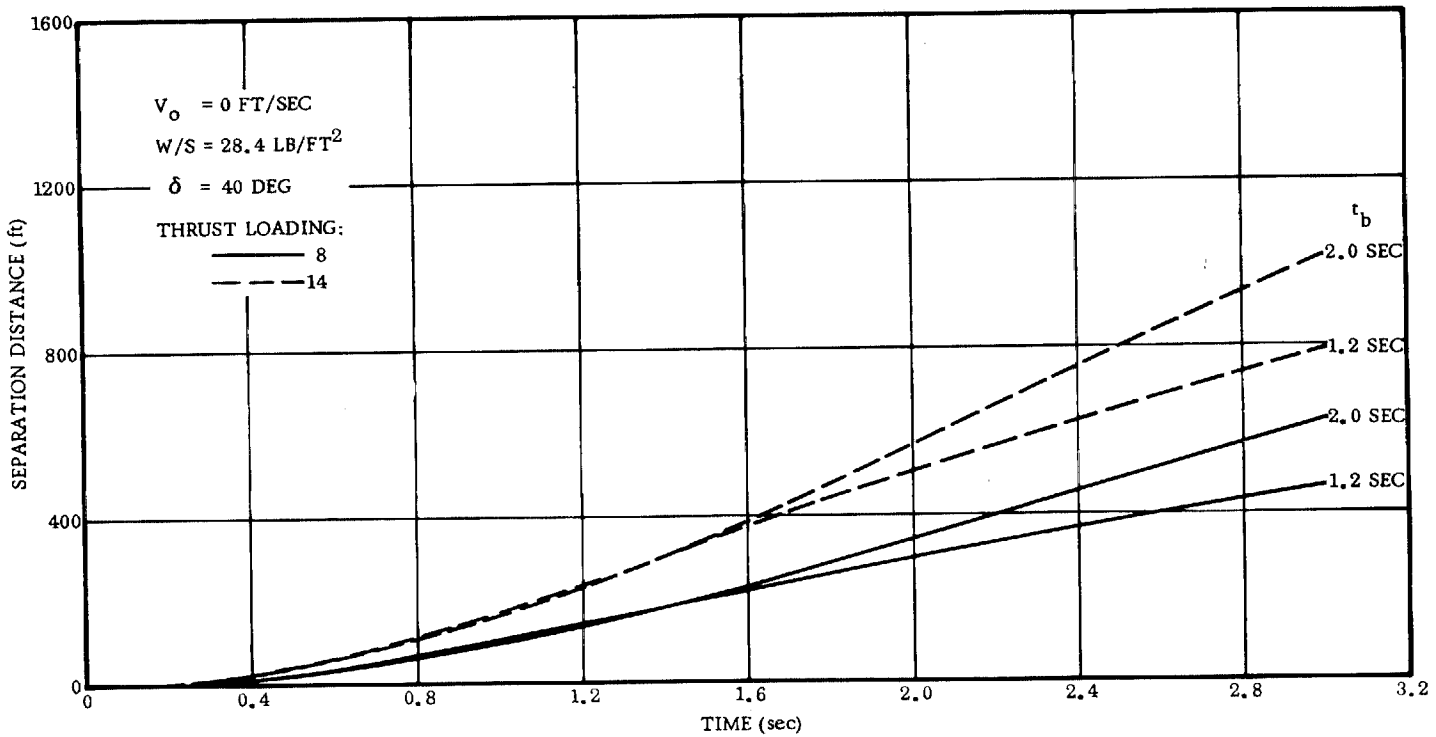

Figure 14. Effect of Rocket Burning Time on On-the-Pad Separation Distance; Lifting Body

criteria can be formulated. The methods described in this section are useful however for preliminary design studies.

A detailed analysis for a specific system must also take account of the possible need for a stabilization and attitude control system. Since this would proceed along established lines once an overall configuration and propulsion system is formulated, it need not be discussed here. The reader may consult Ref. 31 for a detailed discussion of this type of problem.

3.1.2 Atmospheric Abort

The critical abort condition during powered flight through the atmosphere is at the point of maximum dynamic pressure (max q). This is due to the increased drag which considerably reduces the accelerating effects of the abort rockets. However, the shock wave intensity due to an explosion at altitude is considerably less than at sea level.

Consider, for example, the launch vehicle configuration "A" of Sec. 3.1.1 which had a H_2-O_2 propellant weight of 427,000 lb. According to Table IV the equivalent weight of TNT is W_T = 128 tons. For a 5 psi overpressure at sea level, the overpressure ratio, $p/P_X = 5/14.7 = 0.34$.

This corresponds to a scaled distance $d' = 132.5$ ft and a scaled arrival time $t'_X = 0.068$ sec (Table V). Consequently a 5 psi overpressure occurs at

$$d = 132.5 \times 128^{1/3} = 668 \text{ ft}$$

with an arrival time of

$$t_X = 0.068 \times 128^{1/3} = 0.34 \text{ sec}$$

This is in fact the overpressure characteristic shown in Fig. 7. With the spacecraft located 100 ft from the center of the explosion, and assuming a 2 sec warning time (of which 0.5 sec is required for sensing, etc.), the spacecraft is required to move 668 - 100 = 558 ft in 1.50 + 0.34 = 1.84 sec. This implies an acceleration (in vacuum) of 10.42 g.

With the same overpressure stipulation at an altitude of 40,000 ft, the overpressure ratio, $p/P_X = 5/2.72 = 1.84$. From Table V, $d' = 57.9$ ft and $t'_X = 0.0162$ sec. Also, from Table VI, $(\rho/\rho_{SL})^{1/3} = 0.6267$ and $\sigma/\sigma_{SL} = 0.8671$. We find therefore that for an explosion of 128 tons of TNT at an altitude of 40,000 ft, a 5 psi overpressure occurs at

$$d = \frac{57.9 \times 128^{1/3}}{0.6267} = 466 \text{ ft}$$

with an arrival time of

$$t_x = \frac{0.0162 \times 128^{1/3}}{0.6267 \times 0.8671} = 0.15 \text{ sec}$$

This type of result is true in general; namely, that for an equal amount of propellant exploding at altitude, the distance a shock wave travels, and the time required to travel that distance, is shorter than at sea level.

Using the above values, the spacecraft (escape capsule) is required to travel 466 - 100 = 366 ft in 1.50 + 0.15 = 1.65 sec, which implies an acceleration (in vacuum) of 8.34 g (compared to 10.42 g for the sea level condition). This figure is conservative since a substantial portion of the booster fuel is consumed by the time it reaches the max q condition.

One further observation may be made at this point. The explosion shock wave propagates at transonic velocities from the point of detonation, which in itself does not partake of the motion of the booster, and remains stationary in space. For those aborts made when the booster (and hence the abort vehicle) is traveling at velocities above the transonic range, the abort vehicle will outrun the explosion. This will generally be the case for all ascent aborts above approximately 35,000 feet. In short, the explosion hazard is considerably less severe at altitude than at sea level.

In the region of maximum dynamic pressure, the most critical abort problems are: (1) decelerations induced by high aerodynamic forces, and (2) obtaining proper clearance between the abort vehicle and the uncontrolled booster vehicle following separation.

If an abort occurs during powered flight, the escape capsule (abort vehicle) must follow a flight path which avoids the airspace of the booster in uncontrolled flight. This problem is most severe if the booster failure which required abort also nullified the thrust termination capabilities of the booster vehicle. Furthermore, there is an increased booster acceleration due to loss of the abort vehicle mass. Investigation of this problem must also take account of the possibility of "hard-over' main engines. For any specific vehicle configuration, an extensive parameter study must be conducted to determine critical clearance distances in the light of all of these factors. Experience to date has indicated that the abort thrust capabilities are generally marginal in this area. Since it does not appear to be possible to formulate general design rules for this case, computer simulations of varying sophistication must be employed to determine abort thrust requirements.

The second main abort problem at max q arises from the accelerations induced in separating the abort from the booster vehicle. To ensure survival of the crew, these must be within the limits indicated in Fig. 4. On the other hand, the abort thrust must be sufficient to overcome the aerodynamic and gravity forces on the abort vehicle.

The relevent geometry is shown in Fig. 15. It is assumed that positive separation occurs along the body longitudinal axis. Then by summing forces in the longitudinal direction, we have (for zero acceleration)

$$T\cos\delta - W\sin(\alpha+\gamma) - D\cos\alpha + L\sin\alpha = 0 \qquad (5)$$

T = abort thrust; lb

W = weight of abort vehicle; lb

D = drag; lb

L = lift; lb

δ = thrust vector deflection; deg

α = angle of attack; deg

γ = flight path angle; deg

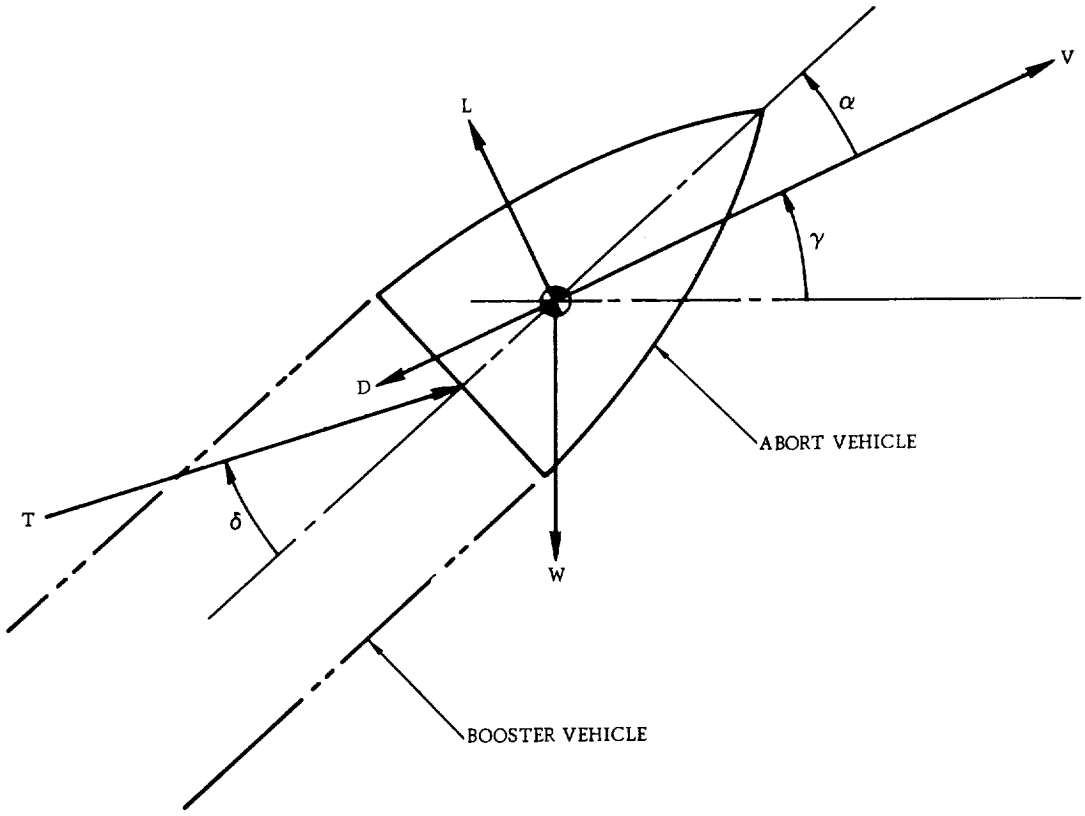

Figure 15. Forces and Geometry at Abort Vehicle Separation

Since

$$D = C_D q S \tag{6}$$

C_D = drag coefficient

q = dynamic pressure; lb/ft^2

S = reference area for abort vehicle; ft^2

we may write Eq. (5) as

$$\frac{T}{W}\cos\delta = \frac{C_D q S}{W}\left[\cos\alpha - \frac{L}{D}\sin\alpha\right] + \sin(\alpha + \gamma) \tag{7}$$

The quantity $(T/W)\cos\delta$ is called the thrust parameter, and $C_D S/W$ is called the drag parameter.

The thrust parameter, given by Eq. (7), is the minimum value necessary to obtain a positive separation between the abort and booster vehicles. The manner in which the thrust parameter varies with dynamic pressure, drag parameter, lift to drag ratio, angle of attack, and flight path angle is shown in Figs. 16 to 19. It is apparent that dynamic pressure and drag parameter are the governing factors, and that the effect of variations in the other parameters is relatively minor.

A critical condition, from the point of view of induced deceleration, is at burnout of the abort rockets. At this time the high aerodynamic forces are no longer opposed by the abort engine thrust. The load factor at burnout is given by†

$$N = \frac{C_D S}{W} q \left[1 + \left(\frac{L}{D}\right)^2\right]^{1/2} \tag{8}$$

This must be within the physiological limits specified by Fig. 4.

Values of the load factor as a function of dynamic pressure, lift to drag ratio, and drag parameter are given in Figs. 20 to 22. It is apparent that the load factor can be quite high especially for the high drag configurations. However, the load factor may decay quite rapidly if the decleration parameter, K, defined by

$$K = \frac{C_D S \rho g V_0}{2W} \tag{9}$$

† See Appendix C.

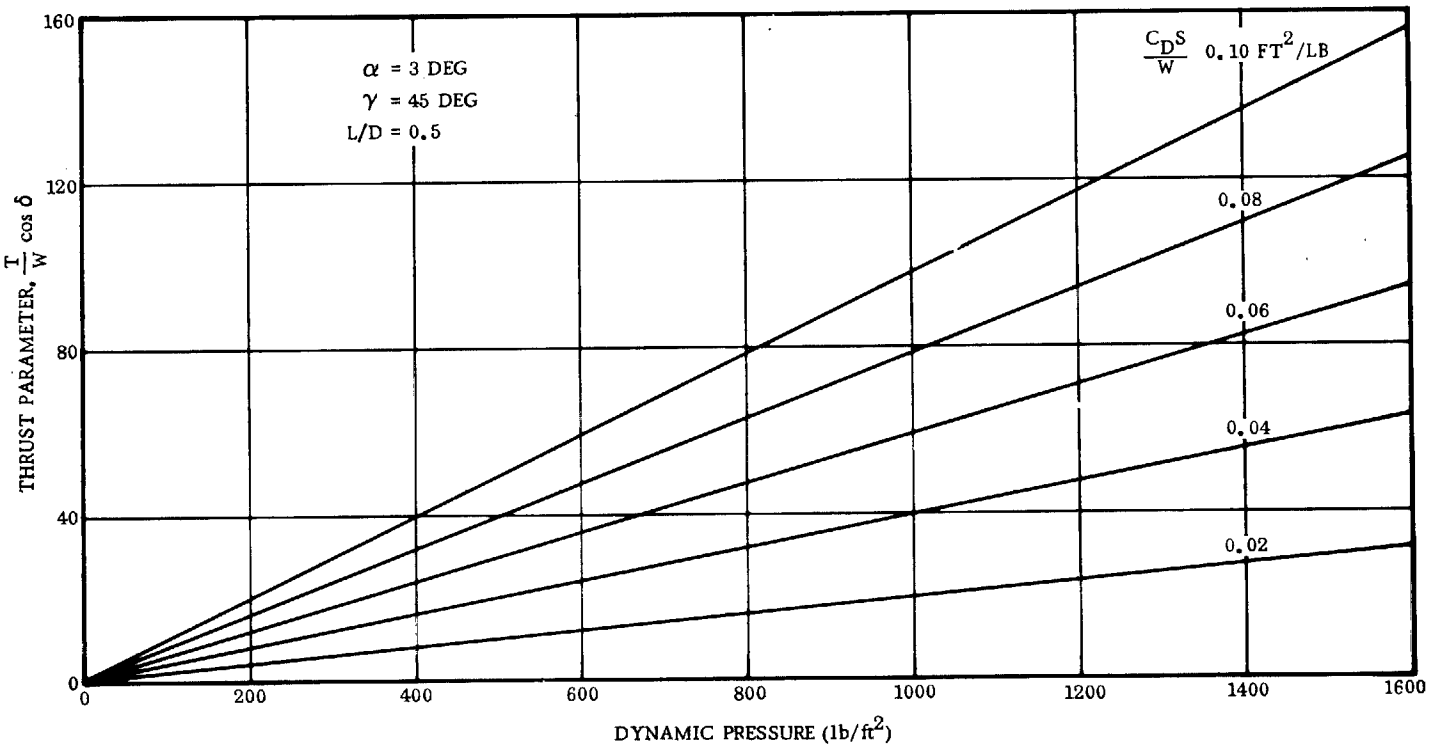

Figure 16. Effect of Dynamic Pressure and Drag Parameter on Separation Criteria

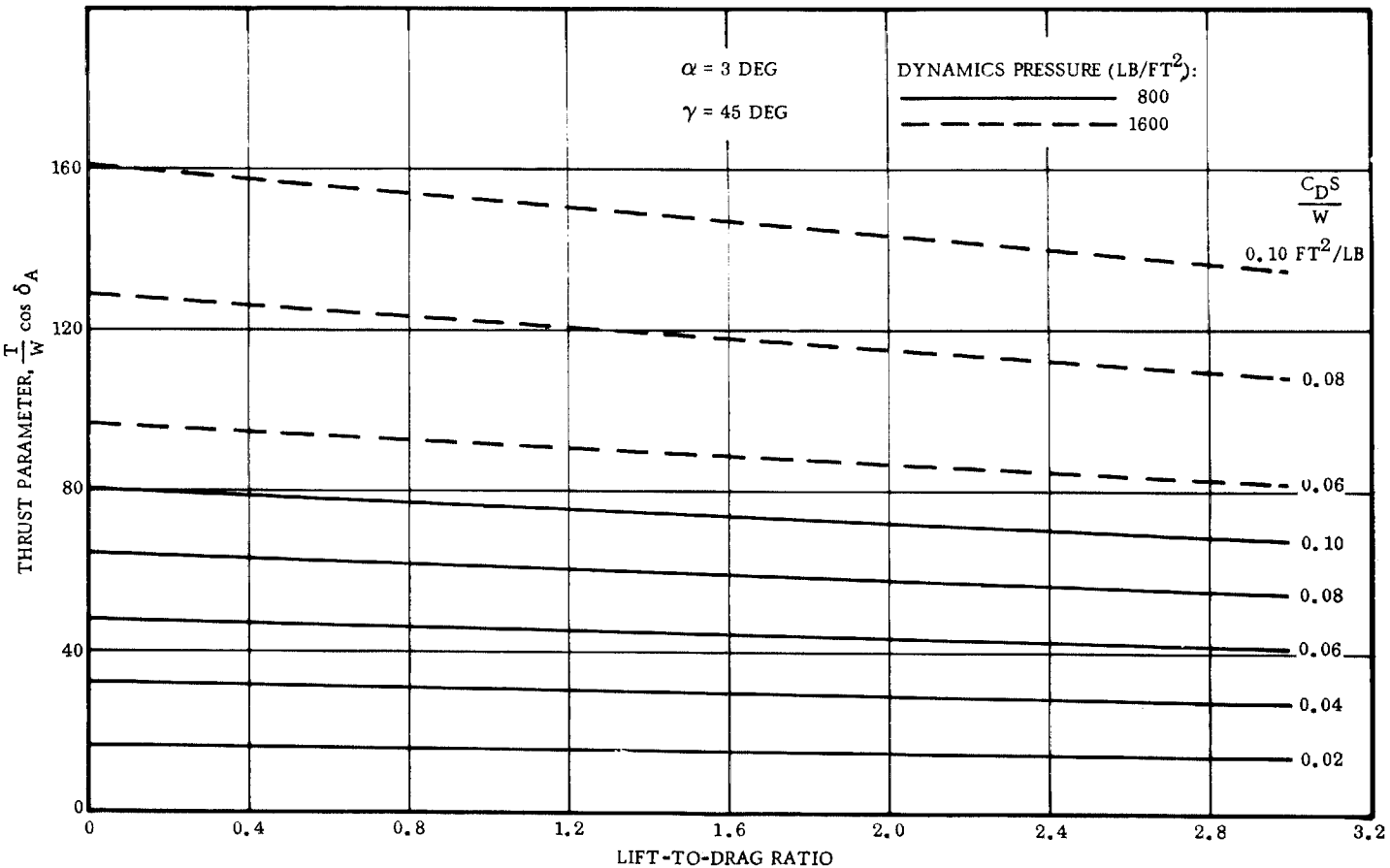

Figure 17. Effect of Lift-to-Drag Ratio on Separation Criteria

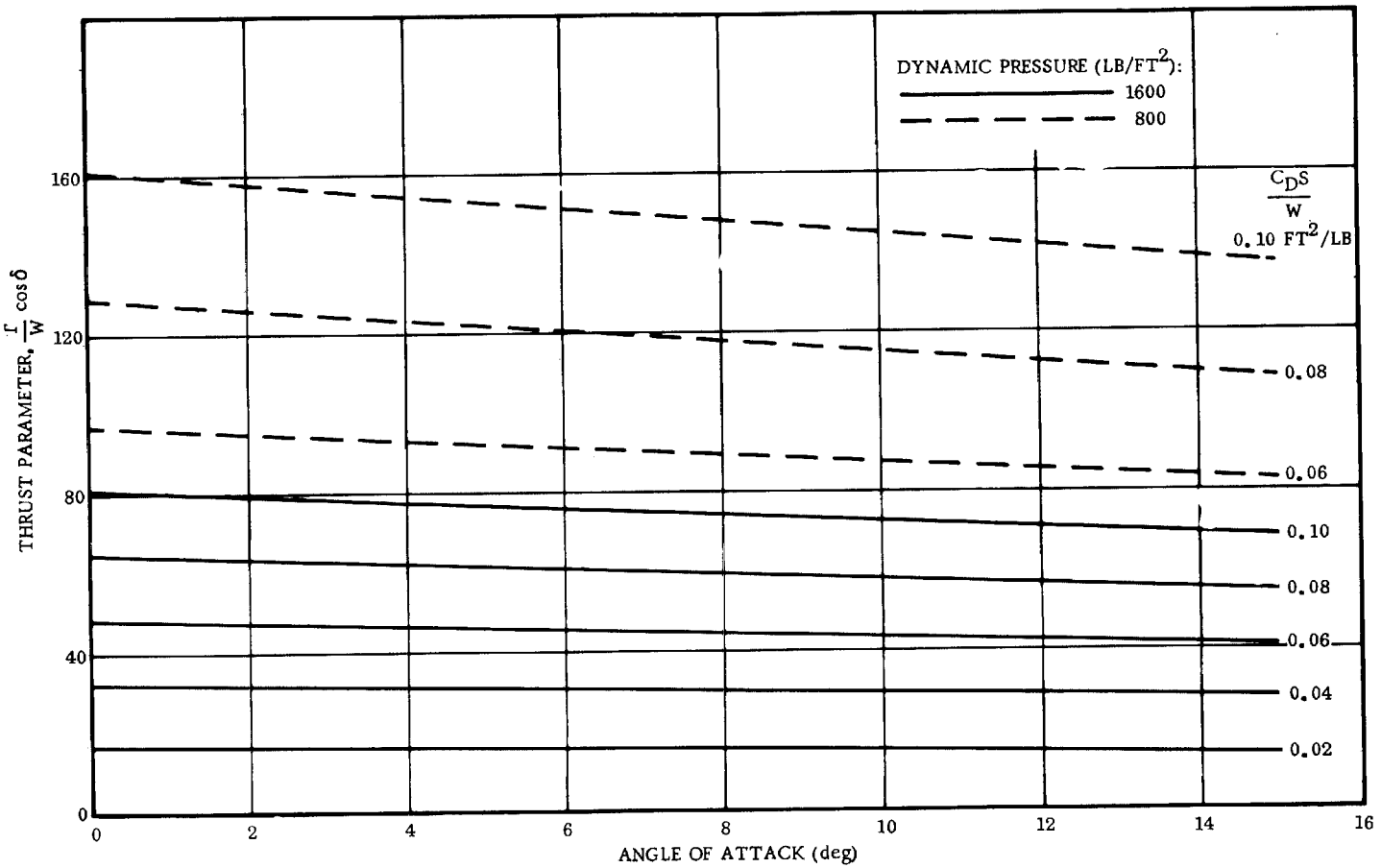

Figure 18. Effect of Angle of Attack on Separation Criteria

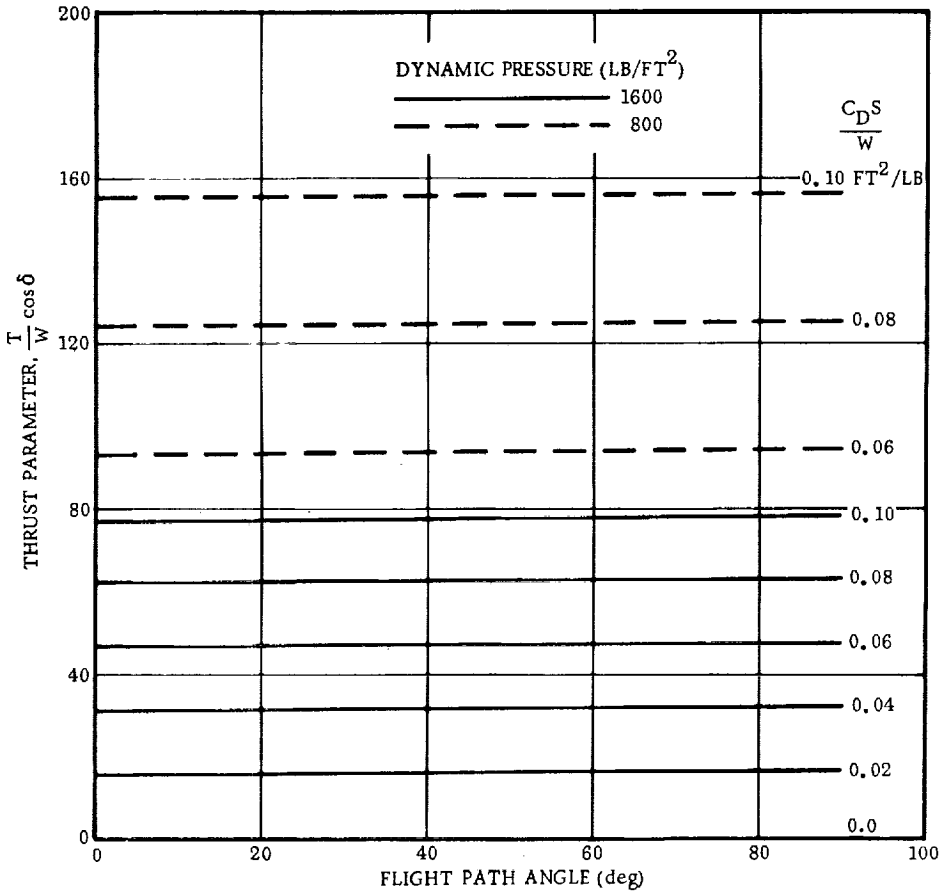

Figure 19. Effect of Flight Path Angle on Separation Criteria

is sufficiently large. Here, g is the gravity acceleration, and V_0 is the velocity of the abort vehicle at rocket burnout. The reasoning is as follows. Suppose that the abort vehicle is separated in the upward vertical direction. Following rocket burnout, the motion is described by

$$m\dot{V} = -D - mg, \qquad V(0) = V_0 \tag{10}$$

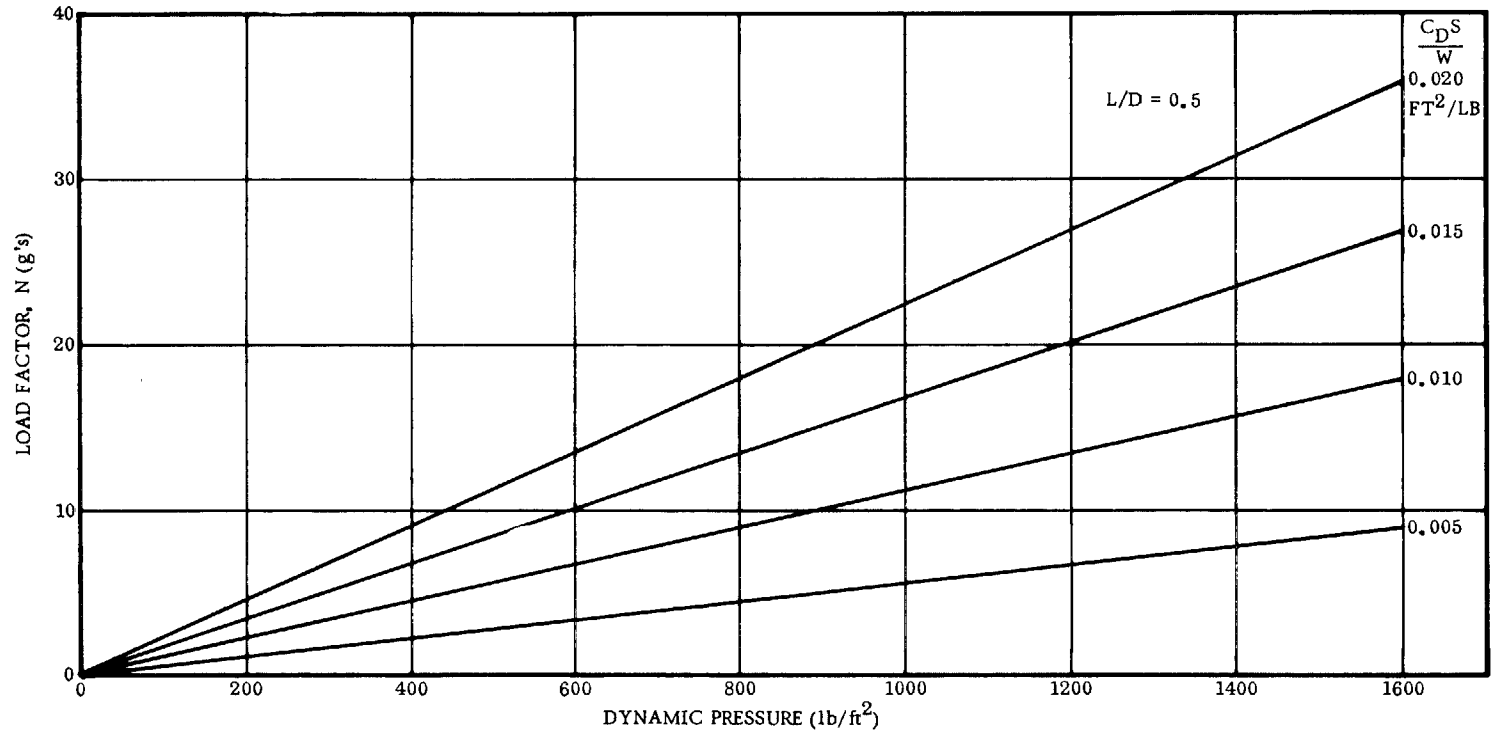

Figure 20. Effect of Dynamic Pressure and Drag Parameter on Acceleration Criteria

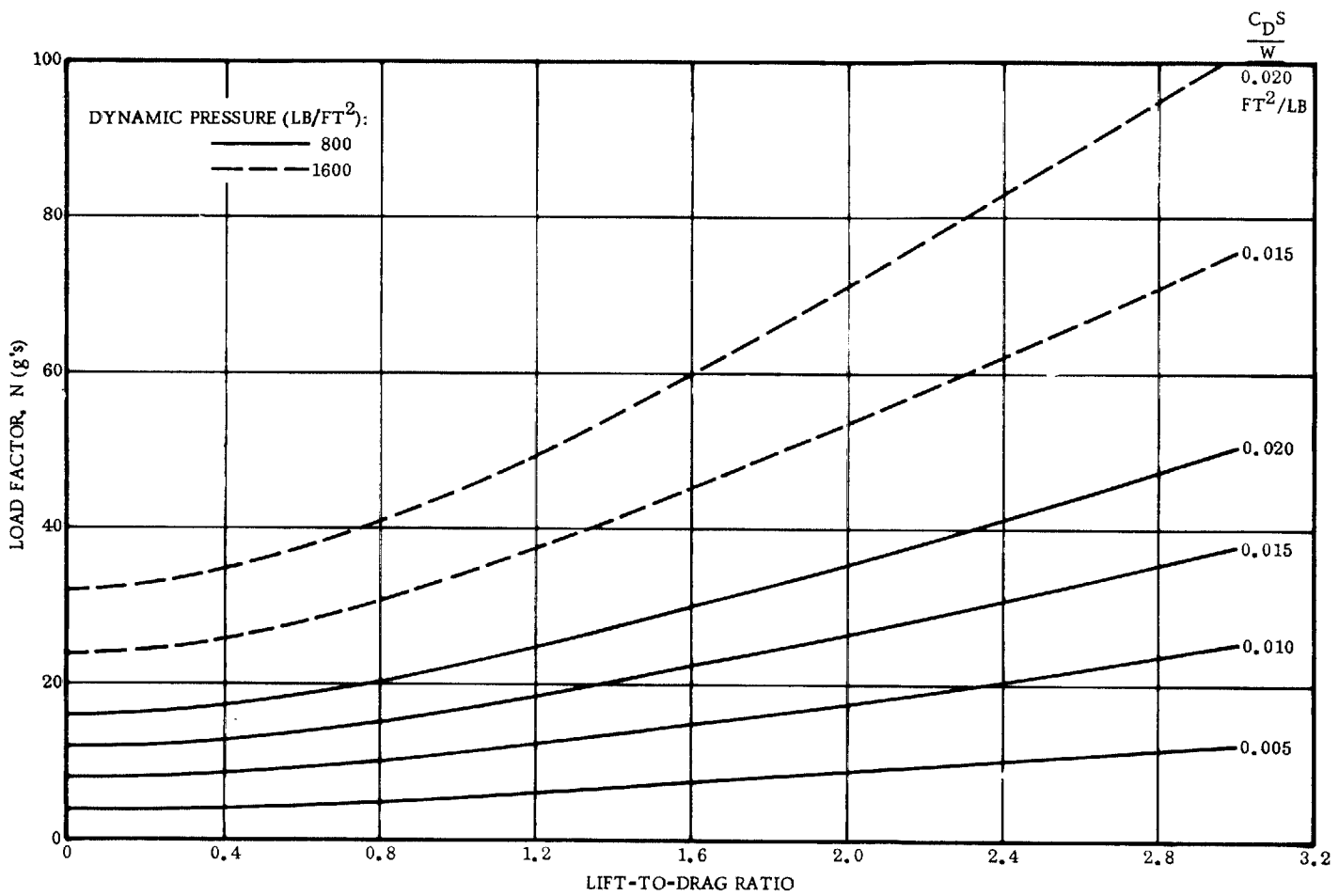

Figure 21. Effect of Lift-to-Drag Ratio on Acceleration Criteria

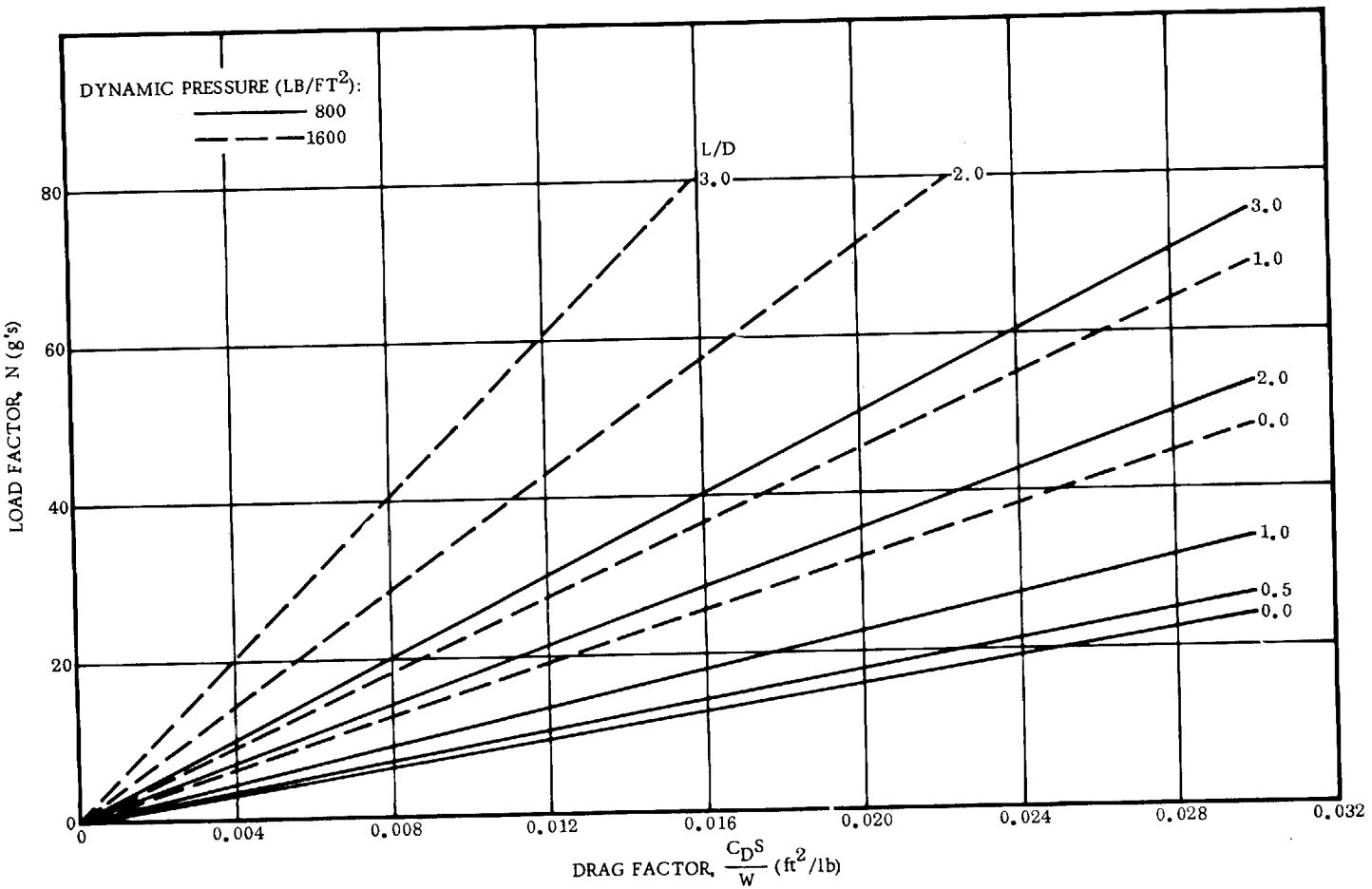

Figure 22. Effect of Drag Parameter on Acceleration Criteria

An elementary integration leads to†

$$\frac{\dot{V}}{V_0} = \frac{K}{(1 + Kt)^2} \tag{11}$$

The quantity $(\dot{V}/V_0)$ is a measure of the time decay of the load factor and is plotted in Fig. 23 for various values of the deceleration parameter, K.

To obtain some insight into the order of magnitude of these quantities, we take

$V_0 = 1660$ ft/sec

$q = 790$ lb/ft^2

$\rho = 0.573$ slug/ft^3

These numbers are representative of the Saturn launch vehicle at max q. With a drag parameter $C_D S/W = 0.020$, we find $K = 0.306$ sec^{-1}. This means that at abort rocket burnout, the load factor is

$$N = \frac{\dot{V}}{g} = \frac{0.306\, V_0}{g} = 15.8\, g$$

However, one second later, we find from Fig. 23 that $\dot{V}/V_0 = 0.180$; the corresponding load factor is

$$N = \frac{0.18 \times 1660}{32.2} = 9.3\, g$$

Thus, in one second the acceleration has been reduced by 6.5 g.

Because of the simplifications in the development, the above results are valid only as first approximations. The main qualitative feature is that a high load factor at abort thrust burnout may be sharply reduced if the deceleration parameter is sufficiently high. This is an important dynamic property since fairly high accelerations may be tolerated if their duration is sufficiently small (see Fig. 4).

Summarizing, the thrust capability for atmospheric abort must be sufficient to

a. Move the abort vehicle from the immediate vicinity of a booster explosion.

b. Provide sufficient clearance to avoid collison with an uncontrolled (possibly powered) booster section.

† We assume that m g is negligible compared to D.

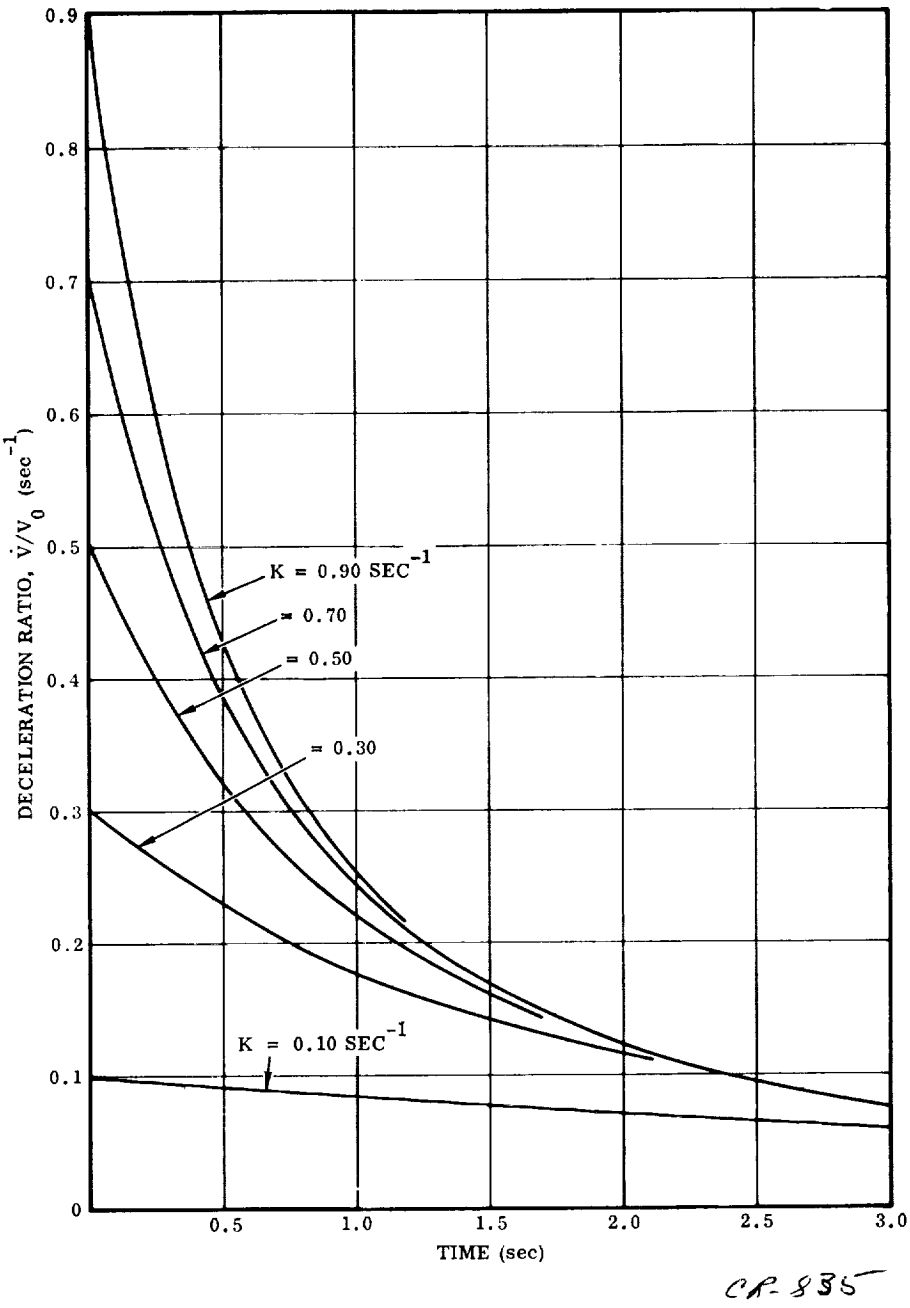

Figure 23. Deceleration Decay

c. Ensure positive separation of the abort from the booster vehicle without exceeding human acceleration constraints.

A cumulative abort thrust requirement could then be formulated in the manner shown in Fig. 24. This would form the basis for specifying the abort propulsion system.

In all of the foregoing discussion, the abort vehicle was analyzed as a point mass. For a detailed application to a specific vehicle, it will be necessary to provide an attitude control and stabilization system.[31]

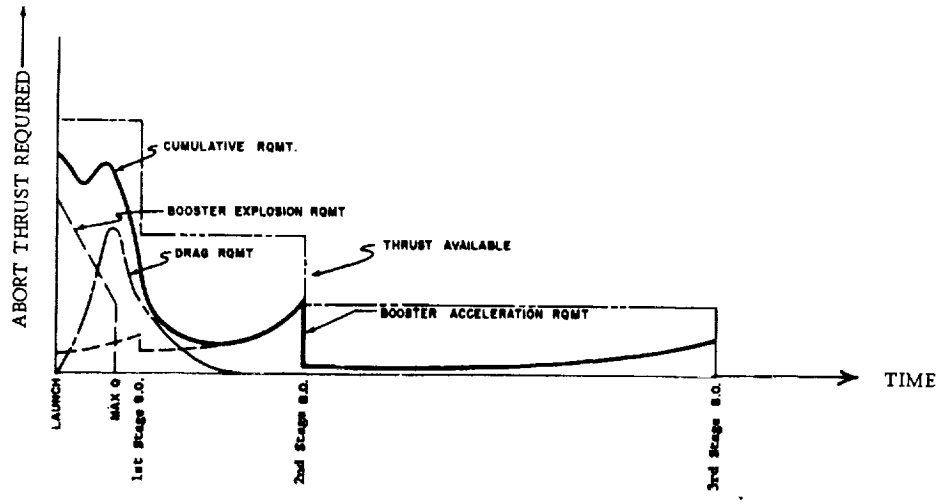

Figure 24. Abort Thrust Requirement Versus Flight Time

3.1.3 Exoatmospheric Abort

The nature of the abort problem changes when the spacecraft is above the sensible atmosphere. Because of the fact that by this time most of the fuel has already been expended, the hazard of a fuel explosion is substantially lessened. Also, for an abort during the atmospheric phase, maximum decleration† was experienced at separation, not reentry. Essentially the reverse is true during the exoatmospheric phase: separation is the lesser problem. It is the nature of the reentry trajectory from the abort conditions (altitude, velocity, flight path angle, etc.) which determines safety from the point of view of deceleration and heating constraints.

† The words "deceleration" and "load factor" will be used interchangeably.

We consider first the situation in which the spacecraft is above the sensible atmosphere and flying at less than parabolic speed. It is pertinent to establish whether an abort thrust capability is indeed required at all at this time. In other words, if an abort condition occurs, is it sufficient merely to separate the abort vehicle (escape capsule) from the booster and permit it to return along a descent trajectory determined by the abort initial conditions? To pursue this question, it is necessary to establish safe "abort corridors;" that is, a map of abort initial conditions which result in descent trajectories that do not exceed permissible deceleration and heating constraints. This may be done in the following way. Suppose that for a specific vehicle, a series of trajectories are calculated (via computer) using the equations of Appendix C. When the abort (initial) velocity is less than circular velocity, the vehicle will always return to the earth's surface. We then plot those specific trajectories in which the maximum deceleration during reentry is precisely 10 g. When the abort (initial) velocity is greater than circular velocity (but less than escape velocity), we plot only those trajectories in which the vehicle does not leave the atmosphere after the first pass and such that the maximum deceleration during reentry is precisely 10 g. This is done in Fig. 25 for a vehicle having a drag parameter, $C_D S/W = 0.02$ ft^2/lb and an L/D ratio of 0.70. Loci of constant flight path angle are denoted by the dotted lines. Connecting equal flight path angles, and eliminating the trajectory lines, produces the complete map of speed, flight path angle, and altitude shown in Fig. 26. Using this, the conditions for a safe abort from the point of view of not exceeding a 10 g deceleration during reentry, may be readily determined. For example, at subcircular velocity, any abort altitude-velocity combination yields a flight path angle (at abort) which if exceeded means that the 10 g deceleration limit will be exceeded during reentry. Similarly,

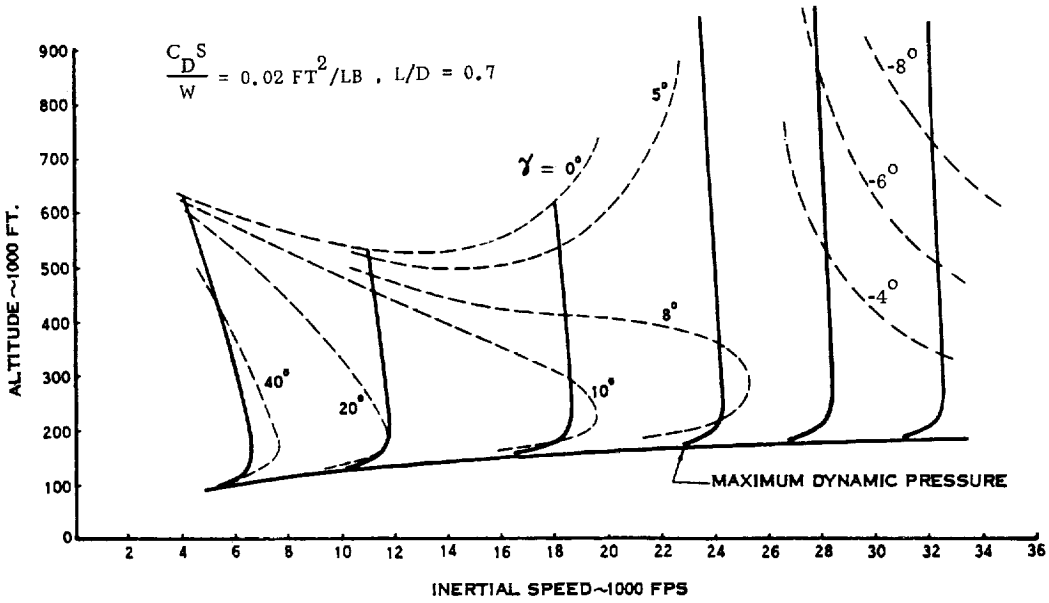

Figure 25. 10G Entry Trajectories

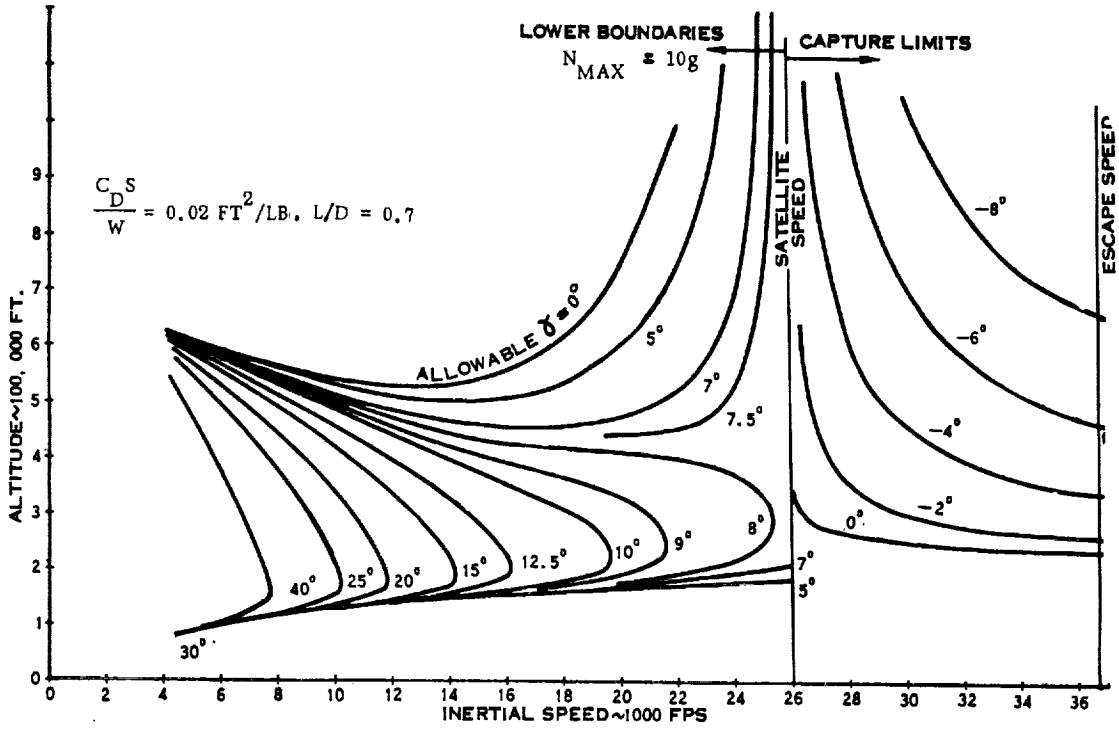

Figure 26. Escape Boundaries

an abort altitude-velocity combination in the supercircular region yields a flight path angle (at abort, which if exceeded, means that the vehicle will not remain in the atmosphere in the first pass. Carter and Kramer[5] call these cases the lower and upper boundaries of the safe abort corridor.

Using Fig. 26, one may determine the safe abort capability for any given ascent trajectory. Consider, for example, the lunar mission ascent trajectory shown in Fig. 27. If this is superimposed on Fig. 26, we have the result shown in Fig. 28. By comparing the flight path angles associated with the trajectory to those defining the corresponding "allowable" values, we find that the crosshatched portion of the trajectory is unsafe from the point of view of maximum decleration or escape during reentry. In other words, some abort thrust capability is necessary at these points in order to modify the reentry path such that the deceleration or escape constraints are satisfied. Fig. 28 may be replotted in the manner shown in Fig. 29, which exhibits the same information from another point of view. This suggests the possibility of shaping the ascent trajectory such that abort conditions are always in the safe region. While this may be feasible to some extent, it is in general impractical since it would seriously compromise primary mission objectives. Thus the main purpose of the above analysis is to define those portions of the ascent trajectory at which an abort thrust capability is required.

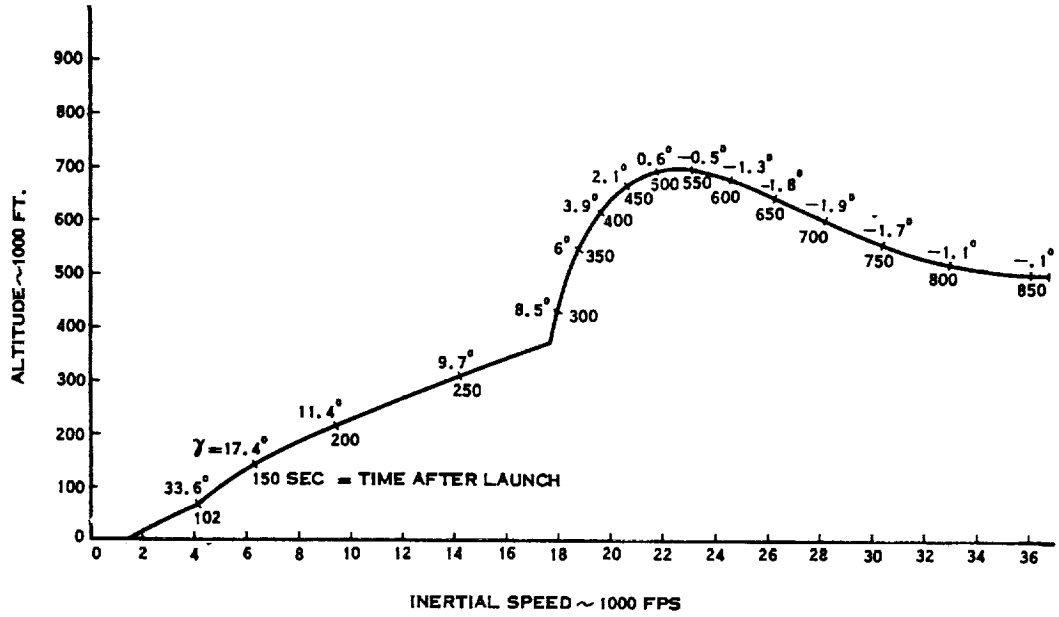

Figure 27. Typical Ascent Trajectory for Lunar Mission

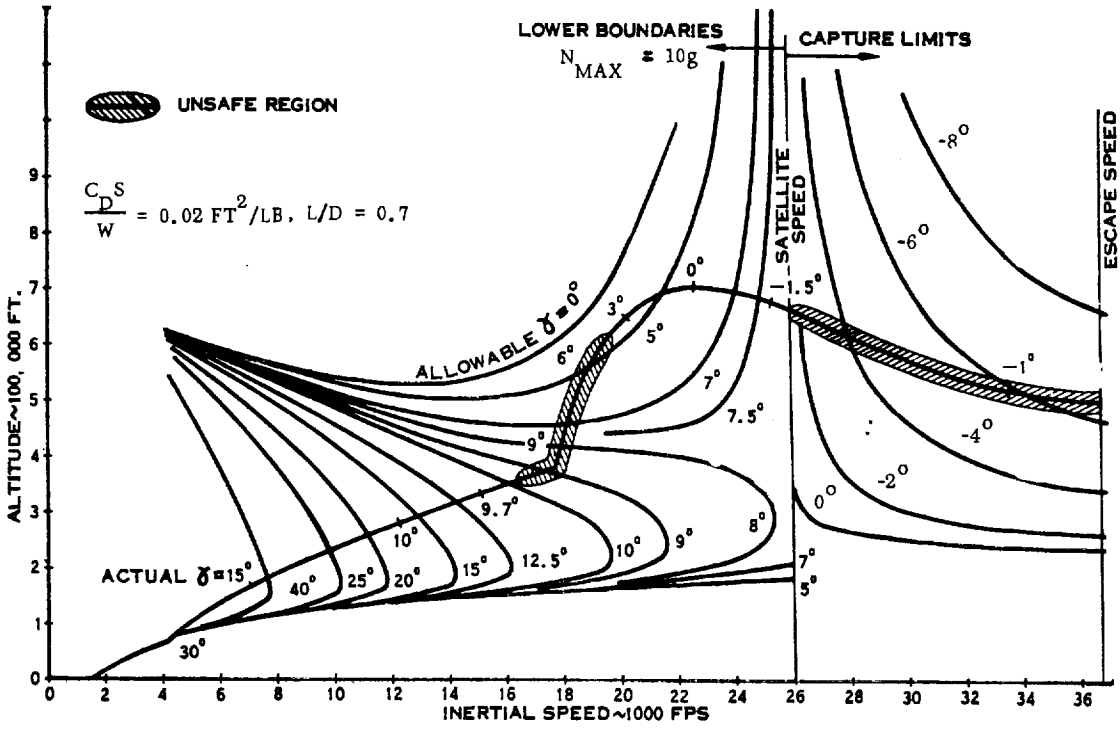

Figure 28. Evaluation of Typical Ascent Trajectory

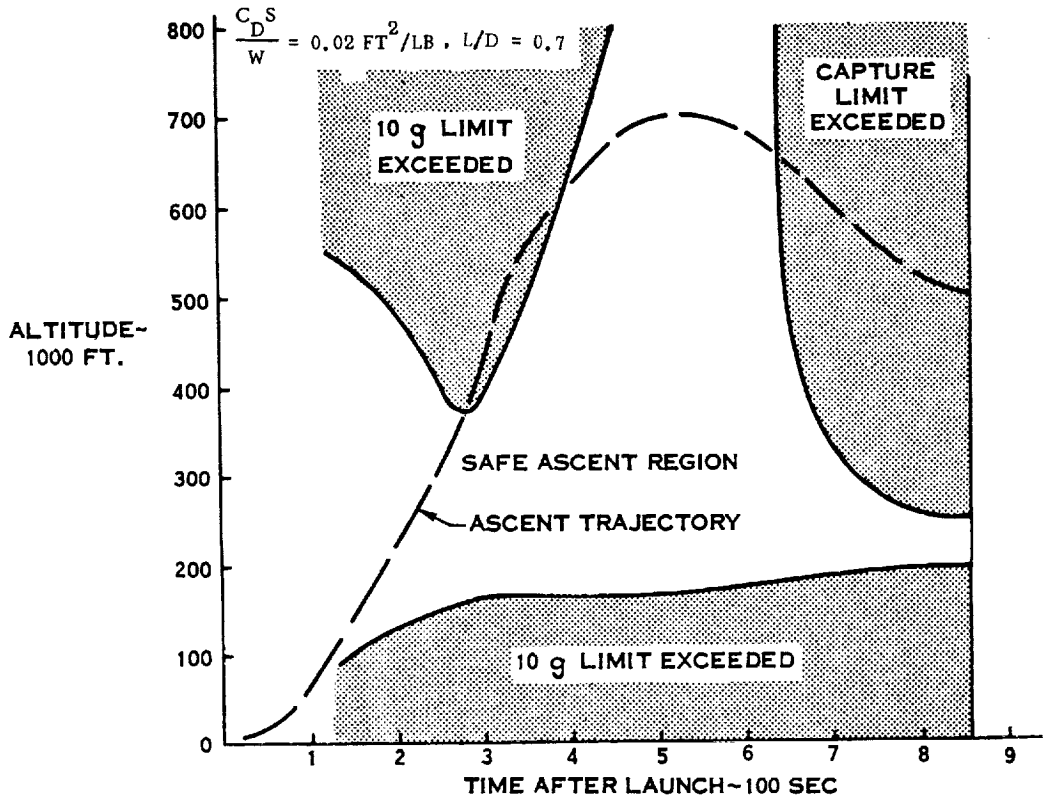

Figure 29. Safe Ascent Corridor - Without Escape Rocket

It should be noted that heating limitations are not accounted for in the escape boundaries presented in Fig. 26. Actually, it is straightforward in principle to construct a diagram of this type in which heating constraints are included. The procedure is the same as for the deceleration limitation alone, except that in plotting Fig. 25, unsafe trajectories from the point of view of excessive heating are rejected. Safe abort corridors, which include deceleration and heating constraints, have been calculated by Diven and Daniel[8], [9] for a wide range of reentry vehicles. The heating constraint used is based on a permissible stagnation point temperature which is due to the surface reradiation capability.†

Several hundred charts are presented showing the safe abort corridors for vehicles having various aerodynamic characteristics with various prescribed values of maximum deceleration and stagnation point temperatures.

† See Appendix D.

3.1.3.1 Determination of Abort Thrust Requirements

In virtually all of the launch trajectories of current interest, there will exist portions in the exoatmospheric regions in which an abort is unsafe from the point of view of deceleration or aerodynamic heating. For lunar ascent trajectories using the Saturn boost vehicle, an exoatmospheric abort is characterized by severe aerodynamic heating such that a cooling by reradiation is not feasible. In this case, some type of ablation cooling is mandatory. In what follows, we will therefore assume that the abort vehicle will have the required heat shield to limit heating,† and we will be concerned exclusively with designing the abort thrust capability to limit the maximum deceleration in reentry.

For any exoatmospheric abort, one may calculate (via the equations of orbital mechanics) the velocity and flight path angle of the abort vehicle at the point where it enters the sensible atmosphere (here defined to be at 300,000 feet). Then using these as initial conditions, the corresponding reentry trajectories may be calculated (using the equations of Appendix C) along with the deceleration-time histories. Such calculations have been made by Slye[4] for entry conditions in the range

$$15{,}000 \text{ ft} < V_E < 18{,}000 \text{ ft}$$

$$-20° < \gamma_E < 0°$$

$$0 < L/D < 2.0$$

with $h_E = 300{,}000$ ft, and for a vehicle having a drag parameter, $C_D S/W = 0.006$ ft^2/lb. The results are shown in Figs. 30 - 33, in which the ordinate represents the maximum deceleration for a particular trajectory.

It will be noted that for entry angles in the range 0° to -10°, the decelerations are more strongly dependent on flight path angle than on velocity over the velocity range of interest. For example, with L/D = 0.5 (Fig. 31), the decelerations are virtually independent of velocity for an entry angle of 6.5°. This result indicates that the abort rocket thrust should be used in such a manner as to reduce the entry flight path angle in order to be most advantageous in reducing the entry deceleration. Furthermore, the abort rocket thrust should be applied immediately prior to reentry.

If the thrust is applied at higher altitudes, the entry angle cannot always be made small. This trend results because the velocity after the abort rocket is fired is normally still subcircular and the trajectory generally has a nonzero eccentricity. After apogee of an elliptical trajectory, the flight-path angle decreases (increases negatively) as the vehicle approaches the atmosphere. For this reason, a steep entry

† The abort vehicle must of course have an attitude control system so that it can be properly oriented for reentry.

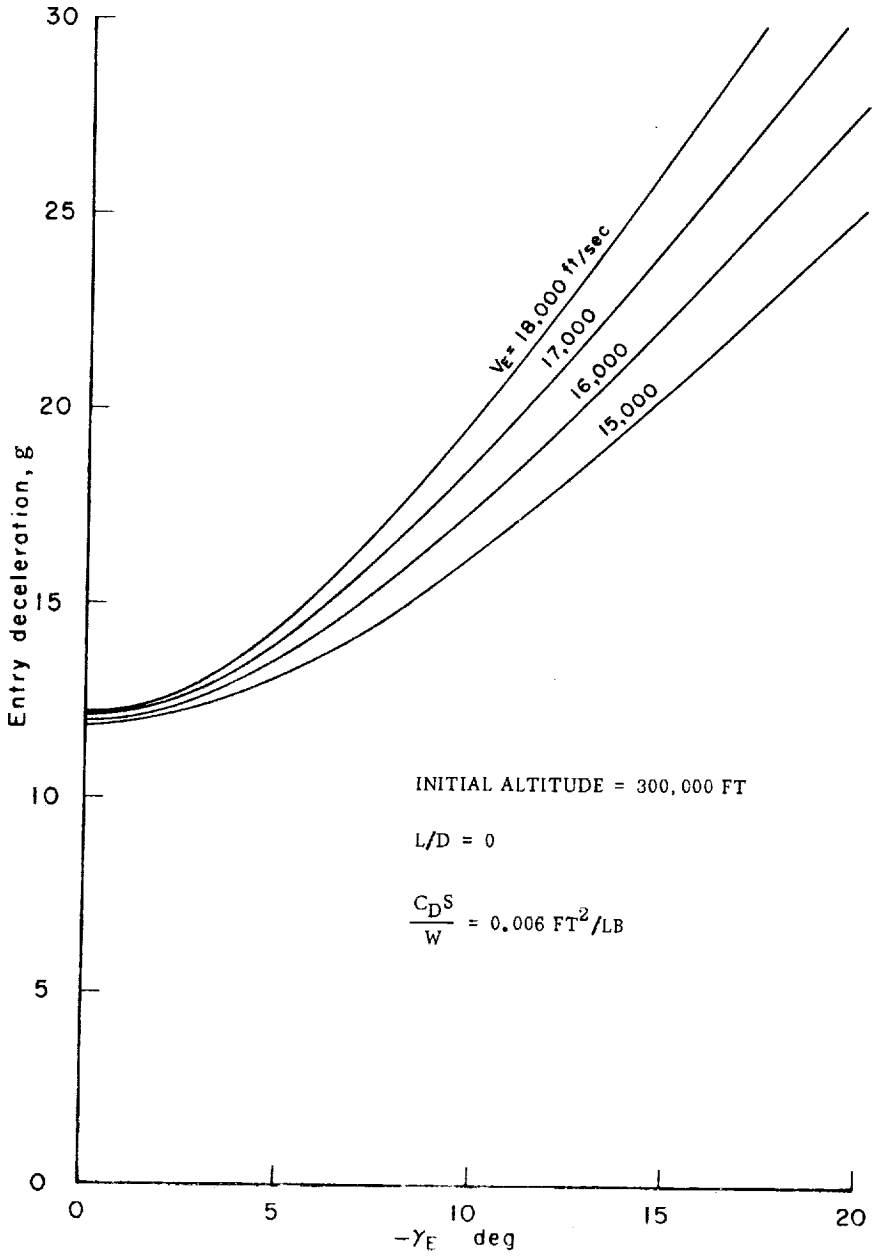

Figure 30. Entry Deceleration, L/D = 0

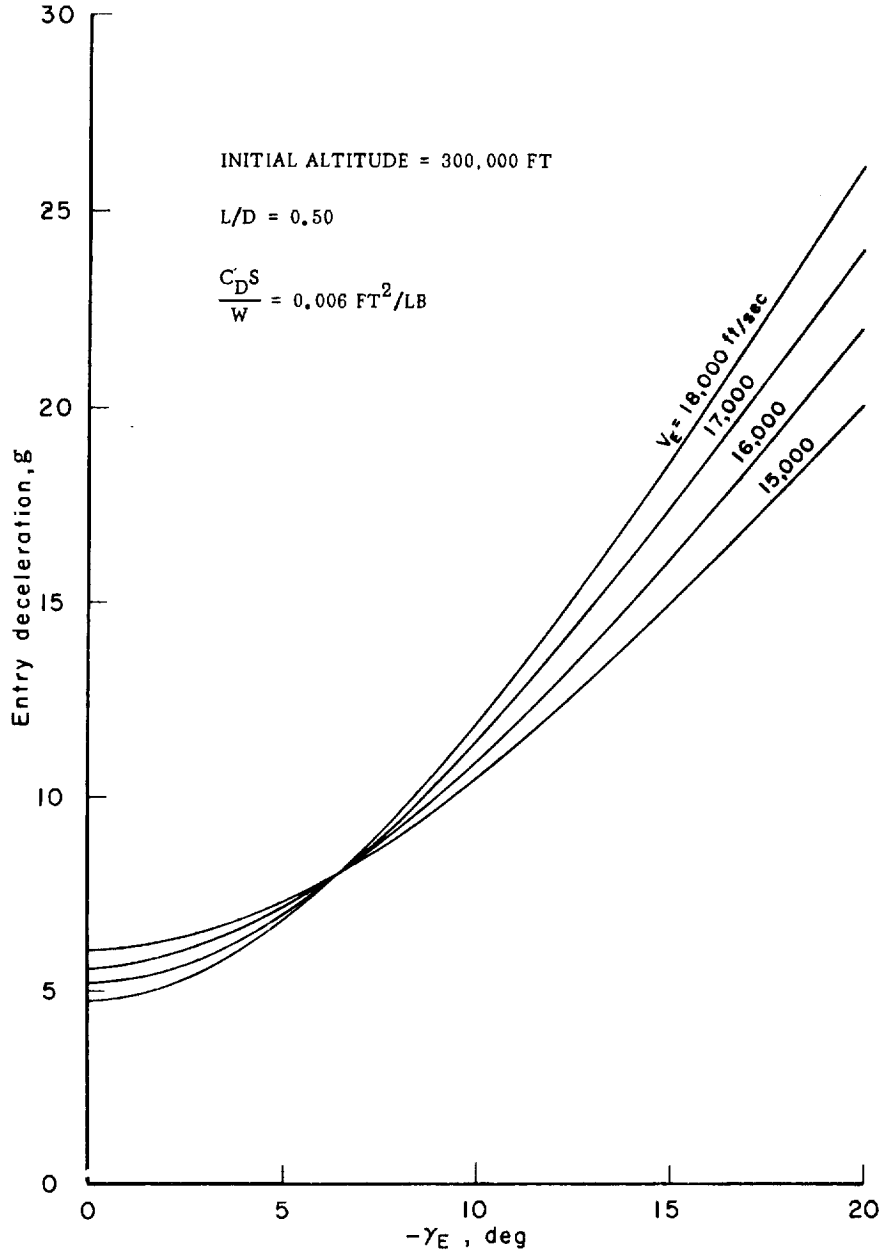

Figure 31. Entry Deceleration, L/D = 0.50

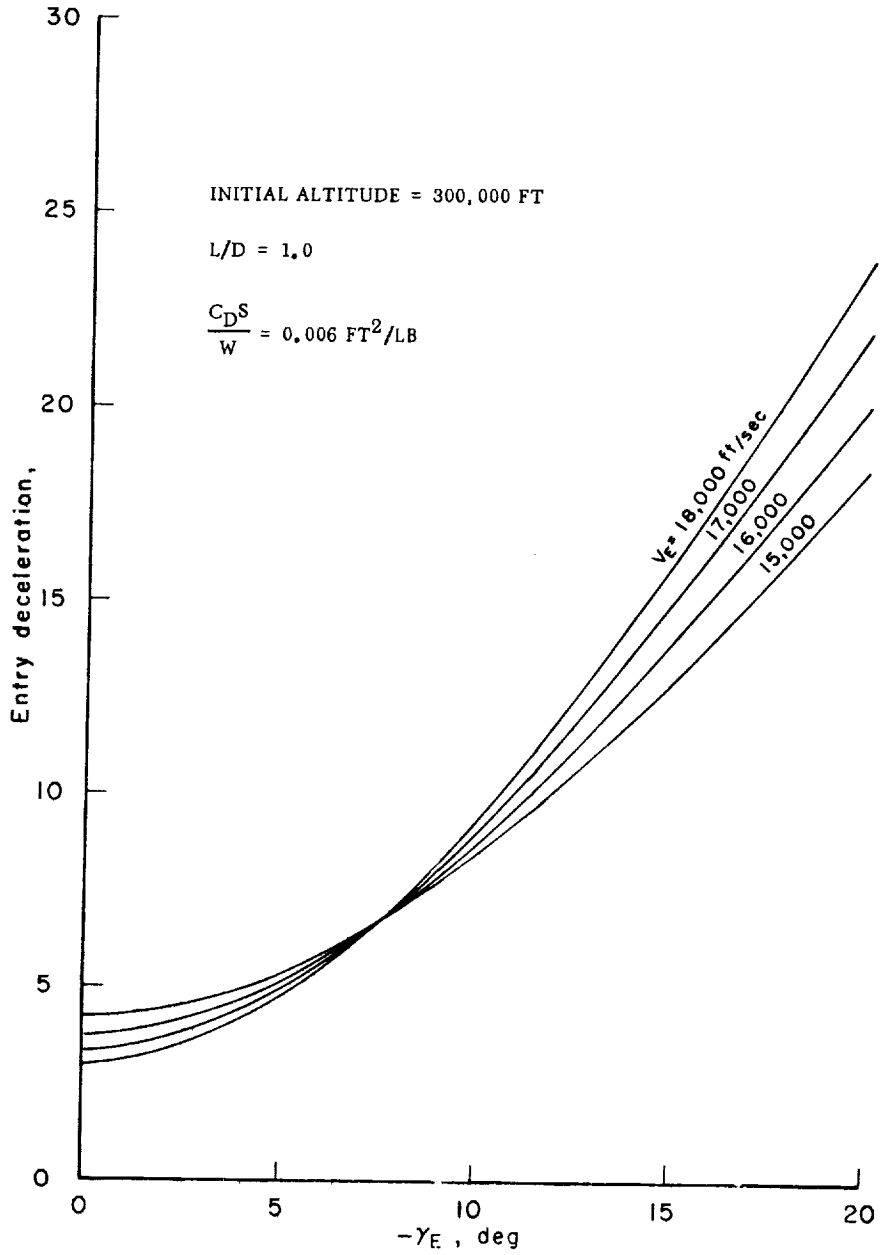

Figure 32. Entry Deceleration, L/D = 1.0

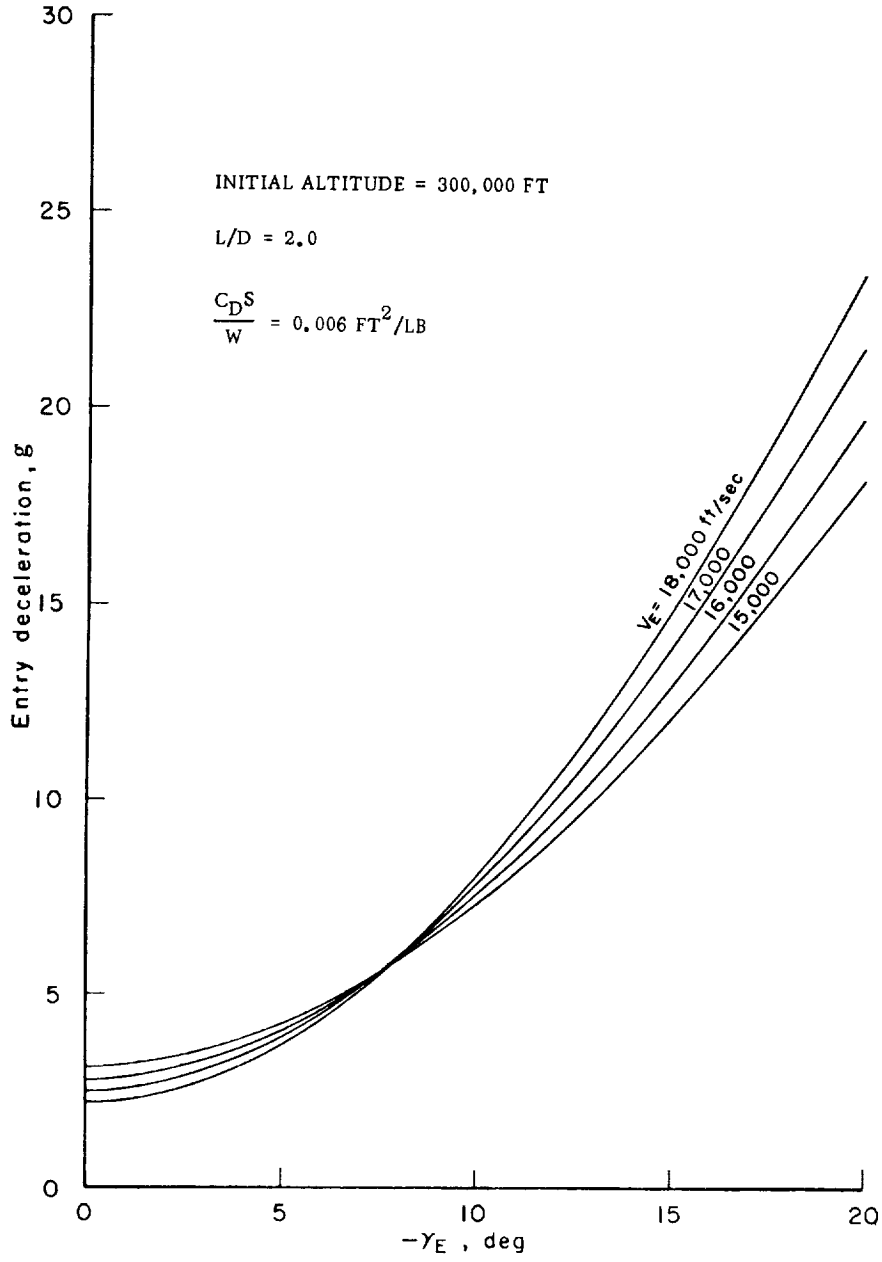

Figure 33. Entry Deceleration, L/D = 2.0

may still result if the velocity impulse is added at too high an altitude. If the use of corrective thrust is delayed until shortly before entry, the entry angle may be reduced directly by applying the abort rocket thrust in a direction normal to the desired flight path after the velocity impulse.

Figs. 30 - 33 may be used directly to determine the ΔV required to limit the reentry deceleration. For example, suppose that a particular exoatmospheric abort results in a V_E = 18,000 ft/sec and γ_E = -15° (at h_E = 300,000 ft). If we require that the maximum deceleration on reentry be 10g, and if the L/D ratio for the vehicle is 0.50, then Fig. 31 shows that the maximum γ_E must be -8.4°. The abort propulsion system must therefore supply a $\Delta V = 18{,}000 \sin 6.6° = 2{,}070$ ft/sec. This corresponds to propellant weight ratios of 0.21 and 0.14 for engines with specific impulse of 275 and 420 sec respectively.

A more critical situation exists when the abort velocities are in the super circular region.† In this case, an immediate return to earth is usually desired in order to avoid (among other things) an extended exposure to the Van Allen radiation belts. If this return is accomplished by direct retrothrust, it is expensive in terms of velocity increment required. For example, if an abort occurs at near escape speed, a velocity increment of some 10,000 ft/sec is required for reduction to satellite velocity alone. A more efficient procedure is to apply rocket thrust in such a manner as to deflect the trajectory so that it lies within a normal entry corridor.[36],[37] Entry along the overshoot boundary using negative lift is generally the least expensive in terms of velocity increment required. For this type of maneuver, the velocity increment required depends not only on the burnout conditions at the abort point but also on the factors which influence the overshoot trajectory. These factors are lift to drag ratio, L/D, drag parameter, $C_D S/W$, entry velocity, and of course the altitude at which the trajectory is altered to coincide with the overshoot trajectory.

The velocity increment required for burnout at a prescribed altitude may be determined from a diagram of the type shown in Fig. 34. In the upper portion of the figure, the burnout (abort) velocity is represented as a vector with origin to the left. Also shown are the corresponding γ_{bo} and $\bar{V}_{bo}$. Here $\bar{V}$ is defined as the ratio of velocity to local circular velocity. The lower portion of the figure shows the entry velocity vector of the overshoot boundary (i.e., a vehicle having this velocity vector at entry will reduce to circular velocity in a single pass using negative lift).

These curves were computed from the results given in Refs. 36 and 37 for vehicles entering with constant $C_D S/W$ and L/D. The velocity increment required of the abort system is represented by the vector between the appropriate burnout point and the curve representing the appropriate vehicle aerodynamics. Since the lowest velocity increment is desired, the vector normal to the appropriate vehicle curve is

† The terms circular velocity and satellite velocity are used interchangeably.

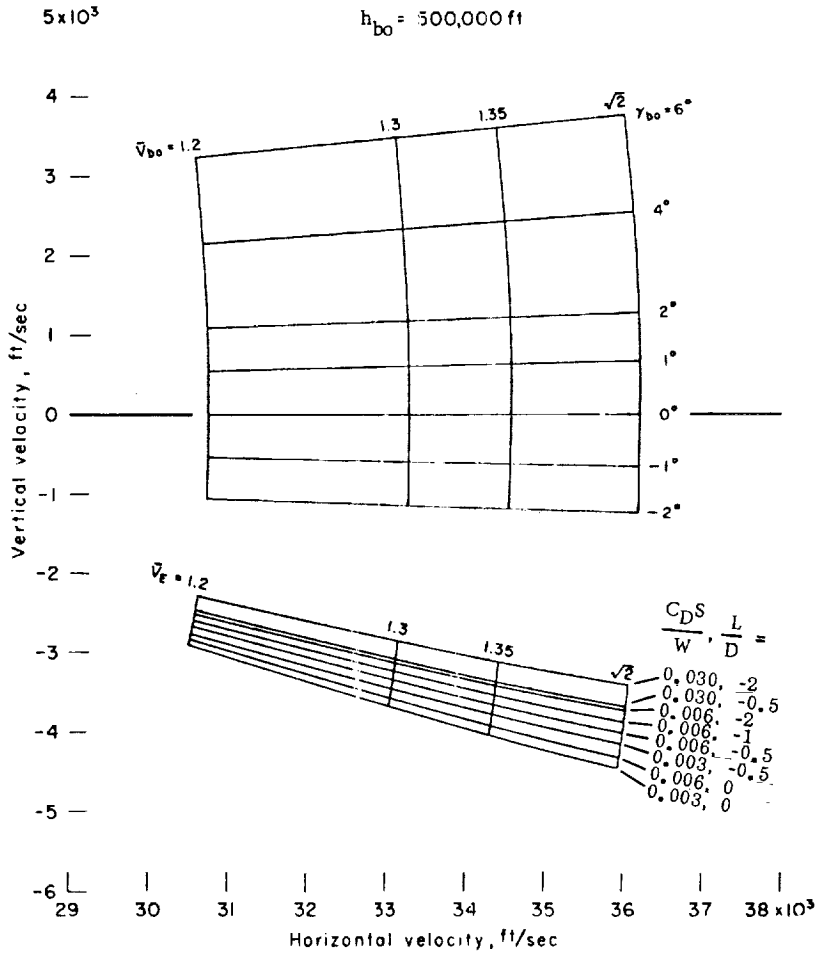

Figure 34. Burnout Conditions at Supercircular Speed and Entry Conditions for the Overshoot Boundary - h_{bo} = 500,000 ft

the one of interest. Similar curves are shown in Figs. 35 and 36 for burnout altitudes of 1,000,000 and 1,500,000 ft respectively.

From a series of curves of the type shown in Figs. 34 - 36, the velocity increments required of the abort system may be calculated and displayed as shown in Figs. 37 - 40.

This series of figures shows the effect on velocity requirements of vehicle $C_D S/W$ and L/D, and of burnout velocity and flight-path angle, respectively. In each case, the velocity requirement is shown as a function of burnout altitude. It is noted that the entry vehicle characteristics $C_D S/W$ and L/D are of secondary importance, except possibly at the lowest altitudes shown. Far more important are the flight

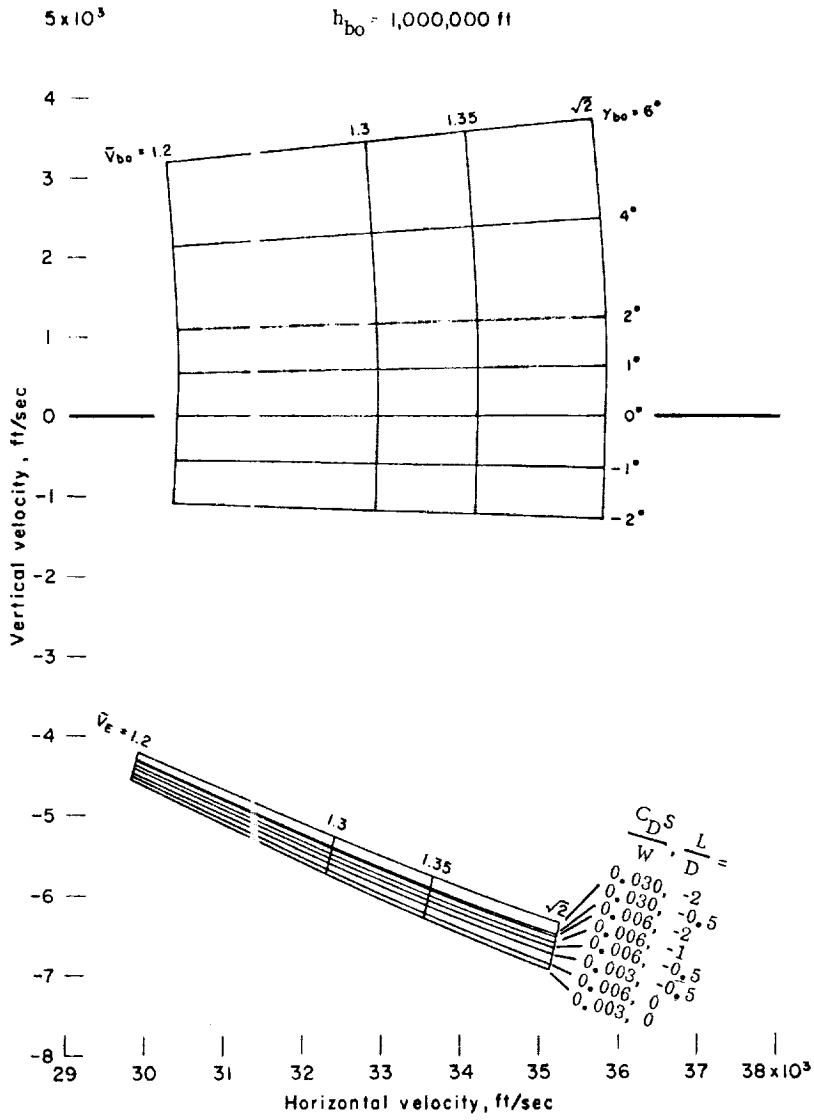

Figure 35. Burnout Conditions at Supercircular Speed and Entry Conditions for the Overshoot Boundary - h_{bo} = 1,000,000 ft

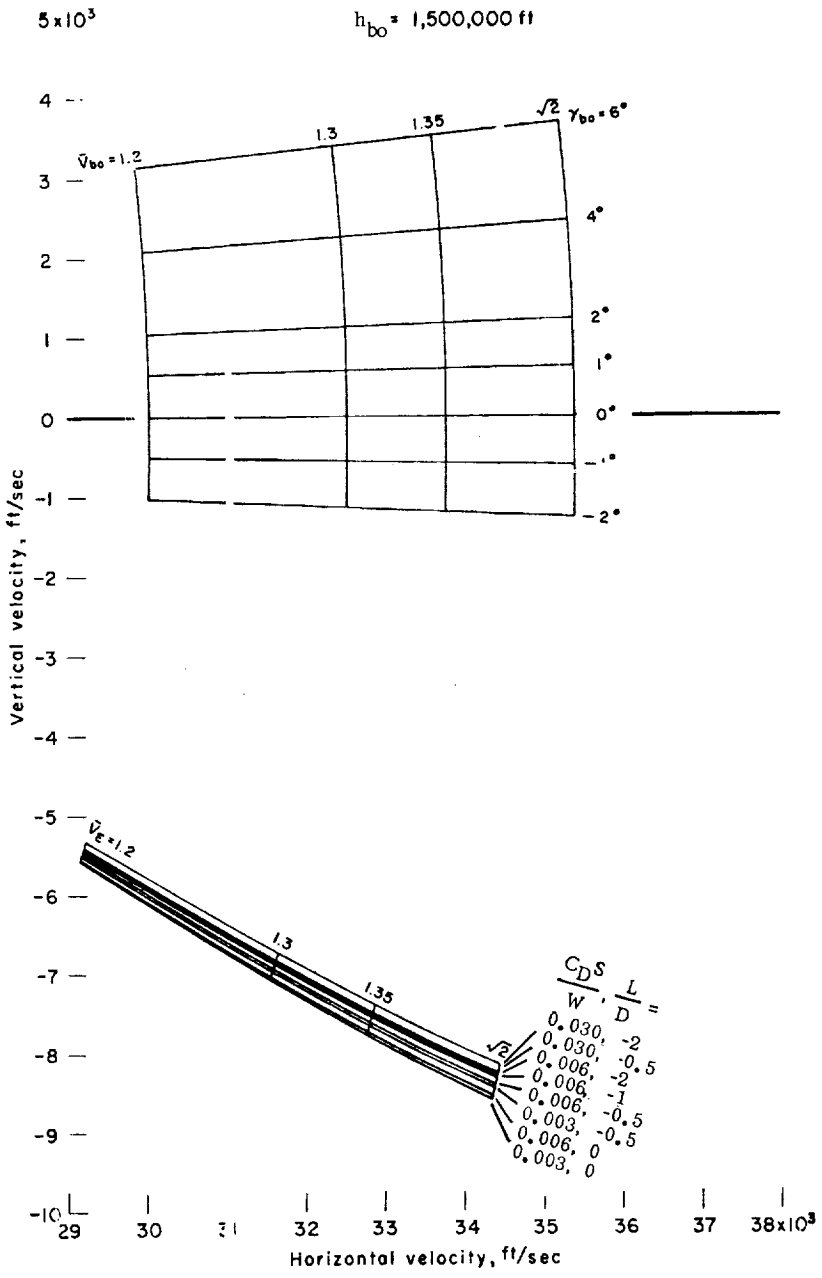

Figure 36. Burnout Conditions at Supercircular Speed and Entry Conditions for the Overshoot Boundary - h_{bo} = 1,500,000 ft

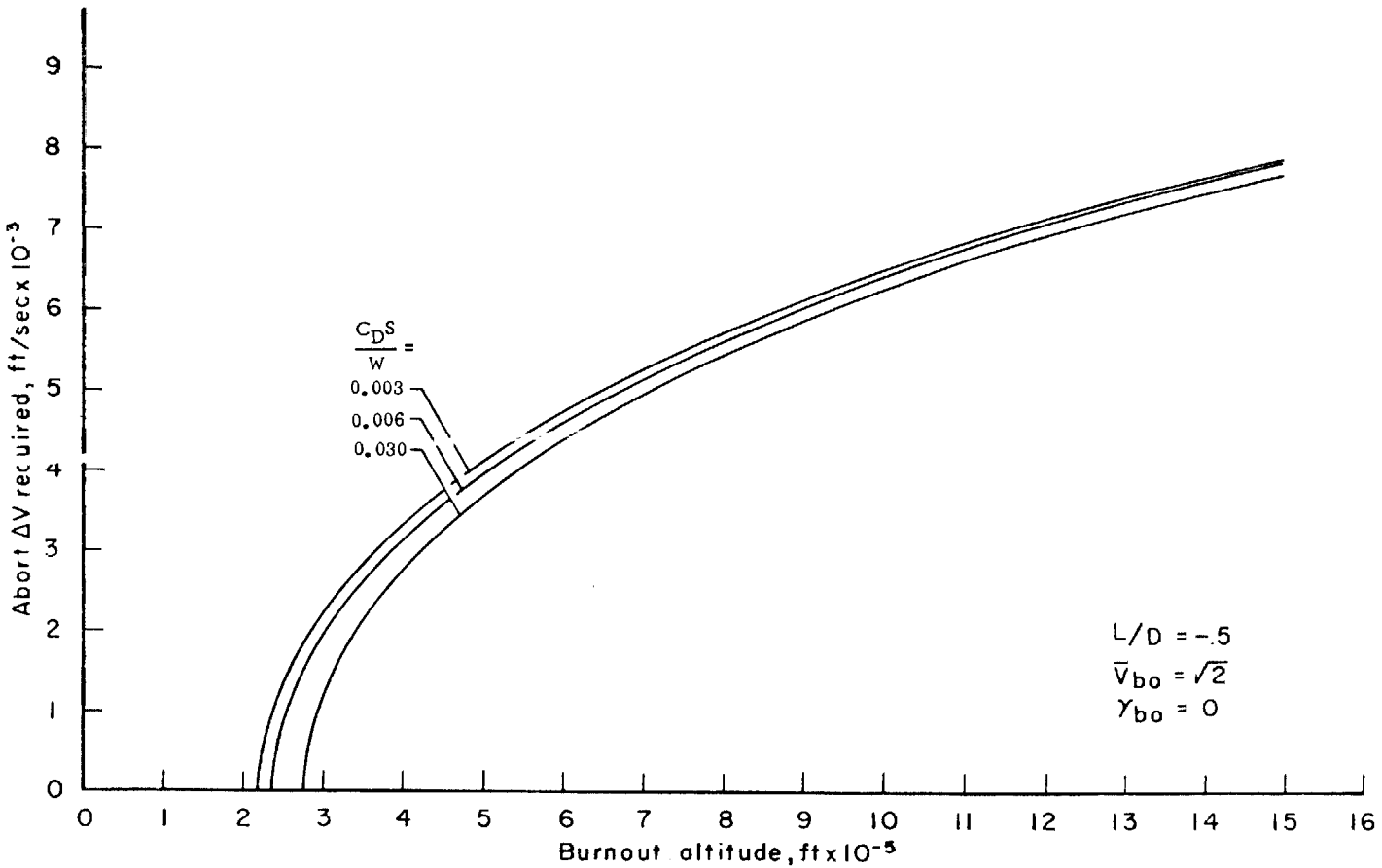

Figure 37. Effect of $C_D S/W$ on Abort Velocity Requirement for Burnout at Escape Speed

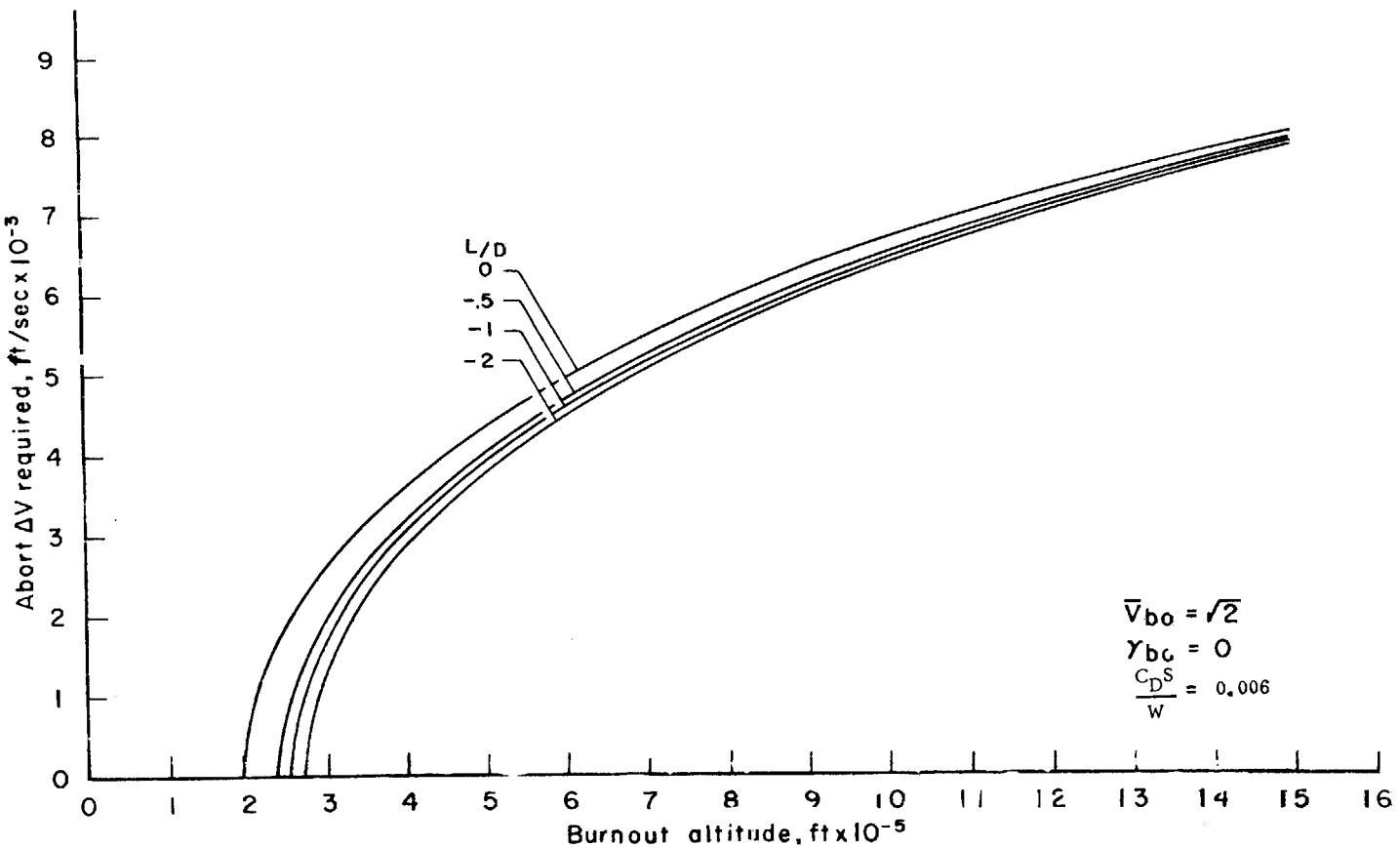

Figure 38. Effect of L/D on Abort Velocity Requirement for Burnout at Escape Speed

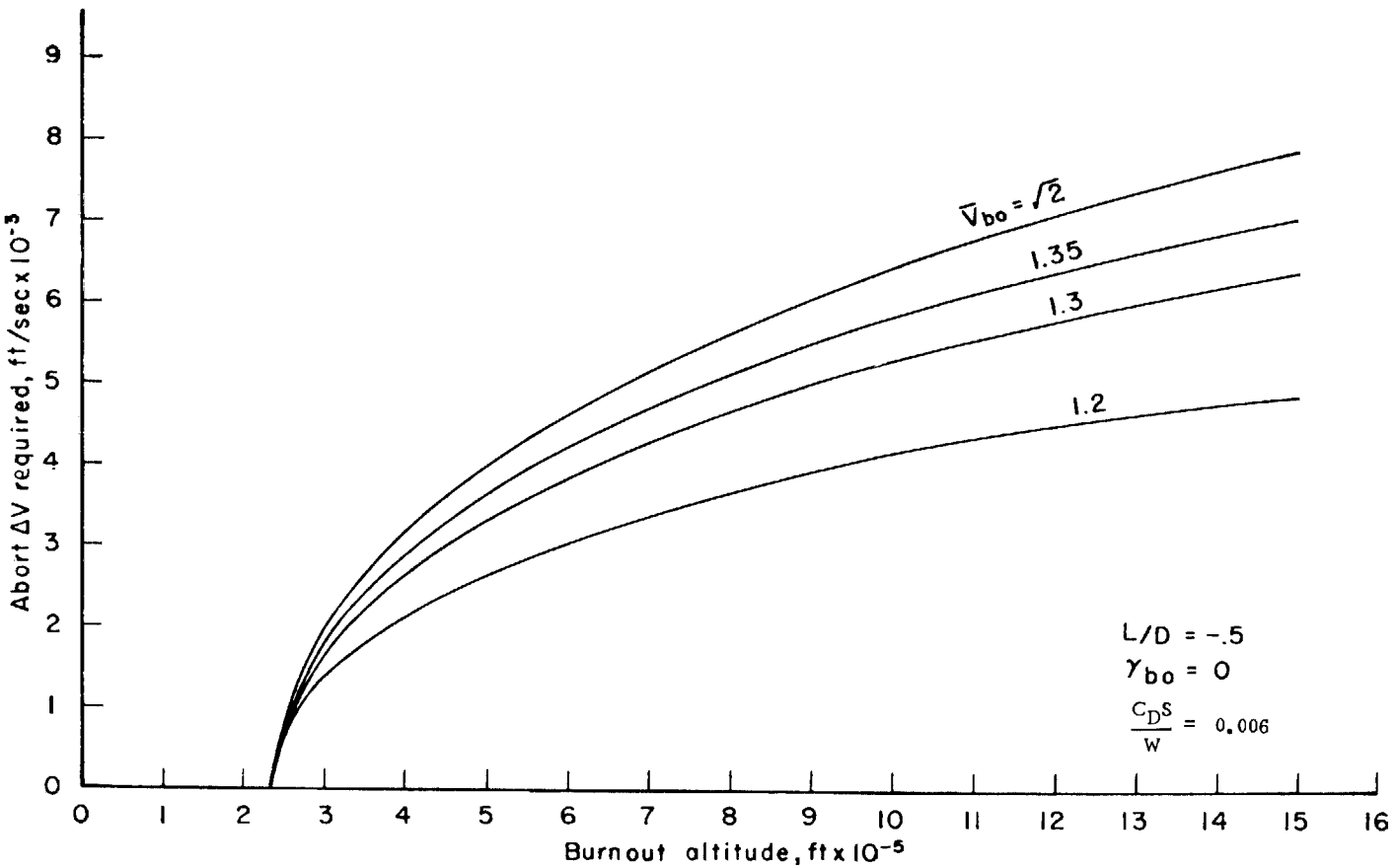

Figure 39. Effect of Burnout Velocity on Abort Velocity Requirement

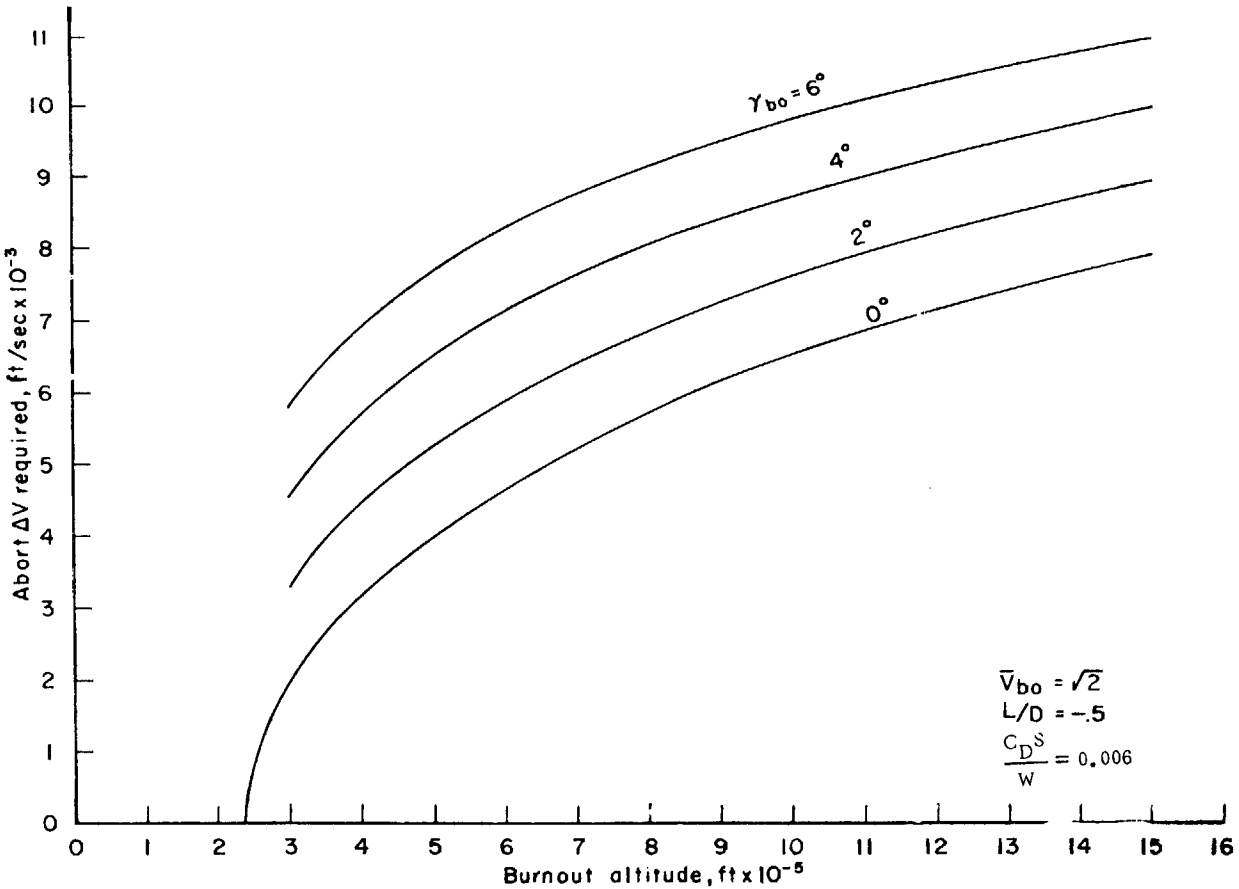

Figure 40. Effect of Burnout Flight-Path Angle on Abort Velocity Requirement for Burnout at Escape Speed

conditions at the point of abort. In this connection it is noted that the abort velocity requirement increases rather markedly with increasing burnout flight-path angle and altitude. For a nominal entry vehicle of $C_D S/W = 0.006$ ft^2/lb and $L/D = -0.5$, abort at escape speed with zero flight-path angle requires a ΔV of approximately 2,000 feet per second at 300,000 feet altitude; 4,000 feet per second at 500,000 feet; and 8,000 feet per second at 1,500,000 feet.

To demonstrate the implications of some of the previous results, we consider an abort situation at burnout for a typical lunar booster trajectory for which

$\gamma_{bo} = 0°$

$V_{bo} = 36{,}300$ ft/sec

$h_{bo} = 500{,}000$ ft

For an entry vehicle with $L/D = -0.5$ and $C_D S/W = 0.006$ ft^2/lb, the abort velocity requirement is 4,000 feet per second (Fig. 38). Application of this velocity increment in the optimum direction is sufficient to place the vehicle on the overshoot boundary where entry is accomplished with negative lift. If L/D is zero, the velocity requirement is increased to 4,300 feet per second and if it is -2, it is decreased to 3,700 feet per second. If the burnout altitude could be decreased to 300,000 feet, the three values of the velocity requirement decrease to 2,000 feet per second for $L/D = -0.5$; 2,600 feet per second for $L/D = 0$; and 1,300 feet per second for $L/D = -2$. It is noted that entry vehicle aerodynamics have a larger effect at the lower altitude. Boost trajectories with burnout altitudes less than 300,000 feet appear to be impractical because of drag effects on the booster itself.

The abort thrust requirements formulated thus far have been based on impulsive velocity (infinite thrust). In practice, of course, the thrust level of a rocket engine is limited, and a finite time is required to expel a given amount of propellant. Assuming finite thrust engines, McGowan and Eggleston[3] investigated the following question: At what time and in what direction and at what engine thrust level should the available ΔV be applied in order to realize the lowest peak deceleration on reentry? It is assumed that the abort velocity is subcircular.

This is significantly different from the problem previously considered; namely, what are the ΔV requirements to be applied at entry (i.e., at 300,000 ft) in order to orient the entry flight path angle such that a specified deceleration is not exceeded.

The McGowan and Eggleston study is based on an abort condition known to be critical from the point of view of entry deceleration. These abort conditions are

$V = 13{,}800$ ft/sec

$\gamma = 10°$

$h = 705{,}000$ ft

with an abort vehicle whose parameters are

$W = 7{,}000$ lb

$S = 75$ ft^2

$C_D = 1.4$

$L/D = 0$ or 0.5

With no abort thrust capability, the resulting entry trajectory is as shown in Fig. 41. It is noted that even with $L/D = 0.5$, the deceleration reaches a peak value of about 18 g. Several points of later interest are marked 1 to 7 along the trajectory.

We consider first the following question: At any given time or position along the trajectory, in what direction should the available ΔV be applied in order to realize the lowest peak deceleration on reentry?

It would appear plausible that the entry decelerations could be most effectively reduced by using all the available thrust to minimize the instantaneous flight path angle. To do this, the ΔV must be applied in a direction which is normal to the resultant velocity vector, V_1. From Fig. 42 and some elementary geometry reasoning, this abort thrust angle is obtained as†

$$\xi = 180° + (\operatorname{sgn}\gamma)\cos^{-1}\frac{\Delta V}{V} \tag{12}$$

In order to investigate the validity of Eq. (12), a cursory study was made with the trajectory shown in Fig. 41. At each of the seven indicated conditions on this trajectory, a thrust of 50,000 pounds was applied for 11 sec ($W_p/W = 0.287$; $I_{sp} = 275$ sec) in the directions of $\xi = 0°$, $60°$, $120°$, $180°$, $240°$, and $300°$. The vehicle's trajectory was then calculated (with $L/D = 0.5$) until the maximum deceleration was reached. A plot of the maximum decelerations as a function of ξ is shown in Fig. 43. Also shown are the values of ξ calculated from Eq. (12) and indicated by the ticks on the curves. The results show that, for the conditions investigated, Eq. (12) does indeed give the

† By definition, $\operatorname{sgn}\gamma = +1$ if $\gamma > 0$
$= -1$ if $\gamma < 0$

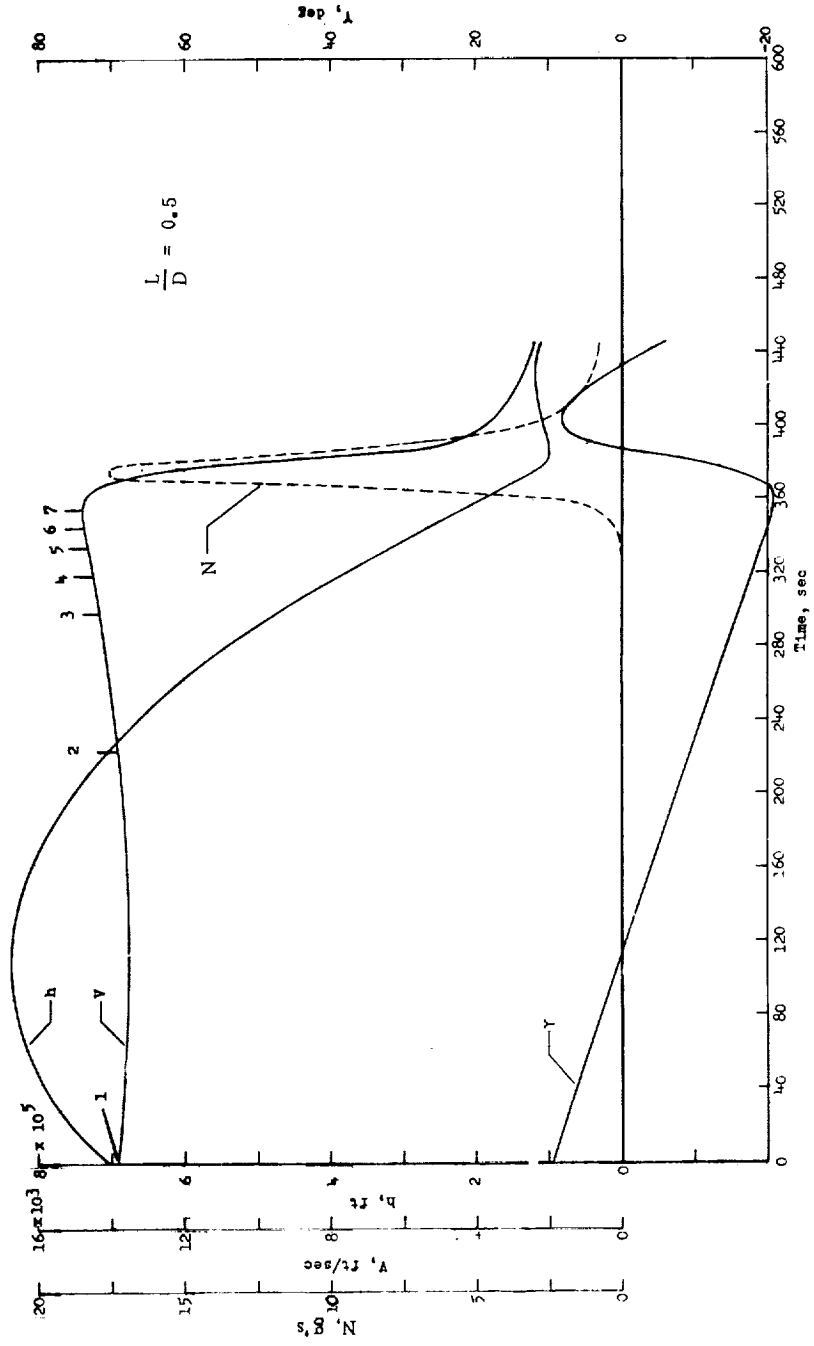

Figure 41. Entry Trajectory With No Abort Thrust

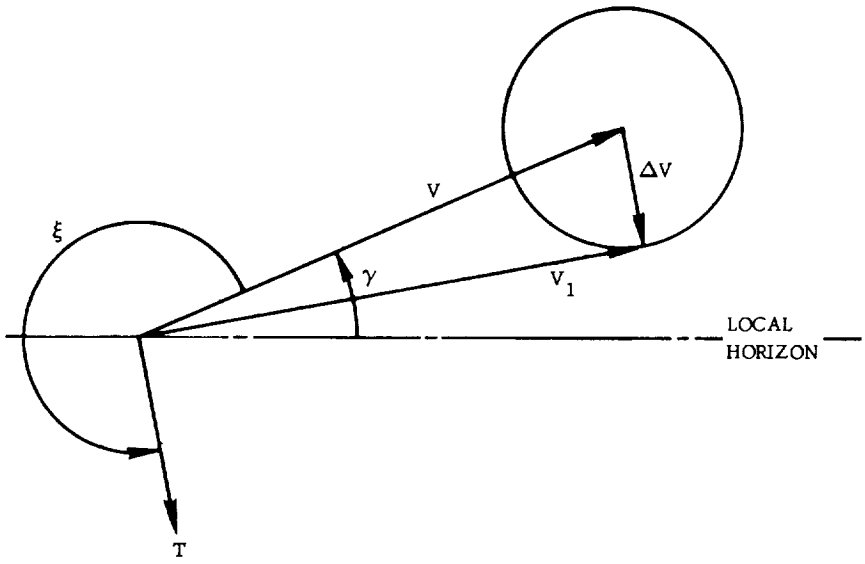

(a) Positive Flight Path Angle

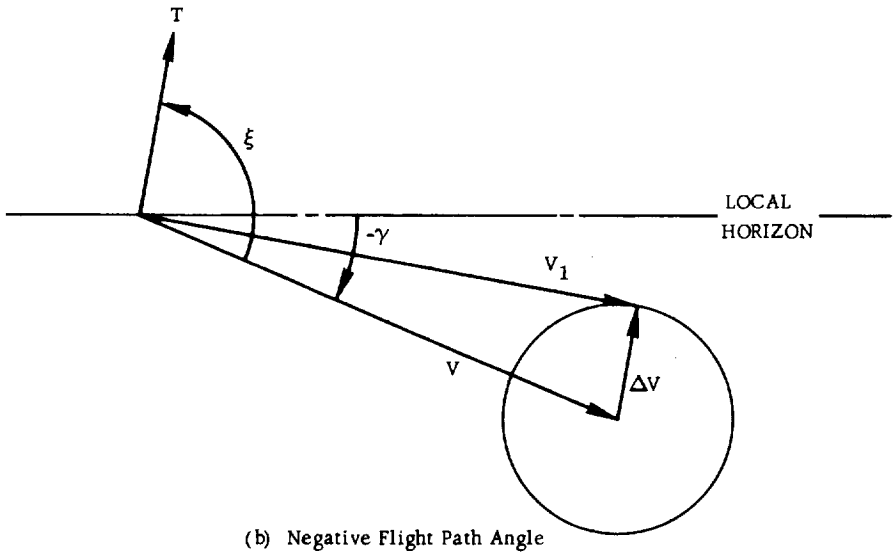

(b) Negative Flight Path Angle

Figure 42. Optimal Direction of Abort Thrust - Subcircular Velocity

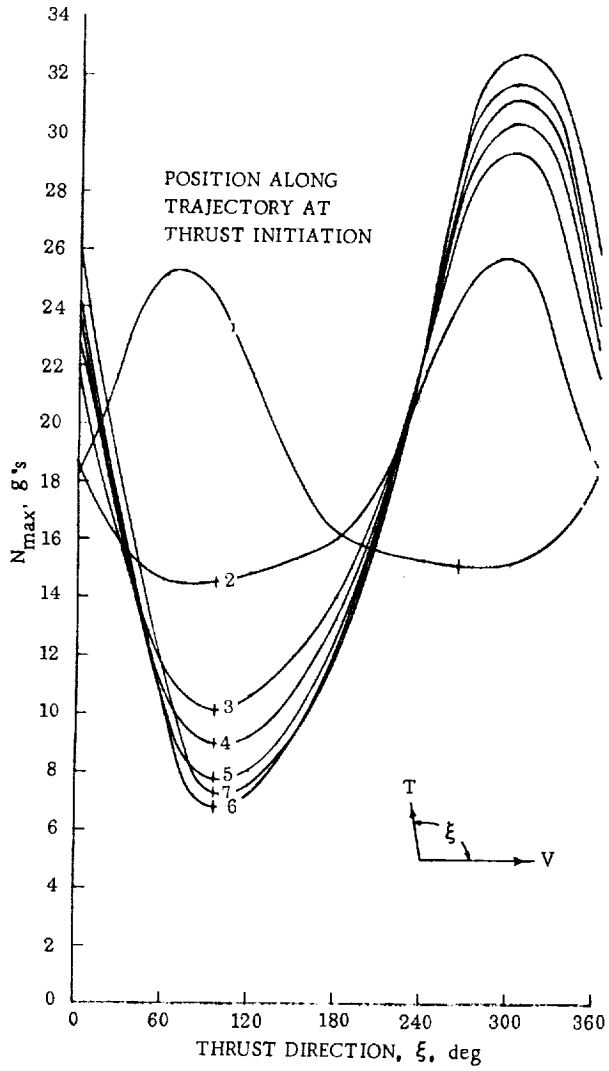

Figure 43. Variation of Peak Deceleration With Thrust Direction

near-optimum direction for thrust application if minimum deceleration is the governing criterion.

Fig. 43 indicates that the position or time at which the thrust is applied also affects the deceleration on entry. This effect is more graphically illustrated in Fig. 44 by plotting the variation of the decelerations of the vehicle as a function of time-from-abort. The same 50,000-pound-thrust engine was applied at the seven positions (identical to those shown in Figs. 41 and 43 in the direction of ξ given by Eq. (12). For reasons of clarity the accelerations due to the engine thrust and the individual variations of V, γ, and h are not shown. The results of Fig. 44 show that, for the given thrust level of 50,000 pounds ($W_p/W = 0.287$; I_{sp} = 275 seconds), the optimum time for thrust application is just prior to a rapid buildup of dynamic pressure (position 6).

This same type of analysis was used to determine peak decelerations on entry for several sizes of abort engines and for thrust initiated at various altitudes from about 500,000 feet to about 185,000 feet along the abort trajectory shown in Fig. 41. The results, summarized in Fig. 45, show maximum decelerations calculated for abort-engine sizes ranging from 8,000 pounds to 50,000 pounds of thrust and for an infinite thrust engine (equivalent to impulsively applied velocity). The calculations were made for an abort-propellant weight ratio W_p/W of 0.287 and specific impulse of 275 seconds. The curves also represent peak decelerations for an abort-propellant weight ratio of 0.199 with specific impulse of 420 seconds. Both sets of numbers represent an ideal velocity increment of 3,000 ft/sec (see Fig. 46). The results are virtually independent of the choices of specific impulse or weight ratio for the given ΔV.

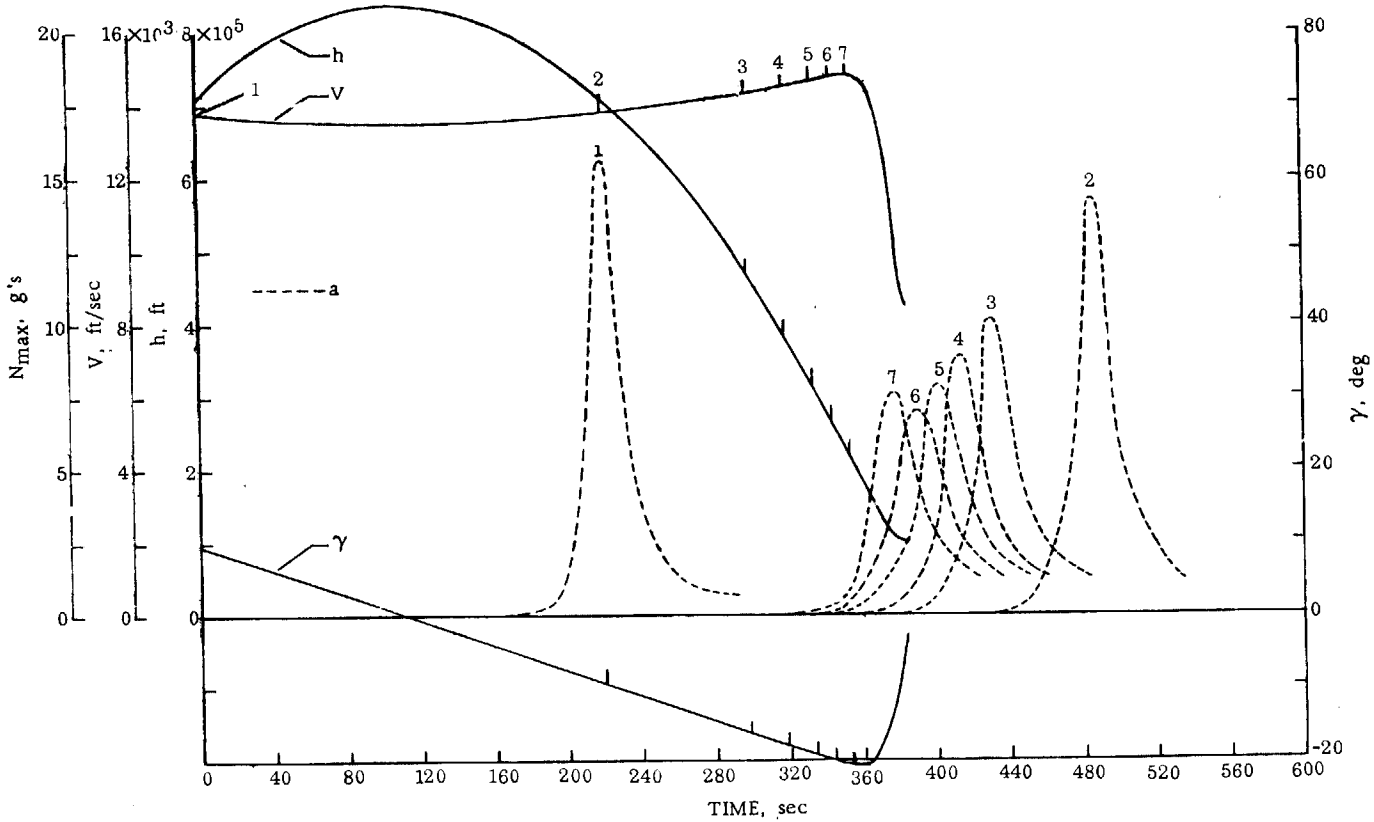

Figure 44. Deceleration-Time Histories for Abort Thrust Applied at Various Points Along Trajectory

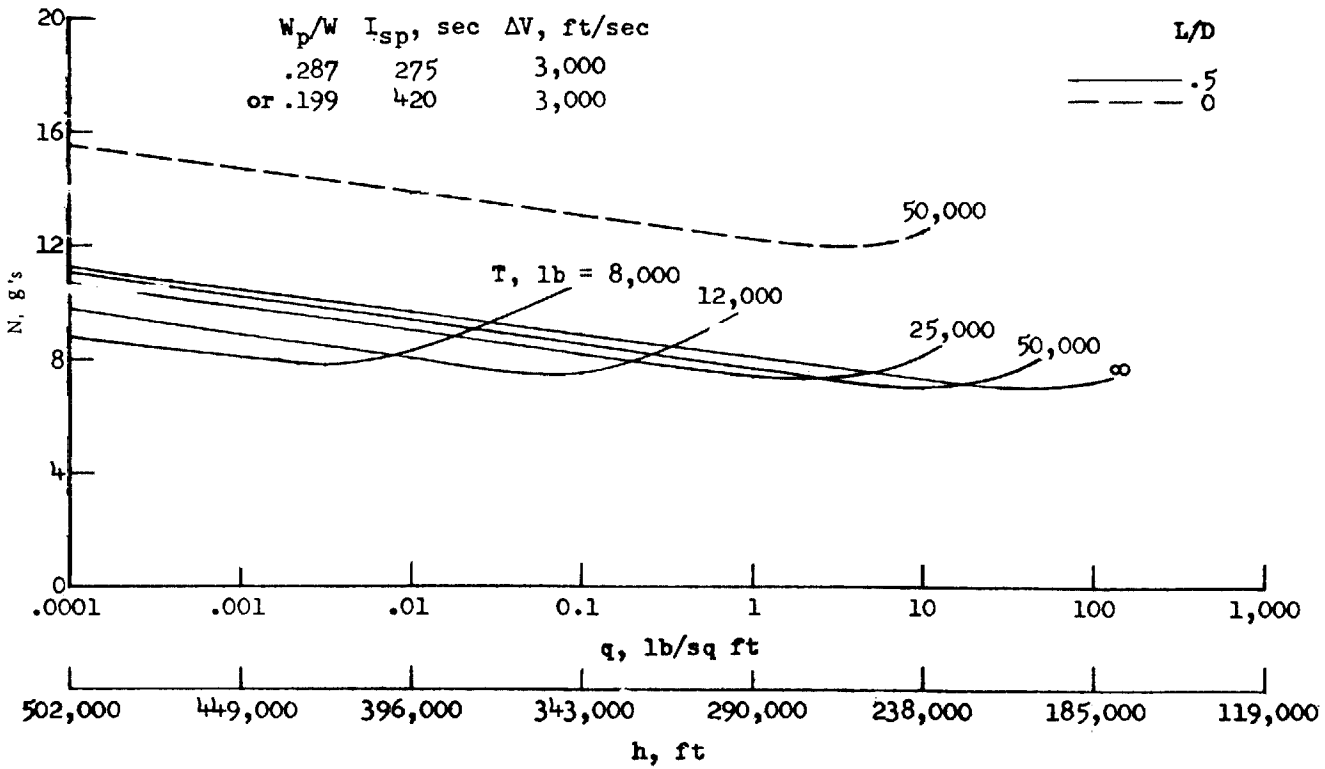

Figure 45. Maximum Decelerations on Entry After Thrust Initiation at Various Altitudes (or Dynamic Pressure) Along Trajectory

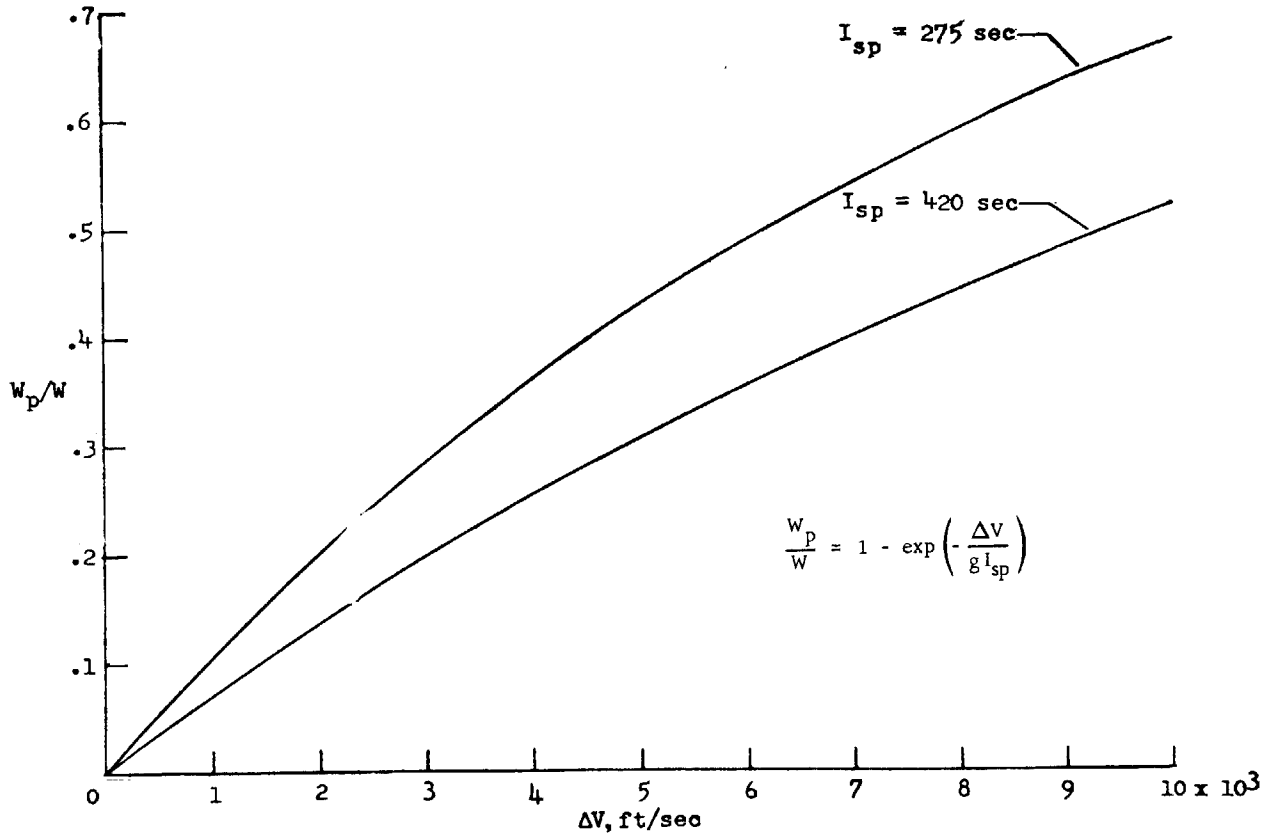

Figure 46. Relationship Between Abort Velocity and Ratio of Fuel Weight to Vehicle Weight

It is apparent that the effect of engine size on the minimum decelerations obtainable is slight - the minimum decelerations range from about 8g to 7g. However, the conditions (altitude and dynamic pressure) at which the thrust is initiated are important for minimum deceleration. For an 8,000-pound-thrust engine the optimum conditions for thrust initiation for minimum deceleration on entry are a dynamic pressure of about 0.001 lb/sq ft and an altitude of about 449,000 feet. For a 50,000-pound-thrust engine the optimum conditions for abort thrust initiation to realize the minimum decelerations are a dynamic pressure of 10 lb/sq ft and an altitude of 238,000 feet. Although most of the data in Fig. 45 are for an L/D value of 0.5, decelerations with a 50,000-pound-thrust engine are also given for an L/D value of 0. The decelerations on entry are of course substantially higher for L/D = 0 than for the equivalent vehicle with L/D = 0.5.

The fuel requirements for an abort at supercircular velocity have been determined earlier in this section based on the requirement that the vehicle enter the earth's atmosphere along an overshoot boundary.

However, these requirements are optimistic since they are based on impulsive velocity changes. When a finite-thrust rocket engine is used, the thrust level of the engine determines the time required to effect a given change in the magnitude and direction of the velocity. At supercircular velocities this time can be extremely critical, since at this condition the centrifugal acceleration is greater than the acceleration due to the earth's gravity and hence the resultant acceleration is away from earth. For an immediate return to earth, the acceleration due to thrust must be large enough to overcome the difference in acceleration between the centrifugal and gravitational accelerations (which is about 1g at escape velocity) and put the vehicle into a trajectory that penetrates the earth's atmosphere. Therefore, the abort thrust is applied to achieve maximum deflection of the flight-path angle toward the earth. The primary consideration in this study was to determine the abort propellant required to return the vehicle to earth when L/D is constant at -0.5 or 0. No attempt was made to modulate the decelerations on entry since various energy management schemes have been developed to cope with this phase of the recovery.

An example of the abort-propellant weight ratio required to return the vehicle to earth is shown in Fig. 47 for a 50,000-pound-thrust engine and propellant with a specific impulse of 420 seconds. Abort was initiated at the burnout conditions of the trajectory where the velocity is 36,000 ft/sec, the flight-path angle is 1.8°, and the altitude is 58.5 miles. For several abort-propellant weight ratios the altitude time histories of the vehicle are plotted from abort initiation. With a 50,000-pound-thrust engine and L/D = -0.5, between 24 and 25 percent of the total vehicle weight would be required to return the vehicle to earth.

In Fig. 48 the propellant weight ratio of 0.282 was held constant and the thrust level was changed for several computed trajectories. With the available abort propellant of 28 percent of the gross vehicle weight, the trajectories enter and remain

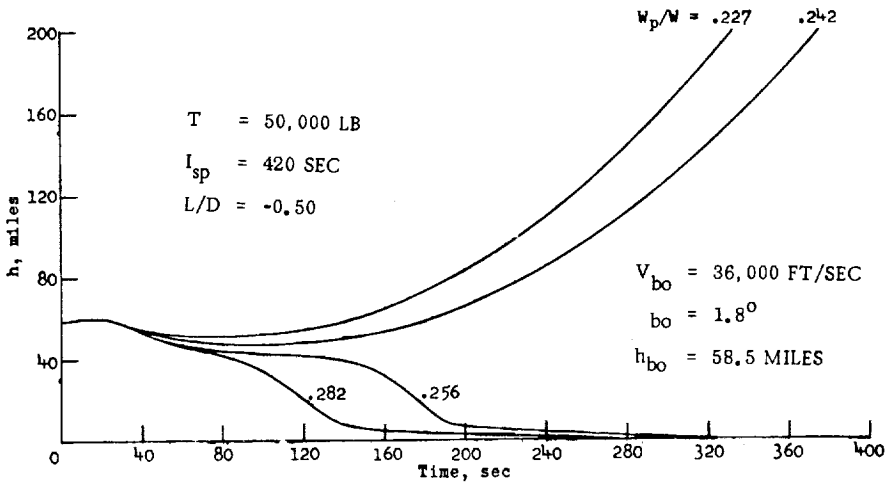

Figure 47. Influence of Propellant Mass Ratio on Supercircular Velocity Abort Trajectory

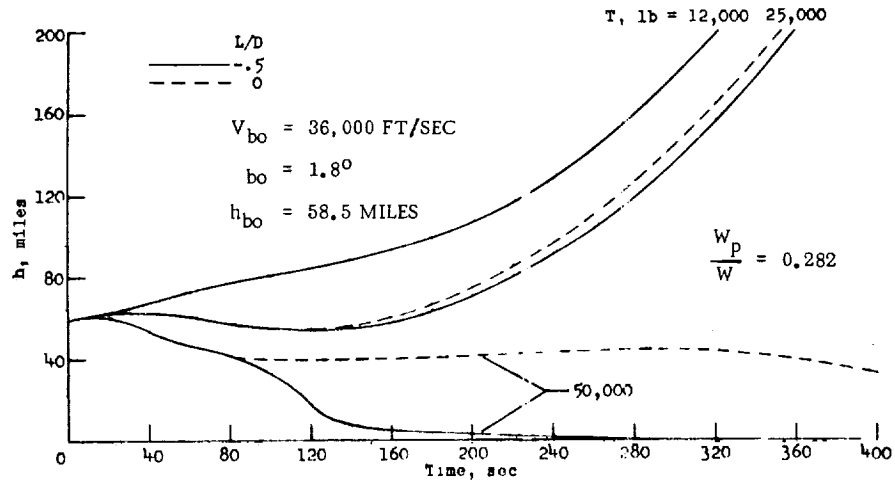

Figure 48. Influence of Abort Thrust Level on Supercircular Velocity Abort Trajectory

within the atmosphere in the case of a 50,000-pound-thrust engine when L/D is -0.5 or 0; however, for L/D = 0 the entry is marginal. On the other hand, with the same propellant weight the trajectory would not return to earth if an engine with 25,000 pounds of thrust or less were used. On the basis of acceleration, the initial ratio of thrust to vehicle weight was 3.53g for the 50,000-pound-thrust engine, 1.76g for the

25,000-pound-thrust engine, and 0.845g for the 12,000-pound-thrust engine. In a similar manner the propellant-weight-ratio requirements for aborts initiated at supercircular velocities were determined.

In Fig. 49 are shown the propellant-weight-ratio requirements to return the vehicle to earth for aborts initiated between near-circular velocity and escape velocity. No thrust is required to return the vehicle to earth for velocities up to about 28,000 ft/sec since a dip trajectory was used for this study (i.e., the flight-path angle had a sufficiently large negative value up to this velocity). Aborts initiated at the injection velocity of 36,000 ft/sec would require a propellant weight of about 25 percent of the gross vehicle weight to return to earth with a 50,000-pound-thrust engine, specific impulse of 420 seconds, and L/D of -0.5. For a 25,000-pound-thrust engine the abort-fuel weight requirement is about 35 percent of the gross vehicle weight for aborts initiated at 36,000 ft/sec. If infinite thrust were assumed, a corresponding propellant weight of only 20 percent would be indicated. The propellant weight ratios are shown at several velocities for a 50,000-pound-thrust engine and L/D = 0; as would be expected, more fuel (on the order of 3 percent of the payload) is needed to return to earth than when L/D = -0.5. The initial ratios of thrust to vehicle weight used are also listed in the figure. For an abort at 36,000 ft/sec with a propellant having a specific impulse of 275 seconds, the propellant weight ratio needed to return the vehicle to earth is at least 10 percent greater than the requirement when the specific impulse is 420 seconds.

For aborts initiated at velocities between 32,000 and 36,000 ft/sec, the fuel requirements increase rapidly by about 18 to 27 percent of the gross vehicle weight for the finite-thrust engines. Also noted is the more rapid increase of the fuel requirements with abort initiation velocity as the engine size decreases. For still further reductions in the engine thrust the initial ratio of thrust to weight approaches unity and indications are that the fuel requirements (percent of payload) to return the vehicle to earth would become prohibitive.

For immediate return to earth during this supercircular velocity phase of the launch it appears that between 25 and 34 percent of the payload must be set aside for abort purposes for the initial ratios of thrust to weight considered.

Another critical factor during aborts at supercircular velocities is the accumulated time delay required to (1) separate the vehicle from the booster, (2) orient the vehicle in the proper attitude, and (3) initiate the abort thrust. This effect of the accumulated time delay from abort until abort thrust initiation on the propellant weight requirements (I_{sp} = 420 seconds) is shown in Figs. 50(a) and 50(b) for aborts occurring at 34,000 ft/sec and 36,000 ft/sec, respectively. With no time delay ($\Delta t = 0$) the propellant weight ratios are the same as those given in Fig. 49 for the respective abort velocities and thrust levels. For example, in Fig. 50(b) an abort-propellant weight ratio of 25 percent is required with a 50,000-pound-thrust engine if applied at the burnout velocity of 36,000 ft/sec ($\Delta t = 0$). If, however, abort thrust initiation is

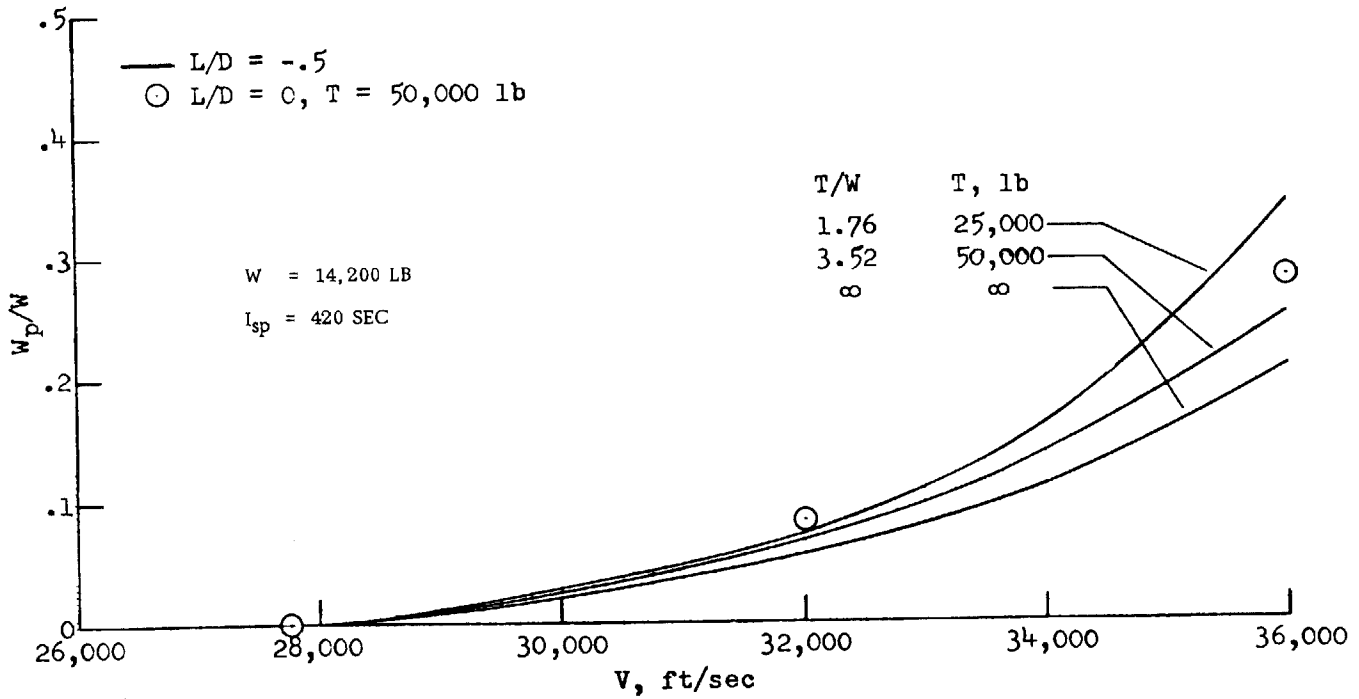

Figure 49. Propellant Weight Required to Return Vehicle to Earth for Aborts Initiated Along the Launch Trajectory

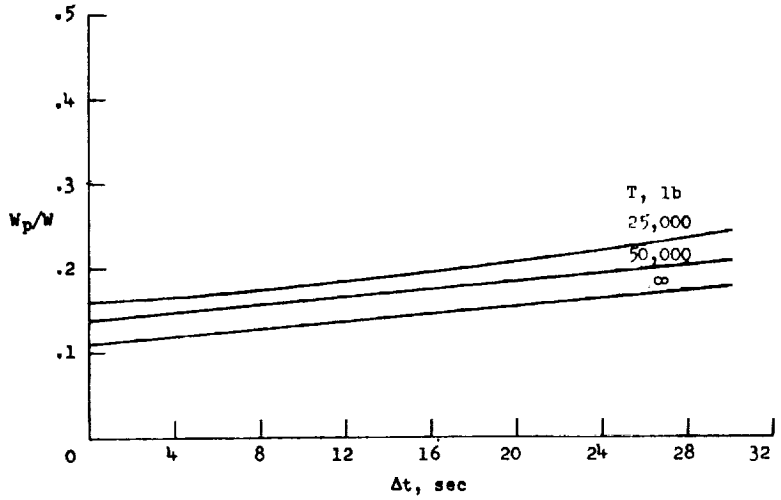

(a) V_{bo} = 34,000 ft/sec; γ_{bo} = 0.4°; h_{bo} = 55.0 miles

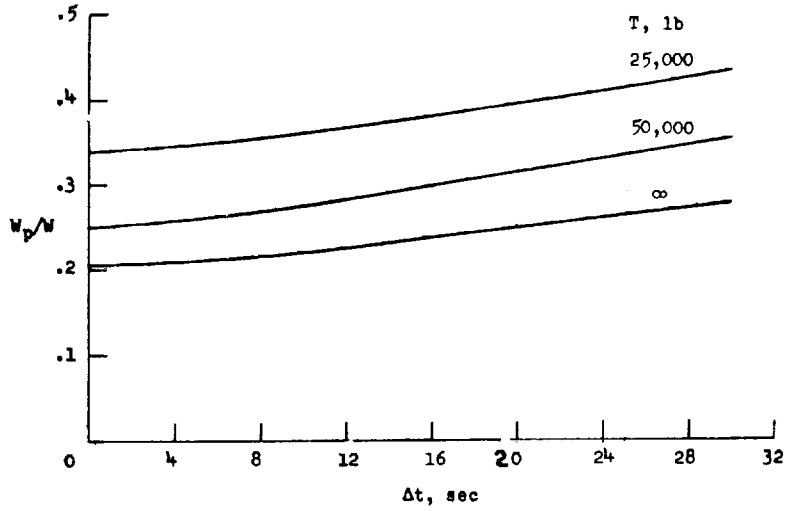

(b) V_{bo} = 36,000 ft/sec; γ_{bo} = 1.8°; h_{bo} = 58.5 miles

Figure 50. Abort Propellant Weight Required to Return Vehicle to Earth With the Time Delay From Abort Initiation to Thrust Initiation

delayed for 30 seconds after injection, a propellant weight ratio of 35 percent is required to return the vehicle to earth. Similar trends are also shown for the delays associated with the other thrust levels.

Summary of Sec. 3.1.3

The main results of this section are collected here for convenience. Since the nature of the abort problem is strongly dependent on whether the abort occurs at subcircular or supercircular velocity, they will be summarized separately. In each case, the main results are derived from an analysis of a typical lunar launch trajectory, in which the abort vehicle is assumed to be a point mass. Also, it is supposed that some form of ablative shielding is provided to cope with aerodynamic heating, since for this type of mission a cooling by reradiation appears insufficient. This also implies that the abort vehicle contains an appropriate attitude control system.

Abort at Subcircular Velocity

The ΔV requirements of the abort propulsion system are based on a maximum allowable peak deceleration on reentry. Impulsive thrust is assumed.

a. The ΔV requirements are relatively insensitive to the drag parameter, $C_D S/W$.

b. For entry angles to approximately -10 degrees, the entry decelerations are more strongly dependent on flight path angle than on velocity. Entry altitude is defined to be 300,000 ft.

c. The critical parameter, from the point of view of entry deceleration, is the entry flight path angle.

d. To minimize the peak deceleration on reentry, the abort ΔV should be applied at the entry altitude in such a way as to obtain the maximum reduction in flight path angle.

e. Some lift capability is required for the abort vehicle. For the launch trajectory considered, a ballistic type of vehicle ($L/D = 0$) will experience intolerable deceleration on reentry whatever the entry flight path angle.

f. The peak decelerations on reentry are relatively insensitive to variations in the abort engine thrust level. In other words, the assumption of impulsive thrust is valid.

Abort at Supercircular Velocity

The ΔV requirements in this case derive from entry corridor considerations. That is, the abort vehicle must return to earth in one pass through the atmosphere. Furthermore, some aerodynamic modulation is required to alleviate peak deceleration problems on reentry.

a. The ΔV requirements are essentially insensitive to variations in drag parameter, $C_D S/W$ and L/D.

b. The ΔV must be applied in such a way as to alter the trajectory such that it enters on an overshoot boundary.

c. The ΔV requirements are minimized if the burnout altitude and flight path angle are held to minimum values.

d. The entry trajectory is very sensitive to engine thrust level for a given ΔV. Assuming impulsive thrust could lead to serious errors.

e. The ΔV requirements increase sharply for abort velocities in the range 32,000 to 36,000 ft/sec.

f. Time delays due to separation of abort from booster vehicle, orienting vehicle to proper attitude, and initiating abort thrust can be significant in terms of fuel requirements, especially at near escape speed.

g. The ΔV requirements are more critical at supercircular (as compared to subcircular) abort speeds.

3.1.4 Abort From Satellite in Orbit

Until the present time (1968), manned orbital flight has been limited to Mercury and Gemini vehicles† which orbited the earth at low altitude and reentered after some prescribed interval. It is expected, however, that manned orbital missions will grow both in number and sophistication, providing many new research and operational vistas unattainable by unmanned satellites. This would include navigational, communications, weather, and reconnaissance systems, each of which may employ twenty or more vehicles in number, properly spaced in orbit in specific arrays to perform their respective functions.

In order to ensure the survival of the astronaut operating in this type of environment in the event of emergencies, three main concepts are presently envisioned: (1) direct abort from orbit and subsequent reentry, (2) rescue via earth-based facilities, and (3) rescue via satellite based facilities. All of these schemes are based on the idea that the astronaut is supplied with (or has immediately available) self contained life support equipment (space suit) which will sustain life for an hour or more. The selection of a specific abort system is then strongly dependent on the space mission itself, state of the art in space technology, and resources available. In the following sections, the general features of each of the abort systems will be described, together with foreseeable problems, and areas for further research.

† Concurrently with the Russian Vostok vehicles.

3.1.4.1 Abort Via Deorbiting

The simplest means of escape from orbit is by decreasing speed to the point from which a satisfactory atmospheric entry can be achieved. Obviously, either the satellite itself or a separate escape capsule may be used to effect the abort. As presently conceived, a manned satellite with a prime function of a scientific or reconnaissance nature would itself not have a reentry capability because of prohibitive weight and propulsion requirements. However, a small escape capsule (whose mass is small compared to that of the space station) appears to be a possible and reasonable solution to the abort problem in this case. A detailed discussion of possible configurations for such an escape (abort) capsule is deferred until later (Sec. 3.3). Here we shall consider the general nature of the abort thrust requirements, and related problems for abort from orbit. The main purpose is to obtain "order of magnitude" results, and for this purpose, the following assumptions are made:

a. Orbital altitudes are confined to the range 100 - 400 nautical miles.

b. Velocity changes are impulsive.

c. Reentry altitude is taken as 60 nautical miles. Thus, in the following, V_E and γ_E mean the velocity and flight path angle at this altitude.

d. The drag factor, $C_D S/W$, is constant.

In order to escape from orbit and return to earth, a retrothrust must be applied to reduce speed. The direction and magnitude of this thrust must be such that the velocity and flight path angle at the entry altitude will result in a safe reentry from the point of view of deceleration and heating constraints. The ΔV required at various orbital altitudes and the resulting values of V_E and γ_E are shown in Fig. 51.† This ΔV must be applied in a direction opposite to the satellite velocity vector. The curves in the figure have been derived on the assumption that the thrust misalignment angle, β, is zero.

An investigation of the influence of abort thrust misalignment yields the results shown in Fig. 52. It is apparent that for all practical purposes, β may vary by as much as 10° without seriously affecting reentry conditions.

Abort conditions usually require that the escape capsule reenter the atmosphere on the first pass. The minimum ΔV required to do this is shown in Fig. 53. The results shown here are derived from the calculation of abort trajectories in which an elliptical Keplerian path is assumed from orbit to reentry altitude, followed by an entry phase in which atmospheric effects are accounted for. The results shown are valid for nonlifting vehicles with drag parameters in the range 0.05 to 0.10.

† The main results in this section are derived from Ref. 15.

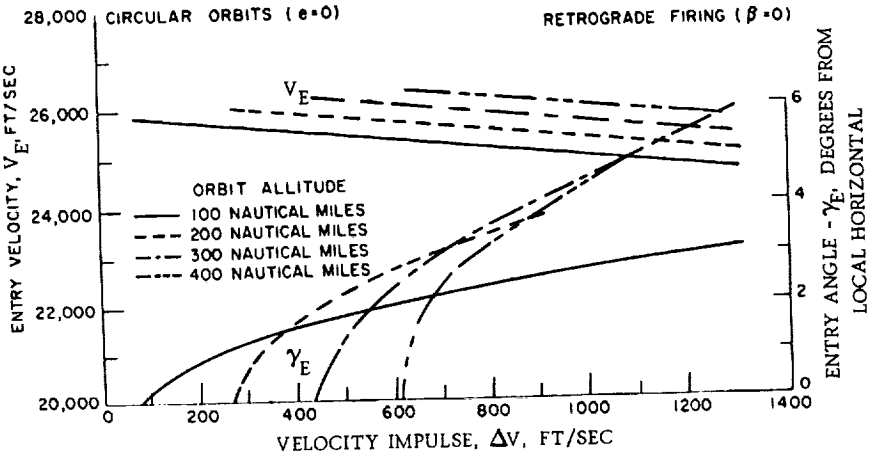

Figure 51. Deorbiting Parameters

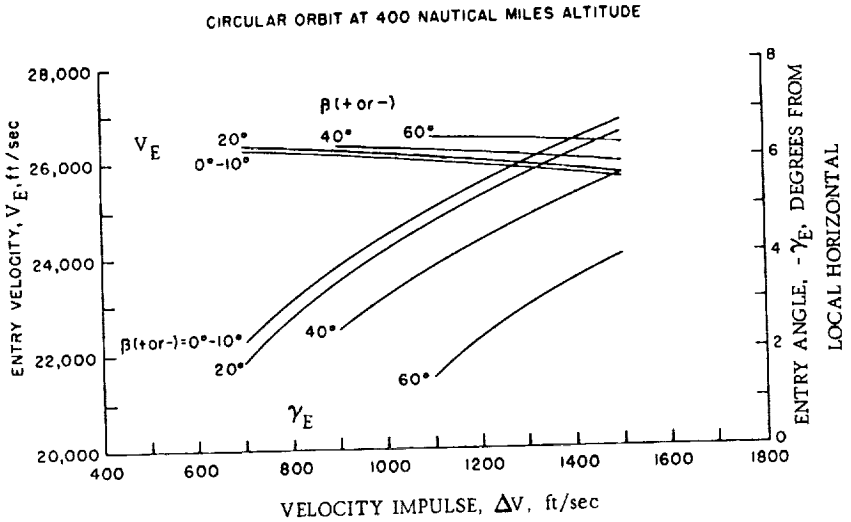

Figure 52. Effects of Angle of Deorbiting Impulse on Reentry

The range associated with abort trajectories, using the minimum ΔV values of Fig. 53, is shown in Fig. 54. This curve is useful in obtaining "order of magnitude" estimates for surface recovery operations.

While Fig. 52 has indicated that abort thrust misalignment produces negligible variations in reentry conditions, a variation in thrust magnitude produces significant downrange dispersions. This is indicated graphically in Fig. 55. The maximum deceleration encountered during reentry is shown in Fig. 56.

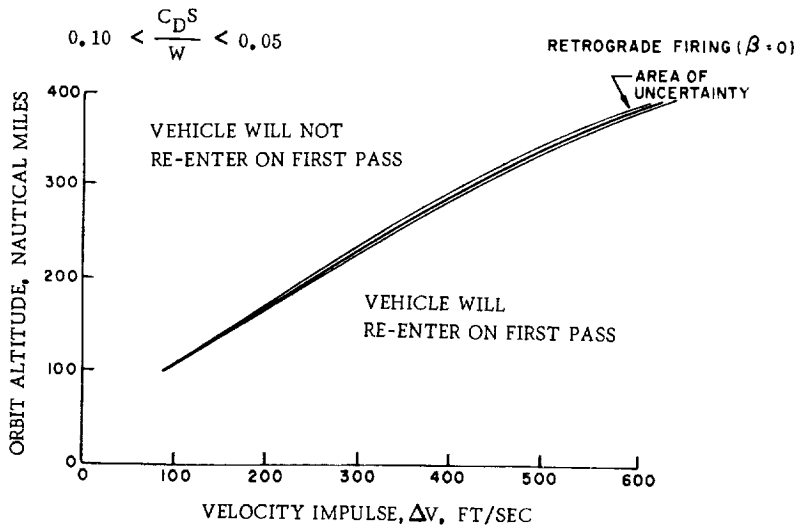

Figure 53. Minimum Deorbiting-Velocity Impulse for Circular Orbits

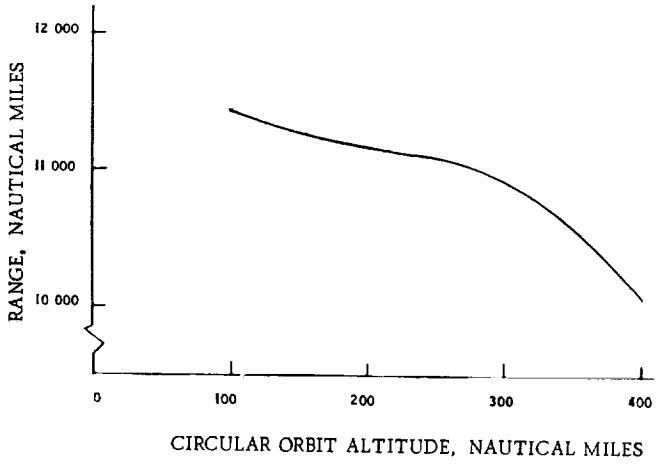

Figure 54. Range From Orbit to Impact Using Nominal Deorbiting Impulse

For more sophisticated systems, a lifting, semi-ballistic configuration for the abort vehicle is desirable. Besides providing for range extension or reduction, the little added complexity affords the extremely desirable capability for crossrange maneuvers.

A typical abort reentry in this case is shown in Fig. 57. Superimposed on this figure are the flight regimes and design criteria for optimization of the trajectory. Typical reductions in maximum deceleration due to the use of a lifting configuration are shown in Fig. 58.

3.1.4.2 Rescue Via Ground Based Facilities

If there is not capability aboard a satellite vehicle to effect an abort and reentry to earth, then a rescue or retrieval by an earth-launched vehicle is an obvious possibility to be considered. This idea requires mainly that the orbit of the satellite be known, and that the earth-based rescue vehicle be launched at precisely the time

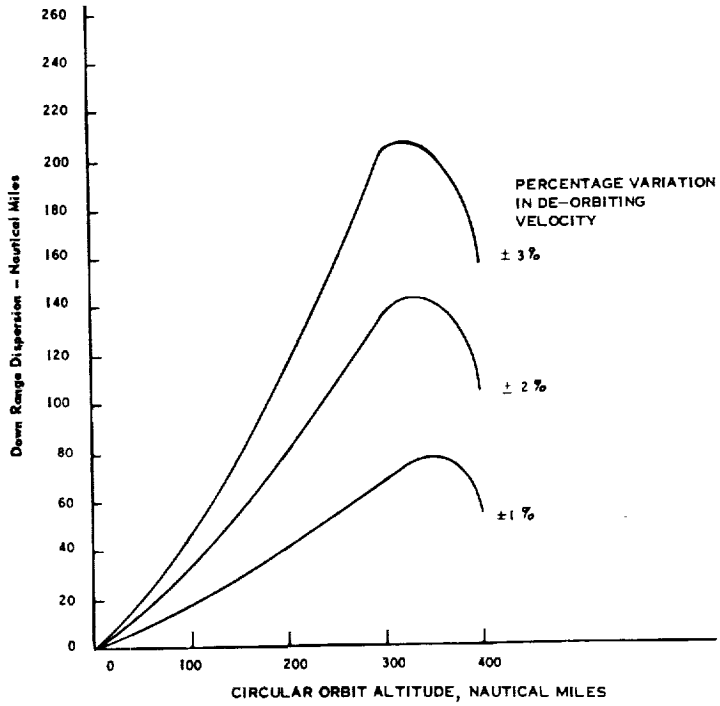

Figure 55. Range Dispersion Due to Deorbiting-Velocity Variations

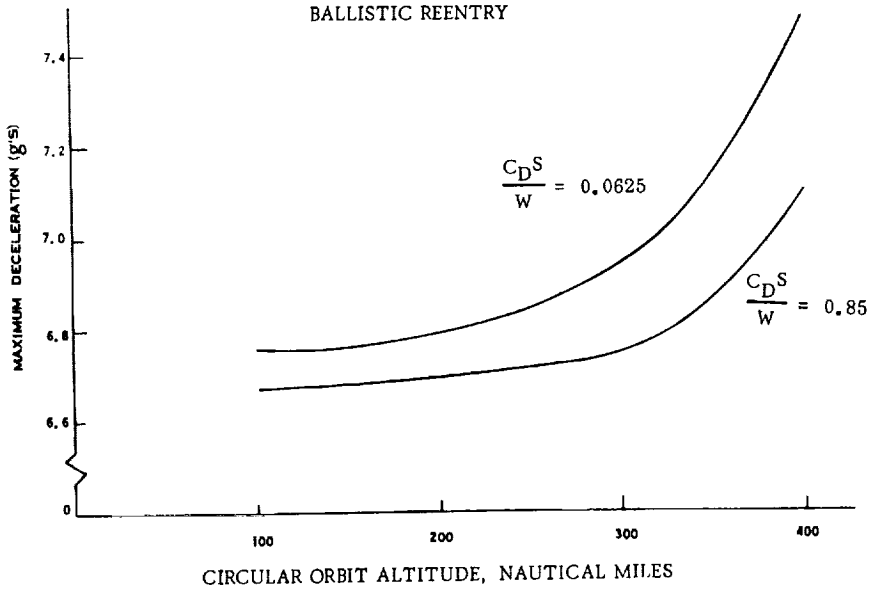

Figure 56. Maximum Reentry Deceleration Using Nominal Deorbiting Impulse

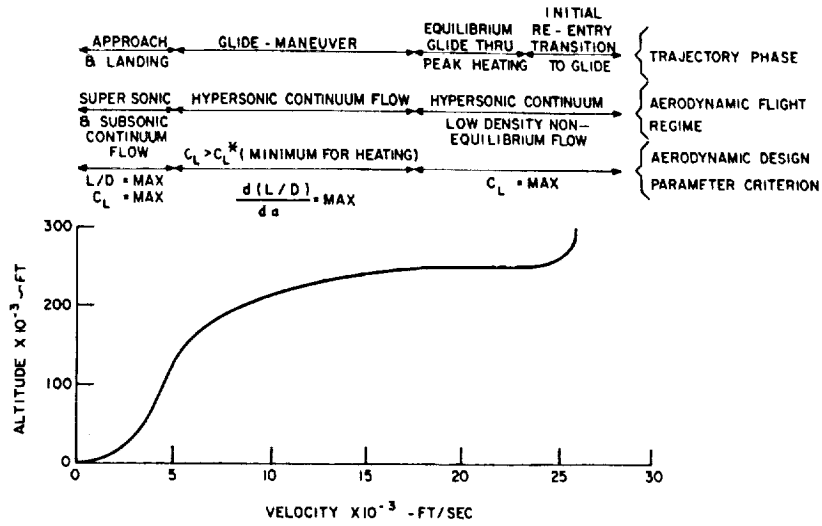

Figure 57. Schematic of Lifting Vehicle Reentry Trajectory

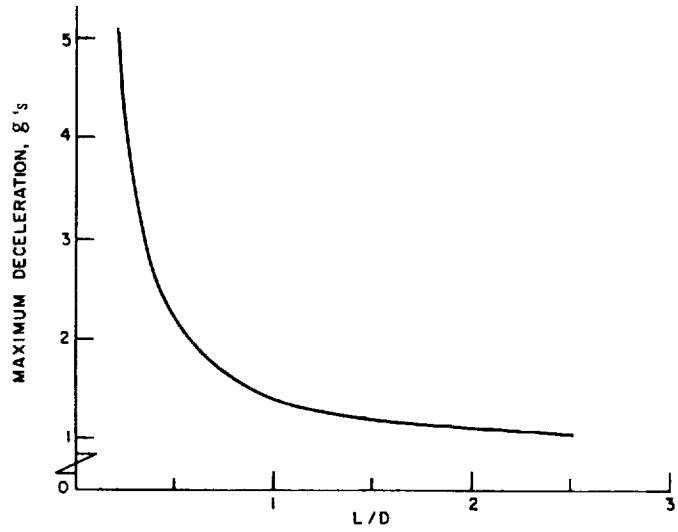

Figure 58. Maximum Deceleration During Lifting Reentry From Orbit

which will ensure rendezvous. This scheme is illustrated in Fig. 59; point (1) indicates the position of the satellite at the moment the rescue vehicle is launched from earth, and point (2) is the position at rendezvous. An operation of this type has already been executed both by the Americans and Russians, and presents no insurmountable problems in principle. However, the adoption of this scheme as a means of rescuing an astronaut in an orbiting vehicle appears doubtful at the moment. First of all,

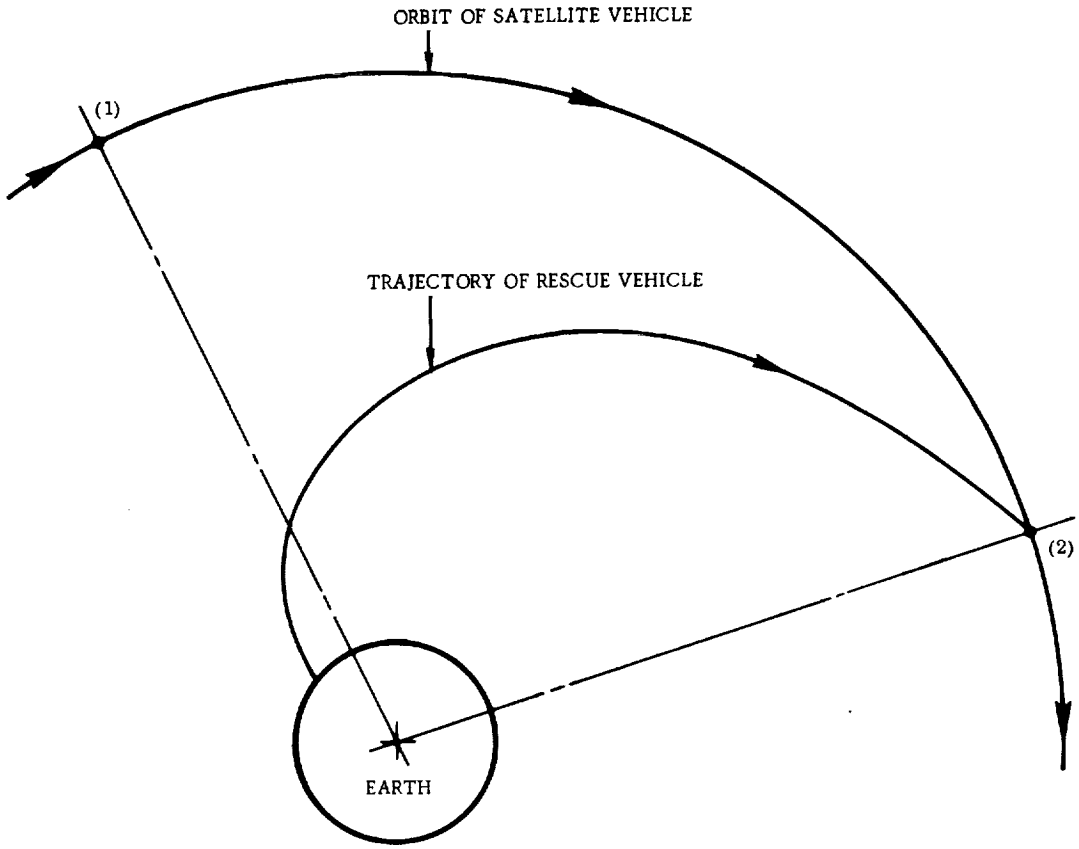

Figure 59. Rescue Via Earth-Based Vehicle

it requires the availability of a launch vehicle in a constant state of readiness, and a flawless launch countdown. Furthermore, considerations of optimum use of available resources suggest that an extensive manned satellite program provide for rescue and retrieval in terms of satellite-based facilities. In this way, abort procedures could readily be incorporated in the preliminary design stages to provide a maximum of crew survival capability with a minimum allocation in terms of weight and fuel. The relevant design philosophies for such a system are discussed in the following section.

3.1.4.3 Rescue Via Satellite-Based Facilities

The basic idea in this approach is that a rescue or retrieval vehicle could be launched from a satellite (space station) in orbit to rendezvous with a satellite in the same or neighboring orbit for the purpose of providing aid in an emergency situation. Specific features of such a scheme will no doubt evolve as more sophisiticated manned space missions begin to take firm shape and sufficient resources are committed to their realization. For present purposes, we will merely explore the general features

of a satellite-based rescue system mainly from the point of view of the problems of orbital transfer, rendezvous conditions, propellant mass ratio requirements, and areas for optimization studies. An analysis of problems of this type will dictate the nature and form of the associated guidance, control, and propulsion requirements.

While orbital transfer problems have been studied intensively for many years, the specific case in which the "interceptor" vehicle achieves a rendezvous with the "target" vehicle, has received less attention. The rendezvous constraint, in fact, adds a new dimension to the problem. Fuel or time optimal maneuvers are not as readily determined. We begin therefore by considering feasible, though not necessarily efficient maneuvers. To simplify the discussion, it will be assumed that the orbits of the interceptor and target vehicles are coplanar. Possible transfer maneuvers in this case are shown in Fig. 60. Parts (a), (b) and (c) of the figure pertain to vehicles on the same circular orbit, and parts (d) and (e) depict transfer between vehicles in different orbits.

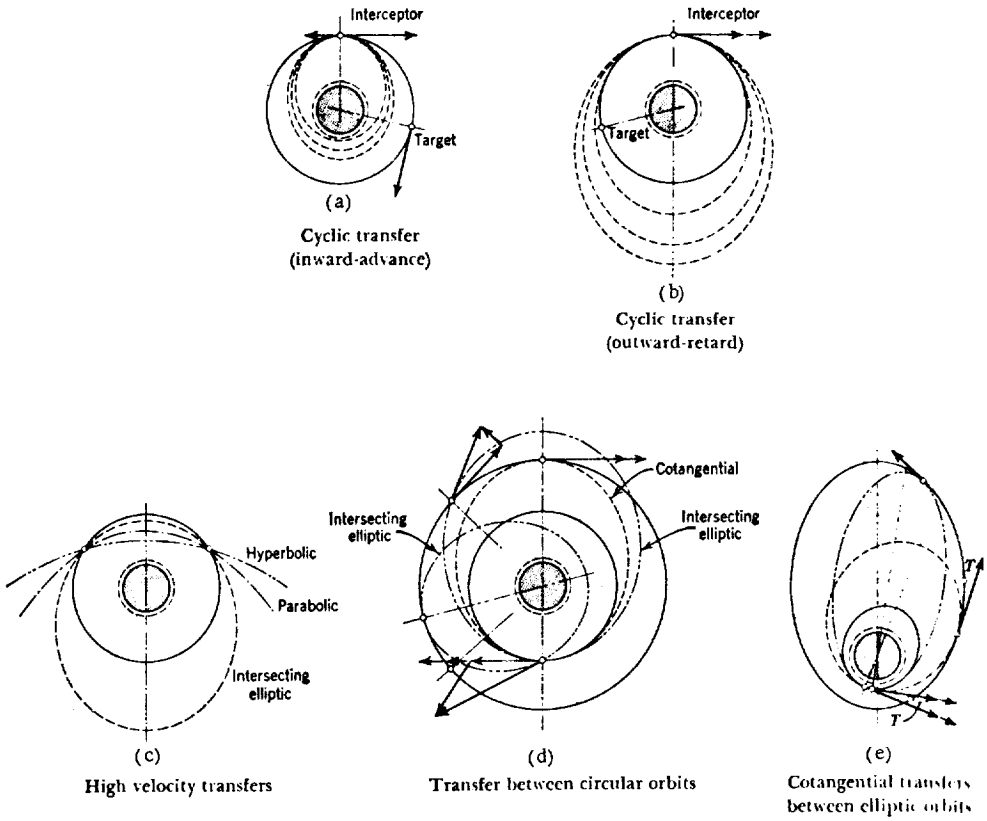

Figure 60. Coplanar Transfer Techniques

To analyze the first of these in more detail, we consider the situation shown in Fig. 61. Here the target vehicle leads the interceptor vehicle by $\Delta\theta$ degrees in the same circular orbit. In order to achieve a rendezvous with the target vehicle, a velocity increment may be applied to the interceptor, causing it to go into the elliptic transfer orbit shown. If the proper ΔV is applied, the interceptor will return to its initial position at a time which coincides with the arrival of the target vehicle. Using the basic relations given in Appendix B, it is a simple matter to show that this velocity increment is given by

$$\Delta V = V_S\left[1 - \sqrt{2 - \left(\frac{2\pi}{2\pi - \Delta\theta}\right)^{2/3}}\right] \tag{13}$$

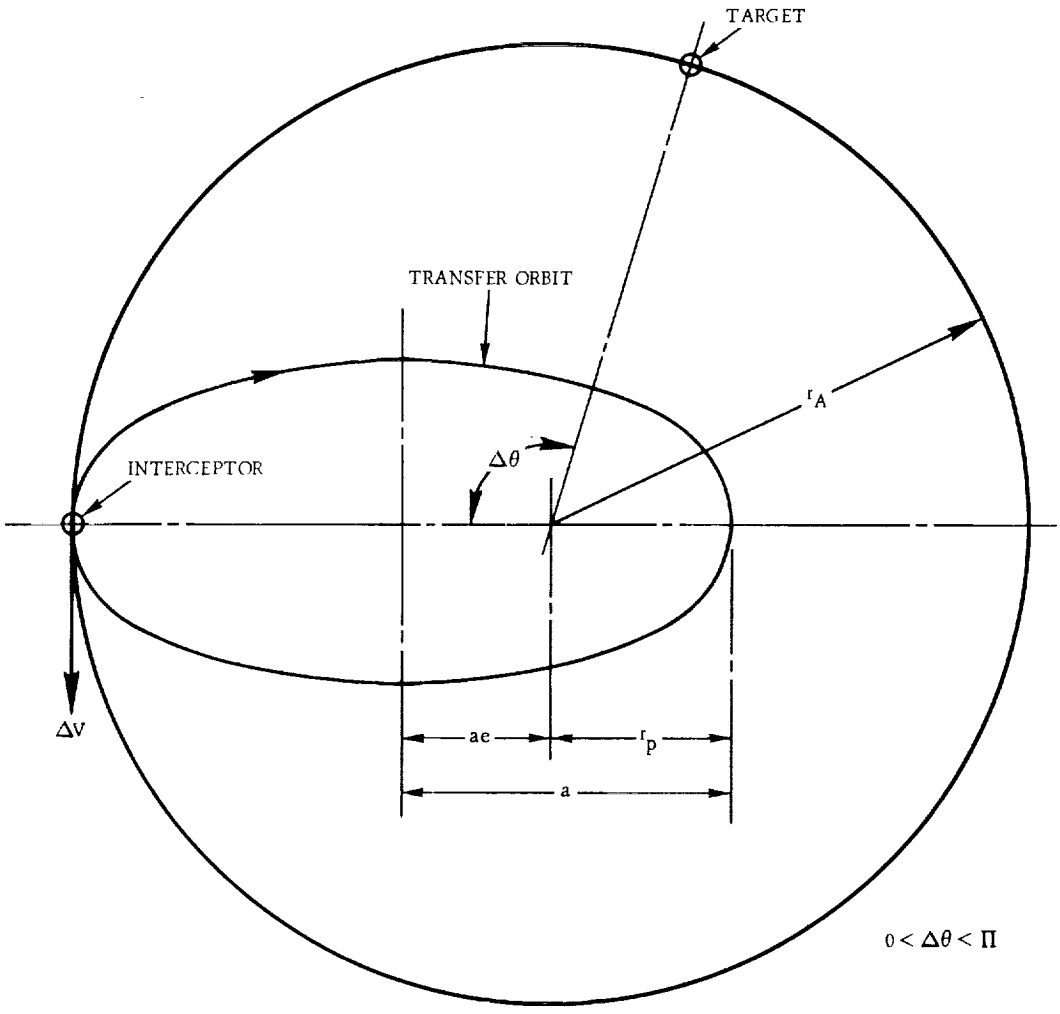

Figure 61. Inward Transfer in Circular Orbit

where

$$V_S = \left(\frac{\mu}{r_A}\right)^{1/2} \tag{14}$$

is the satellite (circular) speed. In this case, the relation between $\Delta\theta$ and r_p, the perigee of the elliptic transfer orbit, is found to be

$$\Delta\theta = 2\pi\left[1 - \left(\frac{r_A - r_p}{2r_A}\right)^{3/2}\right] \tag{15}$$

It is generally required that the vehicle in the transfer orbit remain above the sensible atmosphere at all times. This serves to define an allowable lower limit for r_p. Thus, for a given r_A, the minimum allowable r_p determines the maximum $\Delta\theta$ that can be accommodated by this maneuver. To ascertain some order of magnitude quantities, consider a circular orbit at an altitude of 1000 miles and assume that the atmospheric effects are negligible above a 50-mile altitude. Then

$$r_A = 26.17 \times 10^6 \text{ ft}$$

$$r_p = 21.15 \times 10^6 \text{ ft}$$

$$V_S = 23{,}200 \text{ ft/sec}$$

We find that

$$(\Delta\theta)_{max} = 2\pi\left[1 - \left(\frac{26.17 + 21.15}{2 \times 26.17}\right)^{3/2}\right]$$

$$= 0.882 \text{ rad}$$

$$= 50.5°$$

The required velocity increment is

$$\Delta V = 23{,}200\left[1 - \sqrt{2 - \left(\frac{2\pi}{2\pi - 0.882}\right)^{2/3}}\right]$$

$$= 1{,}260 \text{ ft/sec}$$

The total velocity increment for the maneuver is twice this value since the same ΔV must be applied when the interceptor returns to its initial point in order to recircularize the orbit.

Using Eq. (B19), the total time of the maneuver is obtained as

$$\Delta t = \left(\frac{r_A^3}{\mu}\right)^{1/2} (2\pi - \Delta\theta) = 6{,}090 \text{ sec} = 1.69 \text{ hr}$$

If the lead angle, $\Delta\theta$, is greater than the maximum which can be accommodated by going through one transfer orbit, a multicycle operation is called for. As a matter of fact, the ΔV requirements decrease if multicycle operations are used, even if the given $\Delta\theta$ is within the one cycle capability. The time intervals, however, increase substantially. For example, if the $\Delta\theta = 50.5°$ is reduced to zero by going through two transfer orbits of $\Delta\theta = 25.25°$ each, then the ΔV for each of these two orbits is $\Delta V = 580$ ft/sec or a total of 1,160 ft/sec compared with 1,260 ft/sec for the single cycle case. The time interval is, however, increased to 3.66 hr compared to 1.69 hr.

Similarly for the three cycle case of $\Delta\theta = 16.83°$ each, the total $\Delta V = 1{,}140$ ft/sec but $\Delta t = 5.62$ hr. Obviously, there is a practical limit from the time duration point of view.

If the target vehicle leads the interceptor by an angle greater than 180°, it is preferable to employ an outward elliptic transfer orbit as shown in Fig. 62. Here for

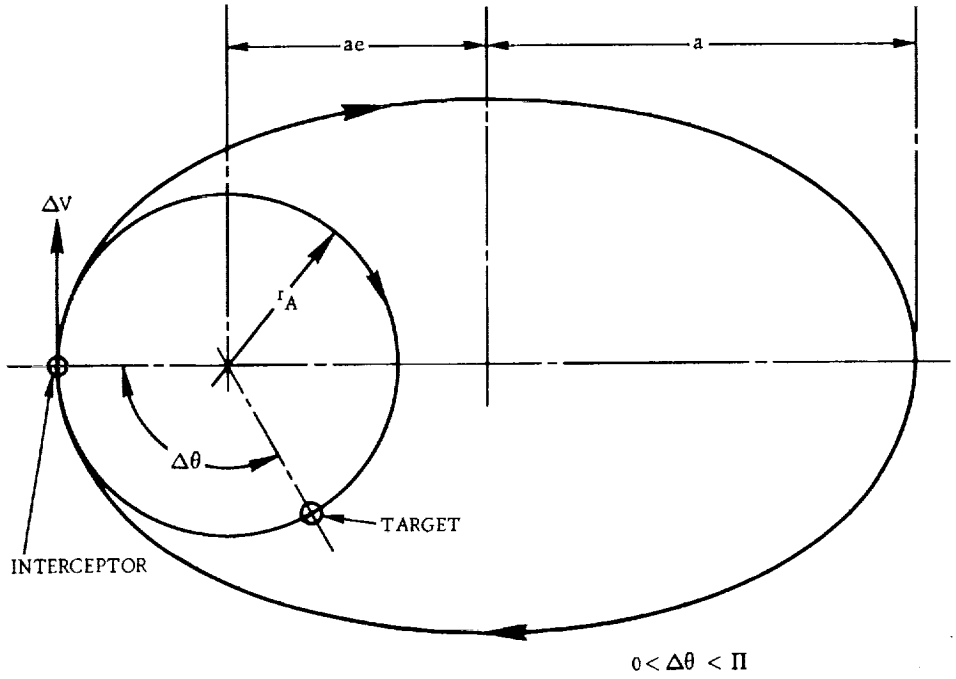

Figure 62. Outward Transfer in Circular Orbit

notational convenience, we call $\Delta\theta$ the lag angle. In this case, the target vehicle traverses an angle $(2\pi + \Delta\theta)$ in orbit as the interceptor completes one cycle on the transfer orbit. The required velocity increment and time duration are now found to be

$$\Delta V = V_S\left[\sqrt{2 - \left(\frac{2\pi}{2\pi + \Delta\theta}\right)^{3/2}} - 1\right] \tag{16}$$

$$\Delta t = \left(\frac{r_A^3}{\mu}\right)^{1/2} (2\pi + \Delta\theta) \tag{17}$$

Velocity increments, as a function of lead angle (for inward transfers) and lag angle (for outward transfer), are shown in Figs. 63 and 64 respectively.

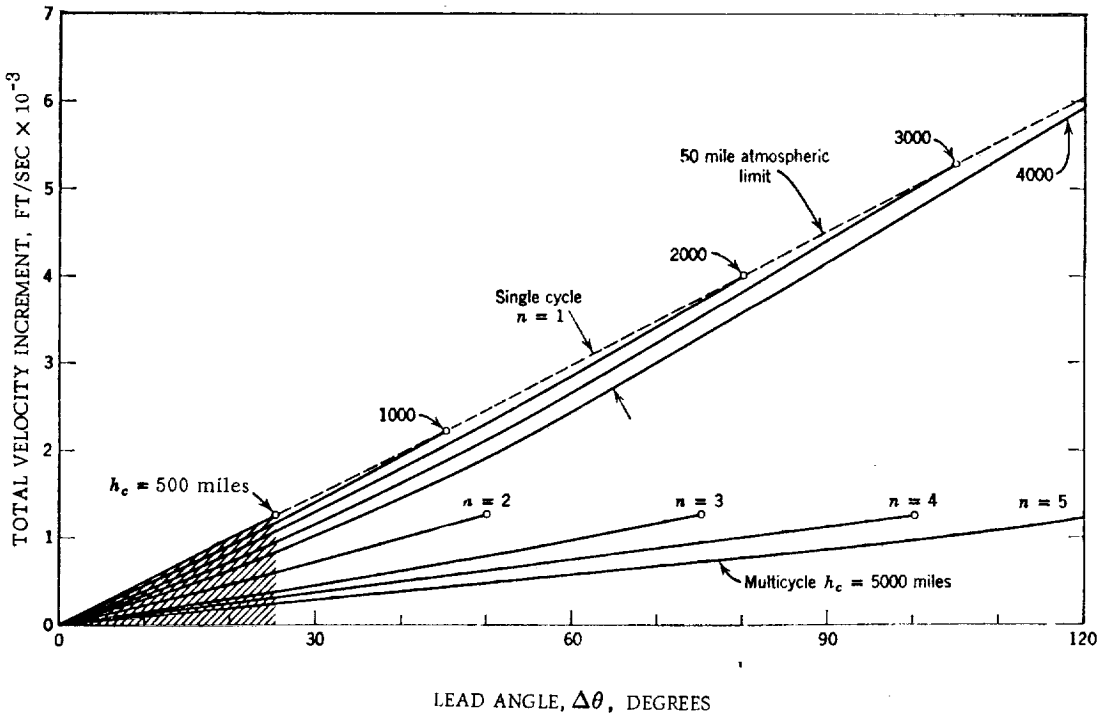

Figure 63. Total Velocity Increment for Cyclic Inward Transfer Between Satellites on the Same Circular Orbit

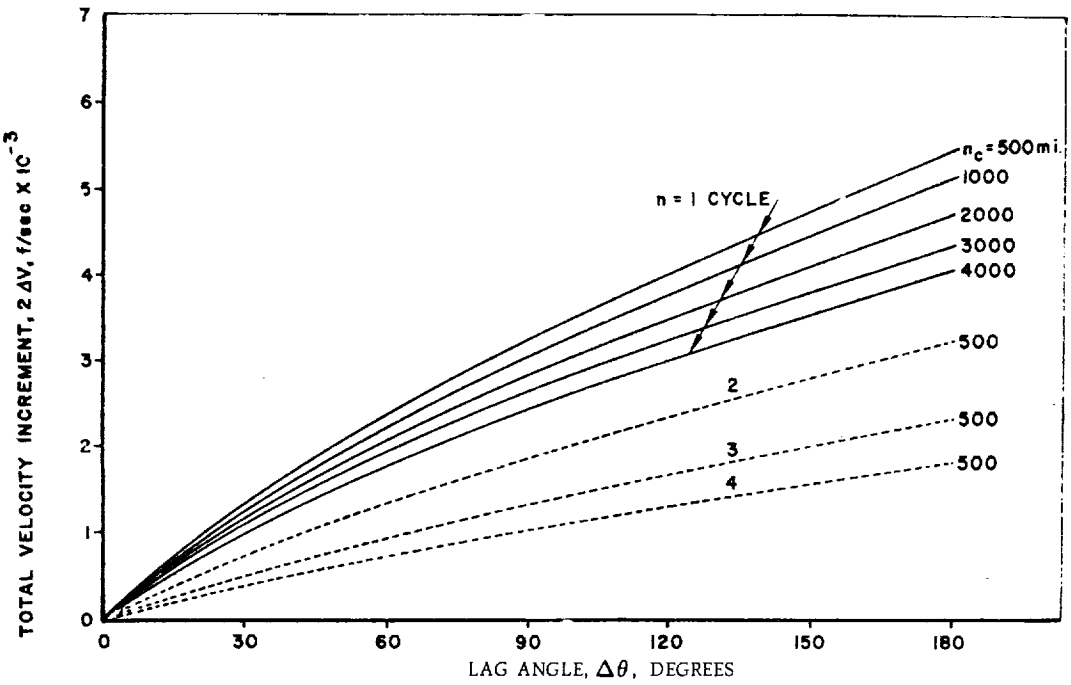

Figure 64. Total Velocity Increment for Cyclic Outward Transfer Between Satellites on Same Circular Orbit

If the target and interceptor vehicles are on different circular orbits, then a minimum energy (fuel) transfer may be accomplished via the Hohmann ellipse as shown in Fig. 65. However a rendezvous will be effected only for one special value of $\Delta\theta$. It is not difficult to show that this value of $\Delta\theta$ must be

$$\Delta\theta = \pi \left[1 - \left(\frac{r_A + r_B}{2 r_B} \right)^{3/2} \right] \tag{16}$$

Thus, in general, in order to achieve a rendezvous, the Hohmann transfer must be followed by an iso-orbital transfer of the type already discussed.†

†Alternately, the interceptor may stay in its own orbit until the required $\Delta\theta$ difference occurs.

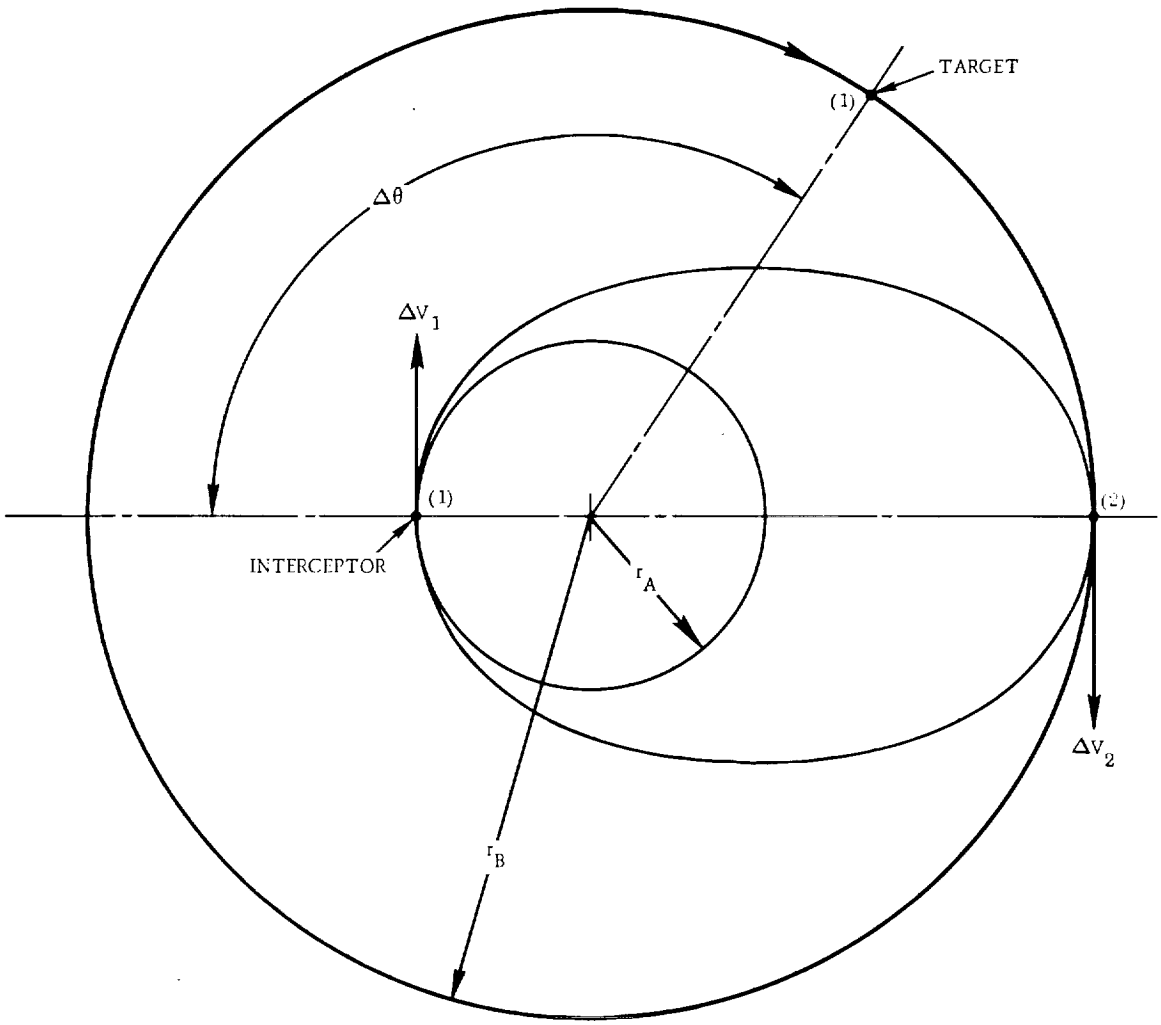

Figure 65. Outward Hohmann Transfer

The necessary velocity increments shown in Fig. 65 are given by

$$\Delta V_1 = \left(\frac{\mu}{r_A}\right)^{1/2}\left[\left(\frac{2\,r_B}{r_A + r_B}\right)^{1/2} - 1\right] \tag{17}$$

and

$$\Delta V_2 = \left(\frac{\mu}{r_B}\right)^{1/2}\left[1 - \left(\frac{2\,r_A}{r_A + r_B}\right)^{1/2}\right] \tag{18}$$

These are plotted in nondimensional form in Figs. 66 and 67. The phase angle, $\Delta\theta$, given by Eq. (16) is plotted in Fig. 68 as a function of the ratio of the orbit radii.

The case of an inward Hohmann transfer between circular orbits is shown in Fig. 69. The required phase angle for rendezvous in this case is

$$\Delta\theta = \pi\left[\left(\frac{r_A + r_B}{2r_A}\right)^{3/2} - 1\right] \tag{19}$$

and is plotted in Fig. 70. In this case, the required ΔV_1 and ΔV_2 are obtained from symmetry considerations from the previous results.

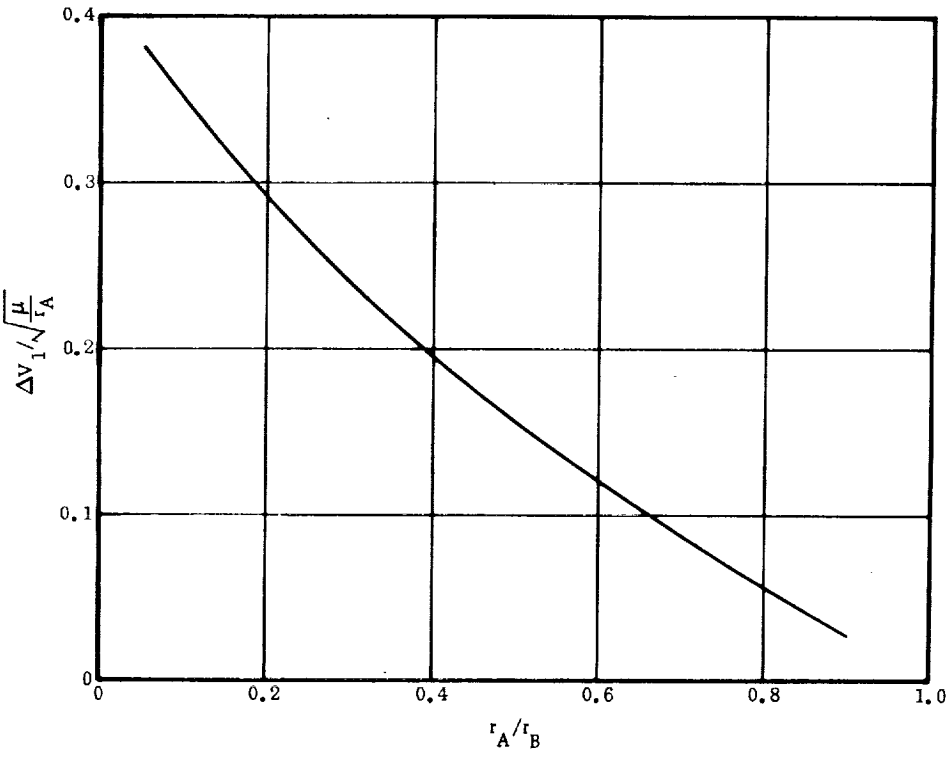

Figure 66. Velocity Increment for Hohmann Transfer

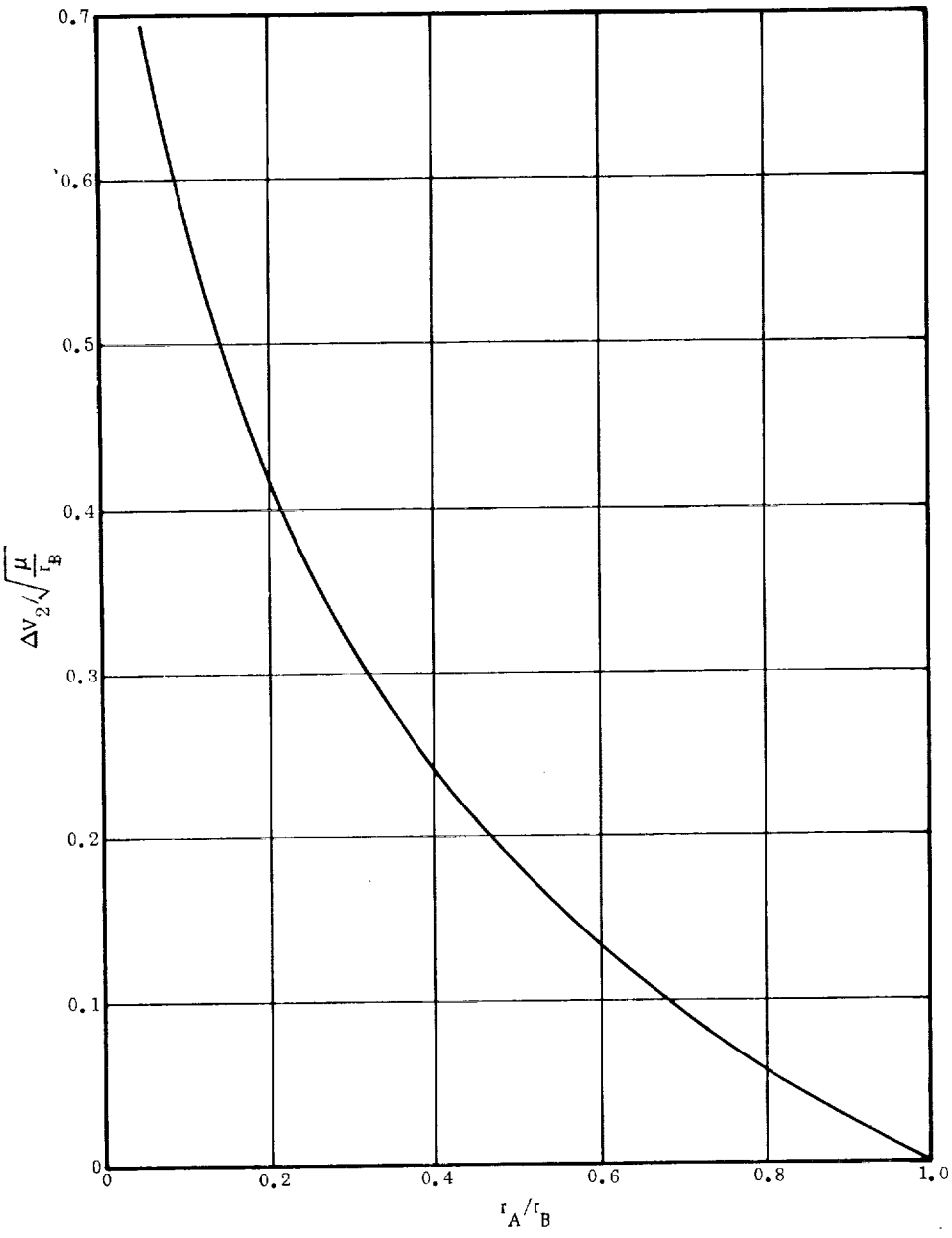

Figure 67. Velocity Increment for Hohmann Transfer

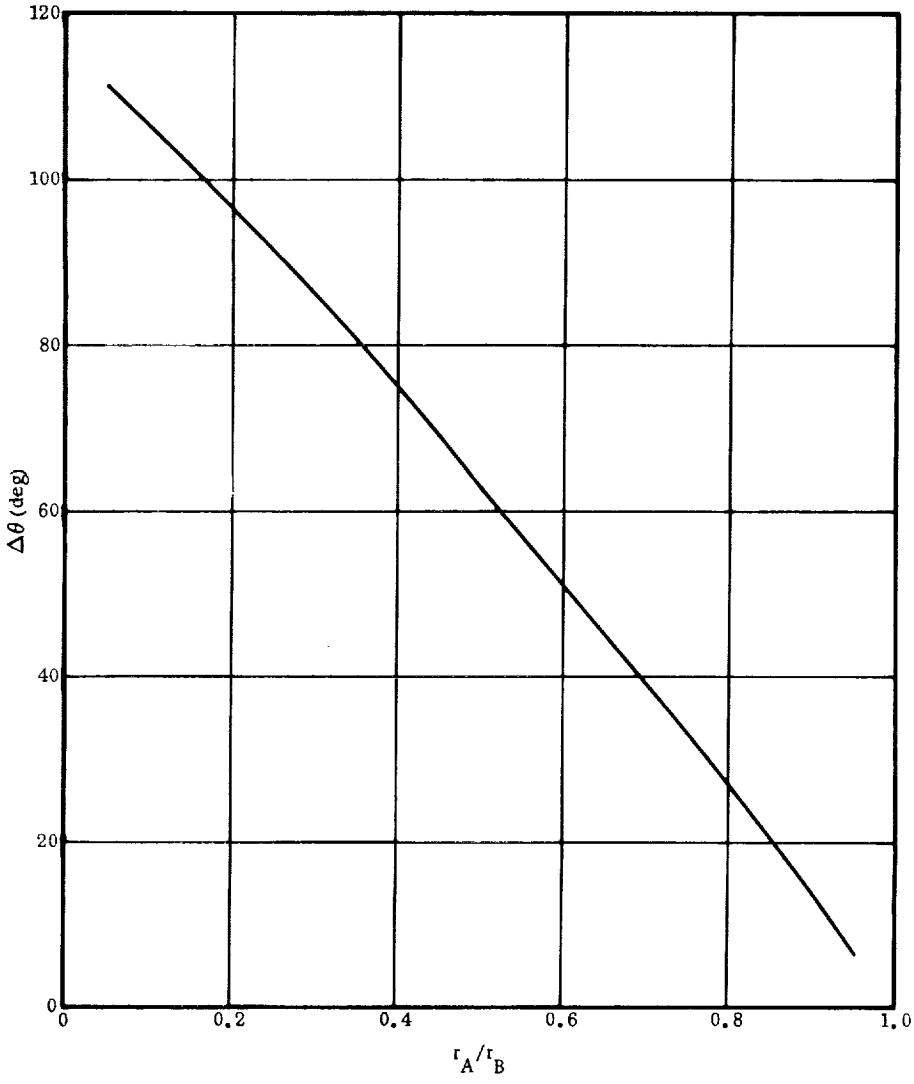

Figure 68. Phase Angles for Outward Hohmann Transfer

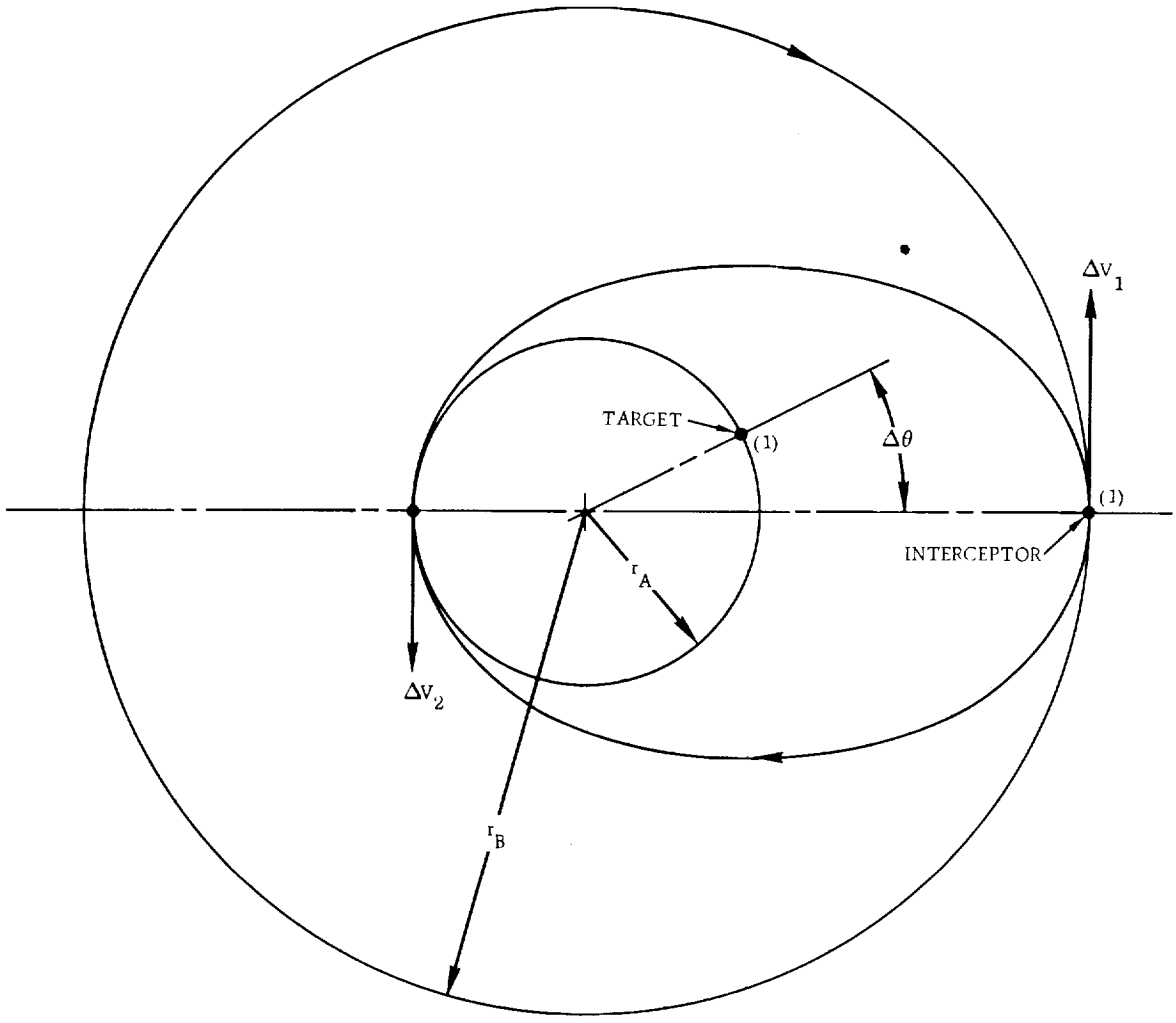

Figure 69. Inward Hohmann Transfer

For purposes of comparison, it is instructive to investigate the high velocity-short time transfers of the type shown in Fig. 60c. A more detailed view is shown in Fig. 71. The initial positions of the target and interceptor are denoted by (1). If the proper ΔV is applied to the interceptor at (1), it will follow a hyperbolic orbit and rendezvous with the target at (2). For definiteness, suppose that the hyperbolic transfer orbit is symmetrical about the line which bisects the angle between (1) and (2). We seek to obtain some insight into the required ΔV and transfer time for this type of

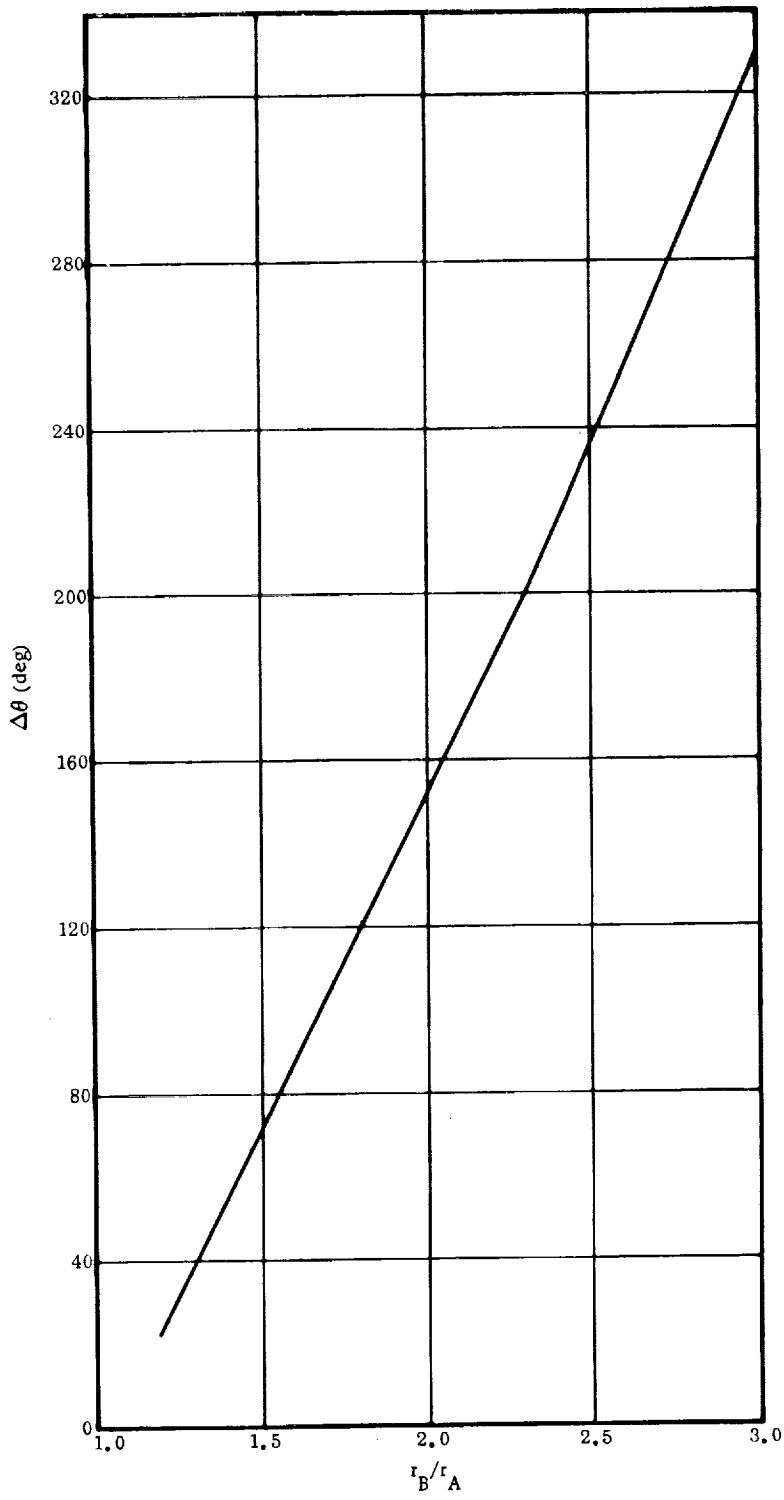

Figure 70. Phase Angles for Inward Hohmann Transfer

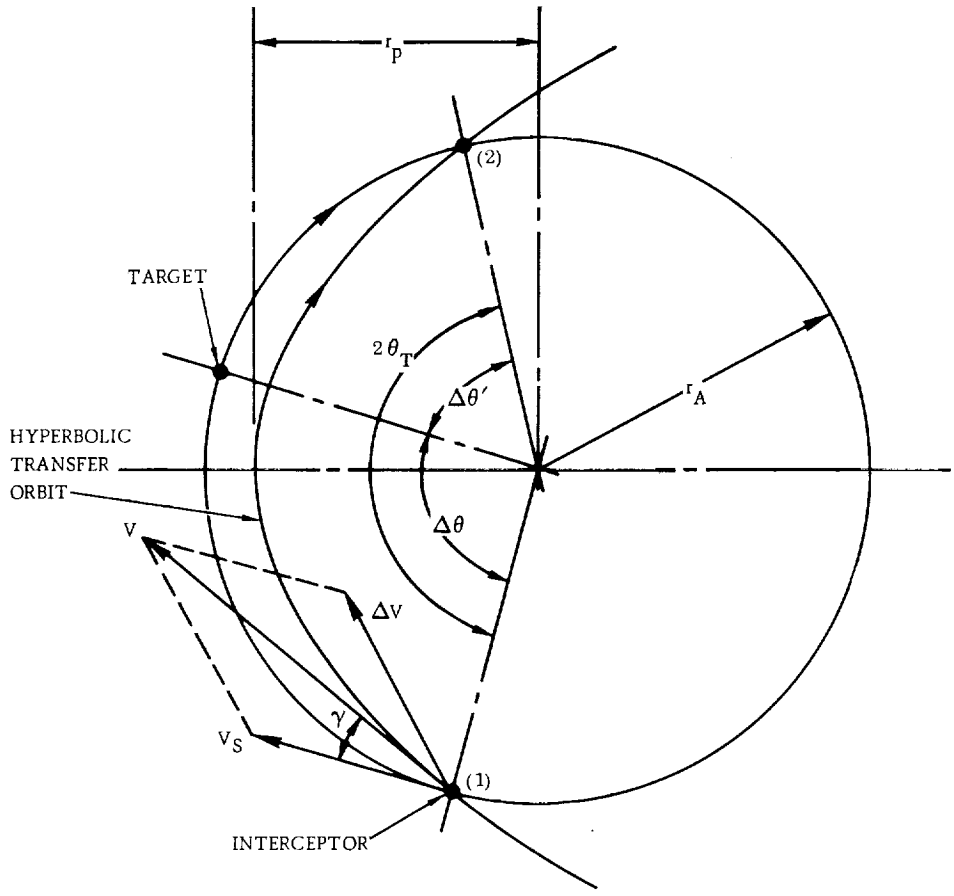

Figure 71. Iso-Orbital Rendezvous Via Hyperbolic Transfer Orbit

maneuver. The following relations for the hyperbolic orbit, given in Appendix B, will be used.

$$\ell = r(1 + e\cos\theta_T) \tag{20}$$

$$\ell = r_p(e + 1) \tag{21}$$

$$r_p = a(e - 1) \tag{22}$$

$$V = \left[\mu\left(\frac{2}{r} + \frac{1}{a}\right)\right]^{1/2} \tag{23}$$

$$\cos\gamma = (1 + e\cos\theta_T)\left[1 + 2e\cos\theta_T + e^2\right]^{-1/2} \tag{24}$$

Transfer time measured from perigee

$$t = \left(\frac{a^3}{\mu}\right)^{1/2} \xi \tag{25}$$

where

$$\xi = \frac{e\sqrt{e^2 - 1}\,\sin\theta_T}{1 + e\cos\theta_T} - \ln\left[\frac{\sqrt{e+1} + \sqrt{e-1}\,\tan\frac{1}{2}\theta_T}{\sqrt{e+1} - \sqrt{e-1}\,\tan\frac{1}{2}\theta_T}\right] \tag{26}$$

From the above relations, it follows that

$$\cos\theta_T = \frac{1}{e}\left[\frac{r_p}{r_A}(e + 1) - 1\right] \tag{27}$$

For some representative values of e and r_p/r_A, we obtain

r_p/r_A	e	θ_T	ξ
0.8	1.2	50.70°	0.0623
0.8	1.4	48.92°	0.1828
0.8	1.6	47.53°	0.2844
0.8	1.8	46.45°	0.4046
0.8	2.0	45.57°	0.5359
0.6	1.2	74.53°	0.1094
0.6	1.4	71.68°	0.2965
0.6	1.6	69.52°	0.5070
0.6	1.8	67.80°	0.7328
0.6	2.0	66.42°	0.9685

It would appear that variations in e have small effect on the angular distance (true anomaly) θ_T, but there are significant variations in ξ, which is a measure of the total time of travel. Thus a requirement of minimum time would imply a minimum eccentricity, e.

To investigate the problem further, we fix the hyperbolic transfer orbit by taking

$$r_p/r_A = 0.8, \quad \text{and} \quad e = 1.2 \tag{28}$$

Now the velocity on the hyperbolic orbit at point (1) or point (2) is given by

$$V = \left(\frac{\mu}{r_p}\right)^{1/2}\left[2\left(\frac{r_p}{r_A}\right) + e - 1\right]^{1/2} \tag{29}$$

We may now calculate the ΔV requirements for circular orbits at various altitudes via the hyperbolic orbit transfer whose parameters are defined by (28). The results of these calculations are summarized below.

Orbital Altitude (miles)	r_A (ft $\times 10^{-6}$)	Circular Velocity (ft/sec)	ΔV (ft/sec)
1,200	27.226	22,740	17,570
10,000	73.69	13,820	10,680
20,000	126.5	10,550	8,150

It is apparent that for near-earth orbits, the ΔV requirements for "short time" transfers are enormous. As a general "rule of thumb," the mass ratio should not exceed about 25% for this type of vehicle. With a specific impulse of 420 sec, this implies a ΔV capability of 4,000 ft/sec. It would appear therefore that this type of maneuver is impractical at the present state of the art, at least for near-earth orbits.

As a matter of interest, in order to compare the transfer times for different types of maneuvers, we may proceed as follows.

The transfer time for the target vehicle (Fig. 71) in going from (1) to (2) is

$$\left(\frac{r_A^3}{\mu}\right)^{1/2}\Delta\theta'$$

The interceptor, in going from (1) to (2) via the hyperbolic orbit, has a transfer time given by

$$2\left(\frac{a^3}{\mu}\right)^{1/2}\xi$$

Equating the above expressions and solving for $\Delta\theta'$, we have

$$\Delta\theta' = \frac{2}{(e-1)^{3/2}}\left(\frac{r_p}{r_A}\right)^{3/2}\xi \tag{30}$$

For the 1,200-mile orbit, and parameters given by (28), we find

$$\Delta\theta' = 0.997 \text{ rad} = 57.13°$$

$$\Delta t = 1{,}194 \text{ sec}$$

$$\Delta\theta = 2\theta_T - \Delta\theta'$$

$$= 0.773 \text{ rad} = 44.27°$$

We note, incidentally, that $r_p = 0.8\, r_A = 21.78 \times 10^6$ ft, so that the nearest point of the hyperbolic orbit to the earth's surface is above the 50-mile atmospheric limit.

To effect a rendezvous on a 1,200-mile circular orbit with $\Delta\theta = 44.27°$ using an inward transfer (Fig. 61), the corresponding ΔV and transfer time are found to be

$$\Delta V = 1{,}060 \text{ ft/sec}$$

$$\Delta t = 6{,}600 \text{ sec}$$

The ΔV requirement is realistic although the transfer time is increased by a factor of about 5.5.

An essentially similar analysis can be performed for hyperbolic transfer between concentric circular orbits as shown in Fig. 72. The hyperbolic orbit is assumed to have an axis of symmetry, which is the line defined by position (1) of the interceptor and the center of attraction. This serves to define the perigee, $r_p = r_A$. Furthermore, θ_T is obtained from

$$\cos\theta_T = \frac{1}{e}\left[\frac{r_A}{r_B}(e+1) - 1\right] \tag{31}$$

Thus, for representative values of e, we find (taking $r_A/r_B = 2/3$)

e	θ_T	ξ
1.2	67.17°	0.0945
1.4	64.62°	0.2464
1.6	62.72°	0.4211
1.8	61.22°	0.6099
2.0	60.00°	0.8069

The same general conclusions can be drawn relative to variations in e as for the iso-orbital transfer discussed previously.

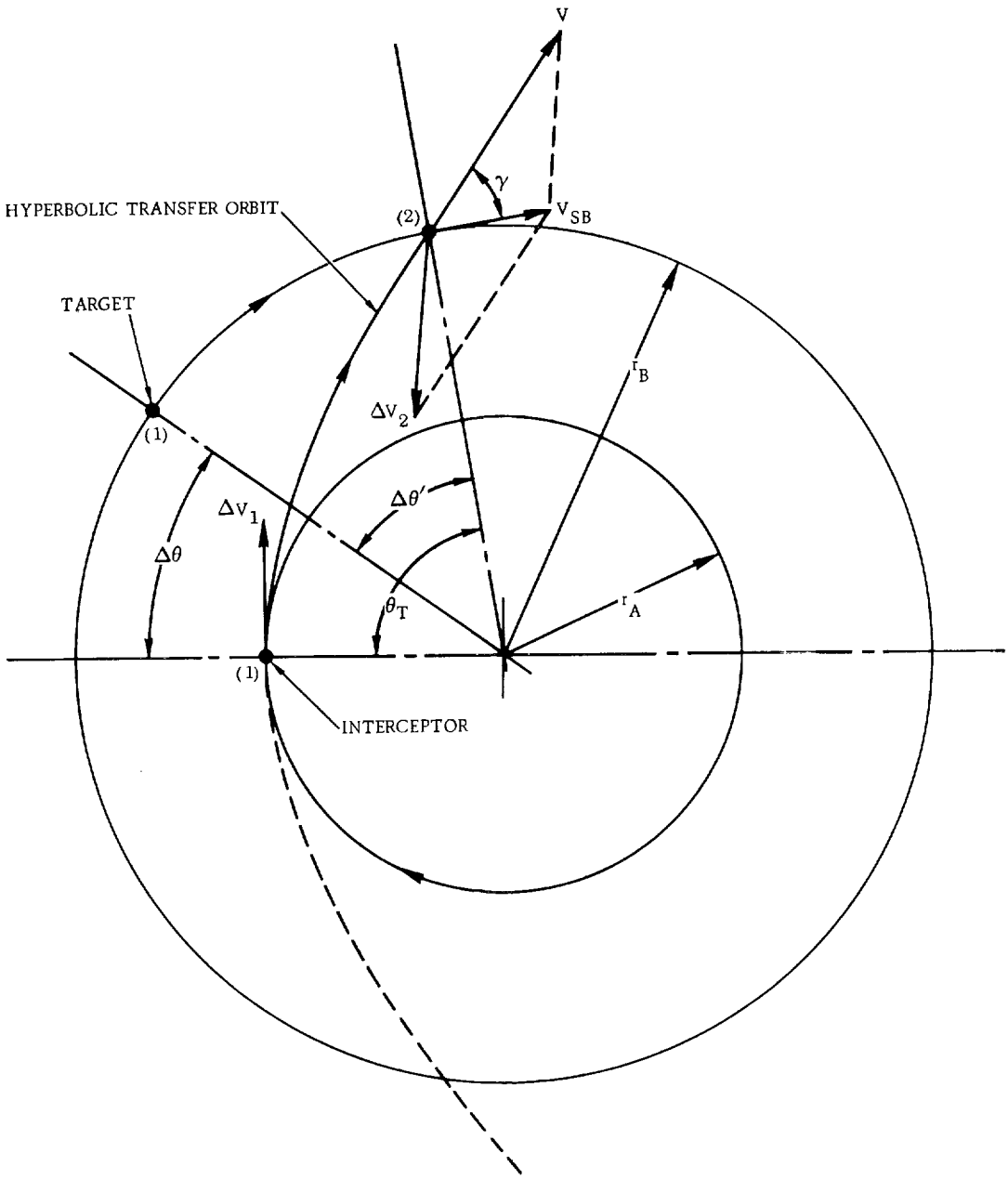

Figure 72. Rendezvous Via Direct Hyperbolic Transfer Orbit

Equating the time required for the target vehicle to travel from (1) to (2) to the time required for the interceptor to go from (1) to (2) along the hyperbolic path, we find

$$\Delta\theta' = \frac{\xi}{(e-1)^{3/2}}\left(\frac{r_A}{r_B}\right)^{3/2} \tag{32}$$

With e = 2.0, we obtain

$$\Delta\theta' = 25.30°$$

$$\Delta\theta = 34.85°$$

Now with

$$r_A = 23.53 \times 10^6 \text{ ft (500-mile orbit)}$$

we have

$$r_B = 1.5\, r_A = 35.29 \times 10^6 \text{ ft}$$

$$\Delta t = 776 \text{ sec}$$

The velocities on the hyperbolic orbit are at point (1);

$$V_1 = 42{,}360 \text{ ft/sec}$$

at point (2):

$$V_2 = 37{,}360 \text{ ft/sec}$$

From which we find (see Fig. 72)

$$\Delta V_1 = 17{,}900 \text{ ft/sec}$$

$$\Delta V_2 = 24{,}750 \text{ ft/sec}$$

With $r_A = 73.69 \times 10^6$ ft (10,000-mile orbit) and other parameters remaining unchanged, the required velocity increments reduce to

$$\Delta V_1 = 10{,}120 \text{ ft/sec}$$

$$\Delta V_2 = 13{,}980 \text{ ft/sec}$$

For purposes of comparison, an outward Hohmann transfer (Fig. 65) with

$r_A = 23.53 \times 10^6$ ft $\qquad r_A/r_B = 2/3$

$\Delta\theta = 34.85°$

results in

$\Delta V_1 = 2{,}450$ ft/sec

$\Delta V_2 = 2{,}100$ ft/sec

$\Delta t = 10{,}000$ sec

The foregoing analyses are illustrative of the following general result:

Short-time hyperbolic orbital transfers require intolerably large velocity increments especially for low orbital altitudes. They become feasible only for very large orbital altitudes (on the order of tens of thousands of miles).

3.1.4.3.1 Optimality Considerations

Most optimal orbital transfer problems studied thus far have been of the non-rendezvous type. In general, when a rendezvous constraint is specified, the problem is enormously complicated. A few simple results are available, however, for optimal transfer and rendezvous between coplanar concentric circular orbits. The Hohmann transfer of Fig. 65, for example, is the fuel optimal transfer if waiting time in the initial orbit is allowed.†

In general, the following factors affect both the formulation and solution of the optimal transfer problem:

a. Is waiting in the initial orbit permitted?

b. Are intermediate parking orbits permitted?

c. Is there a restriction on the allowable number of velocity impulses?

Furthermore, it is often impractical to specify a firm optimality criterion. For example, a fuel optimal maneuver may incur an intolerably high transfer time.

† If the ratio of radii exceeds 11.94, then it is known that a three impulse-bi elliptic transfer is optimal.

A semirational empirical approach to the problem might proceed as follows. Suppose that n velocity impulses are allowed. Then

$$\sum_{i=0}^{n-1} t_i = t_n \tag{33}$$

Here t_i is the time spent by the interceptor on the i^{th} orbit, and t_n is the flight time of the target; t_0 is the waiting time on the initial orbit. Eq. (33) is merely a statement of the rendezvous constraint; namely, that the flight time of the interceptor and target must be equal. In principle, one may calculate the minimum total transfer time, t_m, for a given total ΔV, as a function of n or t_i or both. Writing $U = \sum_{i=1}^{n} \Delta V_i$, the plotted results might appear as shown in Fig. 73. This permits the the determination of an absolute minimum t_m. The complexity of this calculation depends, of course, on the allowable degrees of freedom; i.e., how many parameters may be varied in the optimization procedure.

At present, few general results are available and there is still much to be done with this problem.

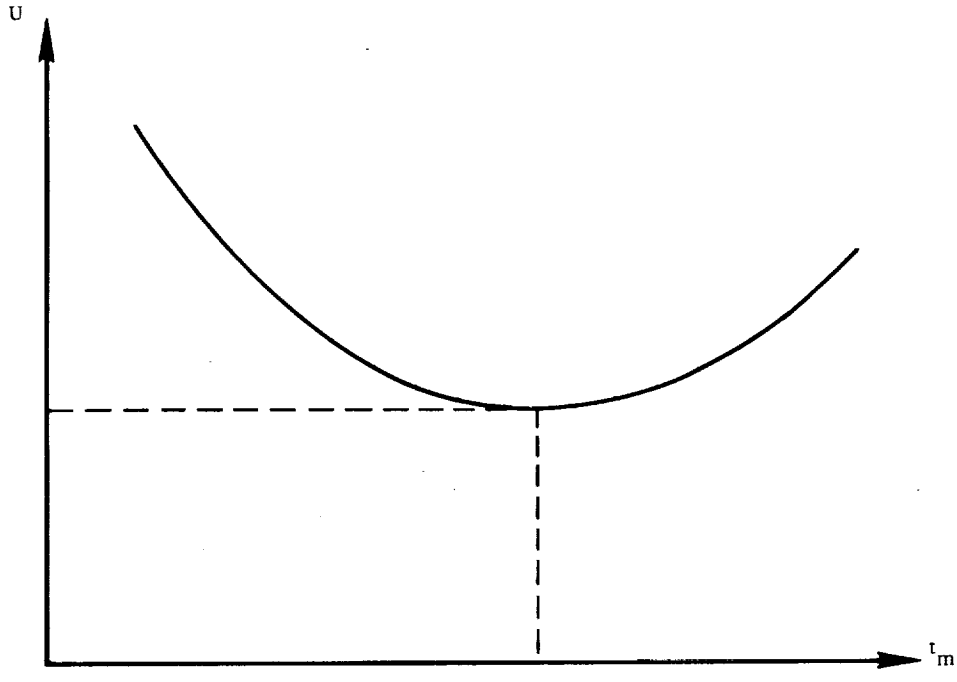

Figure 73. Total Velocity Increment Versus Minimum Time

3.1.4.3.2 Terminal Guidance

At the conclusion of the orbital transfer maneuver, a docking operation will usually be required between the target and interceptor vehicles. Since a theoretically perfect intercept cannot be accomplished in practice, the intercept vehicle must have a certain amount of terminal guidance capability. A discussion of this problem, however, is beyond the scope of the present monograph. An introductory exposition of this topic together with selected references is contained in Chap. 9 of Ref. 39.

3.1.5 Lunar Mission Abort

A typical circumlunar trajectory is shown in Fig. 74. From the point of view of abort considerations, this may be divided into three regions:

a. From point A, where the vehicle is launched into the circumlunar orbit, to some point B. The location of B is such that in the region A to B, a velocity increment may be applied to return the vehicle to earth in less time than the duration of the complete circumlunar mission.

b. In the region B to C. This is the immediate vicinity of the moon where the application of velocity increments is either of marginal value in expediting a return to earth, or else involves highly complex computations.

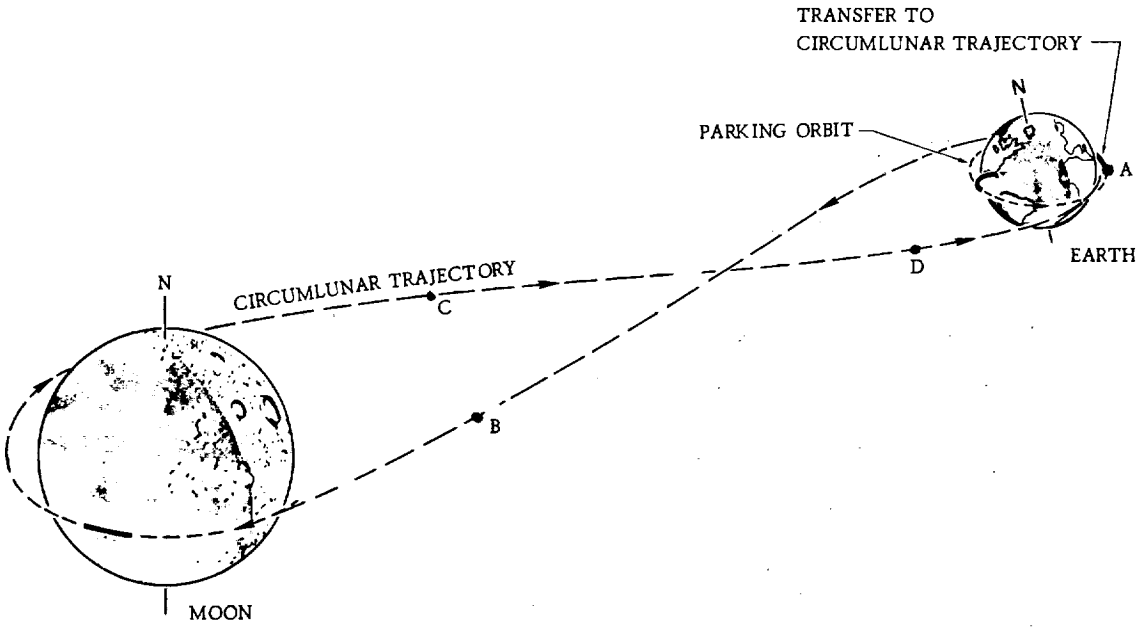

Figure 74. Typical Trajectory for a Lunar Mission

c. In the region C to D. On this portion of the trajectory the vehicle is already on its return route, and the main reason for applying velocity increments is to decrease the return flight time. Beyond some point D, the potential reduction in flight time decreases while the entry velocity penalty increases as the vehicle moves nearer the earth.

The regions a and b above are often called the midcourse regions. The abort problem during this phase of the mission is discussed in Sec. 3.1.5.1. Problems associated with abort from a lunar parking orbit are discussed in Sec. 3.1.5.2.

3.1.5.1 Midcourse Region

It does not appear likely that an abort system designed for the atmospheric phase of flight could be used for abort during the midcourse region of a circumlunar trajectory since the points of emphasis are reversed. An abort in the atmosphere must be executed immediately, must have very high thrust, but requires only moderate aiming accuracy. On the other hand, a midcourse abort has less need for speed of execution, but requires high aiming accuracy.

Should an abort condition occur in the midcourse region, it is usually desirable to effect a return to earth in the shortest possible time. The primary constraints are the velocity increment capability of the vehicle, and the need to ensure safe entry conditions.

In order to simplify the analytical formulation, the gravitational effects of the sun and moon will be neglected. The manner in which this assumption compromises the results obtained will be discussed later.

As shown by Merrick and Callas,[6] the direction of abort thrust for a minimum time abort may then be determined in a very simple way. First of all, a safe entry condition may be ensured by specifying an appropriate flight path angle at the entry altitude. Furthermore, the abort trajectory (whether elliptic or hyperbolic) may be defined in terms of a vacuum perigee and the eccentricity. The situation is illustrated in Fig. 75.

From the relations given in Appendix B, it is readily found that the flight path angle, at any point on a conic trajectory, is given by

$$\tan\gamma = \frac{1}{r_p\sqrt{1+e}}\left[2r_p r - r_p^2(1+e) - r^2(1-e)\right]^{1/2} \qquad (34)$$

For eccentricities between 0.85 and 1.15, the corresponding flight path angle at the entry altitude (taken as 400,000 ft = 121.92 km) is 4° 25' ±10' for a specified vacuum perigee of 6,450 km.

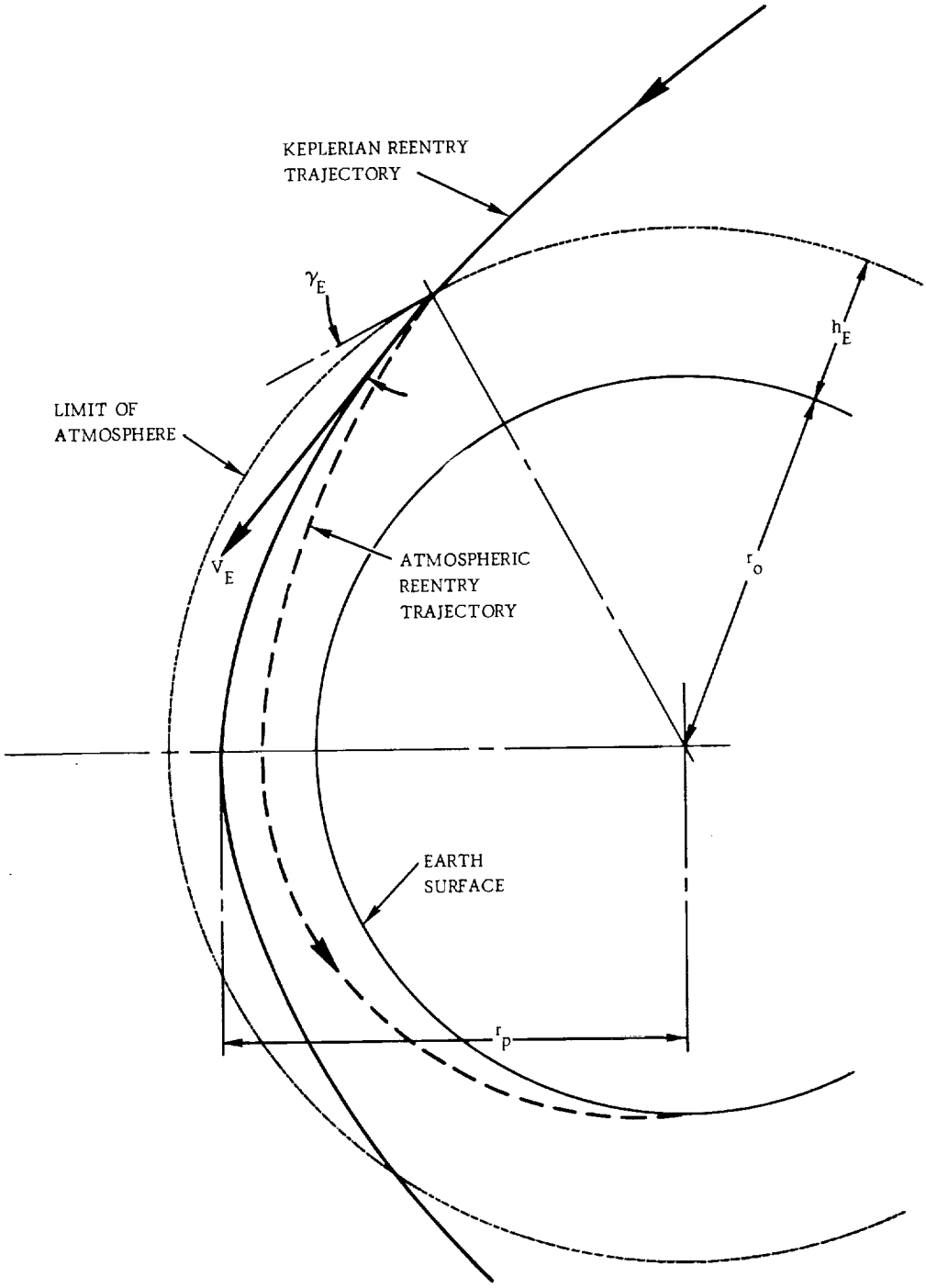

Figure 75. Reentry Geometry

Now the general equation of a conic trajectory is

$$V^2 = \mu\left[\frac{2}{r} + \frac{(e - 1)}{r_p}\right] \tag{35}$$

At perigee

$$V_{per}^2 = \frac{\mu}{r_p}\left[2 + (e - 1)\right] \tag{36}$$

Therefore

$$V^2 - V_{per}^2 = 2\mu\left(\frac{1}{r} - \frac{1}{r_p}\right)$$

Since the angular momentum immediately after abort is the same as the angular momentum at perigee, we have

$$V_{per}\, r_p = V_H\, r$$

Also

$$V^2 = V_H^2 + V_R^2$$

Combining the above three equations, we obtain

$$V_H^2 = \frac{r_p^2}{(r^2 - r_p^2)} V_R^2 + \frac{2\mu\, r_p}{r\,(r + r_p)} \tag{37}$$

This is a hyperbola in the $V_H V_R$ plane and represents another form of the general conic equation. A quantitative indication of the velocities which must exist after an abort firing is shown in Fig. 76. The velocity hodograph, which represents Eq. (37), is shown in Fig. 77 for fixed values of r_p and r.

The total velocity vector achievable by an abort firing is the vector sum of V_0, the velocity just prior to abort, and ΔV, the velocity increment capability of the vehicle. Referring to Fig. 77, the achievable velocities which will effect a safe entry† are those that lie on the circle and also on the hodograph. Several possibilities exist. First of all, if the circle of achievable velocities is very small (corresponding to a

†A safe entry is one for which the entry flight path is within prescribed limits.

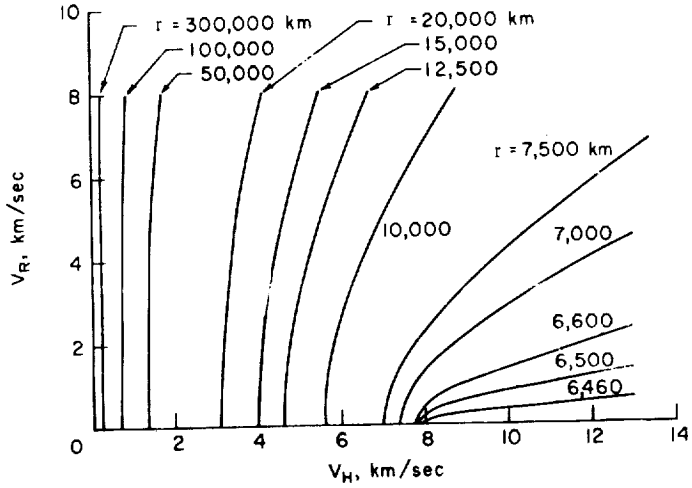

Figure 76. Velocity Hodograph for Perigee Radius of 6,450 km

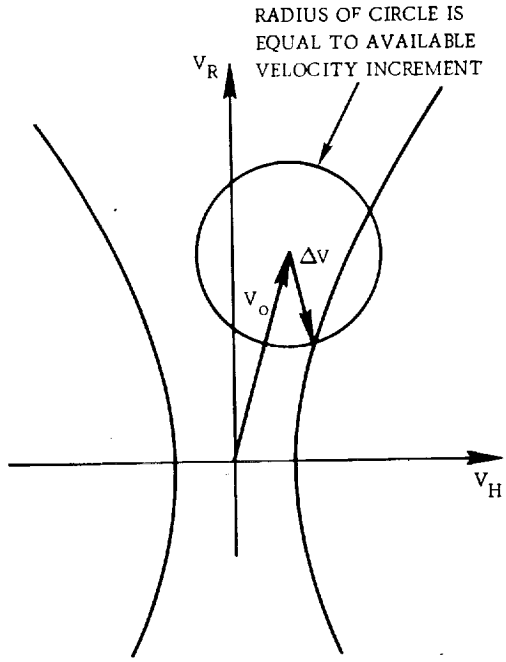

Figure 77. Hodograph of Abort Trajectory

negligible velocity increment), no solutions exist. This corresponds to a condition whereby the vehicle has run out of fuel or has a damaged engine. In this case, reentry conditions cannot be altered.

If the circle of achievable velocities is somewhat larger, or if the symmetrical branches of the hodograph are closer together (because of increased range; see Fig. 76) then there will be one branch of the hodograph going through the circle as shown in Fig. 77.

The third possibility is that both branches of the hodograph go through the circle of achievable velocities. A solution on the left branch of the curve corresponds to an abort maneuver in which the direction of the spacecraft's orbit about the earth is reversed.

For present purposes, we are primarily concerned with that achievable point on the hodograph for which the flight

time to perigee is a minimum. It is shown by Merrick and Callas[6] that this minimum time is associated with that point on the achievable hodograph for which V_R is an algebraic minimum. This is the situation depicted in Fig. 77.

The above results, which are based on two-body gravitational effects (i.e.; neglecting the influence of the sun and moon), are attractive from the point of view of minimizing onboard computational facilities. The errors incurred in this approximation are shown in Fig. 78, in which perigee miss distance is plotted versus range at abort foı selected values of ΔV. Actual perigee values were calculated using the four-body gravitational equations (earth, moon, sun system). As expected, for modest values of range at abort, the errors are small. However, the errors become substantial for large abort range and small ΔV.

For purposes of keeping onboard computational equipment at a modest level, Merrick and Callas[6] develop a so called "modified" two-body analysis which maintains the error at reasonable levels for ranges beyond 100,000 km. This in turn requires that each lunar trajectory be treated individually. The reader may consult Ref. 6 for details.

A summary of the data relating minimum return time to range at abort is presented in Figs. 79 and 80 for the outbound and return legs of a typical circumlunar trajectory. The fact that minimum time to return decreases with ΔV capability is of course in accord with intuitive considerations. At less than 0.5 km/sec, the abort capability is marginal. Indeed, Fig. 81, which is a plot of total time from injection to perigee versus range at abort, shows that an abort which is accomplished at outbound ranges greater than 277,000 km, with $\Delta V = 0.5$ km/sec, is valueless since a quicker return is accomplished by doing nothing. It is also interesting to note that for the lower abort velocities, it is possible to return more quickly by aborting on the return leg of the mission even before the space vehicle has accomplished half of the trip (in terms of hours to the moon). The data of Fig. 81 determines the location of point B in Fig. 74.

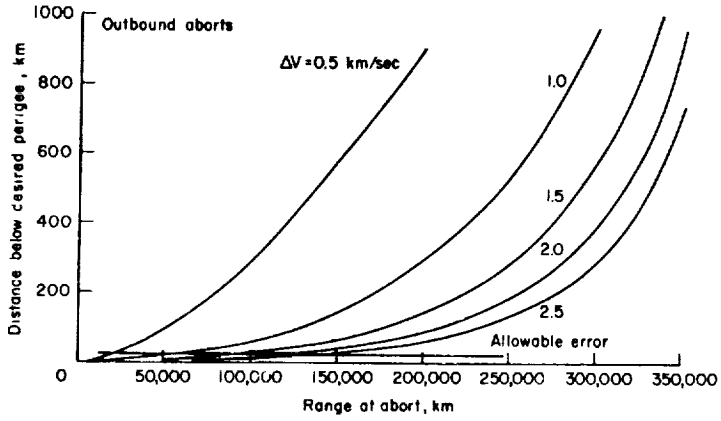

Figure 78. Perigee Miss Distance Due to Two-Body Guidance Law

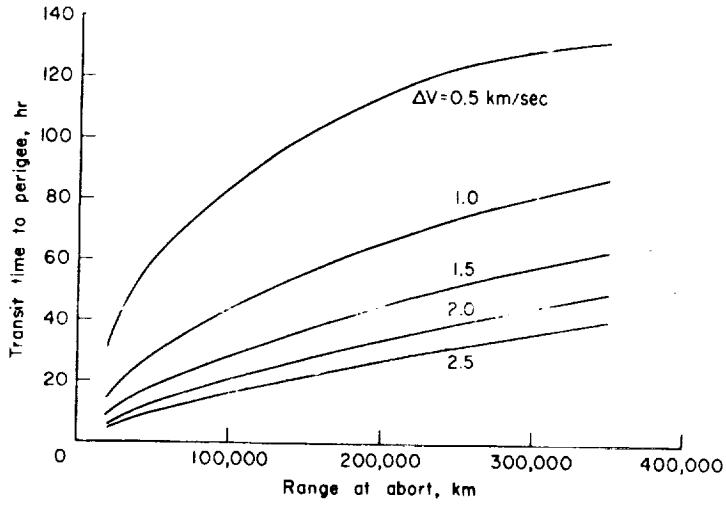

Figure 79. Flight Time From Abort to Perigee; Outbound Leg

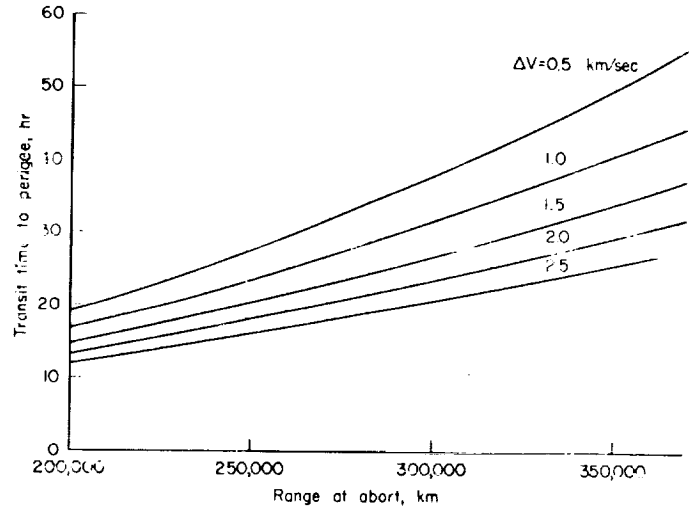

Figure 80. Flight Time From Abort to Perigee; Return Leg

For specific missions, preprinted graphical representations of the hodograph equation, similar to that shown in Fig. 76, can be made available to the astronaut. This, together with current estimates of the range, horizontal, and vertical velocity can be used to determine the abort thrust magnitude and direction, which will accomplish either a minimum time or other type of abort trajectory. This can be done even if the onboard computer and earth communication link have failed. The primary requirement is merely a capability for a reasonable estimate of the range and velocity.

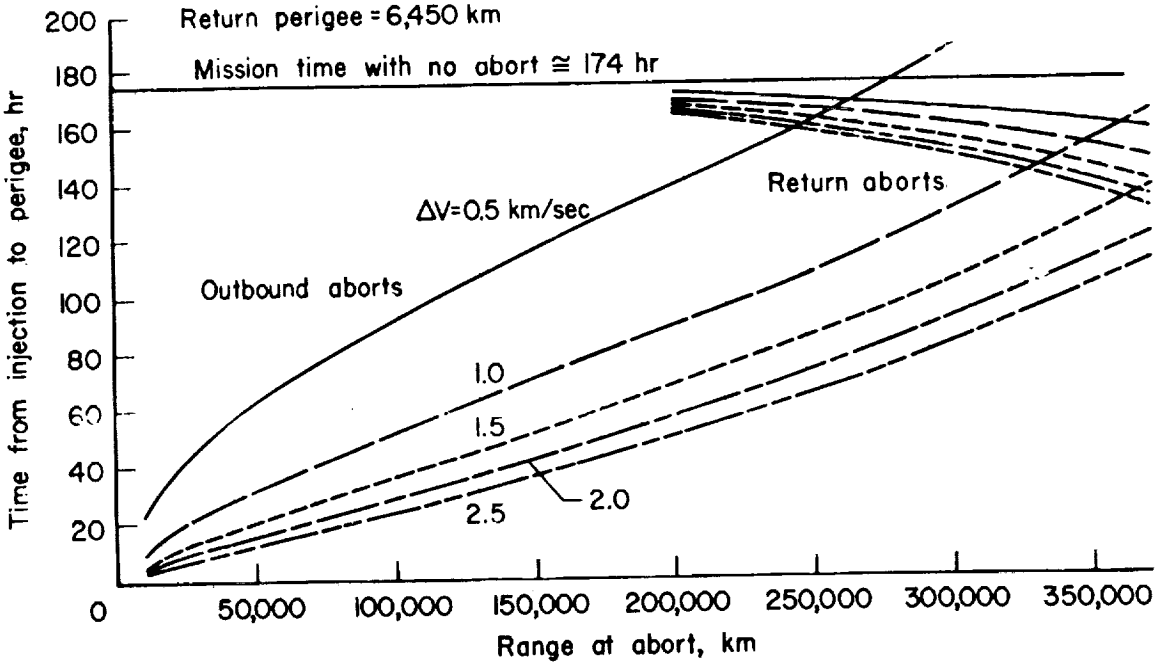

Figure 81. Total Flight Time, Injection to Perigee

Parametric studies of "quick return" abort trajectories from the midcourse region of a lunar mission are contained in the paper by Bartos and Greenberg.[29] Here also, the free flight portions of the abort trajectory were calculated by two-body Keplerian mechanics with a specified vacuum perigee for acceptable entry conditions. Typical abort trajectories from a lunar mission are shown in Fig. 82. Abort

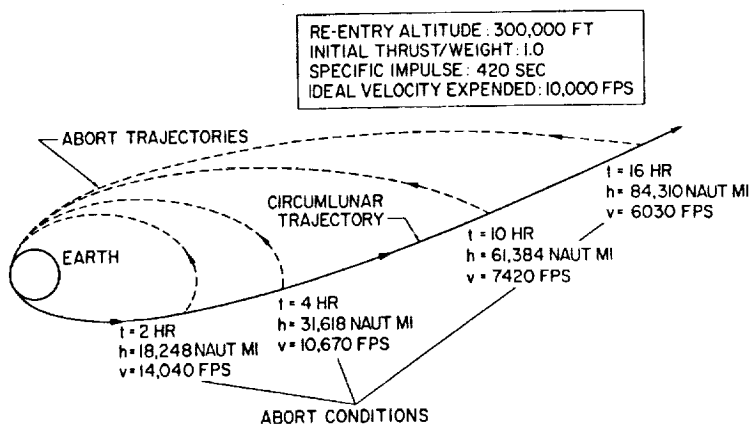

Figure 82. Trajectory Characteristics for Abort During Earth-Moon Transfer With One Lunar Stage

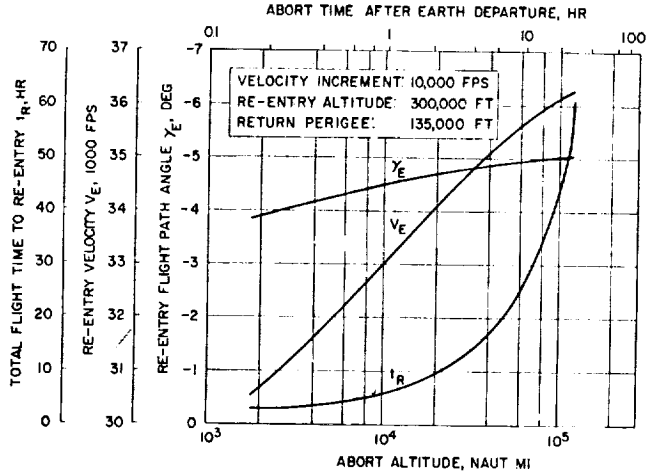

Figure 83. Abort Capabilities During Earth-Moon Transfer Using the Lunar Landing or Launch Stage (Velocity Increment = 10,000 fps)

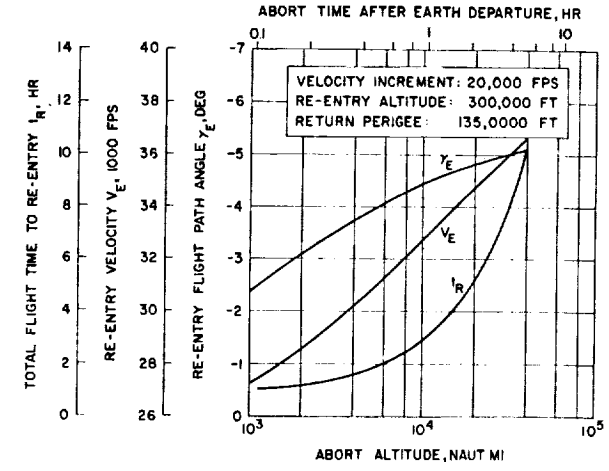

Figure 84. Abort Capabilities During Earth-Moon Transfer Using Both Lunar Landing and Launch Stages (Velocity Increment = 20,000 fps)

capabilities for velocity increments of 10,000 and 20,000 fps are shown in Figs. 83 and 84 respectively. It is noted that reentry velocity increases with increasing altitude at time of abort. This is due to the fact that at high altitudes the abort velocity increment becomes large compared to the local trajectory velocity. Consequently, the abort maneuver not only redirects the flight path angle back toward earth, but increases the magnitude of the velocity vector. The data presented in Figs. 83 and 84 is valid up to abort altitudes for which the resulting reentry velocity is parabolic. At higher altitudes, either smaller velocity increments would have to be utilized (less than vehicle capability, and hence longer flight time) or else additional thermal protection would have to be provided for the space vehicle (with a corresponding weight penalty).

For this reason, an abort with a 20,000 fps velocity increment is limited to flight altitudes from injection to 45,000 nautical miles, whereas an abort with 10,000 fps can be accomplished at altitudes up to approximately 140,000 nautical miles. Beyond that, velocity increments less than 10,000 fps will provide parabolic return to earth as illustrated in Fig. 85. However, in terms of flight time, there is a point beyond which it becomes equally attractive to return to earth along the circumlunar trajectory, a point which has been noted previously in the Merrick and Callas study.

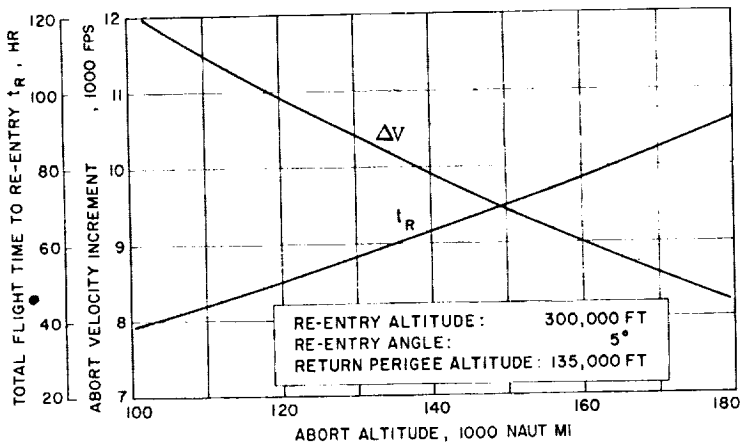

Figure 85. Abort Velocity Requirement and Flight Time for Parabolic Return From the Earth-Moon Transfer Trajectory

3.1.5.1.1 Abort Way-Stations

It was noted in the previous section that with the use of predetermined hodograph charts, the astronaut could effect a safe abort in the midcourse region of a lunar mission if a reasonable estimate of range and velocity were available. With the loss of computational and communication equipment, such an estimate is not feasible. The ensure abort capability in this case, we are led to the concept of abort "way-stations." As proposed by Callas and Merrick,[10] this idea would take the following form.

Consider a manned spacecraft on a typical lunar mission encountering an emergency that necessitates an immediate return to earth. Let us assume that the emergency was caused by a failure in both the communications link and the on-board computer, so that all of the necessary calculations for the abort must be made either on board without the computer, or else prior to the emergency. Such an abort problem can be considered in three parts.

First, the state vector at the time of the abort maneuver must be predicted.

Second, a safe return trajectory must be determined within the existing constraints; that is, landing site restrictions and available change in velocity.

Third, the vehicle must be oriented properly and the abort maneuver performed so that the desired return trajectory is achieved.

One method of predicting the state vector after an emergency has developed is to make a series of celestial observations and process them in some fashion that

will best estimate the current position and velocity. These results can then be updated to the abort time. Several such schemes exist but generally they either require a complex computer to process the results, or they are so simplified that they have marginal accuracy and cannot be used near the moon. Furthermore, sufficient time may not exist to make the necessary celestial observations to determine the state vector accurately. Thus, consideration must be given to the idea of calculating the state vector of the vehicle in advance to minimize the pilot's task in the event of an emergency. If the state vector is predicted for some time in the future, this information gained prior to the emergency can be utilized to give a reasonably accurate prediction. This leads naturally to restricting the number of points on the trajectory from which aborts will be considered. These points are termed abort way stations, and should occur frequently enough to handle all the possible aborts.

If the best estimate of the state vector is routinely computed on board for the next one or two way stations, in the event of computer failure the state vector would be known at those future points and sufficient time would exist for abort calculations and vehicle maneuvering. The abort calculations would be based on trajectories tabulated before the flight for each of the way stations. Since these trajectories are computed before the flight, they can represent the exact physical situation with the inclusion of the earth's oblateness and the perturbing bodies such as the moon and sun. The scheme herein proposed uses precalculated charts computed in this fashion.

After the abort velocity increment is computed, the vehicle must be oriented in the proper direction and the abort executed.

The abort charts consist of velocity hodographs plotted for each reference trajectory. Typical hodograph plots are shown in Fig. 86. The radial velocity is plotted along the abscissa and the horizontal velocity is plotted along the ordinate. The dashed line represents the velocity history of the reference trajectory, and points corresponding to specific ranges are marked. The solid lines represent all of the achievable in-plane safe return trajectories at the respective ranges shown. For example, at the range of 100,000 kilometers, the vehicle would have the velocity represented by the solid circle on the dashed line if it were on the reference trajectory. The vector joining that point with any point on the solid line would represent the abort velocity increment at that range. The further the abort velocity increment extends to the left along the return velocity curve, the shorter will be the return flight time. Since the fuel on board the vehicle will be limited, the curves are terminated on the left. The terminal

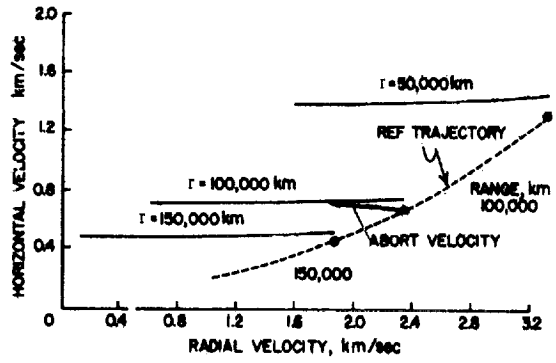

Figure 86. Typical Abort Hodograph Charts

point on the right of each solid line represents the minimum practical abort velocity increment required to return the vehicle to a safe entry. If some velocity on the solid line results in a return to one of the desired landing sites, the velocity is termed a "landing site point" and the corresponding point on the reference trajectory is an abort way station.

When an emergency of the type considered arises, the pilot quickly determines which abort way station he is approaching and selects the proper charts; for example, the one shown in Fig. 87. As in Fig. 86, the solid curve represents all of the achievable safe in-plane aborts for a vehicle at a given range. The hodograph velocities for various specified landing sites can be given in tabular form to any desired accuracy as illustrated by the table in Fig. 87.

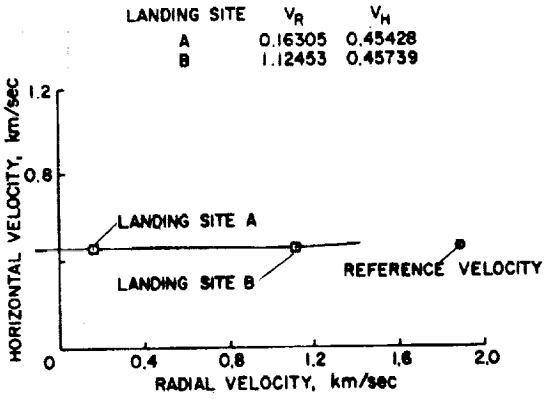

Figure 87. Abort Chart for Way Station

After the abort velocity increment is computed, the vehicle is maneuvered to the proper attitude so that the abort can be executed at the time the vehicle reaches the way station.

The reader may also consult the paper by Kelly and Adornato[14] which treats the concept of abort waystations in a slightly different manner.

3.1.5.2 Lunar Region

In this section, we investigate the problem of aborting the lunar mission once a lunar parking orbit has been established. Obviously, this far from "home," the astronaut has few options available for altering radically the nominal properties of the return trajectory. However, from the point of view of expediting the return to earth on the order of a few hours, various alternatives may be employed, consistent with the thrust capability of the space vehicle.

For a completely accurate analysis of direct moon-to-earth aborts, it is necessary to compute a return trajectory from any point on the lunar parking orbit. In addition, the gravitational effects of the moon, earth, and sun should be accounted for. On the other hand, it is desirable to minimize the computational load on the onboard equipment. Therefore, following Kelly[7] we suppose that one nominal moon-to-earth trajectory is established instead of computing a completely different trajectory for each abort point.

The situation is illustrated in Fig. 88. From any abort point (1) on the lunar parking orbit, a velocity increment is applied, placing the space vehicle on a transfer trajectory. At point (2), another velocity increment is applied, such that the space vehicle now follows the nominal moon-earth return trajectory. This is called direct abort, and requires two velocity increments. Alternately, the space vehicle may remain on the lunar parking orbit until it reaches point (3), at which time one velocity increment will place it on the nominal return trajectory. This is called indirect abort.

By limiting the insertion point (2) to within three lunar diameters, the nominal return trajectory can be represented as a hyperbola in selenocentric coordinates, and the transfer trajectories as ellipses. The transfer ellipse is constrained tangent to the return trajectory at point (2).

For each departure point, θ_1, there are an infinite number of possible insertion points, θ_{T2}. However, to limit r_2 to within three lunar diameters (as mentioned previously), θ_{T2} should be less than 111 degrees. Moreover, since $\theta_{T2} > \theta_1$, we must have $\theta_1 < \theta_{T2} < 111°$.

It is assumed that the orbital elements of the return trajectory (which as noted earlier is a hyperbola) are known. Also the values θ_1 and θ_{T2} can be measured with onboard equipment. The problem of direct abort can then be formulated as

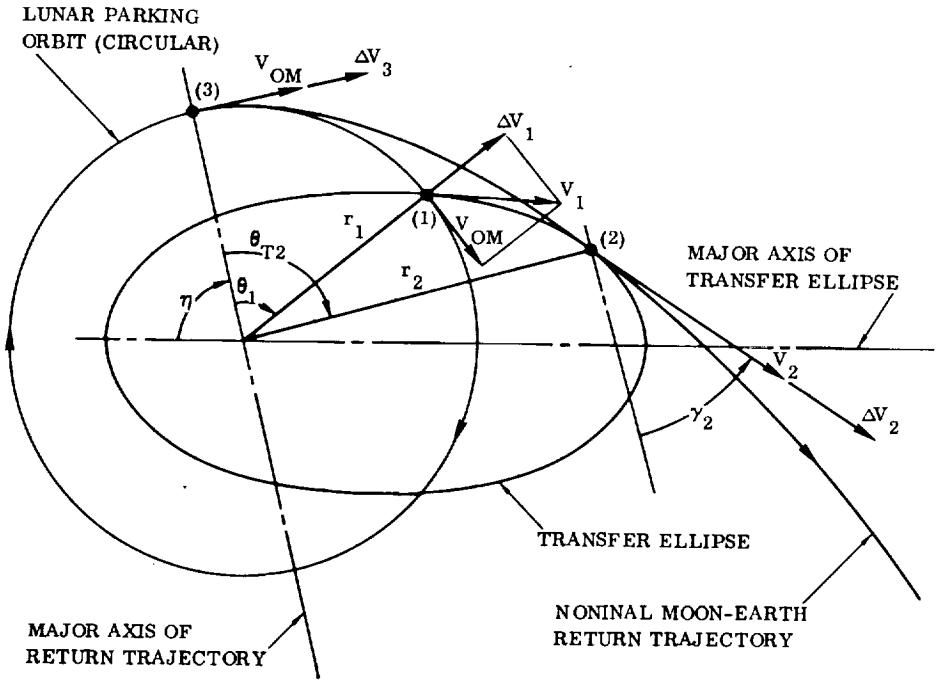

Figure 88. Abort From Lunar Parking Orbit

follows. Given r_1, r_2, θ_1, θ_{T2}, and γ_2, determine the velocity increments ΔV_1 and ΔV_2 together with the orbital elements of the transfer ellipse. Having this, the time to insertion into the nominal return trajectory may be calculated. The time and total velocity increment for this direct abort maneuver can then be compared with the corresponding quantities for the indirect abort.

To obtain the necessary relations, we note that for the transfer ellipse, the true anomalies for points (1) and (2) are $(\eta + \theta_1)$ and $(\eta + \theta_{T2})$ respectively. Therefore, by equating the semilatus rectum at points (1) and (2), we have

$$r_1\left[1 + e\cos(\eta + \theta_1)\right] = r_2\left[1 + e\cos(\eta + \theta_{T2})\right] \tag{38}$$

Using Eqs. (B16) and (B17), we obtain the expression for γ_2 as follows:

$$\tan\gamma_2 = \frac{\sin(\eta + \theta_{T2})}{\left[1 + e\cos(\eta + \theta_{T2})\right]} \tag{39}$$

Eliminating e between the above two equations, and solving for $(\eta + \theta_{T2})$ yields

$$\tan(\eta + \theta_{T2}) = \frac{1 - \cos\Delta\theta}{\sin\Delta\theta - \dfrac{(r_2 - r_1)}{r_1\tan\gamma_2}} \tag{40}$$

where

$$\Delta\theta = \theta_{T2} - \theta_1$$

The value of η serves to locate the major axis of the transfer ellipse relative to the major axis of the return trajectory. The orbital parameters for the transfer ellipse are now readily obtained; viz.

$$e = \frac{\sin(\eta + \theta_{T2}) - \tan\gamma_2}{\tan\gamma_2\cos(\eta + \theta_{T2})} \tag{41}$$

$$\ell = \frac{e\, r_2 \sin(\eta + \theta_{T2})}{\tan\gamma_2} \tag{42}$$

etc.

It is now a straightforward matter to calculate ΔV_1, ΔV_2, and the corresponding transfer time for direct abort.

In Ref. 7, some numerical results are given for the case of a circular lunar orbit of 100 nautical mile radius, with a return trajectory which, in the lunar vicinity, is approximated by a hyperbola with eccentricity, e = 1.485. These are summarized in Figs. 89 - 91.

Fig. 89 shows the elapsed time (Δt) to the insertion point versus the location (true anomaly θ_{T2}) from the abort point θ_1. (In Fig. 88, this is a comparison of transit times on paths (1) - (2) and (1) - (3) - (2), respectively.) Within the θ_{T2} region of interest, a break-even point is seen to exist for each abort location θ_1 at which the direct abort takes just as long to reach point (2) as the indirect abort.

Figure 90 gives the corresponding impulsive velocity requirements for the two-impulse direction return and the single-impulse indirect return. A cross-plot of these results (time saved by direct return versus the associated ΔV penalty) for various abort locations is shown in Fig. 91. The sharp knees represent regions of minimum ΔV penalty because further increases in ΔV produce only slight increases in time saved. Hence, a best operating envelope, such as shown in Fig. 91, can be drawn connecting these regions to uniquely define the potentialities of this mode of direct abort for each initial abort location. The resulting values are tabulated as follows.

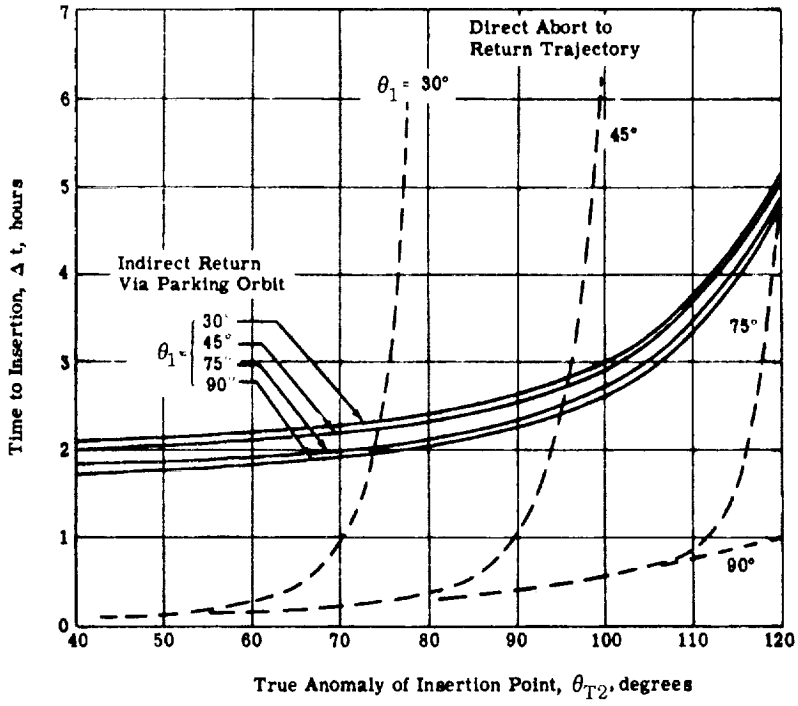

Figure 89. Elapsed Time for Direct and Indirect Returns From 100-Nautical-Mile Circular Parking Orbit

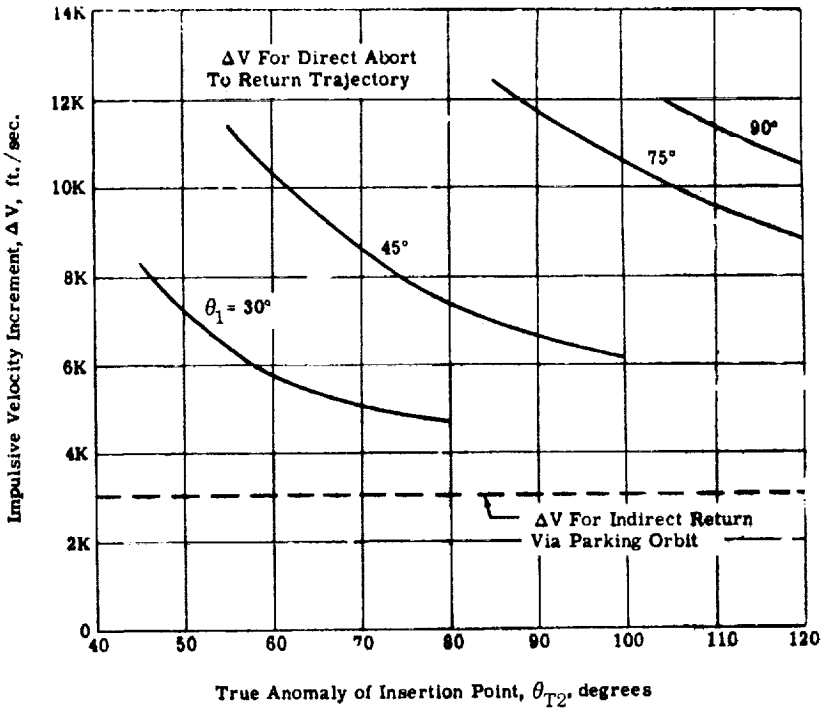

Figure 90. Velocity Increment for Direct and Indirect Returns From 100-Nautical-Mile Circular Parking Orbit

Abort Point θ_1	Δt Saved (hr)	ΔV Penalty (fps)	Insertion Point θ_{T2}
30°	1.88	2,700	60.5°
45°	1.95	4,350	80.0°
75°	2.40	6,080	115.0°

These preliminary results suggest that the time saved by direct abort (using a nominal return trajectory) is rather small compared to the total time for return to earth. Furthermore, since the ΔV requirements are high, this scheme appears to be of limited value. In other words, from the point of view of expediting a return to earth from the lunar vicinity, there are limited options available to the astronaut — other than "heading home" along the initially prescribed return trajectory.

3.2 GEMINI ABORT SYSTEM

Manned space flights have, up to the present time, included the Mercury, Gemini and Apollo space vehicles, which are orbital and suborbital in nature.

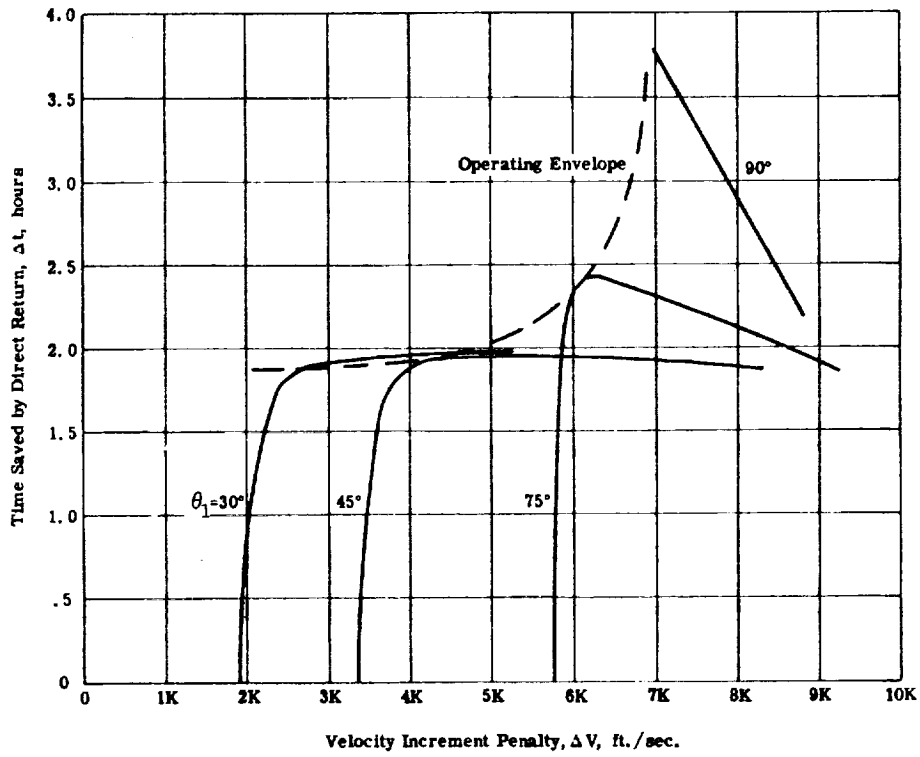

Figure 91. Time Saved Versus Velocity Increment Penalty for Direct Return Abort From 100-Nautical-Mile Circular Parking Orbit

In this section, we will describe the main features of the Gemini abort system. The somewhat more sophisticated Apollo system is described in Sec. 3.3.

To begin with, the booster vehicle itself must be given special attention; it must be "man rated." This means essentially that problems of reliability, via redundancy and otherwise, assume an especially prominent role. For example, a primary area of concern in manned launch vehicles is dynamic behavior in the event of guidance or hydraulic malfunctions in the high dynamic-pressure flight regime. Aerodynamic instability will cause the Gemini launch vehicle to diverge to breakup attitudes within 1 second when control failure occurs at maximum dynamic pressure. Because of the need for immediate switching under this condition, a backup guidance and control system is automatically triggered. Automatic switching is accomplished by abnormal rate gyro signals, full-engine gimbal position, and low-hydraulic pressure. The attitude rate switching level for the first stage is 3.5 degrees per second in pitch and yaw and 20 degrees per second in roll. During second-stage flight, where no aerodynamic divergence is involved, the levels are opened up to 10 degrees per second in pitch and

yaw. Manual switchover can be initiated if guidance or control malfunctions cause a slow divergence which is sensed by the pilot or by ground tracking.

Various other considerations that relate to improving the quality and reliability of systems and components in the Gemini vehicle are discussed in the November 1964 issue of Astronautics and Aeronautics, which is entirely devoted to the Gemini program.

In practice, of course, a system reliability can never attain 100%, which means that an abort system must be provided to enhance the survival probability of the astronaut in the event of emergency. The abort system for Gemini features a Malfunction Detection System (MDS) in which the astronaut plays a significant role.

The MDS senses the following parameters which are displayed on the spacecraft instrument panel for abort decisions and subsequent action by the astronaut:

a. Launch vehicle turning rates in pitch, yaw, and roll (overrate). Information from switches on rate gyros appears as a red light; this is actuated when a certain condition in any one of the three turning axes is exceeded.

b. Stage-I and Stage-II engine-chamber underpressure. Complete or partial loss of thrust (below a design point), as measured by thrust-chamber pressure switches, actuates a red light for Stage-I and an amber light for Stage-II.

c. Stage-I and Stage-II propellant-tank pressures. There are two pressure sensors in each of the four propellant tanks. Pressure information from each sensor is displayed on meters.

d. Switchover to the secondary flight-control system. An amber light is actuated when switchover to the secondary flight-control system occurs.

e. Staging. When staging operations are initiated by sensing a thrust decay in a Stage-I engine, a signal is sent to the spacecraft, causing an amber indicator lamp to light. When staging actually is accomplished by Stage I separating from Stage II, the interstage connectors through which the signal was routed are pulled apart, and the path for lighting the lamp breaks. The lamp lighting and then extinguishing 1 sec later indicates successful staging.

With the Gemini MDS technique, end effects — and not equipment failures — are sensed. From these end effects, lights and meters on the spacecraft instrument panel are activated, and the astronauts evaluate the seriousness of the situation and the best procedure to follow during any special circumstance. With this type of manual system, more than one cue can be used to verify an abort situation.

Besides the MDS displays, the astronauts use physiological cues (accelerations from thrust and turning rates), get information from other spacecraft instruments, and have voice communication with the ground, as indicated in Fig. 92. Simulations

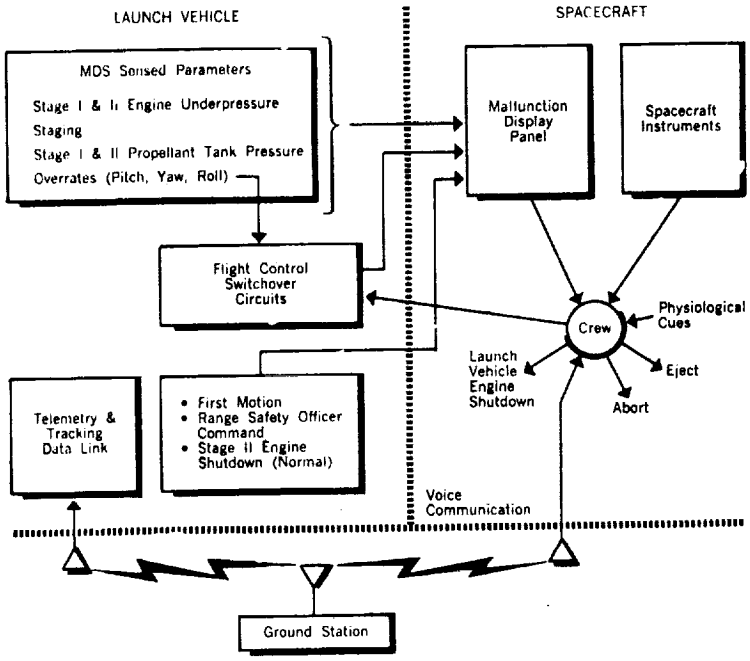

Figure 92. Cues for Astronaut Abort in Gemini

revealed that, in many cases, astronauts placed much reliance on audio-kinesthetic cues. These cues not only are very dependable, but they also instill pilot confidence in the validity of the MDS indications when thus checked.

The general features of the Gemini MDS are shown in Fig. 93.

NASA conducted simulation studies, using Mercury astronauts, to determine the reaction required to effect a successful abort in the event of a launch-vehicle malfunction. With the exception of the hard-over engine condition, the astronauts were able to simulate a successful escape with appropriate instrument-panel indications and a manual abort system. However, a warning time of 1 sec — which is the amount available for malfunction detection, display, observation, reaction, escape-mechanism initiation, and escape-system operation if an engine hardover occurs during the maximum-g regime — was not sufficient. This lack of adequate time for a succesful escape was the major reason for establishing the requirements for a redundant guidance and flight-control system.

Fig. 94 shows the launch acceleration and dynamic pressure time histories. Also indicated are the three Gemini launch escape modes. Ejection seats are used from the launch pad to an altitude of 70,000 feet. Ejection seats are feasible for Gemini because of the low order pressure wave which originates from burning

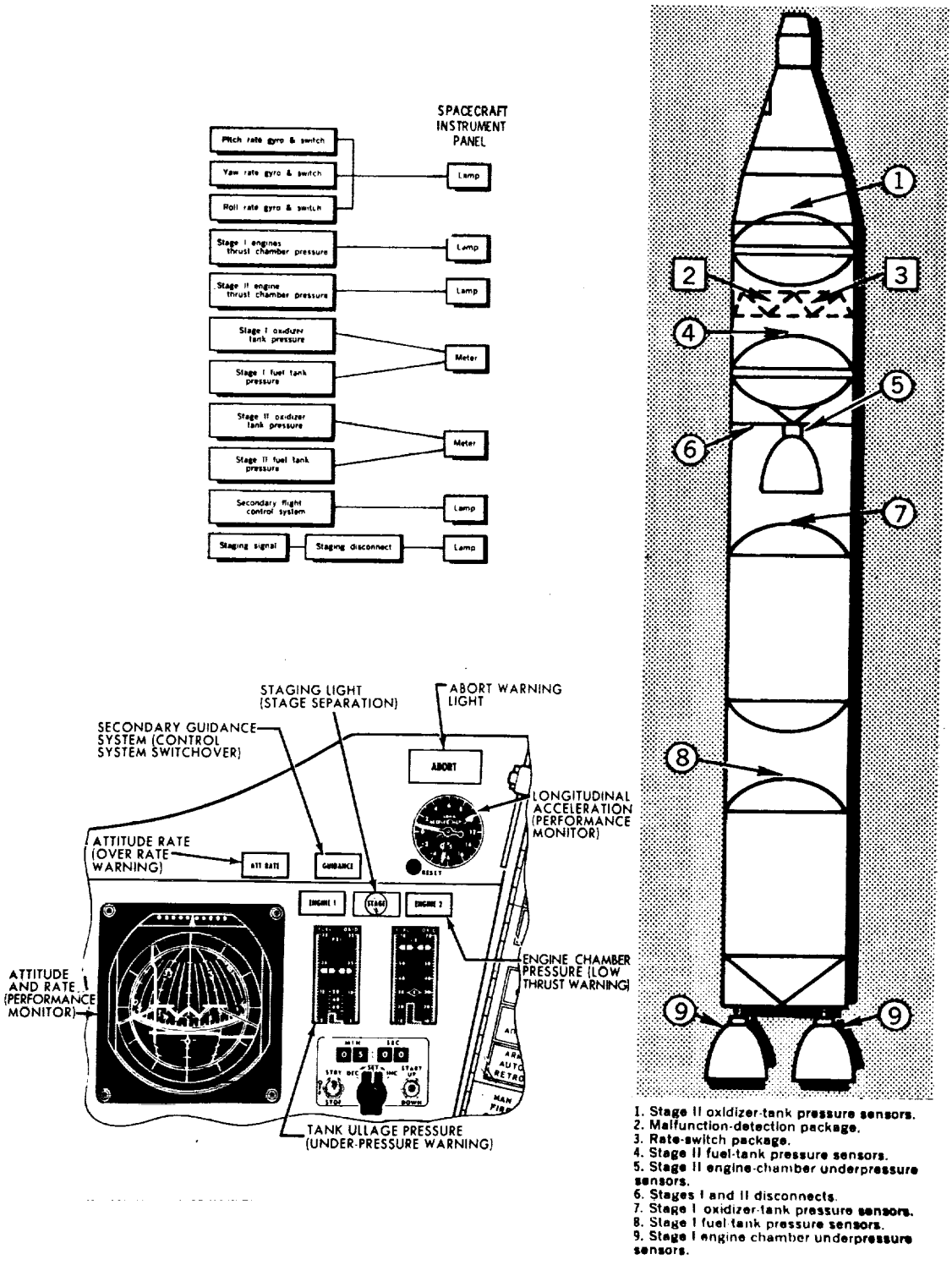

Figure 93. Gemini Malfunction Detection System (MDS)

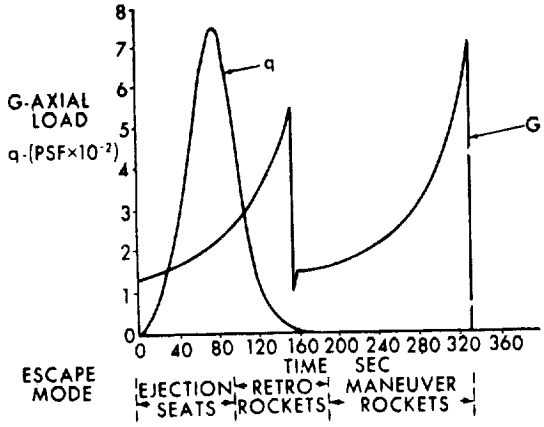

Figure 94. Gemini Launch Parameters

hypergolic propellants as in Titan II. Above 70,000 feet, the spacecraft drag has reduced sufficiently to permit separation of the spacecraft by salvo fire of the retro-rockets. For this escape mode, the top section of the adapter is retained and the resulting configuration is aerodynamically stable, small end forward. The adapter section is separated at apogee of the escape trajectory. After staging, when dynamic pressure is negligible, the escape mode involves shutting down the booster and separating with the translational rendezvous propulsion system.

The escape hatches and the ejection seats are triggered by the actuation of either pilot's D-ring located on the forward portion of the seat. The launch vehicle is shut down and the retro-rockets are fired by a control of the left console. The maneuver rockets are fired by a translational control handle located just above the pilot's left knee.

The abort sequences in each mode are illustrated in Fig. 95.

Requirements for an off the pad abort govern the ejection seat and thrust design characteristics. As noted earlier, the low order pressure wave characteristics of the Titan II hypergolic propellants constitute a less severe overpressure condition than that associated with a conventional LO_2-RP1 fuel combination. Typical off-the-pad ejection trajectories are shown in Fig. 96 in relation to fireball growth. These trajectories have been verified by numerous full scale tests, which show that adequate safety margins exist.

The results of an extensive simulation program are reported by North and Cassidy.[12] This program involved 51 malfunction runs representing 9 major types of malfunctions:

a. Partial loss of thrust - one engine (Stage I).

b. Total loss of thrust - one engine (Stage I).

c. Total loss of thrust - both engines (Stage I).

d. Staging failures.

e. Tank (fuel and oxidizer) pressure losses.

f. Roll malfunction (Stage I).

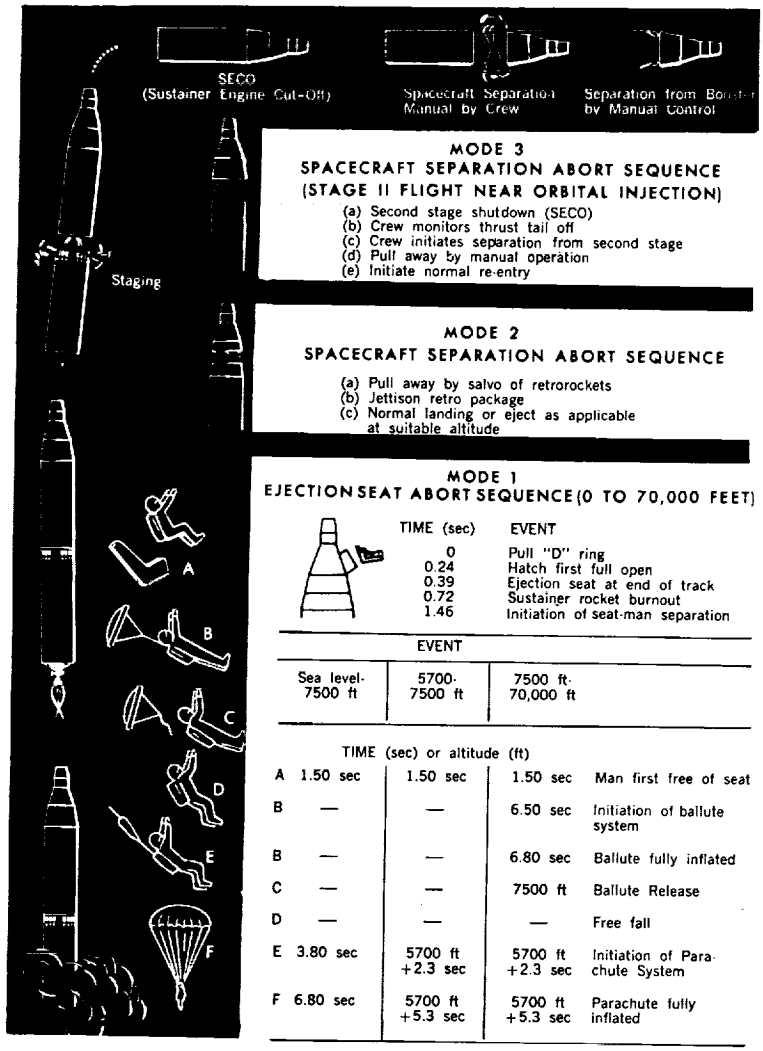

MODE 3
SPACECRAFT SEPARATION ABORT SEQUENCE
(STAGE II FLIGHT NEAR ORBITAL INJECTION)

(a) Second stage shutdown (SECO)
(b) Crew monitors thrust tail off
(c) Crew initiates separation from second stage
(d) Pull away by manual operation
(e) Initiate normal re-entry

MODE 2
SPACECRAFT SEPARATION ABORT SEQUENCE

(a) Pull away by salvo of retrorockets
(b) Jettison retro package
(c) Normal landing or eject as applicable at suitable altitude

MODE 1
EJECTION SEAT ABORT SEQUENCE (0 TO 70,000 FEET)

TIME (sec)	EVENT
0	Pull "D" ring
0.24	Hatch first full open
0.39	Ejection seat at end of track
0.72	Sustainer rocket burnout
1.46	Initiation of seat-man separation

	TIME (sec) or altitude (ft) EVENT			
	Sea level-7500 ft	5700-7500 ft	7500 ft-70,000 ft	
A	1.50 sec	1.50 sec	1.50 sec	Man first free of seat
B	—	—	6.50 sec	Initiation of ballute system
B	—	—	6.80 sec	Ballute fully inflated
C	—	—	7500 ft	Ballute Release
D	—	—	—	Free fall
E	3.80 sec	5700 ft +2.3 sec	5700 ft +2.3 sec	Initiation of Parachute System
F	6.80 sec	5700 ft +5.3 sec	5700 ft +5.3 sec	Parachute fully inflated

Figure 95. Gemini Abort Sequences

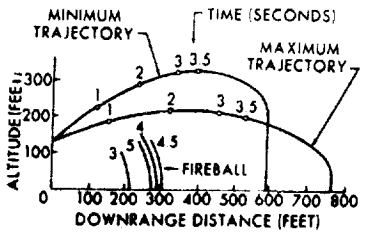

Figure 96. Off the Pad Escape

g. Direct-current power failure.

h. Instrument malfunction.

i. Display-light failure.

The selected malfunctions were based on failure analysis data for the Titan II launch vehicle. They were also derived from considerations relating to criticality of the malfunctions with respect to anticipated pilot

difficulty in detecting and evaluating the cues and the response time for taking corrective action. Normal launch vehicle runs were interspersed throughout the simulation. The most difficult malfunction runs were selected for use in the simulation regardless of their probability of occurrence in actual flight.

The NASA astronauts who participated in the simulation were given only 1 day of indoctrination. Each pilot was scheduled for approximately 75 runs, 65 runs having malfunctions and 10 being normal. Each of the 51 malfunction runs was presented to the pilots at least once, and the 14 most difficult runs were presented twice to each pilot. The runs were randomly distributed so that the pilots had no way of knowing which problem would be presented next. They were aware of the general nature of the possible malfunctions, but they were not aware of the time during flight at which the malfunctions were programmed.

It became readily apparent to the pilots that the most critical malfunctions were engine failures or tank pressure losses immediately after liftoff or immediately after staging. The critical engine failures were readily detectable through redundant cues, including decrease in sound level, decrease in acceleration, and illumination of the combustion chamber pressure light. Pilot reaction time to this failure was as low as four-tenths of a second. Reaction time requirements varied from approximately 1 second to 2 1/2 minutes, depending upon the type and time of malfunction. Several of the malfunctions, such as sensor failures and gradual tank pressure losses, were noncritical and required no abort action. For the majority of the failure modes, there were multiple cues such as is the case with engine failure. Tank pressure losses were sensed by redundant transducers driven by redundant power sources and presented on redundant meters. For tank pressure failures which occurred after the first 5 seconds, the rate of decay was relatively slow. The pilots were able to let several pressure failures decay parallel to and just above the structural limit or were able to wait until the pressure dropped to within 1 psi of the structural margin before taking abort action.

Some typical reaction times required of the astronaut in the event of malfunction are shown in Figs. 97 and 98. For example, (Fig. 97) with engines hardover in roll during Stage-I flight, the physiological limit would be exceeded in about 1 sec. For engine hardover in pitch and yaw during the high-dynamic-pressure regime (approximately 75 sec after liftoff), the time until the structural limits are exceeded is less than 2 sec. The warning time the astronauts have to initiate action is somewhat shorter than the time shown.

Loss of thrust, too, requires immediate action from the astronauts. Fig. 98 shows the time from inadvertent thrust termination until critical limits are exceeded. If an engine failure occurred approximately 75 sec after liftoff, the launch vehicle would break up in about 3 sec.

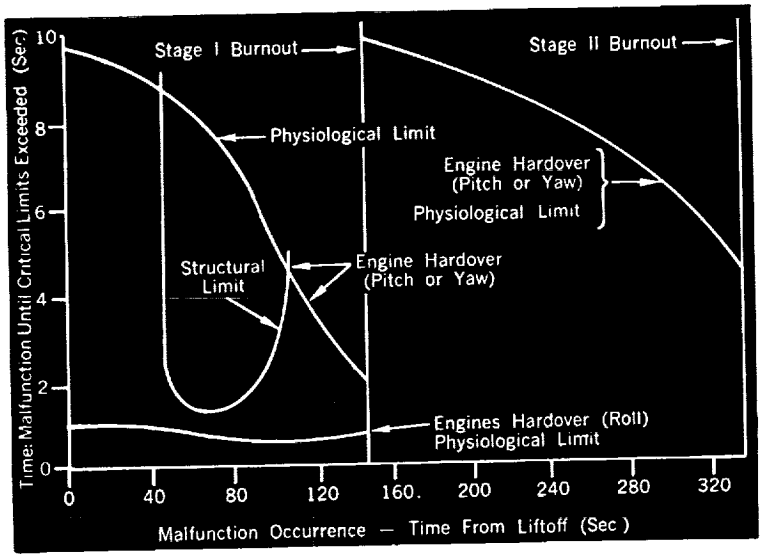

Figure 97. Violent Controls Malfunction

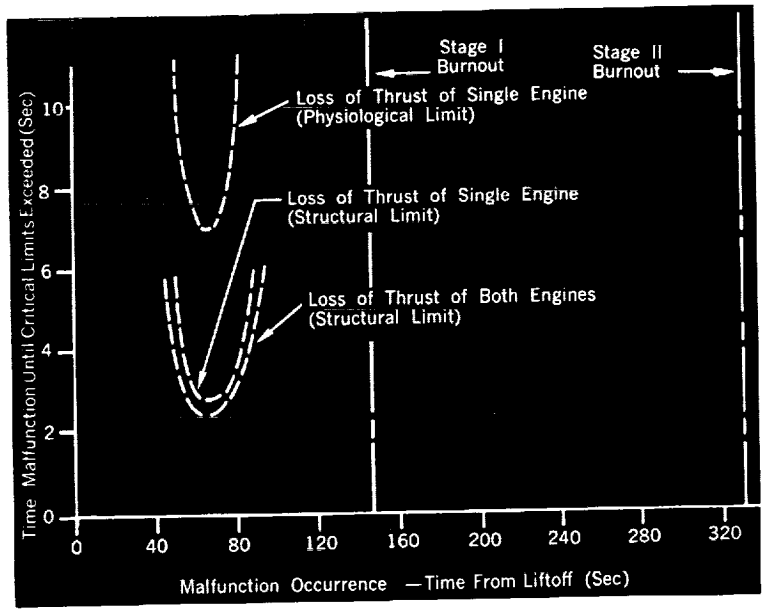

Figure 98. Inadvertent Thrust Termination

The reported studies have shown that the astronaut can readily familiarize himself with the abort procedures, and react quickly enough to apply corrective action to virtually all anticipated malfunctions.

3.3 APOLLO ABORT SYSTEM

3.3.1 General

The abort system for Apollo is conceptually similar to that for Gemini, although there are differences in complexity and refinement.

The abort system for Saturn/Apollo vehicles is semiautomatic. The system can sense failure modes that slowly lead to catastrophic conditions and indicate these failures on a display panel to the flight crew to allow them to make the abort decision.

The system can also automatically initiate an abort when it senses a failure mode that will lead to a rapid vehicle breakup. Studies of many failure modes have shown that despite the tremendous mass and inertia of the Saturn launch vehicles, the time from occurrence of a malfunction until the vehicle reaches a "breakup" angle of attack can be very short. Therefore, a fast responding automatic capability must be included in the crew safety system.

The Saturn V Apollo crew safety system is very similar to the Saturn IB system but has three stages to monitor. Because of increased loading, the system must also monitor propellant tank pressures in the S-II and S-IVB Stages.

The Apollo spacecraft consists of the components above the instrument unit as shown in Fig. 99. The different Saturn vehicle configurations are shown in Fig. 100.

The launch escape system (LES) and command module (CM) comprise the launch escape vehicle (LES).

The LES provides the capability to abort the mission up to a point following second-stage ignition where the dynamic pressure is sufficiently low to abort using service module propulsion. To minimize payload penalty, the system is jettisoned as soon as the service module offers an effective abort capability.

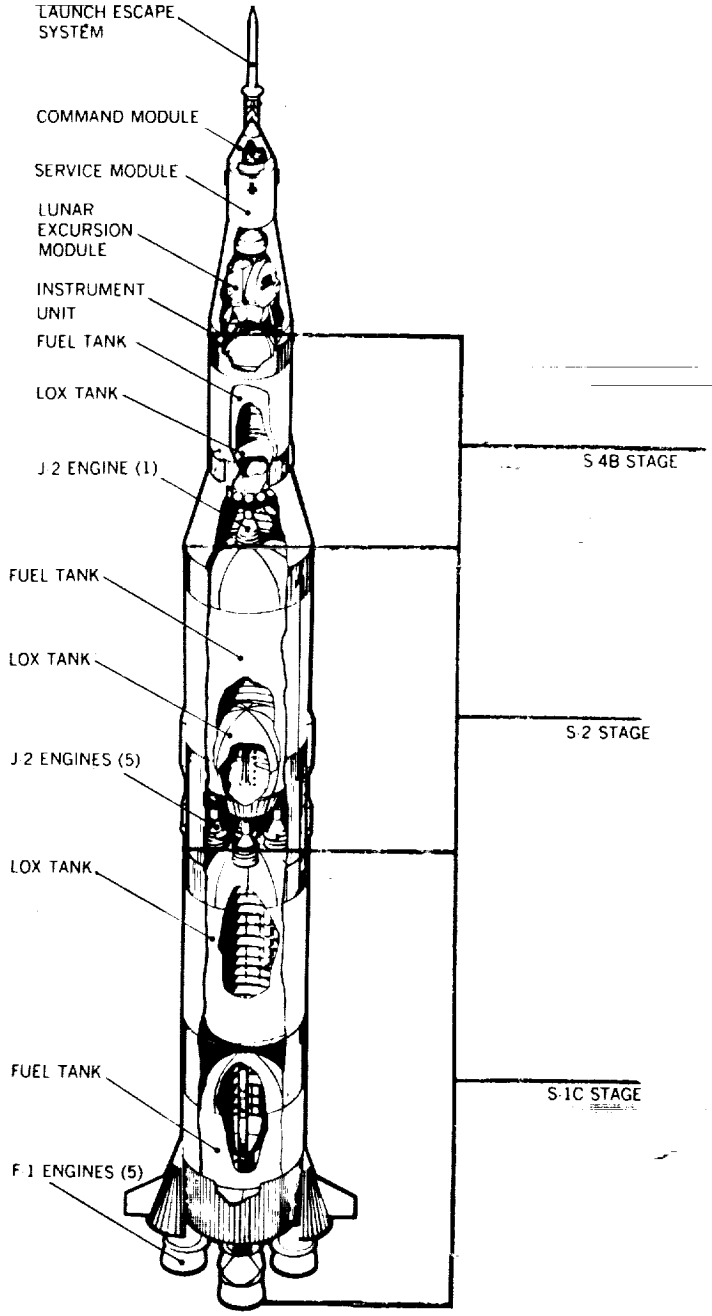

Figure 99. The Saturn V Configuration

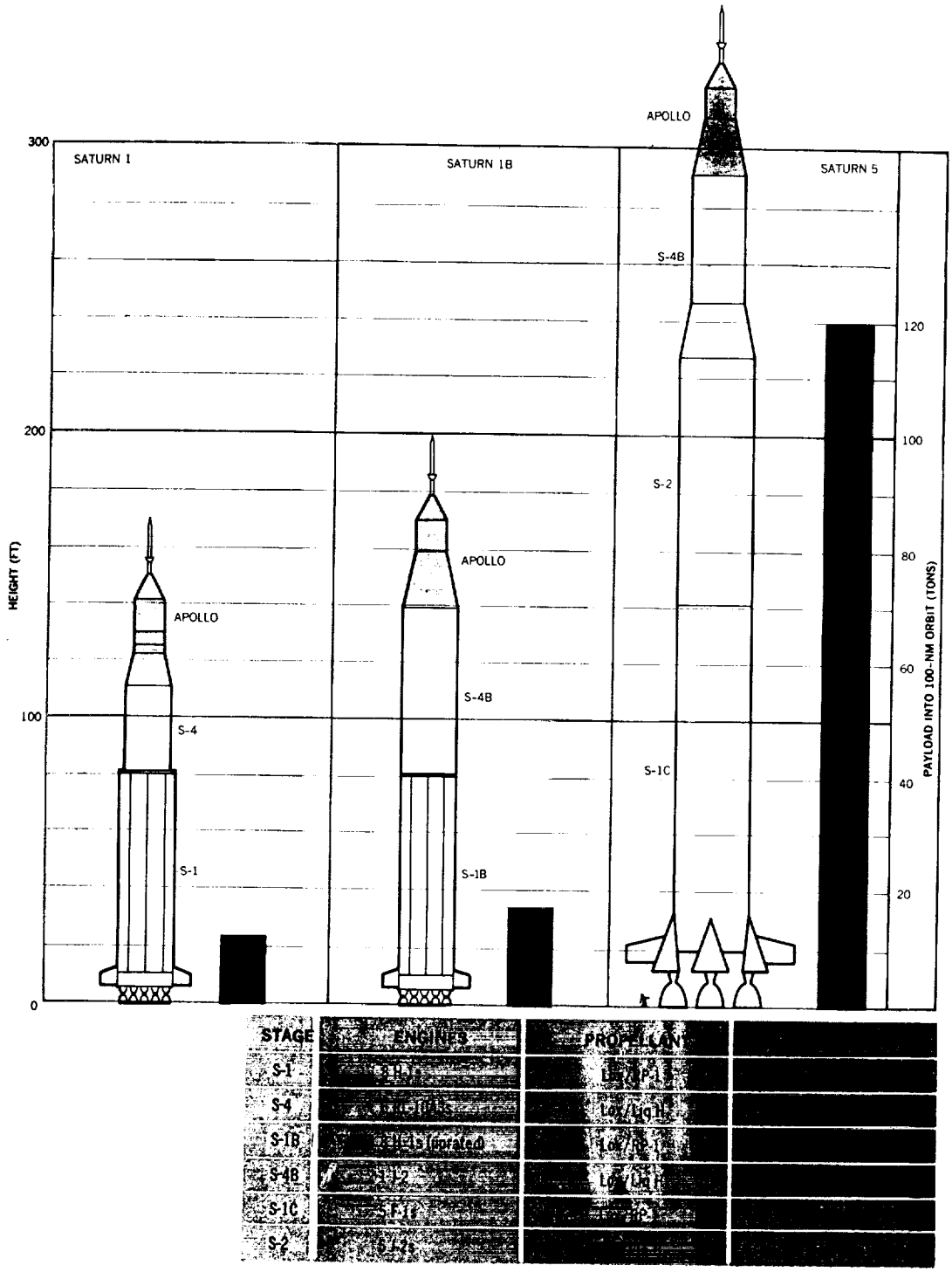

Figure 100. The Saturn Vehicles

The launch vehicle emergency detection system (EDS) monitors critical launch vehicle parameters, and emergency conditions are displayed to the crew to indicate the necessity for abort action as indicated below.

Launch Vehicle Function	Display
Excessive Rate	Indicator light
Total Angle of Attack	Analog display from Q-ball
Guidance Failure	Indicator light
Propellant Tank Pressure	Analog displays
Engine Status	Indicator light for low thrust also indicates stage separation
S-II Stage Second Plane	Indicator light
Separation Abort Request	Light indicating ground control advising immediate manual abort

The EDS can initiate an automatic LES abort in the event of extremely time critical conditions occurring during the early part of the first-stage burn. Such conditions are loss of thrust on two or more engines of the first stage and excessive vehicle angular rates (in excess of 3°/sec in pitch and yaw and 20°/sec in roll) normally associated with an engine hardover malfunction. Concurrent with abort initiation, emergency detection system provides launch vehicle engine cut-off action except for the first 30 seconds following lift-off, during which period this action is inhibited for range safety reasons.

An important guideline used in the development of the Saturn/Apollo abort system is that, whenever enough time is available, the abort decision will be left to the flight crew rather than automatically initiated. It was felt that no matter how reliable the automatic abort system is made, it can never replace the logic, judgement, and observation powers of the flight crew. However, many of the failure modes of the vehicle do not allow sufficient time for the flight crew to make a decision and react to the emergency; in these cases, the crew must rely on the automatic abort system.

The design of the emergency detection system is based on failure mode and effect analysis. This is a complete analysis of each stage, system, subsystem, and component within the vehicle to determine which component failure modes can cause a failure of the subsystem, which subsystem failures can cause failure of the system, and which system losses can cause loss of the stage and/or vehicle. A failure mode and effect analysis begins at the component level and investigates each possible way in which the component can fail (i.e., open, short, rupture, leak). The effect of the particular failure is analyzed on higher levels of assembly until the effect of that particular component failure on the space vehicle is determined.

Once the failure analysis of a component is completed, a criticality number is assigned to the component. For example, a number 10 indicates that this component can be expected to cause a vehicle loss about 10 times out of 1 million flights.

After the criticality number has been derived for each component, the numbers are summarized for each subsystem, system, and stage of the vehicle — vehicle dynamics must be analyzed and structural limits determined. For example, a failure mode and effect analysis shows that a particular group of control component failures can cause the engines to gimbal "hardover"; this would mean vehicle loss and a criticality number could be derived to show the expected frequency of this failure.

The criticality numbers are summarized on a summary chart which is referred to as a failure tree. (Fig. 101.) In this figure, the failure is traced back only three or four levels and does not reach the component mode in most cases.

Beyond this analysis of failures, the length of time between the occurrence of the failure and the time of reaching the critical angle of attack must be known. This is a function of the time of flight. If the failure occurs about maximum q, we may have the worst case condition and less time is available between the occurrence of the failure and structural breakup of the vehicle. To determine these limits, the structural limit curves must be drawn for each type of failure (control engines hardover, engines null, engines out, etc.). These curves show the various combinations of vehicle angle of attack and engine gimbal angle at which the structural limits of the vehicle are exceeded, as a function of time of flight. Typical curves of this type are shown in Fig. 102.

From the information on the effect of these failures and the information on the vehicle dynamics or structural limits, the time available between occurrence of the failure and catastrophic loss of the vehicle can be derived. This time will indicate the response time required of the detection mechanism. The time will determine whether the crew has sufficient time to recognize the emergency warning and make a decision as to when to abort. If human response would be too slow, the abort or escape must be automatically initiated. A range of safe limits is assigned to each parameter selected for monitoring. Performance within these limits assumes the parameter to be functioning normally. Generally, the selected parameter could have a range of acceptable tolerance bounded by both an upper and lower level of safety (e.g., over pressure and under pressure in a pressurized tank). However, in some conditions only one safety limit is needed (e.g., high angles of attack). As long as conditions of the measured parameter stay within the safety zone, it is assumed that all components are operating satisfactorily. If the measured value approaches the danger level, a catastrophic failure is imminent.

The problem is to decide at what level to place the abort level. If the abort level is placed too close to the tolerance limit, an abort might be needlessly triggered. If, on the other hand, it is moved too close to the danger level (to hedge against a

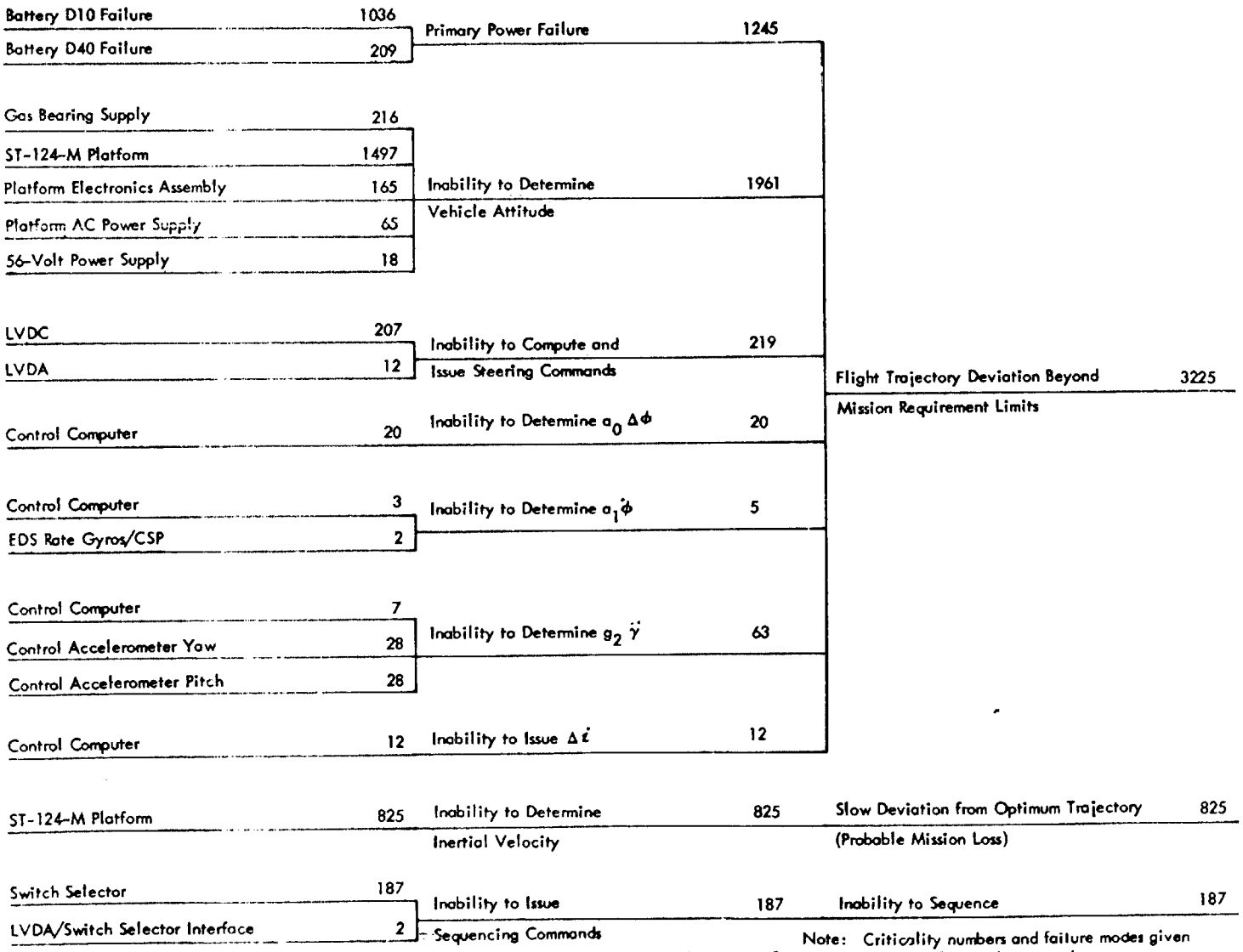

Figure 101. Saturn IB Failure Modes

Note: Criticality numbers and failure modes given are typical and subject to change.

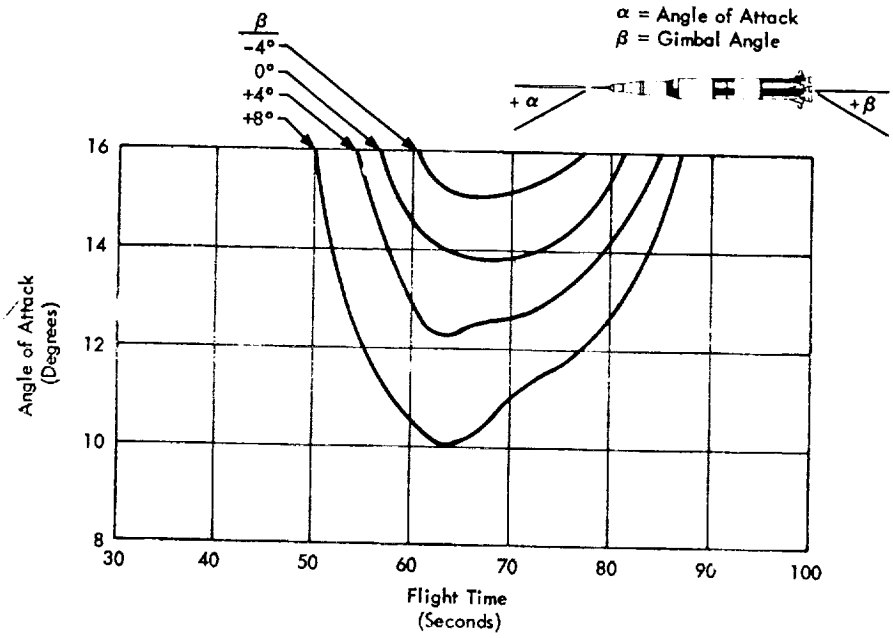

Figure 102. Saturn IB Critical Angle of Attack Versus Flight Time

needless abort), there may not be time enough for a safe escape because of various systems delays. The task is often complicated because the danger levels, as well as the tolerance zone, of certain parameters may change as a function of time. Other factors that further complicate the problem are transients which momentarily exceed the danger level but offer no catastrophic threat.

Consequently, extensive computer simulation studies are required to determine satisfactory abort parameters. Various malfunctions are then introduced (e.g., engine out, high angular rate, etc.) and the vehicle dynamic response noted (primarily angle of attack). In this way, abort problems can be defined, and the proper corrective procedure specified. Studies of this type are contained in Refs. 42 and 43.

In the case of an abort following a booster explosion, the warning time required to abort safely is shown in Fig. 103 for a given propellant ratio and capsule overpressure (taken from Ref. 43). It is noted that the required warning time is of the order of magnitude calculated in Section 3.1.1 for vehicles of this size. The trajectories of the booster vehicle and command module (following abort separation) are shown in Fig. 104 (also taken from Ref. 43).

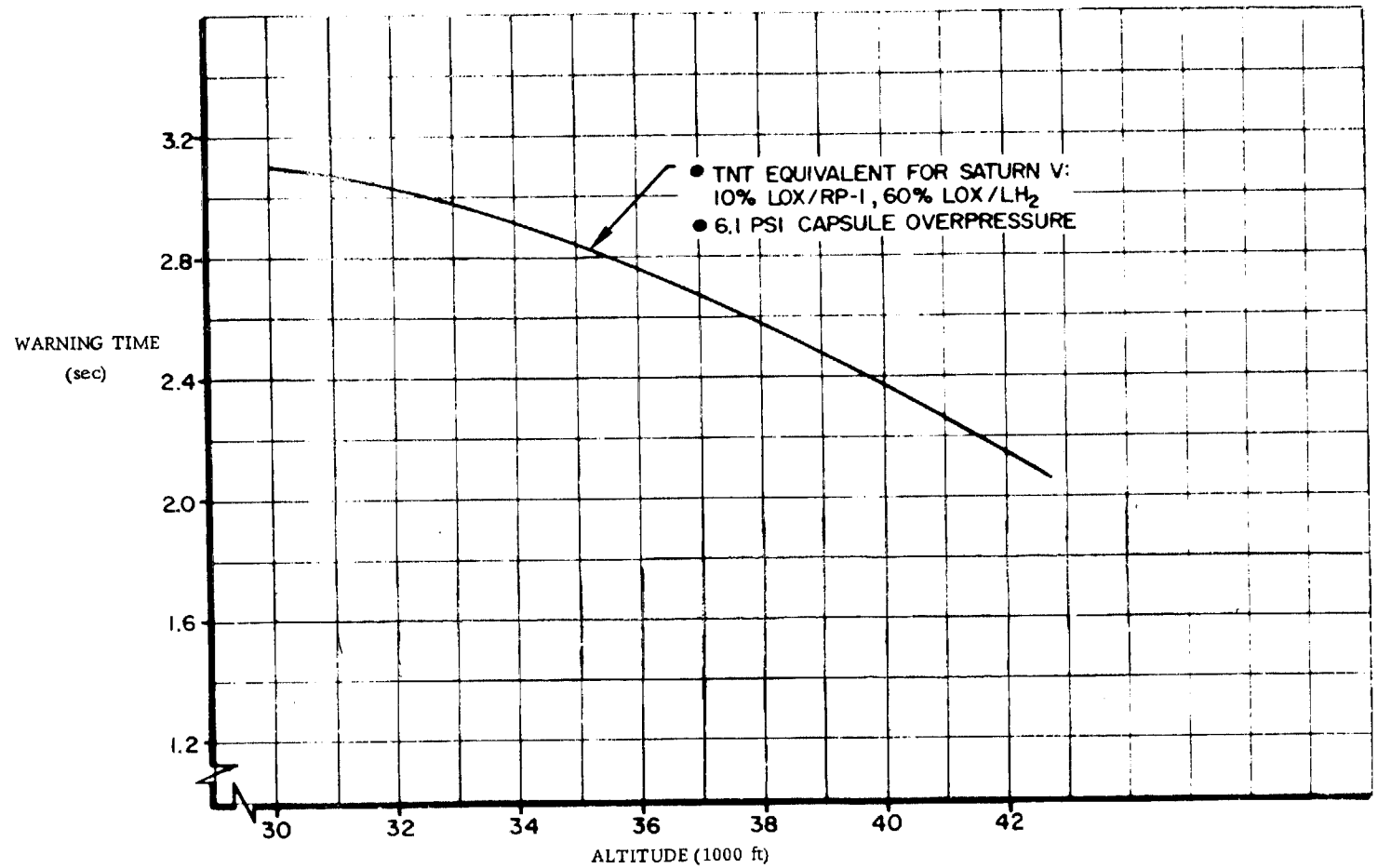

Figure 103. Abort Warning Time Requirements for Saturn V Explosion

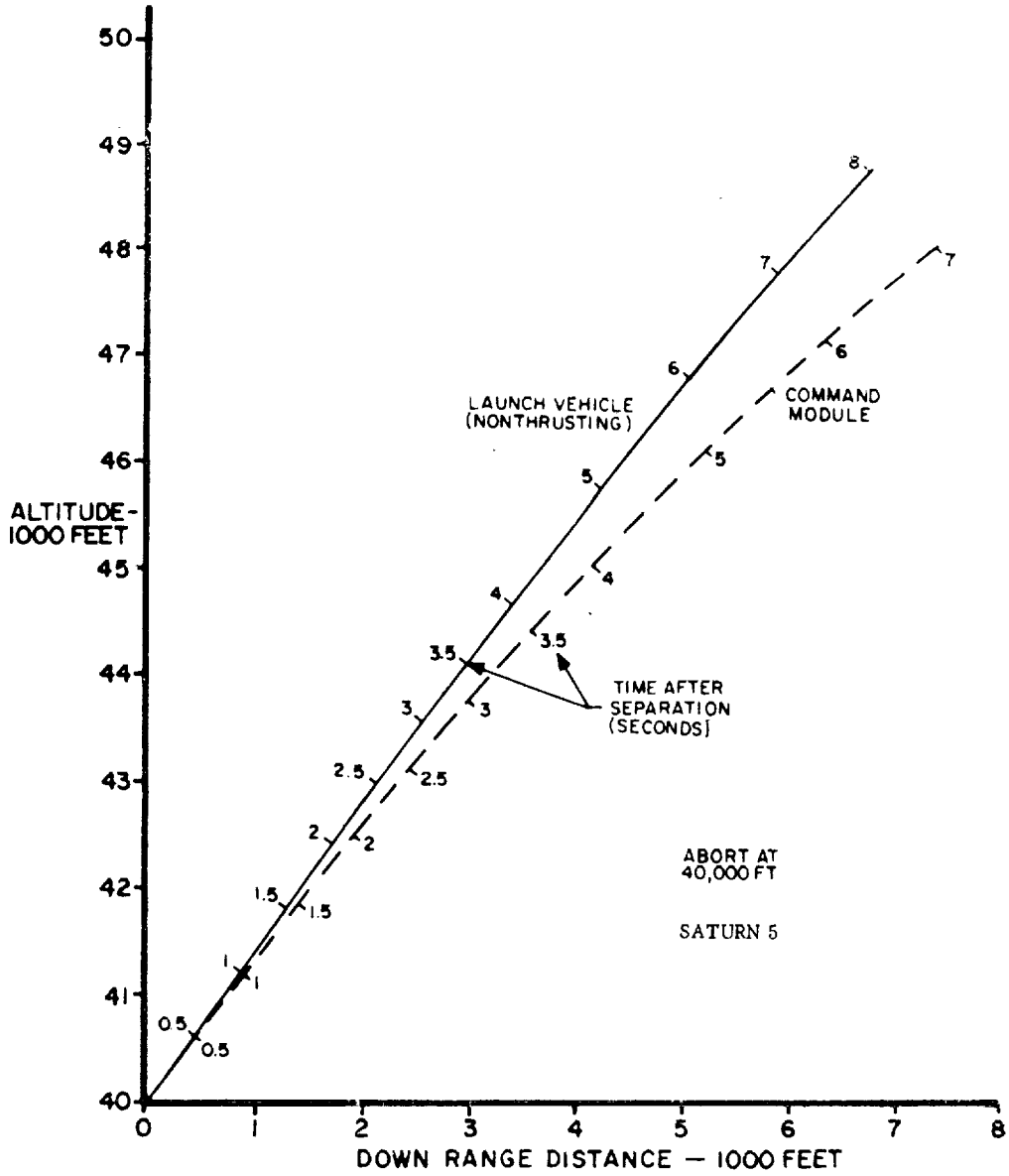

Figure 104. Command Module and Launch Vehicle Trajectories Following Abort

3.3.2 Design Philosophy

The Saturn/Apollo emergency detection system has triple redundant sensors and majority voting logic for all the automatic abort parameters. Dual redundancy is used for most of the manual abort sensors. The redundancy is so arranged that the predominant failure mode of the sensing system has been protected against. The guideline rule of having at least two separate and distinct indications of failure before initiating a manual abort is a protection against any inadvertent aborts from malfunctioning sensor systems. The displays used in the spacecraft are "fail safe" wherever practical. Where possible, the meters used for display of analog singals are "zero offset". This means that the predominant failure modes of the sensing system (loss of power, etc.) will indicate off scale conditions (either high or low) rather than readings within the scale of interest. The indicator lights used for discrete indications to the flight crew are dual-bulb lights and so arranged that the crew cannot distinguish whether one or both lights are on. A failure of one light will not be noticed by the flight crew. The other failure mode (inadvertent light) is protected against by requiring two separate and distinct indications of failure.

The Saturn IB/V crew safety system is shown in the functional diagram, Fig. 105. Monitored parameters are: stage thrust for both stages, guidance computer status, angular attitude rates, attitude error, and angle of attack for spacecraft display. Automatic abort is initiated for S-IB and S-IC two-engine-out or for excessive angular rates in pitch, roll, or yaw; these automatic abort limits are switched out either automatically by the flight programmer or manually by the crew according to mission rules. Provision is also made for an abort request light to be energized from the ground control center. At the ground control center, all of the various crew safety system parameters are monitored by using telemetry information from the vehicle. Other telemetered data is available at the mission control center (MCC) so that the flight director can scan all flight critical data and warn the flight crew by voice communication of any impending danger. This facility provides an early warning to the flight crew by giving information on trends of various vehicle parameters, thereby alerting them to certain types of failure indications which may appear on their display panel. The flight crew will not abort on the telemetry information alone but they may use it as backup data for an abort decision.

A detailed functional description of the EDS together with component specifications is contained in Ref. 44.

3.3.3 Operational Features

3.3.3.1 Abort Parameters

Initiation of a manual abort will be based on at least two separate and distinct indications. These may be a combination of EDS sensor displays, physiological

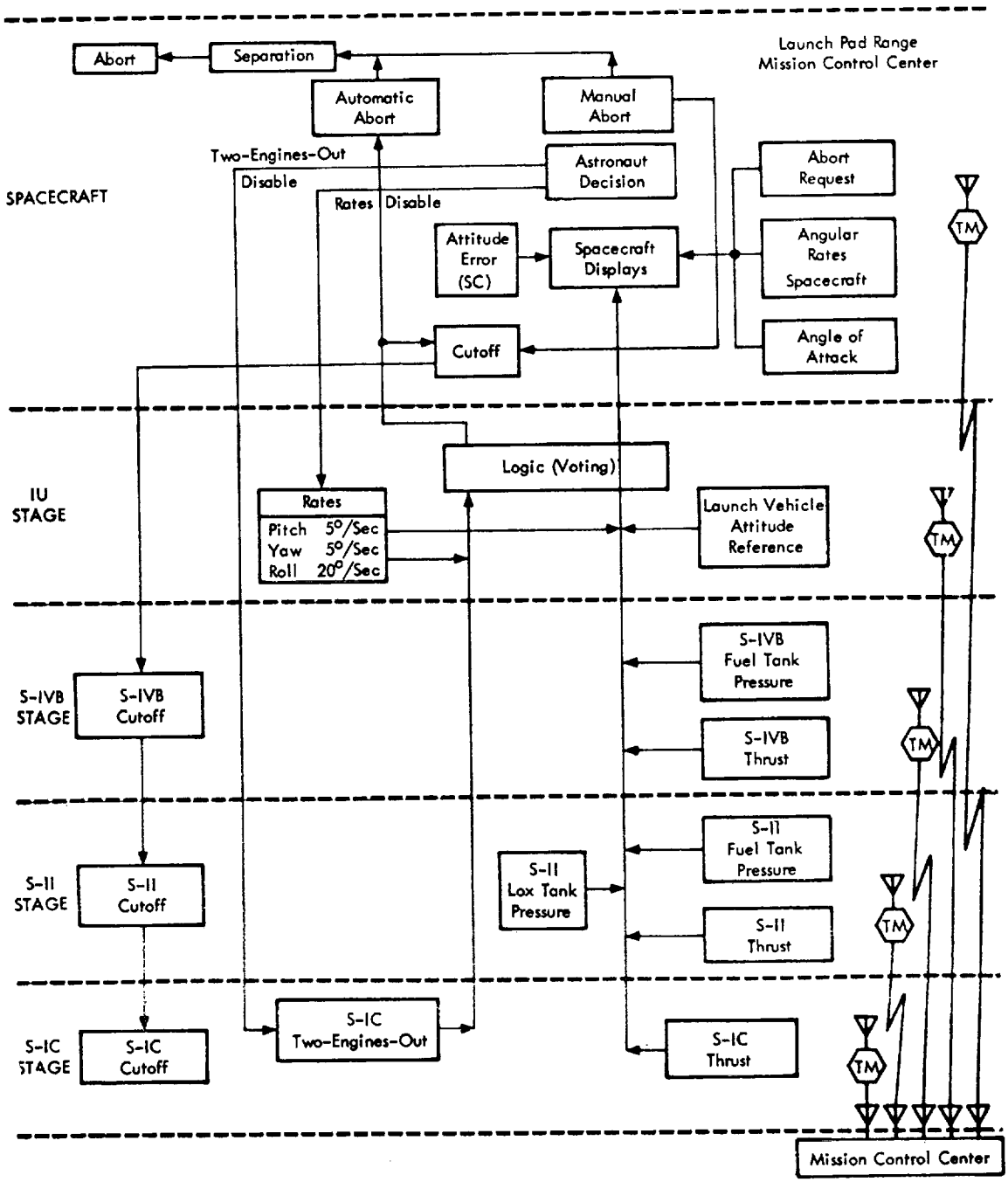

Figure 105. Crew Safety System (Saturn V)

indications, and ground information to the astronaut. In some cases, the two indications may come from the same parameter, but the indication and sensor systems will be independent.

In the event of conflicting information from the onboard EDS and telemetered data relayed to the spacecraft from the ground, the onboard information will always take precedence.

The parameters which govern the decision for manual abort are:

S-IC Stage Thrust. The status of each engine of the S-IC Stage is displayed in the spacecraft (five indicator lights). Upon loss of engine thrust, these engine status lights are energized by a discrete signal.

- An Abort for one-engine-out will be governed by mission rules.
- A minimum of two thrust sensors are used on each S-IC engine to activate the engine-out status lights.

S-II Stage Thrust. The status of each engine of the S-II Stage is to be displayed in the spacecraft (five indicator lights). Upon loss of engine thrust, these engine status lights are energized by a discrete signal.

- Abort on one-engine-out will be governed by mission rules.
- A minimum of two thrust sensors are used on each S-II engine to activate the engine-out status lights.
- Transition from S-IC monitoring to S-II monitoring at staging is accomplished within the launch vehicle circuitry.

S-IVB Stage Thrust. The status of the S-IVB engine thrust is displayed in the spacecraft (one indicator light). Upon loss of engine thrust, the engine-out status light is energized by a discrete signal.

- Engine thrust is monitored throughout S-IVB burn.
- Abort because of thrust loss is governed by mission rules.
- A minimum of two thrust sensors are used on the S-IVB engine to activate the engine-out status light.
- Transition from S-II monitoring to S-IVB monitoring at staging is accomplished with the launch vehicle circuitry.

Staging Sequence. Physical separation of stages including the S-II second plane separation, is indicated in the spacecraft by lights, or other suitable discrete indications. In case of no separation, abort will be governed by mission rules.

Launch Vehicle Attitude Reference Failure. Improper operation of the launch vehicle attitude reference (sensed by the IU guidance and control system) will energize an indicator light in the spacecraft.

Abort or switchover to spacecraft guidance will be governed by mission rules.

Angle of Attack. An angle-of-attack function is displayed by an analog indicator in the spacecraft. This parameter is an indication of slow control failures which lead to excessive angles of attack.

The measured pitch and yaw components are combined in vector form into a total angle-of-attack indication.

The type of measurement to be displayed and the limit settings (if necessary, as a function of flight time) will be determined later. Limit settings will govern abort action.

S-II Propellant Tank Pressures. LO_2 and LH_2 tank pressures in the S-II Stage are displayed in the spacecraft by means of an analog display. This parameter requires a redundant sensor and display system.

S-IVB Propellant Tank Pressures. LO_2 and LH_2 tank pressures in the S-IVB Stage are displayed in the spacecraft by means of an analog display. This parameter requires a redundant sensor and display system.

Attitude Error (Spacecraft). Attitude errors from the spacecraft guidance and navigation system are displayed in analog form on the flight director attitude indicator. This parameter is an indication of slow control failures leading to excessive angles of attack or excessive attitudes.

The spacecraft guidance and navigation system will be preprogrammed with the launch vehicle tilt program for the S-IC flight period. Limit settings as a function of flight time (to be determined later) will govern abort actions.

Angular Rates. A single launch vehicle overrate indicator light in the spacecraft is energized by the IU Control EDS Rate Gyro package when permissible angular rates are exceeded in any plane. This indication primarily covers the flight period in which the overrate automatic abort capability is deactivated.

Spacecraft angular rates are presented by analog display on the flight director attitude indicator. The sensing device for this information is the Apollo rate gyro package. Limit settings, as a function of flight time, determine abort actions.

Activation of automatic abort is based on two basic parameters as follows:

Angular Overrates. This automatic abort parameter covers all control failures which rapidly lead to an excessive angle of attack and subsequent vehicle breakup. Information will be supplied by the control EDS rate gyro package which consists of three rate gyros for each control plane. These gyros are located in the instrument unit. An automatic abort will be initiated when two out of three gyros in any plane indicate that permissible angular rates are exceeded.

Provisions are made to manually deactivate the automatic abort signal for all three planes simultaneously with one switch located in the spacecraft. Manual deactivation time is to be established by mission rules. Capability for deactivating either the roll or pitch/yaw/roll signals by sequencing, prior to first stage inboard engine cutoff, will be available within launch vehicle circuitry.

Adjustable sensor limit settings are provided in pitch and yaw within 2 to 10 degrees/second and in roll within 5 to 20 degrees/second. Sensing hardware must be removed from the launch vehicle to accomplish these adjustments.

S-IC Two-Engines-Out. The loss of thrust on two or more engines will initiate an automatic abort. This automatic abort mode covers failures occurring near the pad and possible range safety action. Deactivation of the automatic abort capability prior to inboard engine cutoff arming is provided by the launch vehicle sequencer.

This automatic abort capability may be manually deactivated from the spacecraft. Manual deactivation times will be established by mission rules.

A minimum of two thrust sensors are used on each S-IC engine to provide inputs into the EDS circuitry. Action of at least two sensors is required to indicate loss of engine thrust.

3.3.3.2 Abort Modes

The LEV configuration is shown in Fig. 106. Abort sequences are illustrated in Figs. 107 and 108 and can be divided into three altitude regions: low altitude (pad abort to 30,000 ft), intermediate altitude (30,000 ft to 100,000 ft), and high altitude (100,000 ft to LES jettison). The sequence of events for the first few seconds of abort flight is common to aborts in any of the three regions. It consists of (1) abort initiation by astronaut or by EDS, (2) booster engine cutoff (only for aborts after 30 sec of launch vehicle flight time, (3) command module/service module interface separation, (4) launch escape and pitch-control-motor ignition and reaction-control-system propellant dump (only during aborts initiated up to 42 sec after lift-off), and (5) canard deployment 11 sec after abort initiation.

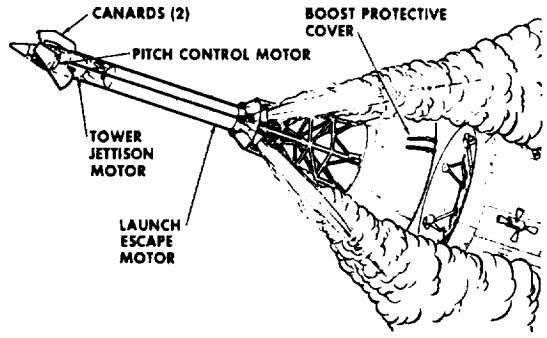

Figure 106. Launch Escape Vehicle

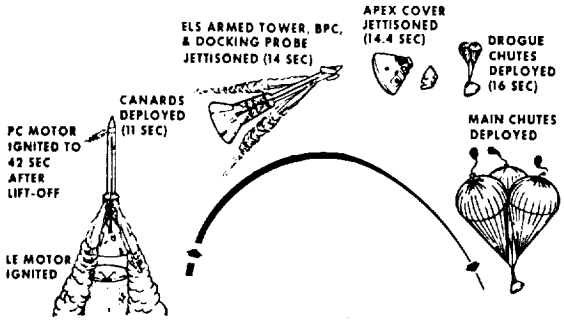

Figure 107. Low-altitude Abort Mode

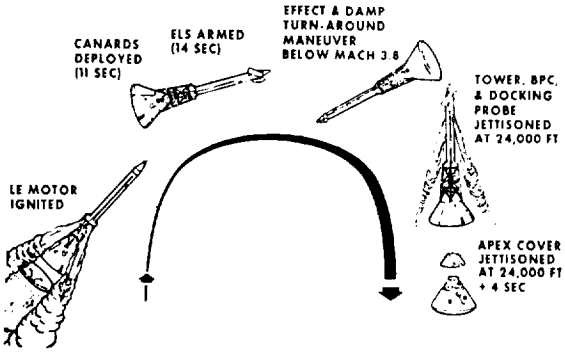

Figure 108. High-altitude Abort Mode

Initiation of the earth landing system (parachute sequence) can occur either 16 sec after abort initiation or during descent at approximately 24,000 ft if abort occurs above 30,000 ft. For aborts initiated above 100,000 ft, a special procedure has been established because of the lower aerodynamic stability encountered; following LES motor burnout, the crew is to establish a specific pitch rate using the reaction control system to avoid acquiring an undesirable trim condition and associated adverse acceleration during subsequent descent.

3.3.3.3 Aerodynamic Characteristics

A canard system reorients the LEV shortly after abort to minimize undesirable "eyeballs-out" acceleration following high-altitude aborts, and reorient the CM to the normal entry attitude for apex cover jettison and subsequent parachute deployment. The canard surfaces are deployed by a pyro-technically operated actuator 11 sec after abort initiation. This delay was established by the time critical pad abort case.

The requirement for a system to reorient the CM stems from the existence of a stable trim point for the CM in the apex forward condition. Thus, if the LES were jettisoned while the launch escape vehicle were in stable flight following abort, the CM could trim apex forward resulting in severe eyeballs-out accelerations and adverse attitude for apex cover jettison and parachute deployment.

The LEV has aerodynamic characteristics that vary grossly over the α range of interest and cannot be

linearized. To predict vehicle motion following canard deployment, it was necessary to define the characteristics throughout the full 360° of rotation. In addition, the Mach number range of interest varies from 0 to 10, depending on the conditions at abort initiation, and can vary over a wide range for any given abort. Although the launch escape vehicle is aerodynamically symmetric prior to canard deployment, the vehicle is dynamically asymmetric because of the offset c.g. of the command module. Moreover, the motor plumes shadow the CM producing a pronounced destabilizing effect, and aerodynamic symmetry is lost, further complicating the analysis.

In view of foregoing considerations, the prediction of vehicle dynamics requires the determination of the static force and moment coefficients as functions of the angles of attack and sideslip, Mach number, thrust coefficient, and proximity effects. Vehicle aerodynamic damping characteristics were also required as a function of Mach number in the vicinity of the two trim points of primary interest.

The nonaerodynamic factors that influence vehicle dynamics are the launch escape motor thrust time history, the large destabilizing movement of the c.g. because of depletion of propellant, and the rapid variation in q_0 during oscillations of the vehicle. Sophisticated three- and six-degree-of-freedom digital computer programs were necessary to handle the large amount of stored data and to undertake the step-by-step, time-dependent solution for the dynamics of the vehicle.

Further details, including the results of wind tunnel tests, may be found in Ref. 41.

The objectives of the Gemini and Apollo programs were limited in scope, so the demands placed on an abort system were relatively modest. For the more ambitious manned space missions, a different abort methodology will be required along with some new rescue and retrieve configurations. Some of the abort guidance and control problems of these missions have already been discussed. In the following sections, some specific rescue and retrieve configurations will be considered.

3.4 EMERGENCY ESCAPE SYSTEMS

While it is hazardous to speculate on the precise form of future manned space vehicles, certain basic conceptual philosophies for emergency escape from a disabled vehicle appear to remain valid. The basic ideas embodied in the parachute and ejection seat (in the case of aircraft), or the lifejacket and liferaft (for sea going vessels) will probably be embodied in the rescue systems for manned spacecraft, albeit at substantially higher levels of complexity and sophistication.

The abort procedure will be dictated first of all by the category of emergency that arises (Table I). Typical "in-space" emergencies are summarized in Table VII.

Table VII. In-space Emergency

Emergency	Category
Loss of Supply Ferry	A-1
Collison (Major)	A-1
Propulsion Explosion	A-1
Meteoroid Penetration (Major)	A-1
Exteme Solar Flare	B-1
Attitude Control Failure	B-1
Stage Separation Failure	B-1
Control Failure	B-1
On-Board Propulsion Failure	B-1
Power Supply Failure	B-1
Major Structural Failure	B-1
Fire in Vehicle	B-1
Human Failure - Physiological	B-1
Human Failure - Psychological	B-1
Leaks	B-2
Meteoroid Penetration (Minor)	B-2
Collision (Minor)	C-1
Communications Failure	C-1
Electrical Arcing	C-1
Vehicle Instrumentation/Display Failure	C-1
Environmental Control Failure	C-1
Toxic Gas Generation	C-1
Mission Instrumentation Failure	C-2

The abort vehicle itself may be classified as to function and configuration in the manner shown in Fig. 109. Most studies to date have been performed on abort vehicles having a reentry capability — and are particularly attractive for escape from low earth orbits. No rescue vehicle is required, and escape can be rapid, which is an important consideration for category A-1 emergencies.

The main advantages of erectable escape capsules are minimum weight and capability for storage in a confined area. It is also conceivable that in certain space missions, it may be preferable to abandon a disabled vehicle in an escape capsule which has no reentry capability; subsequent rescue would then be accomplished by a secondary vehicle launched either from earth or another vehicle in orbit.

A nonseparable abort vehicle is one which, as the name implies, does not separate from the main vehicle but which can be effectively sealed against whatever hazard arises in the main vehicle. This might be considered analogous to the closing of bulkhead hatches on submarines or ships for damage control. Special life support systems must be provided in this case, and here also, rescue must be accomplished by a secondary vehicle.

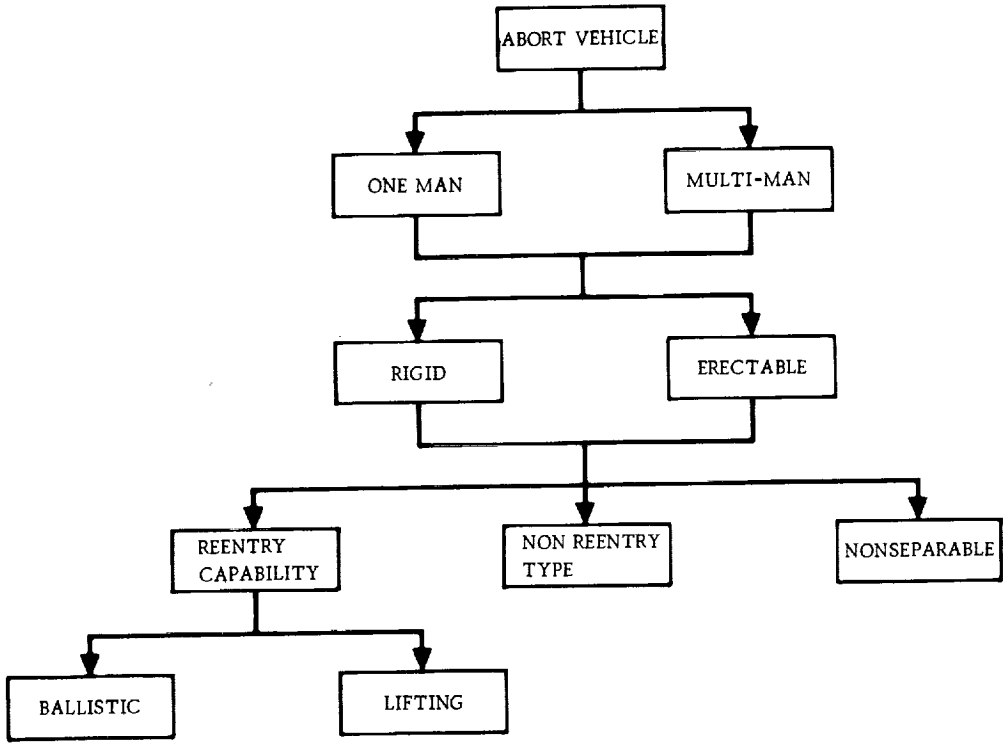

Figure 109. Types of Abort Vehicle Configuration

The abort configurations described in the following sections represent a sampling of schemes which have been proposed to rescue a crew in a disabled spacecraft. Which, if any, of these will reach operational status in the foreseeable future is, at the moment, pure speculation. All that can be said for now is that extensive development work is still required.

3.4.1 Satellite Life Jacket

It is not inconceivable that an astronaut may eject from a disabled spacecraft in the manner of a man abandoning a "burning ship" by donning a life jacket and jumping into the water. This is, in fact, precisely the scheme proposed by Bloom and Quillinan,[15] and designated by the acronym MOOSE (man out of space easiest).

As shown in the sequence of Fig. 110, when it is necessary to abandon the spacecraft, the man dons a space suit (or he may already have it on) and with it the attendant oxygen supply, recovery aids, and survival gear. As part of this design, the space suit is enclosed in a plastic covering and has attached to it tanks containing a foaming plastic and mixer. The man is also provided with a retrorocket package. To deorbit, the man visually orients himself to the earth and measures the altitude and direction of flight with an optical sight mounted on the retrorocket. Using the altitude information and precalculated range tables mounted in a display on the rocket

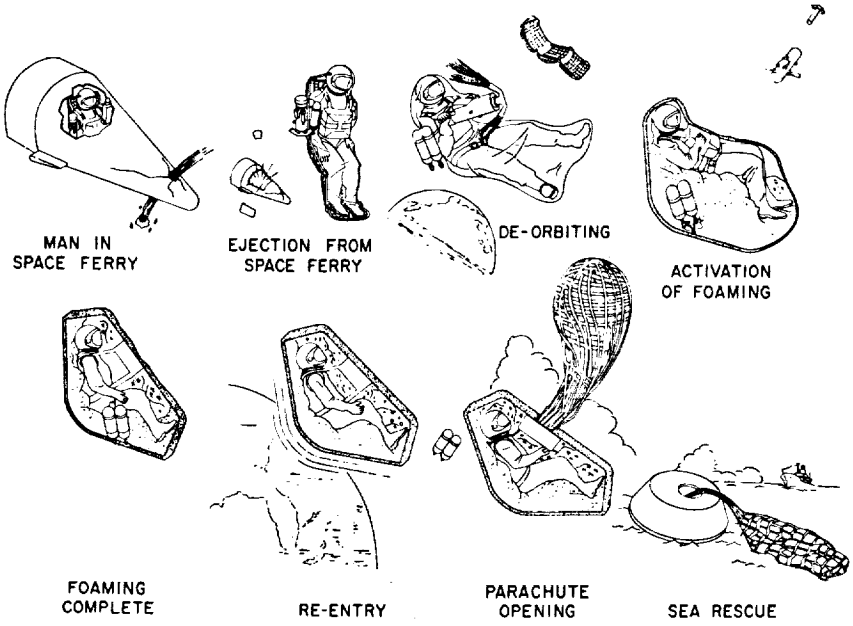

Figure 110. MOOSE Operation

structure, the man is able to aim and fire the rocket motor at the proper orientation in order to achieve reentry. Since there is little effect due to small retrothrust misalignment, visual aiming with a simple gunsight type of device should provide sufficiently accurate alignment. In many cases, the man will avail himself of the option of delaying the firing of the retrorocket until his position in orbit is advantageous to landing in a particular area. The procedure then calls for the astronaut to orient himself for reentry, using the cold control jets on the retrorocket and inflating the plastic covering to the designed shape for reentry. Straps attached to the man and the plastic covering position him in the proper relationship to the plastic covering. The foaming process then fills the space between the man and the plastic covering with foam plastic. A dense plastic foam of 50 lb/ft^3 forms the ablation shield, a less dense foam of 3 lb/ft^3 forms the afterbody, and a very low density foam of 1 lb/ft^3 "pots" the man and equipment in the vehicle. Prior to reentry, the high-intensity flare is fired and the beacon activated. The design shape is highly stable and orients itself early in the reentry. During reentry, the dense foam plastic ablates, protecting the man from the thermal environment, and the very low density plastic cusions him against the deceleration. After maximum reentry heating, radar chaff is expelled, and another high-intensity flare is fired. At an altitude of about 30,000 ft the parachute is deployed on signal from a baroswitch. Parachute-opening shock and drag pulls cutting cords which remove the lightweight foam plastic from around the man's hands and arms. The parachute is designed to limit the impact velocity to 30 ft/sec at sea level. This is well below the maximum allowable impact velocity. At impact, Sofar bombs are released to provide location aids if the impact is on water. After impact the man releases himself from the lightweight foam by pulling on cutting cords with his freed hands and arms. He then obtains the survival kit embedded in the plastic foam. MOOSE can be used as a raft if the impact is on water, and the survival kit is equipped to maintain him in almost any earth environment.

Figs. 111 and 112 show the MOOSE design. The entire unit weighs on the order of 470 lb.

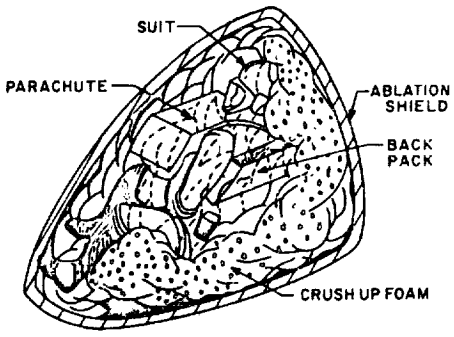

Figure 111. Satellite Life Jacket, MOOSE

A typical reentry trajectory for the MOOSE system is shown in Fig. 113, and the resultant reentry stagnation heating flux and total heating are shown in Figs. 114 and 115 respectively. Fig. 116 shows the calculated resultant ablation of the MOOSE shield. Urethane foam appears to perform well as the ablation material.

Improvements beyond the capability of the early MOOSE system may come in the control of the impact area. This can be accomplished by providing the capability of remaining in orbit until a more desirable position has been reached and then firing the retrorocket. The extended time in orbit requires additional oxygen, CO_2 removal, and

moisture removal. Altitude-, direction-, and angle-measuring equipment is another area of improvement. The optical sight is replaced by an IR sight of the vaporgraph type, thus enabling the man to view the dark side of the earth more clearly. Photo cells used to scan the IR sight could measure the included angle of the earth, and a simple computer, calculating the altitude and time to go to retrorocket firing, would also control the attitude jets from the photocell information. Air-, water-, and land-snatch capability could also be provided.

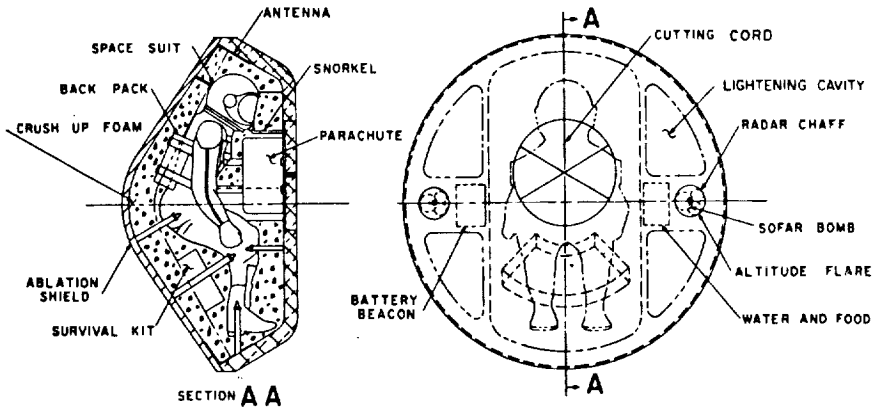

Figure 112. Satellite Life Jacket, MOOSE Profile

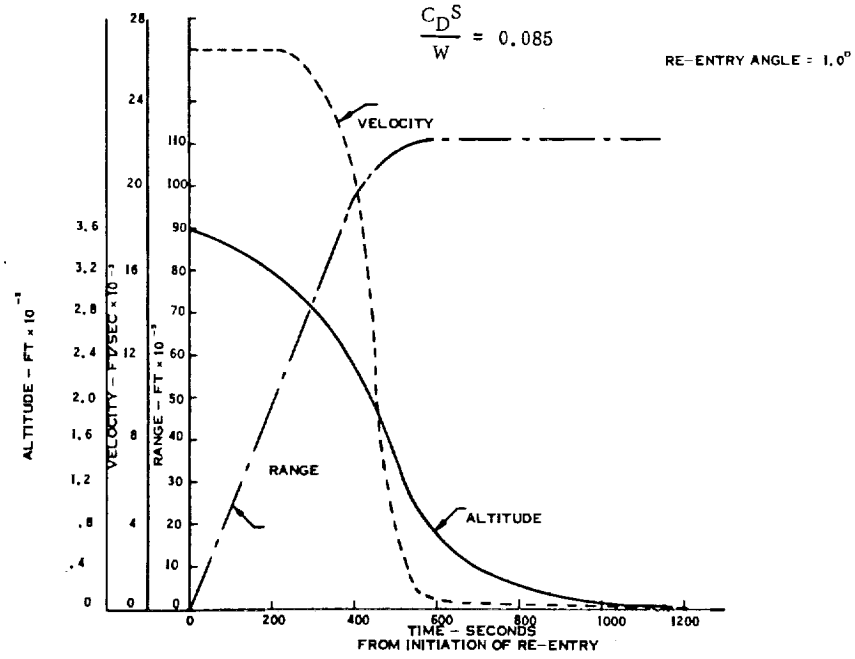

Figure 113. MOOSE Trajectories

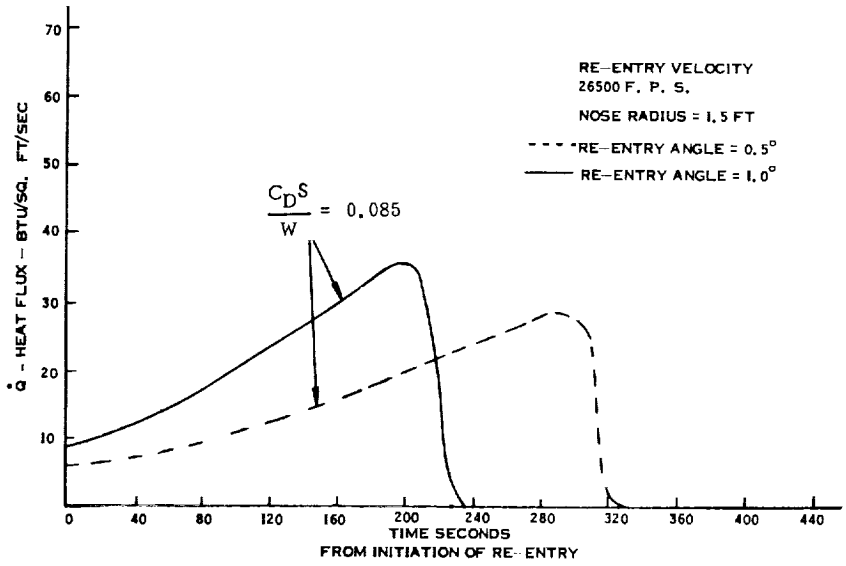

Figure 114. Reentry Heat Flux, Stagnation Point, Space Life Jacket, MOOSE

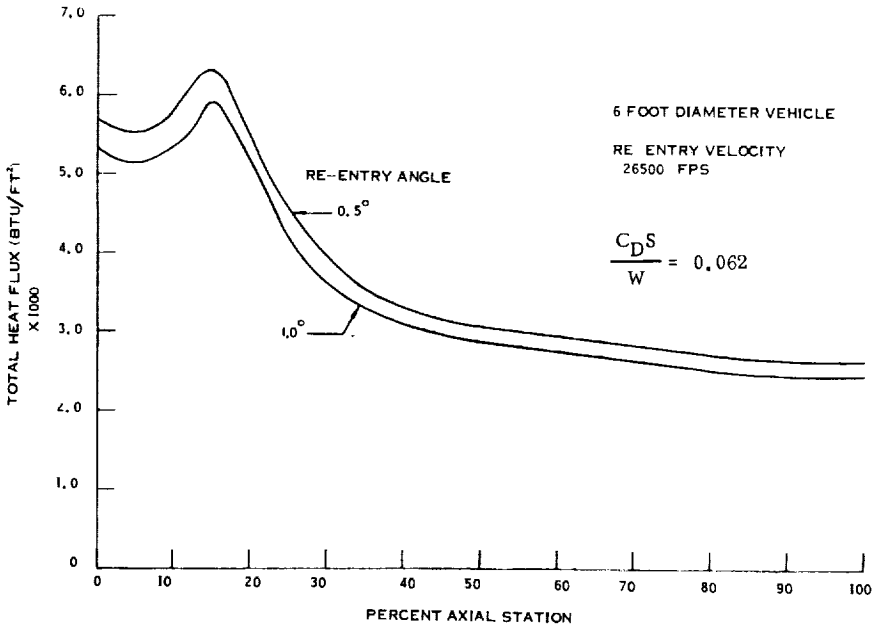

Figure 115. MOOSE Reentry Total Heating

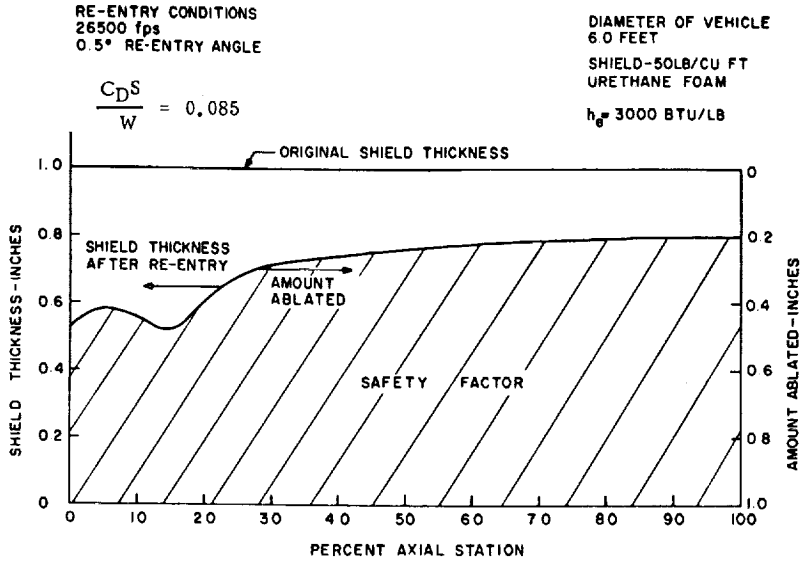

Figure 116. Satellite Life Jacket, MOOSE Ablation Shield

3.4.2 Satellite Life Raft

It is common practice for ships to carry life rafts as part of their emergency equipment. Utilized at sea, a lift raft separates the shipwrecked sailor from the hostile sea environment, and lacking power and controls, drifts toward shore at the mercy of the currents. Its counterpart in space, the satellite life raft, insulates the shipwrecked astronaut from the hostile space environment while it hurtles toward earth (after deorbiting) without propulsive power or course control, under the influence of gravity.

This concept, as well as that of the satellite lifejacket, is due to Bloom and Qullinan.[15]

The satellite life raft, shown in Fig. 117, although utilizing the same reentry shape, is a rigid vehicle with a 0.052-in. thick fiberglass liner protected by a nylon-reinforced phenolic plastic ablation shield 3/4 in. thick. With a 1/4 in.-thick aluminum-honeycomb-cored fiberglass afterbody to complete the closure, this rigid device gains in structural integrity and reliability over the life jacket which must be foamed into shape in space.

Typical operation of the life raft escape is shown in the sequence of Fig. 118. During normal operations, the satellite life raft is mounted in the wall of the satellite, shield protruding, entrance hatch open to living or working quarters, and

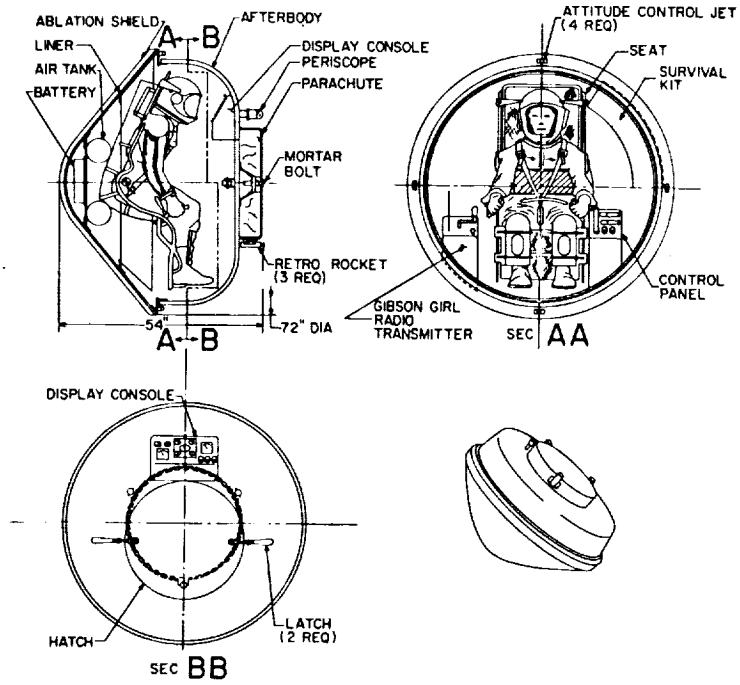

Figure 117. Satellite Life Raft

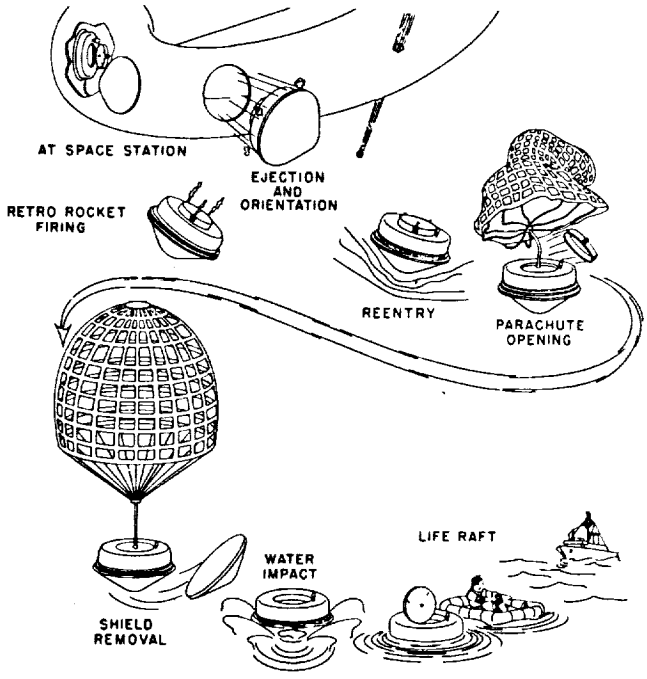

Figure 118. Satellite Life Raft Operation

airtight seal and clamps holding the life raft in its position. On initiation of the "abandon ship" signal, the astronaut climbs into the life raft, secures the hatch, and loosens the clamps (explosive or magnetic). Springs eject the life raft, and after seating himself in the seat composed of aluminum frame with a supporting web of partially drawn nylon, he secures his acceleration-deceleration harness and utilizes the periscope with 180° lens and scribed display face to determine proper orientation for deorbiting. Stored gas (which is air, available for breathing in case malfunction of deorbiting rockets necessitates a wait for rescue) is employed in the attitude jets to orient the life raft for retrorocketing. Attitude is adjusted according to visual observation of the juxtaposition of the earth with scribed circles on the periscope display. The emergency signaling procedure detailed earlier, consisting of flares, radio beacon, and Sofar bombs, is employed in sequence by the life raft.

Reentry heat protection is furnished by the ablating heat shield, which also furnishes the insulating properties to prevent the reentry heat pulse from penetrating to the interior. Subsequent to traversing the extreme reentry conditions, the parachute is deployed by baroswitch signal at an altitude of 30,000 ft. The heat soaking that would take place during parachute descent and that would raise the inside temperature is avoided by jettisoning the heat shield at parachute opening. Landing impact is maintained at about 30 ft/sec (well below man's tolerance in the orientated seat of partially drawn nylon). After landing, the entrance hatch may be opened for air or egress. Since the device floats, there is no need to leave it if it lands on water. In the event it becomes necessary to leave, the rubber life raft from the survival kit may be launched through the hatch, which provides quick escape capability. As before, the survival kit provides sufficient equipment to maintain the man in almost any earth environment, and the hand-powered "Gibson Girl" radio transmitter provides searchers with a homing signal.

A typical trajectory for the satellite life raft is shown in Fig. 119, and Fig. 120 presents a plot of the stagnation point heat flux resulting from such a trajectory. The total stagnation point heating is given in Fig. 121, and it is this value which fixes the amount of ablating material required.

By employing phenolic nylon as the ablative heat shield, the life raft design is able to take advantage of that material's higher effective heat of ablation, and thus it requires a heat shield thickness of only 3/4 in. while still maintaining a safety factor of at least 100%. This information is shown graphically in Fig. 122 which, for an extreme reentry condition, indicates the amount of heat shield ablated from the surface of the life raft during reentry. In addition, the char and remaining ablative material form such effective insulation that the inner surface of the fiberglass liner remains below 160° during the heating portion of the trajectory.

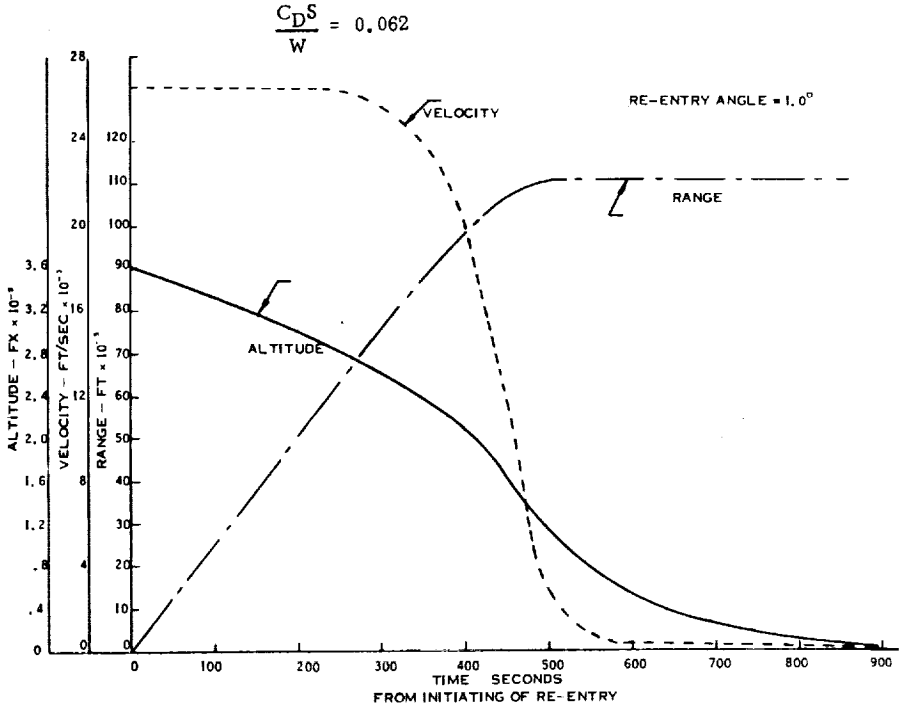

Figure 119. Satellite Life Raft Trajectories

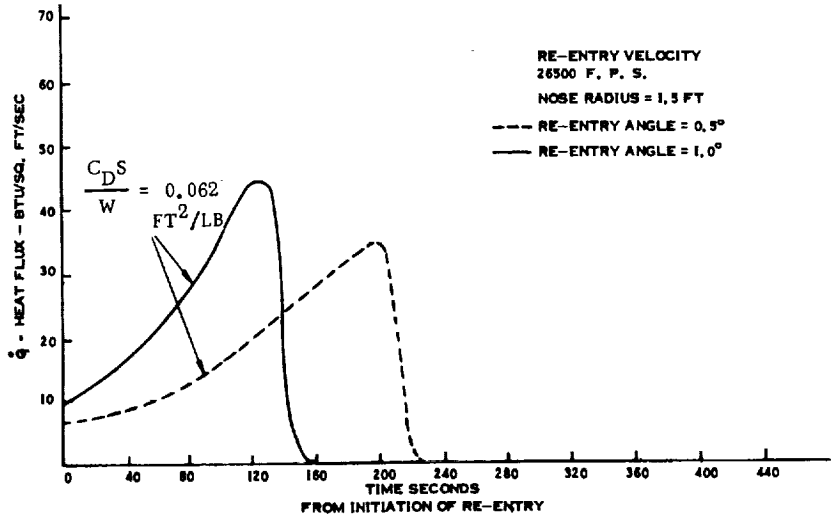

Figure 120. Reentry Heat Flux Stagnation Point Satellite Life Raft

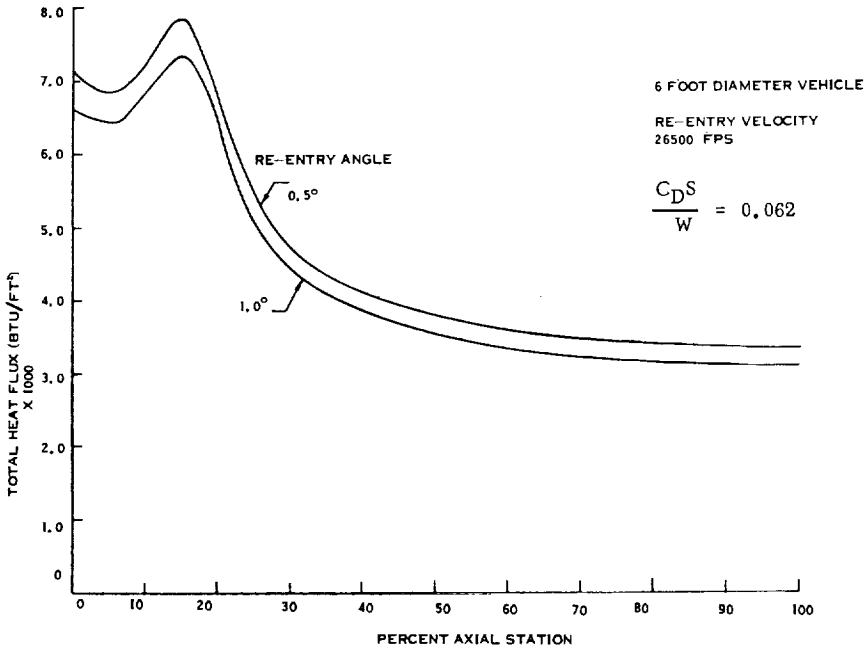

Figure 121. Life Raft Reentry Total Heating

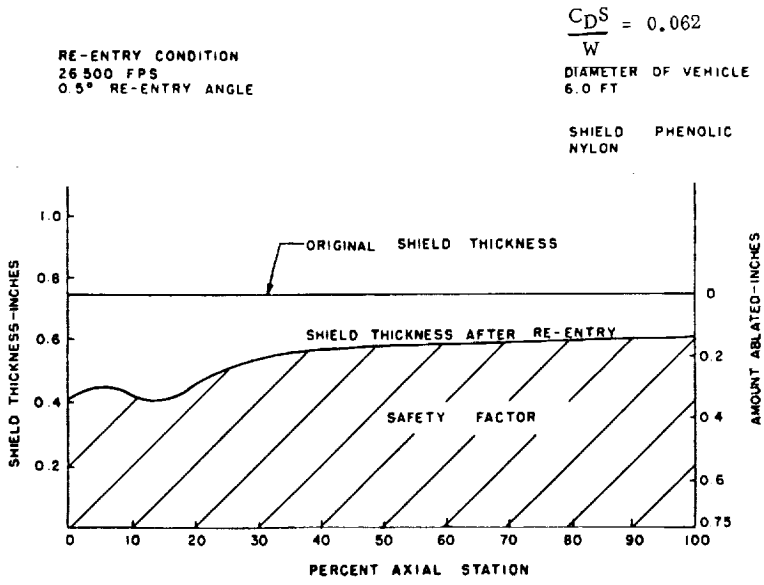

Figure 122. Satellite Life Raft Ablation Shield

3.4.3 Satellite Life Boat

Continuing the analogy with sea rescue equipment, a higher degree of survival capability is afforded by the use of a satellite lifeboat. This idea, also developed by Bloom and Quillinan,[15] is best studied with respect to stipulated crew size and degree of maneuverability desired.

Arbitrary selection of a three-man team, with associated equipment and a 500- nautical mile cross-range maneuver, combined with a requirement to initiate the maneuver at 0.8 to satellite velocity in order to avoid maneuvers when stagnation heat fluxes are highest, fixes payload weight at about 1,000 lb, and L/D at about 1.5 (Fig. 123). These, together with compact design and simplicity requirements, helped set shape factors in the design selection. The resulting device is shown in Fig. 124.

An interesting feature of this lifeboat is the combination of heat shields used. On the windward surface, where reentry heat fluxes and air temperatures are high, this device employs the ablating phenolic nylon shield. On the lee side, the lower air temperatures allow the use of a reradiation heat control provided by a refractory coating backed by 4 in. of insulation.

In operation, the sequence of Fig. 125 seems reasonable. At the "abandon ship" signal, the astronauts scramble into the lifeboat which is sealed to the outside of the space station. The access hatch of the lifeboat is open to the interior of the station, and the astronauts occupy the aluminum-nylon web chairs, the hatch is fastened, seal is broken with station, and the lifeboat is sprung away from the station. Using a periscope version of the alignment sight previously discussed, the lifeboat is positioned by cold jets for deorbiting, and the retrorocket fired. With periscope retracted, instrumentation aboard provides information on reentry loads, vehicle orientation at reentry, and time to initiate maneuver. At the "maneuver" signal, the periscope is once again extended and maneuvers begin when the pilot astronaut, using navigation aids aboard, locates a suitable landing area. The previously described location aids are still used in sequence; e.g., flares, beacon, and chaff. On approach to the landing area, the parachute is deployed and the landing is almost vertical. Should the landing

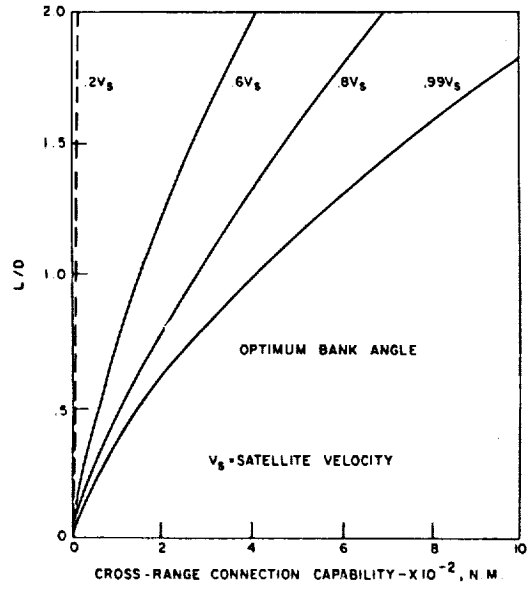

Figure 123. Variation in Cross-Range Maneuver With Initial Velocity

take place on water, the lifeboat floats more than half out of the water. When required or desired, the forward half of the device is released and jettisoned. The rear half can continue to float and is provided with a watertight plastic cover for insertion in the space left by the ejected nose section. If the lifeboat is to be abandoned, the rubber raft of the survival kit can be inflated, and, as before, survival kit and "Gibson Girl" provide excellent survival capability.

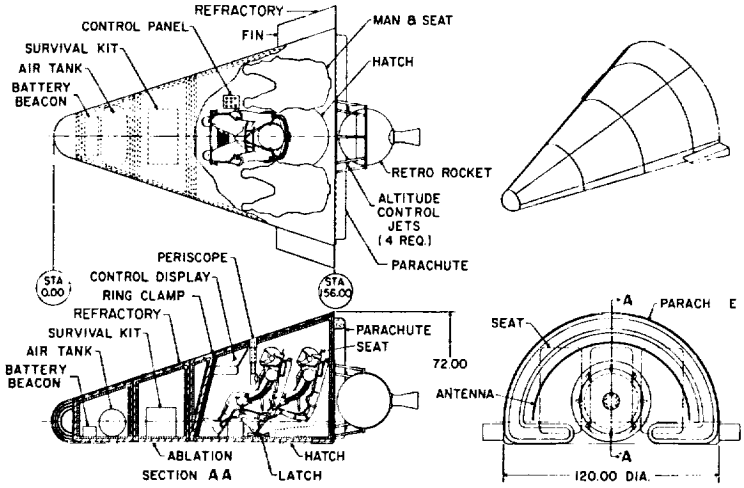

Figure 124. Satellite Lifeboat

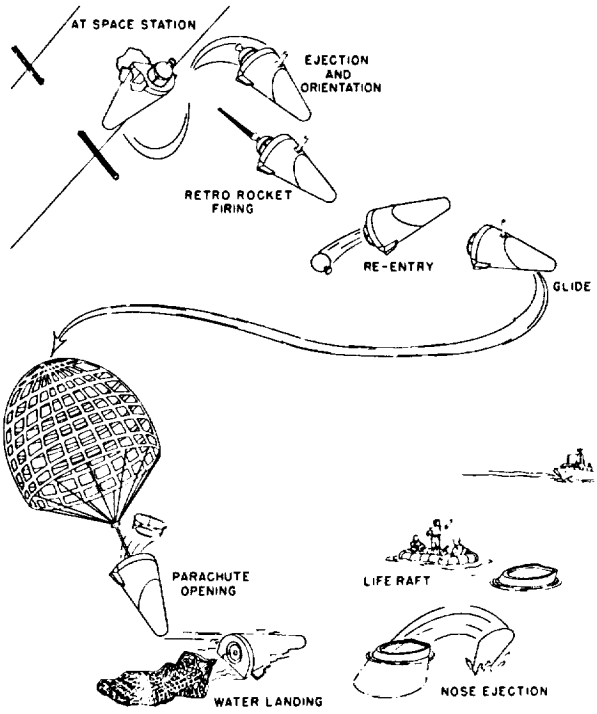

Figure 125. Satellite Lifeboat Operation

3.4.4 EGRESS

As noted earlier in this monograph, a complete manned space mission profile is generally divided into prescribed regions, each of which exhibits its own peculiar abort problems. It would seem to imply that several different abort systems would have to be incorporated in the same vehicle.

EGRESS, which is an acronym for Emergency Global Rescue Escape and Survival System, is an attempt to provide an abort capability over a complete range of flight profiles from on-the-pad, through atmospheric boost, orbit injection, orbit, reentry, and landing.† The EGRESS vehicle is illustrated in Fig. 126. Its basic design employs the existing B-58 cockpit ejection capsule. Space rescue additions include an attitude control system, guidance unit, environmental control system, UHF communications link, retrorocket, and a drag stabilization system. The total weight is 716 lb.

† The presentation follows Dunn and Carroll[11] from which most of the material in this section is derived.

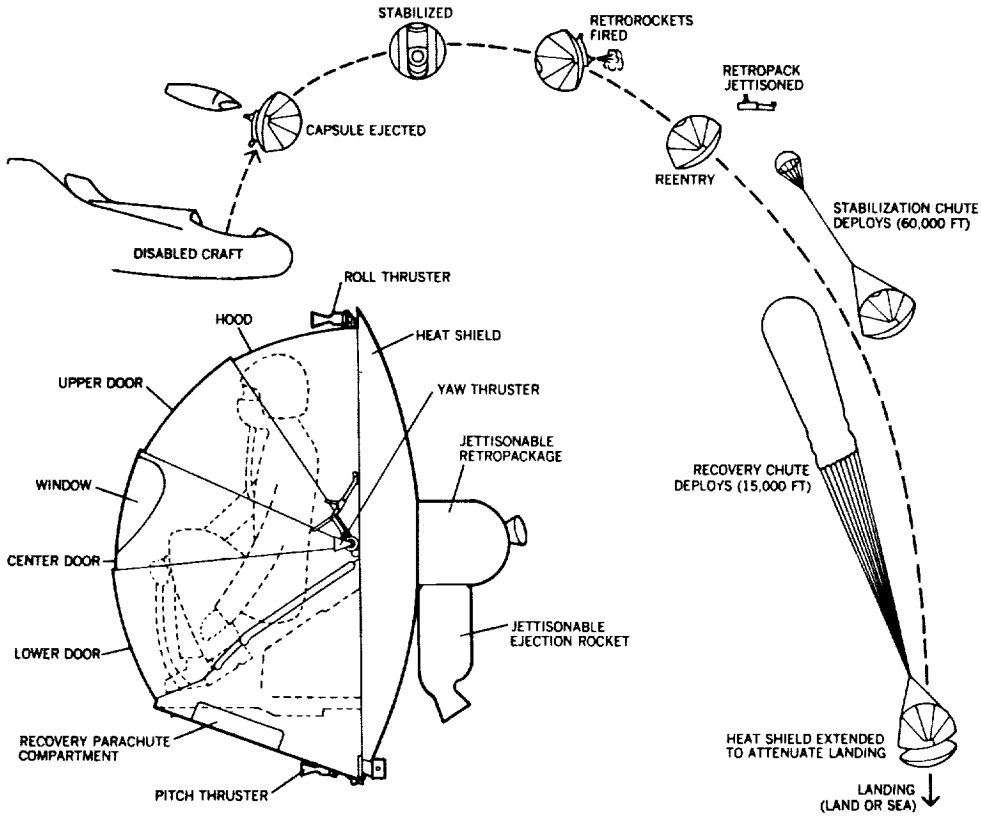

Figure 126. EGRESS Vehicle

The system operation varies with different phases of the flight profile. For this reason, a manual selector switch is incorporated in the design thereby allowing the astronaut to preprogram the ejection and recovery operation for the particular flight condition at abort.

A typical abort sequence begins with encapsulation; that is, the upper, center, and lower doors (which are normally positioned above the hood in Fig. 126) are moved to the down position, thereby completely sealing the astronaut from the environment. The astronaut ejects the capsule by squeezing one or both of the ejection triggers on the ejection handles or firing a canopy or hatch jettison actuator; after a 0.3-sec delay, the ejection catapult is fired, giving the capsule a separation velocity of 50 fps. The rocket provides an impulse of 3,000-lb-sec, which is enough to ensure tail clearance for a 1,000-lb capsule at a dynamic pressure of 1,600 psf. Since peak dynamic pressure during boost is only 800 psf, this combination of rocket and catapult should be sufficient to provide separation and attenuate decelerations.

Nominal spinal accelerations imposed on a man by the catapult are approximately 13 g. If the ejection occurs in any suborbital period, the sequence fires the ejection rocket. Since the capsule drag is quite high and is only partially offset by thrust, the vehicle deceleration rate can be as high as 22 g. As the capsule clears the vehicle, aerodynamic forces (if they exist) will position the capsule so that the heat shield is forward and positive acceleration (eyeballs in) is imposed on the capsule occupant. Stabilization is provided aerodynamically by the capsule/heat shield combination, and it is augmented by a drag chute stabilization system during sub-orbital periods.

If ejection occurs during orbit, the ejection rocket is locked out and the ejection sequence fires only the small ejection catapult. The catapult provides minor acceleration; thus the capsule is simply pushed out of the primary vehicle. At this point, the attitude control system is used to orient the vehicle manually and stop tumbling. The astronaut then uses the onboard clock for time information. Knowing the exact time, and using an onboard position location chart (based on time), the occupant decides when to initiate retrofire. The onboard life support system is designed to provide oxygen and environmental control for approximately 1.5 orbits to allow adequate landing site selection. Before retrofire, the capsule is oriented manually so that the telescope reticle is in line with the horizon. Manual retrothrust then is initiated; alignment is maintained by using the large attitude control nozzles. After retrothrust, the capsule is oriented to the reentry position and manually retained by using the attitude control system.

The 50-ft-diameter ring-sail recovery parachute reduces the capsule's rate of descent to 25 fps. Ground impact forces are absorbed by four shock attenuators that are part of the heat shield attachments. The closed capsule can float without using auxiliary buoyancy devices. However, to provide stability in rough seas and maintain an upright attitude to open the upper capsule door, four outriggers with inflatable flotation bags are provided. The bags can be inflated quickly from a pressure

container on the upper flotation outriggers. A hand-operated pump is provided for inflating the flotation bags on the lower outrigger. The most critically needed items of survival equipment are accessible to the occupant of the closed capsule. After landing, the capsule can serve as a shelter or life raft.

A typical abort sequence is illustrated in Fig. 126. It is essentially the same with slight, but important, variations over the entire flight profile.

The boost phase establishes design criteria for the maximum dynamic pressure and maximum airloads; the reentry phase establishes design criteria for the aeroheating condition. The stability problems are somewhat different in these phases because of the differences in the Mach number and dynamic pressure combinations.

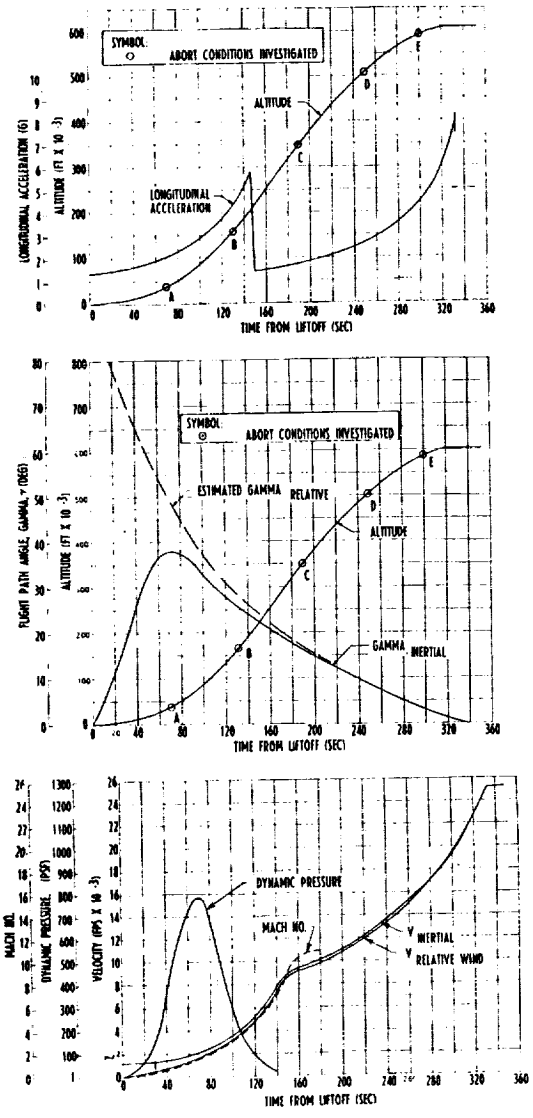

Figure 127. Typical Boost Time History

The escape environment has been investigated for several points during ascent, which comprises powered flight to a low perigee, coast, and final injection at the mission altitude. The escape conditions during the period of coast are not significantly different from the normal orbit conditions. A typical boost trajectory is presented in Fig. 127. Critical escape points are: (1) at launch, (2) at maximum dynamic pressure, (3) near staging, and (4) before orbit injection.

Results that affect design criteria are summarized in Table VIII; the first columns show the first critical conditions the capsule would experience when it is separated from the basic launch vehicle during boost; the second critical condition represents the period when the capsule falls back to earth or reenters from the launch-abort trajectory.

The maximum airload and deceleration occur during case A, the low-altitude booster, maximum dynamic pressure condition. However, the heating rates are low in this case. The most critical combination of deceleration and heating occurs in case E, the near-orbit injection case. Although the initial

Table VIII. Escape Conditions During Boost

Abort Conditions		First Critical Condition, Initial Abort (up-bound)			Second Critical Condition (down-bound)		
During Boost (Fig. 117)	Initial Flight Path Angle (deg)	Dynamic Pressure (psf)	Deceleration (g)	Heat Rate $\left(\frac{\text{Btu}}{\text{ft}^2\text{-sec}}\right)$	Dynamic Pressure (psf)	Deceleration (g)	Heat Rate $\left(\frac{\text{Btu}}{\text{ft}^2\text{-sec}}\right)$
A	49.5	752	22.1	1.4	42	1.24	0
B	28.5	44	1.3	2.3	210	6.2	2.1
C	17.0	0	0	0	502	14.7	12.7
D	8.5	0	0	0	664	19.5	29.0
E	3.0	0	0	0	670	19.7	52.0
Typical reentry trajectory	-2	310	7.8	60	-	-	-

flight path angle at abort is only +3°, the trajectory dynamics and velocity combine to give a return-to-earth, or reentry, angle of about -6° or -7° at a velocity of about 20,000 fps and an altitude of 300,000 ft. This relatively steep reentry angle results in high decelerations and heating rates.

Table VIII also shows the nominal orbital reentry conditions for comparison. The orbital reentry trajectory shows the most critical heating rates, but the dynamic pressures are about one-half those shown for case E. The critical design limits imposed by the reentry trajectory include maximum allowable decelerations encountered for shallow reentry. The capsule retrorocket will provide a predetermined reentry angle; the trajectory data shown in Figs. 128 and 129 represent the proposed capsule reentry. If the capsule is ejected from a lifting parent vehicle during reentry, the deceleration and aeroheating conditions generally will be no more severe since lift vehicles typically reenter at shallow angles.

The aeroheating environment is nearly identical to that of the hardware-proved Mercury capsule. The proposed capsule heat shield has a slightly smaller diameter than the Mercury shield (70 in. as compared with 74.5 in.), and the W/C_DS is about one-half (25 psf vs 55 psf). No particular problem areas are anticipated for the forward ablative heat shield, since the heating rates of 50 to 60 Btu/ft^2-sec and heat loads of 6,000 to 8,000 Btu/ft^2 are similar to those experienced by the Mercury capsules.

For escape from the parent vehicle during reentry, the capsule may eject at a maximum heating condition. In this event, the ablative heat shield briefly faces rearward until the capsule can rotate (yaw) 180°. A check of the yaw maneuver showed low total heat loads on the doors.

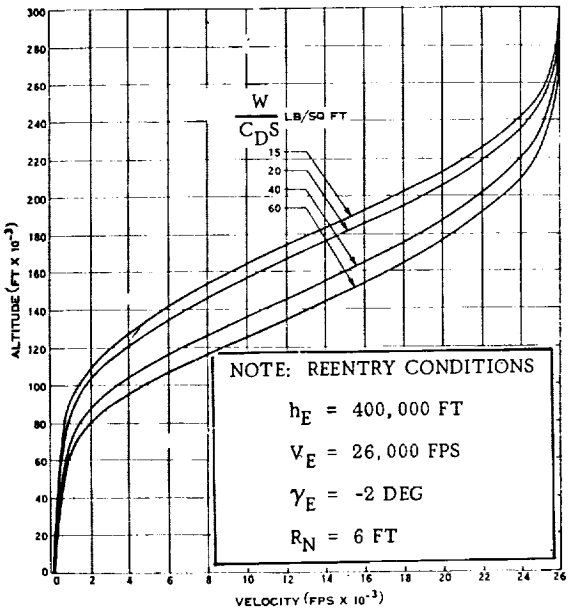

Figure 128. Ballistic Reentry Phase

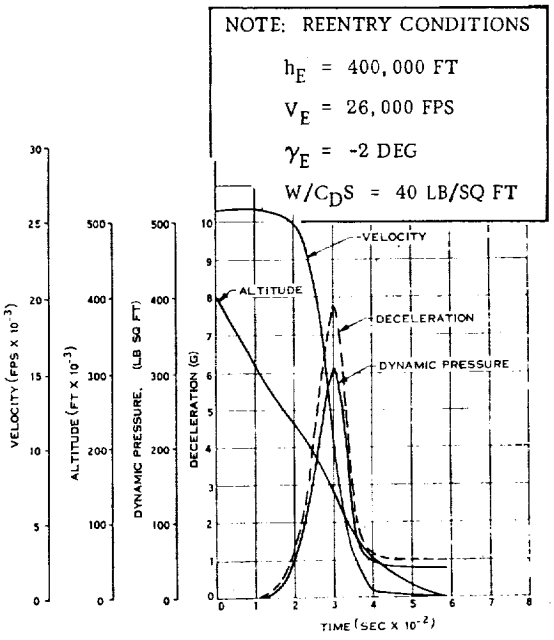

Figure 129. Ballistic Reentry Phase Time History

3.4.5 Paracone

Another system which has an abort capability throughout the flight profile is the paracone.[28] This concept, which is illustrated in Fig. 130, exhibits marked similarities to the satellite life raft (Sec. 3.4.2) and EGRESS (Sec. 3.4.4). Its distinctive feature is the use of an inflatable cone. It is claimed that this affords advantages by providing:

a. Automatic stability and orientation during atmospheric entry and descent to impact due to its peculiar shape.

b. Protection for the crew from temperatures generated by the reentry forces.

c. Absorption of the drag force of reentry due to atmospheric deceleration. For this application this force will be over 2-g for 3 min with a 10-g peak with the crew in the prone position.

d. Atmospheric deceleration to impact.

e. Impact attenuation to minimize the landing force.

f. Shielding against immersion, forest impact, or landing hazards in other adverse terrain.

g. Flotation in the event of a water landing.

h. A large, three-dimensional target for visual or radar search.

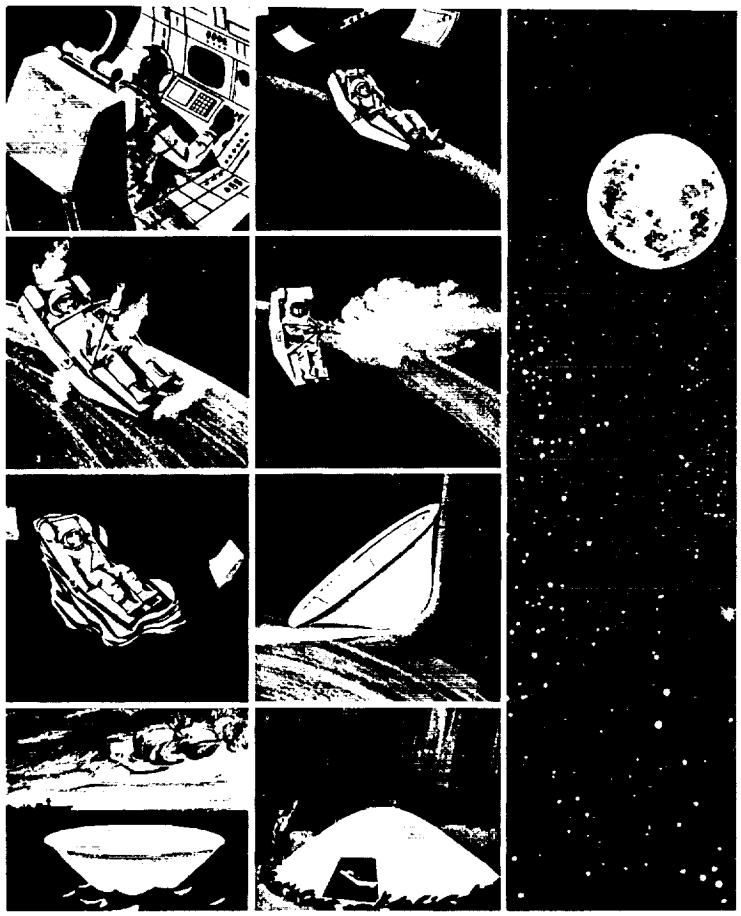

Figure 130. Paracone Concept

i. Shelter for the crew against the elements until recovery.

j. Psychological support to the crew by providing him with a large vehicle during the long minutes of the return.

Basically, the paracone is a gas-inflatable structure shaped like a cone with a large spherical nose. The astronaut is positioned and supported within the cone approximately one third the length of the cone as measured from the leading edge of the spherical nose. He is suspended over an air mattress flotation plenum chamber which, in turn, is located over the impact attenuator (see Fig. 131).

The paracone is part of the crew control seat, and includes the ejection device which enables the crew to clear the stricken vehicle, the stabilizing unit for retro postion alignment, the retro unit to allow deorbiting, the Paracone inflation system that inflates the deploys the Paracone, the life support pack, and the survival pack (Fig. 132). When deployment occurs, the astronaut is so positioned within the

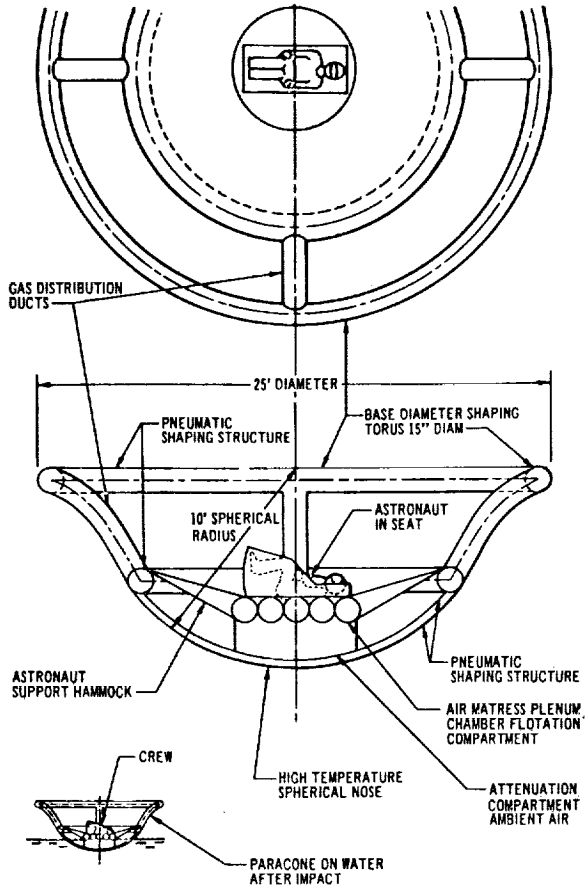

Figure 131. Paracone Configuration

paracone that he is protected during the reentry-temperature and aerodynamic-deceleration phase. In addition, as an integral part of its expandable structure, the paracone provides a terminal velocity impact decelerator, impact attenuation system, flotation and anti-immersion devices, and a large, three-dimensional search target for recovery.

The Paracone is weight-limited rather than size- or shape-limited, and is designed to handle any payload of reasonable size or shape within its weight accommodation design envelope. The astronaut or the crew-containing capsule rests within the Paracone with the crew in the prone position. Deployment of the Paracone may take place either before or after the retrograde force is applied to the payload removing it from orbit.

In a de-orbit abort sequence, the astronaut actuates the ejection handle which (1) vents the cabin; (2) removes the emergency access door in the vehicle; (3) ejects the astronaut, his seat, and the paracone system at a predetermined rate; and (4) actuates

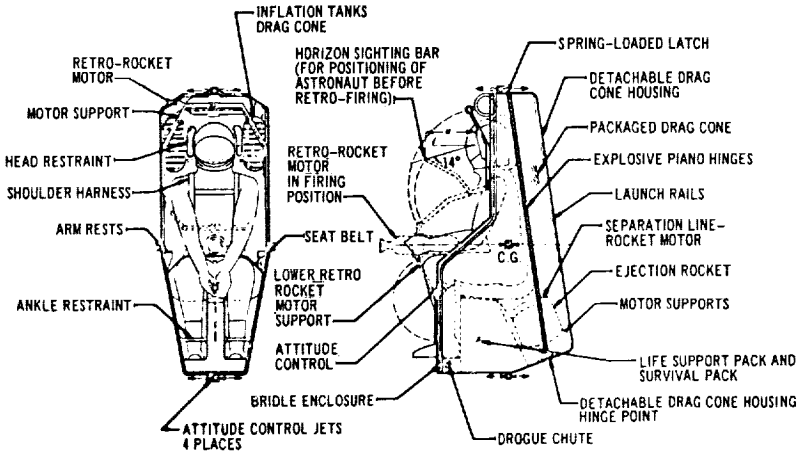

Figure 132. Paracone Survival Pack

the radio beacon transmitter. At a safe distance from the stricken vehicle, the astronaut stabilizes his seat with his attitude controls. He rotates the retrorocket into firing position, observes his position above the earth, and determines when he will fire his retrorockets. He has one orbit's time in which to do this. As he approaches his selected retrorocket firing point, he stabilizes to the correct firing attitude by using his horizon sighting bar, by orientation through star observation, or by radio instructions from earth. At the selected time, he fires his retrorockets and continues to made his attitude adjustments until the retrorocket impulse is completed (see Fig. 120).

The velocity increment of 550 fps applied in the retrograde direction will result in an initial entry speed of approximately 26,000 fps and an angle of 2.5°. If a ±10% tolerance in velocity increment and 30° tolerance in application angle in any direction are allowed, the minimum entry angle is 1° and the maximum angle is 2.5°. The paracone has been designed to operate successfully while not exceeding human tolerance limits over this range of entry conditions. These tolerances should provide impact with a range error of less than 500 n.mi.

After the retrorocket firing, the astronaut jettisons the empty retrorocket and actuates the paracone inflation system which allows the inflation gas to enter the pneumatic shaping structure of the paracone. From this point until after earth impact the astronaut has no other operation requirements. As the Paracone inflates, the internal gas pressure forces the protective housing segments apart until the segments reach a point at which they are automatically jettisoned. The pressurizing gas inflates, the internal gas pressure forces the protective housing segments apart until the segments reach a point at which they are automatically jettisoned. The pressurizing gas inflates the shapes the paracone around the crew. The internal shaping pressure of the paracone is maintained at a pressure differential of 3 psi during the atmospheric reentry and descent to earth. Time of descent from retro to impact will be approximately 1 hour.

As in the case of EGRESS, the precise details of the abort sequence vary with the particular phase of the flight profile.

An on-the-pad abort is illustrated in Fig. 133.

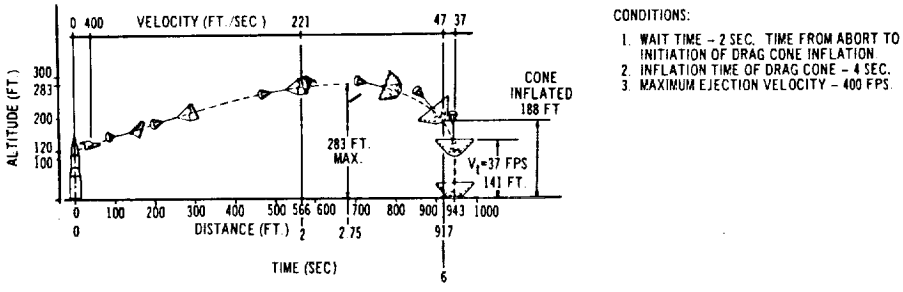

Figure 133. On-the-Pad Emergency Escape; Paracone

Some basic testing has been performed on the paracone structure including (1) wind-tunnel tests for drag and stability information, (2) free-fall model drop tests for dynamic stability information, (3) full-size impact attenuator tests, and (4) flow tests of various attenuator materials for use in comparative analyses seeking the most efficient material for the attenuator.

It is reported that these tests have been sufficiently encouraging to demonstrate basic feasibility of the design. Further details may be found in the paper by Kendall.[28]

4. REFERENCES

1. Miller, E. S., and Bloom, H.L., "Design Considerations for Boost Phase Abort of Manned Space Flights," IRS Paper No. 62-133, June 1962.

2. Gervais, R. L., and Johnson, M. C., "Abort During Manned Ascent into Space," AAS Preprint No. 62-36, January 1962.

3. McGowen, W. A., and Eggleston, J. M., A Preliminary Study of the Use of Finite Thrust Engines for Abort During Launch of Space Vehicles, NASA TN D-713, December 1961.

4. Slye, R. E., Velocity Requirements for Abort from the Boost Trajectory of a Manned Lunar Mission, NASA TN D-1038, July 1961.

5. Carter, W., and Kramer, P. C., "Escape of Manned Vehicles from Lunar Mission Ascent Trajectories," AAS Preprint No. 61-20, January 1961.

6. Merrick, R. B., and Callas, G. P., Prediction of Velocity Requirements for Minimum Time Aborts from the Midcourse Region of a Lunar Mission, NASA TN D-1655, April 1963.

7. Kelly, T. J., Adornato, R. J., and Speiser, K., "Abort Considerations for Manned Lunar Missions," ARS Paper No. 2478-62, July 1962.

8. Diven, J. L., and Daniel, J. W., Ascent and Descent Abort Flight Corridors for Orbital Transport Vehicles, Technical Note R-142, Brown Engineering Co., March 1965.

9. Diven, J. L., and Daniel, J. W., Graphs of Ascent and Descent Abort Flight Corridors for Orbital Transport Vehicles, Brown Engineering Co., March 1965.

10. Callas, G. P., and Merrick, R. B., "A Manual Abort Technique for the Midcourse Region of a Lunar Mission," Proc. 2nd Manned Space Flight Meeting, Dallas, 1963, p. 217-223.

11. Dunn, J. P., and Carroll, P. C., "Project EGRESS," J. Spacecraft, Vol. 4, No. 1, 1967, p. 9-14.

12. North, W. J., and Cassidy, W. B., "Gemini Launch Escape," Proc. 2nd Manned Space Flight Meeting, Dallas, 1963, p. 213-216.

13. Eggleston, J. M., "Some Abort Techniques and Procedures for Manned Spacecraft," Proc. Nat'l Meeting on Manned Space Flight, St. Louis, 1962.

14. Kelly, T. J., and Adornato, R. J., "Determination of Abort Way-Stations on a Nominal Circumlunar Trajectory," ARS Journ. June 1962, p. 887-893.

15. Bloom, H. L., and Quillinan, J. H., "Manned Satellite Emergency Escape Systems," Adv. in Astro. Sci., Vol. 8, Plenum Press, New York, 1961.

16. Young, J. W., and Goode, M. W., "Fixed Base Simulator Studies of the Ability of the Human Pilot to Provide Energy Management along Abort Trajectories," Proc. Nat'l. Aerospace Elec. Conf., Dayton, Ohio, 1962.

17. Ehricke, K. A., "Rescue from Space by a Secondary Vehicle," Physics and Medicine of the Atmosphere and Space (Benson and Strughold eds.), Wiley and Sons, New York, 1960, p. 505-526.

18. Stanley, R. M., "Escape at Launching and in the Atmosphere from a Space Vehicle," Physics and Medicine of the Atmosphere and Space (Benson and Strughold eds.), Wiley and Sons, New York, 1960, p. 497-504.

19. Campbell, P. A., "Introduction to the Problem of Escape and Rescue During Space Operations," Physics and Medicine of the Atmosphere and Space (Benson and Strughold eds.), Wiley and Sons, New York, 1960, p. 493-496.

20. Miele, A., Flight Mechanics, Addison Wesley Publishing Co., Reading, Mass., 1962.

21. Peterson, N. V., "Rescue and Retrieve Space Missions," Physics and Medicine of the Atmosphere and Space (Benson and Strughold eds.), Wiley and Sons, New York, 1960, p. 527-557.

22. Richards, P. B., "A Concept for Space Flight Safety," Proc. Fourth Space Congress, Cocoa Beach, Florida, 1967.

23. Carter, C. V., and Huff, W. W., "The Problem of Escape from Satellite Vehicles," IAS Reprint No. 59-41, January 1959.

24. Duncan, R. C., Dynamics of Atmospheric Entry, McGraw Hill Book Co., New York, 1962.

25. McCuskey, S. W., Introduction to Celestial Mechanics, McGraw Hill Book Co., New York, 1963.

26. Makemson, M. W., Baker, R. M., and Westrom, G. B., "Analysis and Standardization of Astrodynamic Constants," J. Astro. Sci., Vol. 8, No. 1, 1961, p. 1-13.

27. Leitmann, G., Optimization Techniques, Academic Press, New York, 1962.

28. Kendall, R. T., "Techniques for Space and Hypersonic Flight Escape," Proc. SAE Aerospace Systems Conf., Los Angeles, 1967, p. 394-400.

29. Bartos, G., and Greenberg, A. B., "Abort Problems of the Lunar Landing Mission," Progress in Aeronautics and Astronautics, Vol. 10, Academic Press Inc., New York, 1962, p. 735-759.

30. Cohan, C. J., et. al., Crew Escape Criteria for Two Stage Recoverable Aerospace Vehicles, Wright Patterson AFB, FDL-TDR-64-145, October 1964.

31. Chew, F. E., et. al., Investigation of Stabilization and Control Systems for Application to Aerospace Vehicle Escape Capsules, Wright Patterson AFB, ASD-TDR-62-243, June 1962.

32. Glasstone, S., The Effects of Nuclear Weapons, U. S. Atomic Energy Commission, April 1962.

33. Brode, H. L., A Calculation of the Blast Wave From a Spherical Charge of TNT, Rand Corp. Report No. RM-1965, 21 August 1957.

34. Kinney, G. F., Explosive Shocks in Air, McMillan Co., New York, 1962.

35. Kovit, B., "Space Rescue," Space/Aeronautics, May 1966, p. 95-103.

36. Wong, T. J., and Slye, R. E., The Effect of Lift on Entry Corridor Depth and Guidance Requirements for the Return Lunar Flight, NASA TR R-80, 1960.

37. Chapman, D. R., An Analysis of the Corridor and Guidance Requirements for Supercircular Entry into Planetary Atmospheres, NASA TR R-55, 1959.

38. Altman, S. P., and Pistiner, J. S., "Hodograph Analysis of the Orbital Transfer Problem for Coplanar Nonaligned Elliptical Orbits," ARS Journ., September 1961, p. 1217-1225.

39. Leondes, C. T., Guidance and Control of Aerospace Vehicles, McGraw Hill Book Co., New York, 1963.

40. Levine, S., "Man-rating the Gemini Launch Vehicle," Astronautics and Aeronautics, November 1964, p. 52-56.

41. McCarthy, J. F., Dodds, J. I., and Crowder, R. S., "Development of the Apollo Launch Escape System," J. Spacecraft and Rockets, Vol. 5, No. 8, August 1968, p. 927-932.

42. Dinger, R. J., and Norman, J. R., Flight Mechanics Analysis of the AS-205/CSM-101, Chrysler Corp. Report No. TN-AP-68-330, 30 May 1968.

43. Morgan, W. B., Saturn V Launch Vehicle Emergency Detection System Analysis, Boeing Co. Report No. D5-15555-4, 17 June 1968.

44. Anon., Apollo Saturn Emergency Detection System Description, IBM Report No. 111-5-509-7, 1 August 1966, (revised 1 April 1968).

APPENDIX A

LIST OF SYMBOLS

a = semi major axis of elliptic orbit; ft

A_s = acceleration sensed by crew or instrumentation; ft/sec^2. (Defined by Eq. C6)

A_T = acceleration; ft/sec^2 (Defined by Eq. C6)

b = semi minor axis of elliptic orbit; ft

C_D = drag coefficient; N.D.

d = distance from center of explosion; ft

D = drag; lb

e = eccentricity of orbit; N.D.

E = specific energy of body in orbit; ft^2/sec^2

G = universal constant of gravitation

= 3.442×10^{-8} ft^3/(slug sec^2)

g = gravity acceleration; ft/sec^2

g_o = mean value of gravity acceleration at surface of planet; ft/sec^2

h = altitude above surface of planet; ft

H = specific angular momentum; ft^2/sec

I_{sp} = specific impulse of rocket engine; sec

K = acceleration parameter; sec^{-1} (Defined by Eq. 9)

K_b = Stefan Bolzmann constant

= 4.81×10^{-13} Btu/(ft^2 sec °R^4)

where °R = degrees Rankine

K_c = convective heating rate constant; Btu/(ft$^{3/2}$ sec), (See Eq. D2)

K_r = surface radiation emissivity; N.D.

ℓ = semi latus rectum: ft

L = lift; lb

m = mass; slugs

m_p = propellant mass; slugs

M = mass of planet; slugs

n = mean motion; sec^{-1} (See Eq. B20)

N = load factor; G's (See Eq. C10)

p = overpressure; psi (See Fig. 1)

P_x = ambient pressure; psia

P_y = peak pressure; psia

q = dynamic pressure; lb/ft^2

$\dot{Q}_c$ = convective heating rate; $Btu/(ft^2\ sec)$

$\dot{Q}_R$ = radiant heating rate; $Btu/(ft^2\ sec)$

r = distance to center of gravitational attraction; ft

r_o = mean radius of planet; ft

r_p = perigee of orbit; ft (See Fig. B1)

R_N = nose radius, ft (See Eq. D2)

S = reference area; ft^2

t = time; sec

t_b = burning time of rocket; sec

t_d = duration of overpressure; sec

t_x = arrival time; sec

T = thrust; lb

T_s = surface temperature of body; °Rankine

T_w = stagnation point temperature; °Rankine

V = velocity; ft/sec

ΔV = velocity increment; ft/sec

V_E = entry velocity; ft/sec

V_H = horizontal component of velocity; ft/sec

V_R = radial component of velocity; ft/sec

V_p = parabolic (escape) velocity; ft/sec

V_s = satellite (circular) velocity; ft/sec

$\overline{V}$ = V/V_s

W = weight of vehicle; lb

W_T = weight of TNT explosive charge; tons

α = angle of attack; deg

γ = flight path angle; radians

δ = thrust vector angle; degrees

θ = angular position; rad

θ_E = eccentric anomaly; rad

θ_T = true anomaly; rad

μ = gravitational parameter for planet

= $GM = gr^2$

ξ = angle of abort thrust vector; deg (See Fig. 42)

ρ = atmospheric density; slugs/ft^3

ρ_{SL} = atmospheric density at sea level conditions; slugs/ft^3

σ = speed of sound; ft/sec

σ_{SL} = speed of sound at sea level conditions; ft/sec

τ_P = orbit period; sec

φ = range angle; rad (See Fig. C1)

APPENDIX B

ORBITAL MECHANICS

The basic relations of orbital mechanics are summarized here for convenience. Details and derivations may be found in standard texts.[25]

B.1 ELLIPTIC ORBITS

The equation of the orbit is

$$\frac{1}{r} = \frac{1}{\ell}\left[1 + e \cos \theta_T\right] \tag{B1}$$

The eccentricity is given by

$$e = \left[1 + \frac{2H^2E}{\mu^2}\right]^{1/2} \tag{B2}$$

For an elliptic orbit, $e < 1$. If $e = o$, the orbit is a circle, while for $e > 1$, the orbit is a hyperbola.

The following well known relations are written down without further comment. (See Figure B-1).

$$E = \frac{1}{2}V^2 - \frac{\mu}{r} \tag{B3}$$

$$H = r^2 \dot{\theta} \tag{B4}$$

$$\mu = GM \tag{B5}$$

$$g = \frac{\mu}{r^2} \tag{B6}$$

$$\ell = \frac{H^2}{\mu} \tag{B7}$$

$$r_p = \frac{\ell}{(1+e)} \tag{B8}$$

$$V_H = r\dot{\theta} \tag{B9}$$

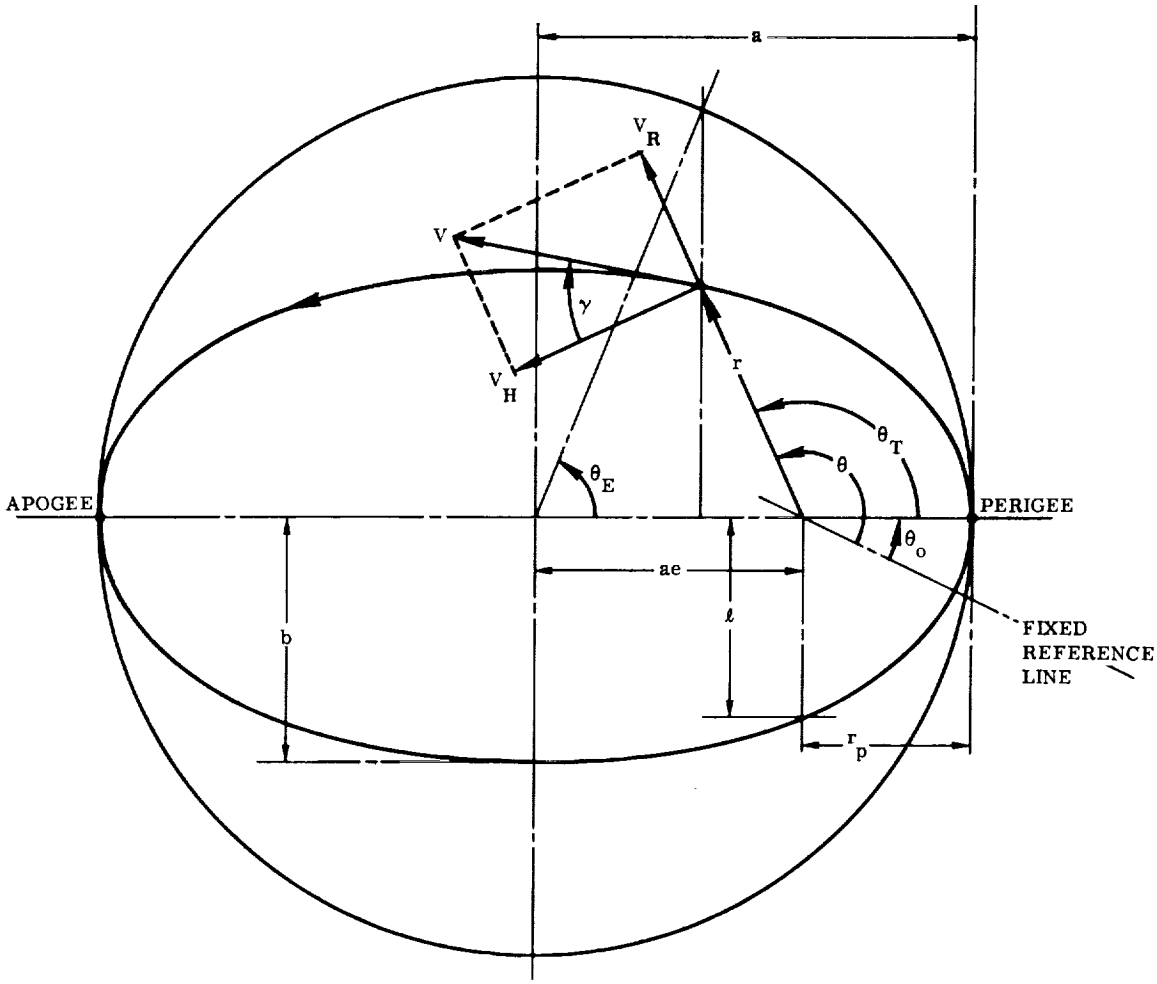

Figure B-1. Elliptical Orbit Geometry

$$V_R = \frac{\mu e}{H} \sin \theta_T \tag{B10}$$

$$V^2 = \mu\left[\frac{2}{r} - \frac{1}{a}\right] \tag{B11}$$

$$r_p = a\,(1 - e) \tag{B12}$$

$$\cos \theta_E = \frac{e + \cos \theta_T}{1 + e \cos \theta_T} \tag{B13}$$

$$\sin \theta_E = \frac{\sqrt{1 - e^2} \sin \theta_T}{(1 + e \cos \theta_T)} \tag{B14}$$

$$\ell = a (1 - e^2) \tag{B15}$$

$$\tan \gamma = \frac{e r}{a (1 - e^2)} \sin \theta_T \tag{B16}$$

$$V_p = \sqrt{\frac{2\mu}{r}} \tag{B17}$$

$$V_S = \sqrt{\frac{\mu}{r}} \tag{B18}$$

The time required for a body in orbit to move from θ_{EO} to θ_E is given by

$$t = \frac{1}{n}\left[(\theta_E - \theta_{EO}) - e (\sin \theta_E - \sin \theta_{EO})\right] \tag{B19}$$

where

$$n = \sqrt{\frac{\mu}{a^3}} \tag{B20}$$

The time required to make one complete revolution is therefore

$$\tau_p = \frac{2\pi}{n} \tag{B21}$$

Using the above relations, it is a simple matter to determine the orbital parameters given the conditions at burnout. For example, suppose that at burnout the altitude, velocity, and flight path angle are given by r_1, V_1, and γ_1, respectively (the subscript 1 denotes burnout). We may then calculate

$$V_{H1} = V_1 \cos \gamma_1$$

from which we obtain the angular momentum as follows.

$$H = r_1 V_{H1}$$

The specific energy is

$$E = \frac{1}{2} V_1^2 - \frac{\mu}{r_1}$$

This permits us to calculate the orbit eccentricity, e, from Eq. (B2). For e = 1 (>1), the orbit is a parabola (hyperbola). Otherwise the orbit is elliptical. Having e and H, all of the other orbit parameters may be readily calculated.

B.2 ORBITAL TRANSFER

Transfer of a vehicle from one orbit to another is usually accomplished by applying velocity increments which are assumed to act instantaneously. A simple case is illustrated in Figure B-2. In order to transfer the vehicle from orbit A to orbit B, a velocity increment, ΔV_1, is applied at point (1), the point of intersection of the orbits. Letting the subscripts A, B, C, ... denote the specific orbits, with subscripts 1, 2, 3, ... referring to particular points on an orbit, we see that the vector sum, $V_{B1} = V_{A1} + \Delta V_1$, must be such that V_{B1} is the velocity which corresponds to the given r and θ_T at point (1) for orbit B.

To accomplish a transfer between nonintersecting orbits, two velocity increments are usually required, in which the vehicle travels from orbit A to orbit B via an intermediate orbit C (see Figure B-3). As before the velocity increments must have a magnitude and direction such that the resulting velocity vector corresponds to

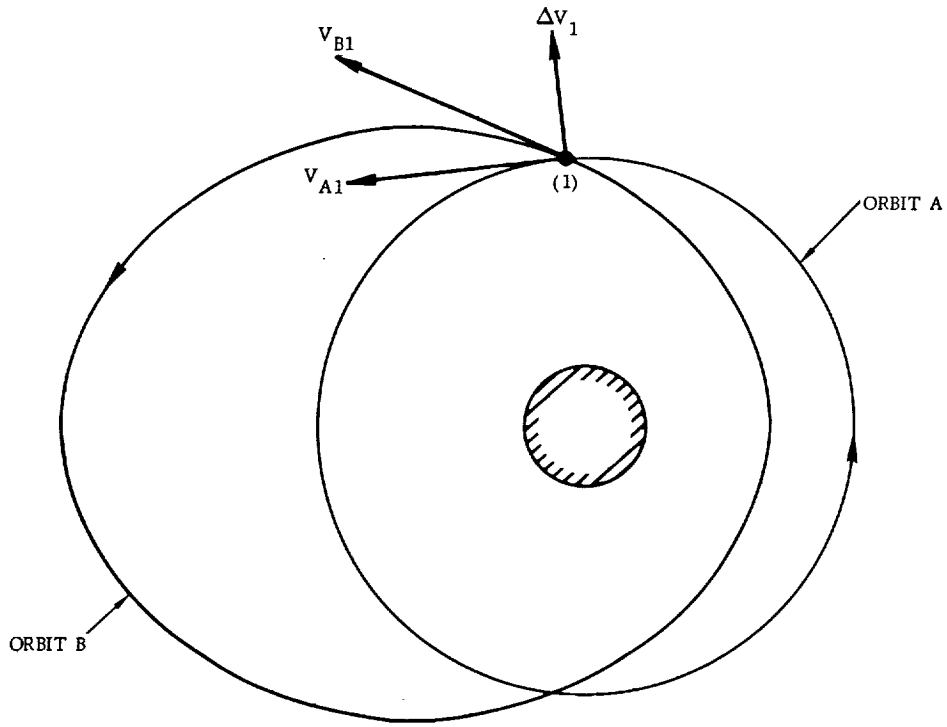

Figure B-2. Orbital Transfer: Intersecting Orbits

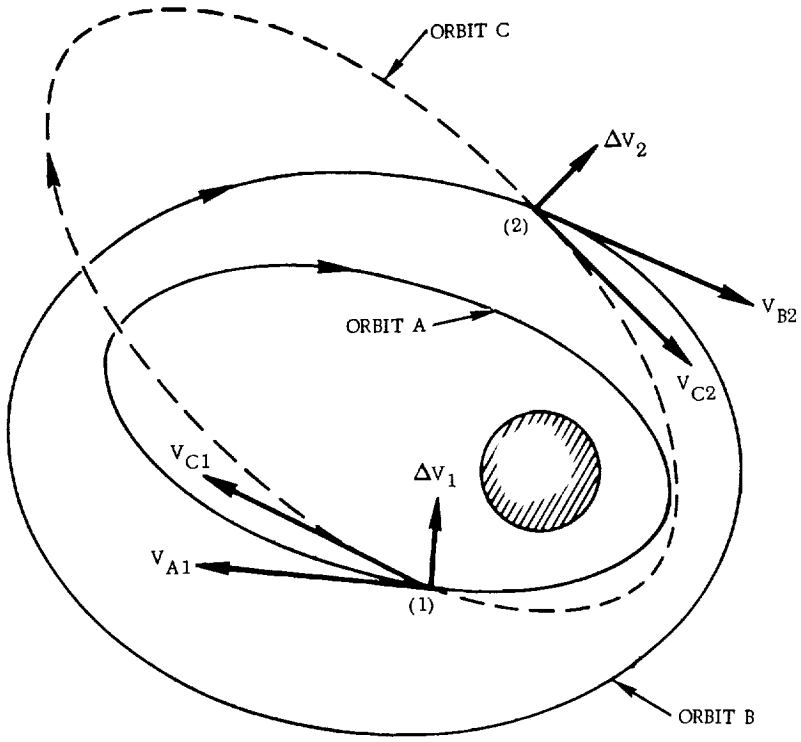

Figure B-3. Orbital Transfer: Nonintersecting Orbits

the proper value for the new orbit at the given r and θ_T. A transfer orbit which is tangent to the new and old orbits is shown in Figure B-4. Here the velocity increments are applied parallel to the vehicle's velocity vector. This type of transfer often represents a minimum fuel orbital transfer. The general problem of optimal orbital transfer is too extensive to be treated here.‡ We will mention only the classical Hohmann transfer shown in Figure B-5. The problem is generally stated as follows:

"Given a vehicle in a circular orbit with radius r_A. Determine the velocity increments which transfer the vehicle from orbit A to (circular) orbit B (radius r_B) such that the fuel expenditure is a minimum."

‡ Cf. Ref. 27

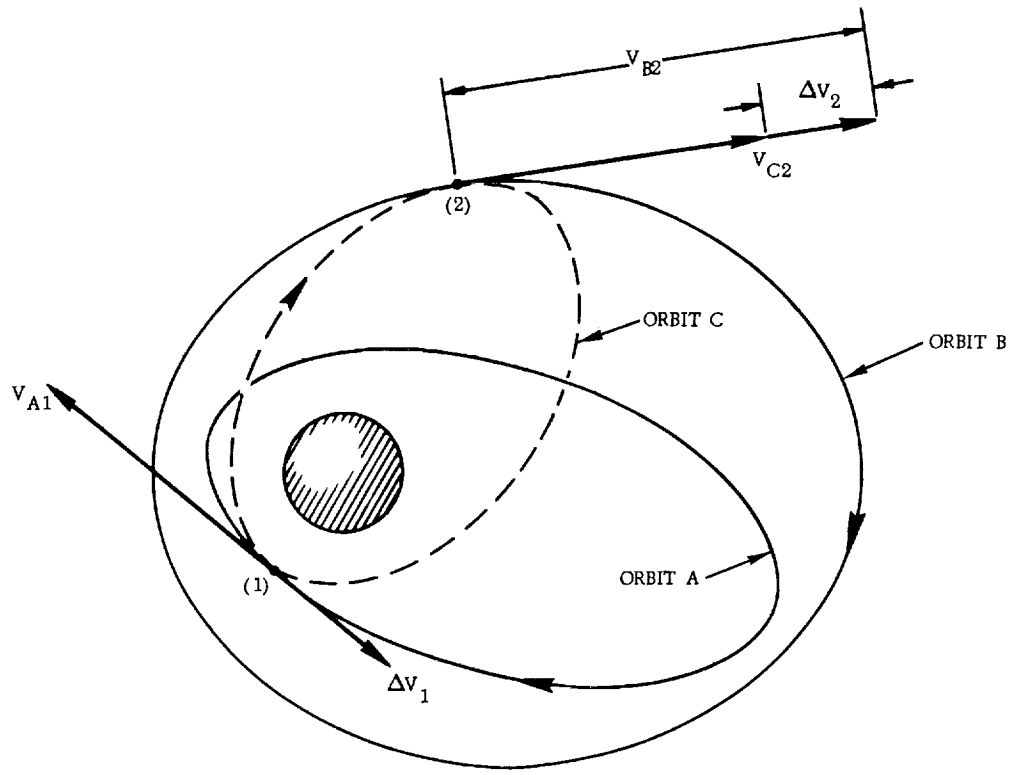

Figure B-4. Orbital Transfer: Nonintersecting Orbits; Tangent Transfer Orbit

It can be shown that the required velocity increments are given by

$$\Delta V_1 = \left(\frac{\mu}{r_A}\right)^{1/2} \left[\left(\frac{2\, r_B}{r_A + r_B}\right)^{1/2} - 1\right] \tag{B22}$$

$$\Delta V_2 = \left(\frac{\mu}{r_B}\right)^{1/2} \left[1 - \left(\frac{2\, r_A}{r_A + r_B}\right)^{1/2}\right] \tag{B23}$$

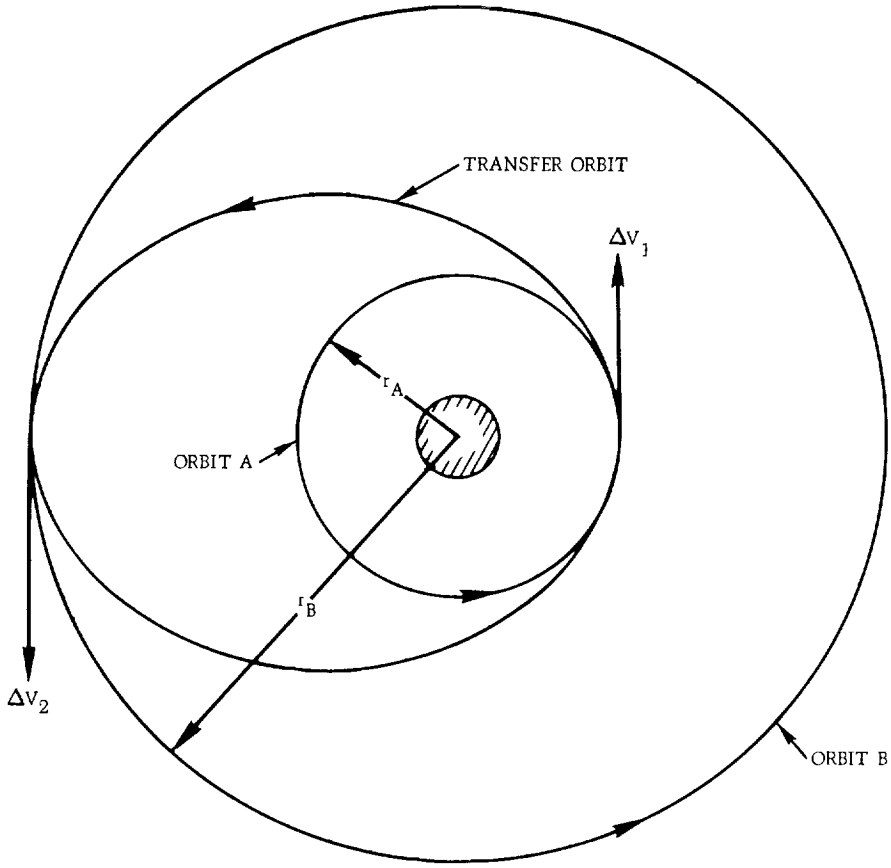

Figure B-5. Hohmann Transfer

The ideal‡ velocity increment is related to the propellant mass ratio by

$$\frac{m_p}{m} = 1 - \exp\left[-\frac{\Delta V}{I_{sp}\, g}\right] \tag{B24}$$

B.3 HODOGRAPH METHODS

The determination of the required velocity increments for transfer between coplanar intersecting elliptical orbits may be simplified materially by emplying hodograph methods.[38] The main ideas in this approach are derived from elementary considerations as follows. Eq. (B3) may be written as

‡ Ideal is used in the sense that atmospheric and gravitational effect are negligible.

$$E = \frac{1}{2}\left(V_R^2 + V_H^2\right) - \frac{\mu}{r} \tag{B25}$$

Also, from (B4) and (B9), we have

$$H = rV_H \tag{B26}$$

Eliminating r between the above equations yields

$$R^2 = V_R^2 + (V_H - C)^2 \tag{B27}$$

where

$$C = \frac{\mu}{H} \tag{B28}$$

$$R = (2E + C^2)^{1/2} \tag{B29}$$

The elliptic orbit is completely defined by the quantities C and R, which are called the hodograph parameters. Eq. (B27), which relates V_R and V_H in terms of C and R is a circle in the V_H - V_R plane as shown in Figure B-6. The velocity vector at a prescribed true anomaly, θ_T, is shown on this figure, corresponding to the point on the elliptic orbit shown in Figure B-7. Thus, using the hodograph of Figure B-6, it is a simple matter to determine the velocity at any point on the elliptic orbit.

A slightly modified hodograph can be constructed which relates the cartesian components, V_x and V_y, of V, rather than the polar components, V_H and V_R.

From Figure B-6 we have

$$V_H = C + R\cos\theta_T \tag{B30}$$

$$V_R = R\sin\theta_T \tag{B31}$$

while from Figure B-7

$$V_x = V_H\sin\theta_T - V_R\cos\theta_T \tag{B32}$$

$$V_y = V_H\cos\theta_T + V_R\sin\theta_T \tag{B33}$$

It follows that

$$V_x = C\sin\theta_T \tag{B34}$$

$$V_y = R + C\cos\theta_T \tag{B35}$$

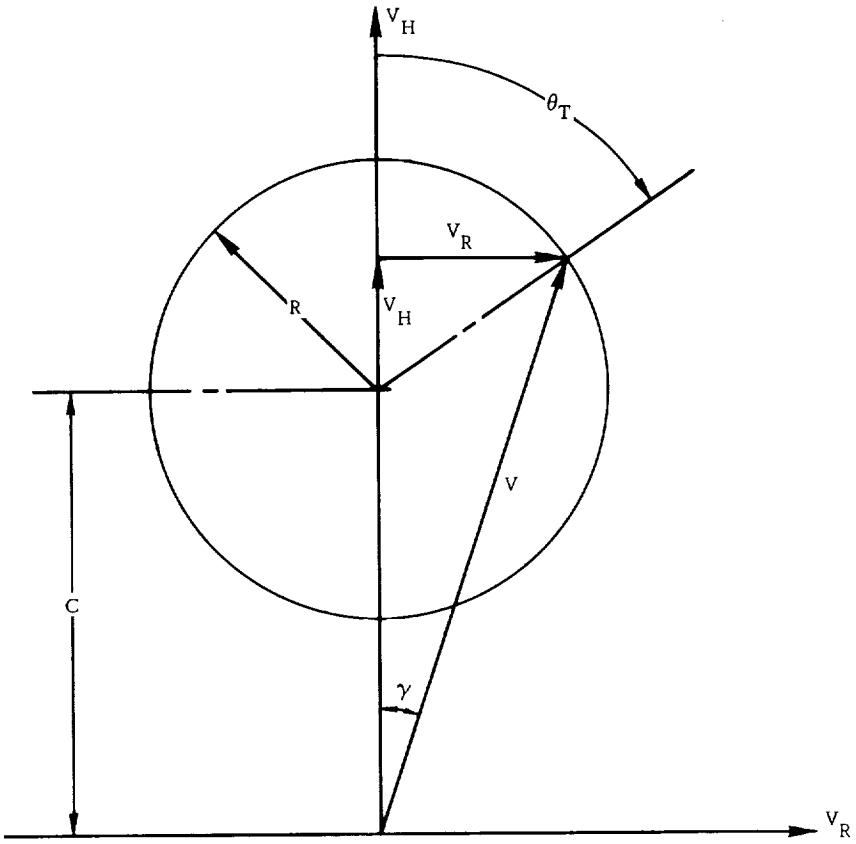

Figure B-6. Hodograph of Elliptic Orbit

This leads to the modified hodograph for the elliptic orbit shown in Figure B-8. The modified hodograph has the property that the velocity vector at a given θ_T is parallel to the velocity vector at the corresponding point on the actual orbit with orientation as defined in Figure B-8.

It is a simple matter to express the elliptic orbit parameters in terms of R and C. For example, it is readily verified that

$$e = \frac{R}{C} \tag{B36}$$

$$a = \frac{\mu}{C^2 - R^2} \tag{B37}$$

$$n = \frac{(C^2 - R^2)^{3/2}}{\mu} \tag{B38}$$

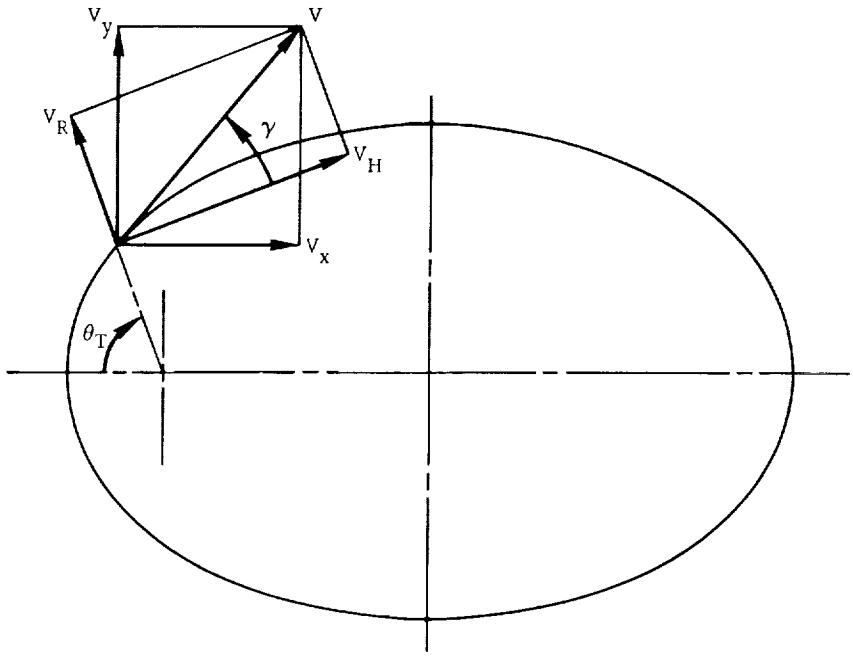

Figure B-7. Elliptic Orbit

To adapt the foregoing ideas to orbital transfer problems, one further property of the hodograph parameters needs to be established.

Suppose that elliptic orbits A and I intersect at point 1. Then‡

$$C_A V_{HA1} = C_A \frac{H_A}{r_{A1}} \tag{B39}$$

$$C_I V_{HI1} = C_I \frac{H_I}{r_{I1}} \tag{B40}$$

But if the orbits intersect at point 1, it means that

$$r_{A1} = r_{I1} \equiv r_1 \tag{B41}$$

Therefore, by virture of (B28), it follows that at a point of intersection,

---

‡ The notation has the following meaning:

$C_A \equiv$ value of C for orbit A

$V_{HA1} \equiv$ horizontal velocity at point 1 on orbit A etc.

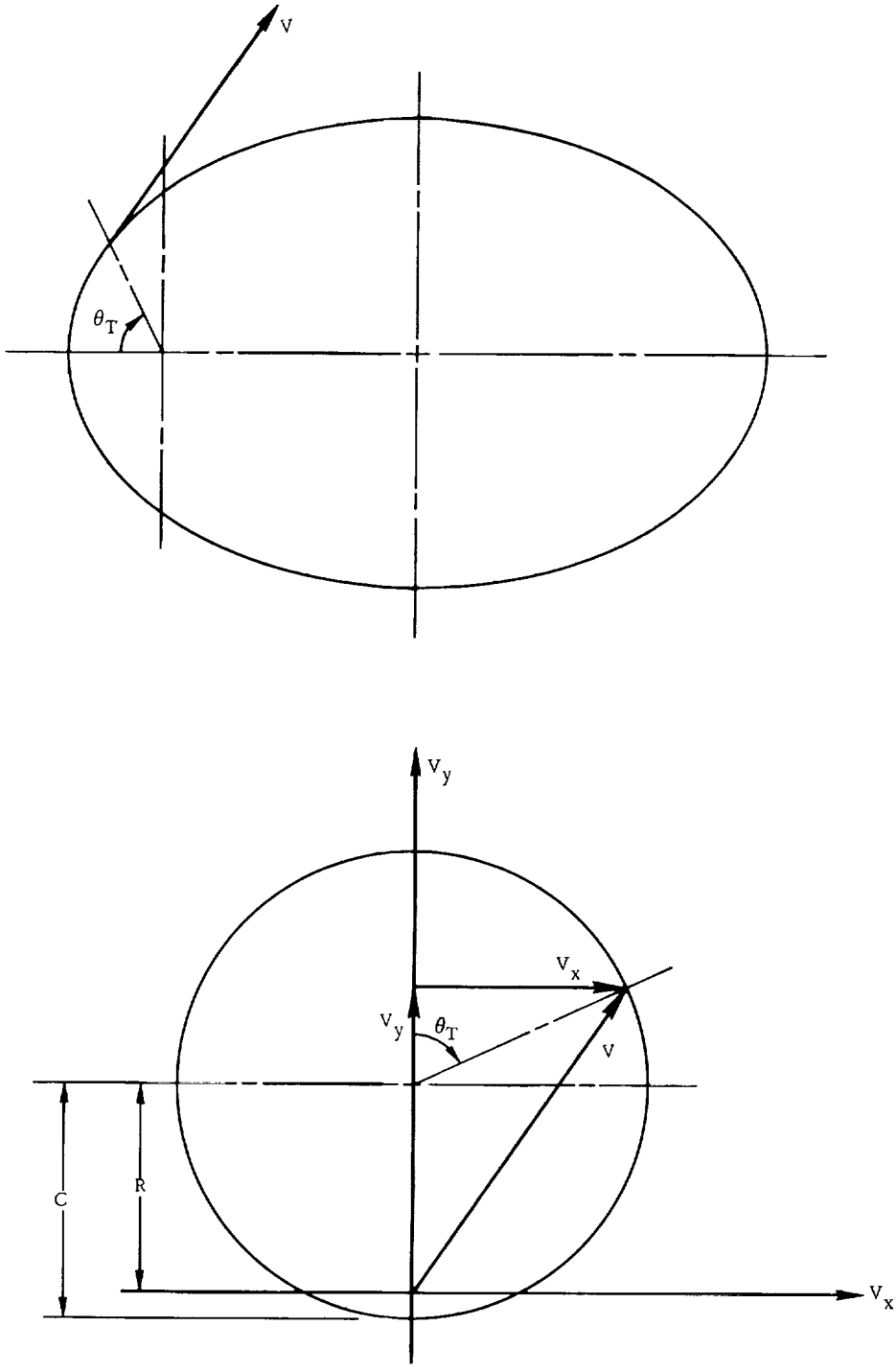

Figure B-8. Modified Hodograph for Elliptic Orbit

$$(CV_H)_{A1} = (CV_H)_{I1} = \frac{\mu}{r_1} \tag{B42}$$

From Figure B-6 we see that

$$\tan \theta_T = \frac{V_R}{V_H - C} = \frac{CV_R}{CV_H - C^2} \tag{B43}$$

Consequently

$$CV_H = C^2 + CR \cos \theta_T \tag{B44}$$

$$CV_R = CR \sin \theta_T \tag{B45}$$

These relations lead to the construction shown in Figure B-9. This particular form of the hodograph is particularly useful for intersecting elliptic orbits since it permits a very simple determination of the velocity increment required to transfer from one orbit to the other. To demonstrate this, consider the intersecting nonaligned elliptic orbits shown in Figure B-10.

When a vehicle in orbit I is at point 1, it is desired to apply a velocity increment such that it continues along orbit A. To determine the magnitude and orientation of this velocity increment, we begin by constructing the modified hodograph for the two orbits as shown in Figure B-11. Laying off the true anomalies, θ_{TA1} and θ_{TI1}, for the two orbits, we obtain the vectors $C_A V_{A1}$ and $C_I V_{I1}$. These vectors terminate at a line 0'0'' which is horizontal since the quantities $C_I V_{HI1}$ and $C_A V_{HA1}$ must be equal at a point of intersection. Dividing $C_A V_{A1}$ and $C_I V_{I1}$ by C_A and C_I respectively yields the vectors V_{A1} and V_{I1} shown in the figure. From this we obtain ΔV directly by vector addition. The foregoing scheme is particularly convenient since the velocity vectors on this hodograph are parallel to the same vectors drawn on the elliptic orbit of Figure B-10.

An application of the foregoing methods to an orbital transfer via an intermediate transfer orbit is now completely straightforward. Referring to Figure B-12, it is required to determine the velocity increments required to transfer from point 1 on orbit A to point 2 on orbit B using an intermediate transfer orbit C. The orbital parameters are summarized in Table B-1, and the corresponding true anomalies are

$$\theta_{TA1} = 40°$$

$$\theta_{TC1} = 100°$$

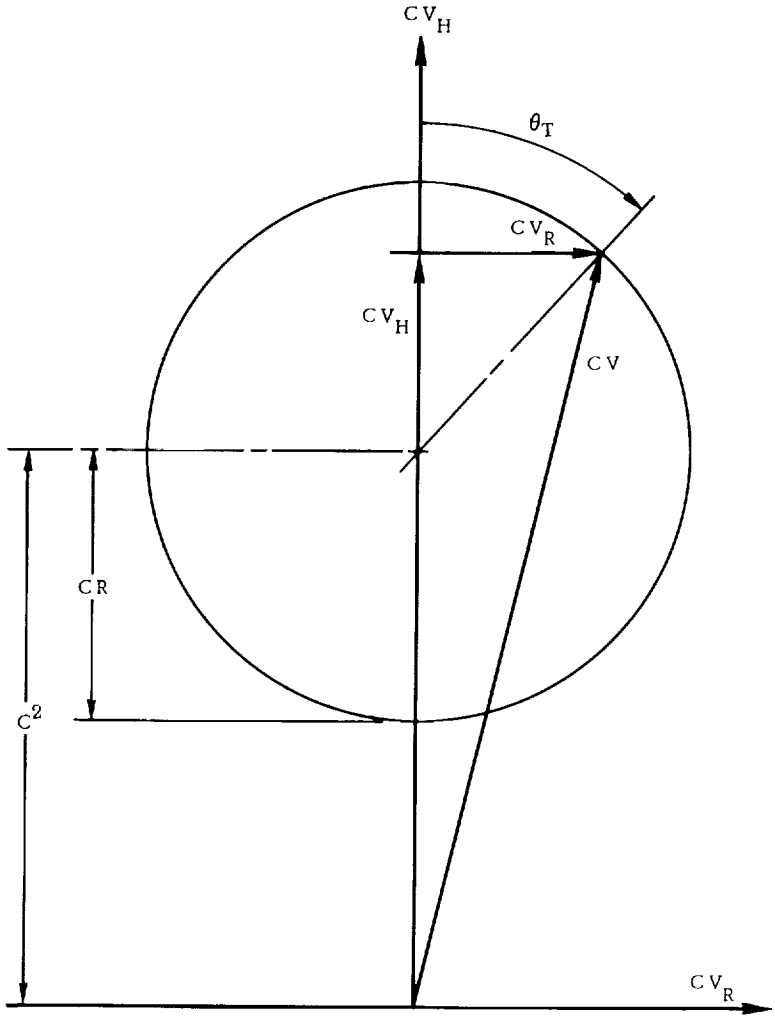

Figure B-9. Modified Hodograph for Elliptic Orbit — Alternate Form

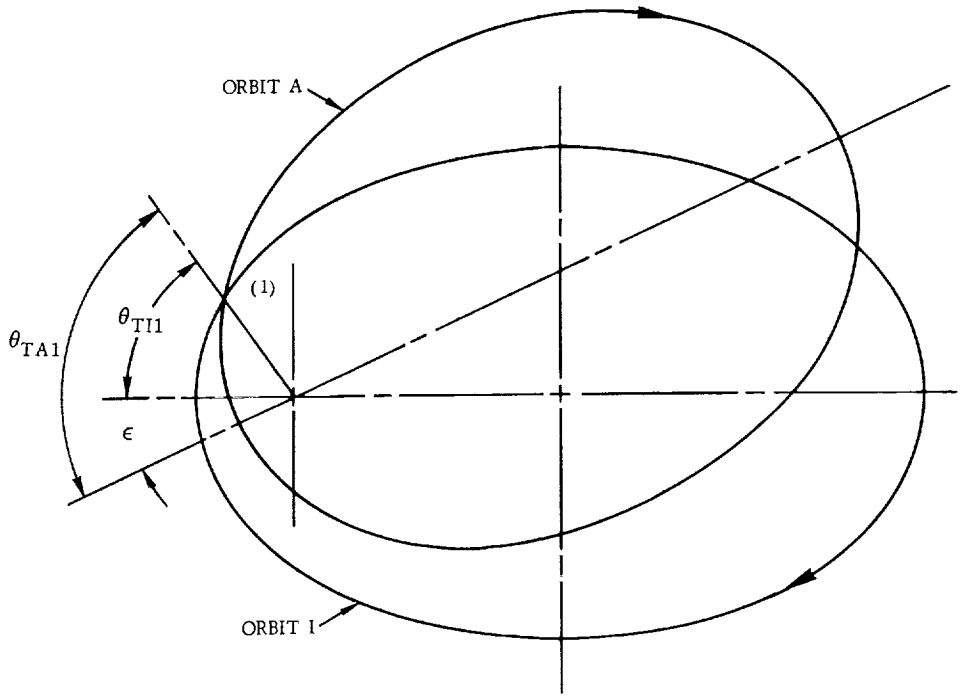

Figure B-10. Intersecting Elliptic Orbits

$\theta_{TC2} = 140°$

$\theta_{TB2} = 105°$

The complete hodograph for the problem is shown in Figure B-13. The velocity increments are now obtainable from this diagram in the manner discussed previously.

B.4 HYPERBOLIC ORBITS

The geometry of the hyperbolic orbit is shown in Figure B-14. The main relations for the parameters are given below.

$$H = r^2 \dot{\theta} \tag{B46}$$

$$E = \frac{1}{2} V^2 - \frac{\mu}{r} \tag{B47}$$

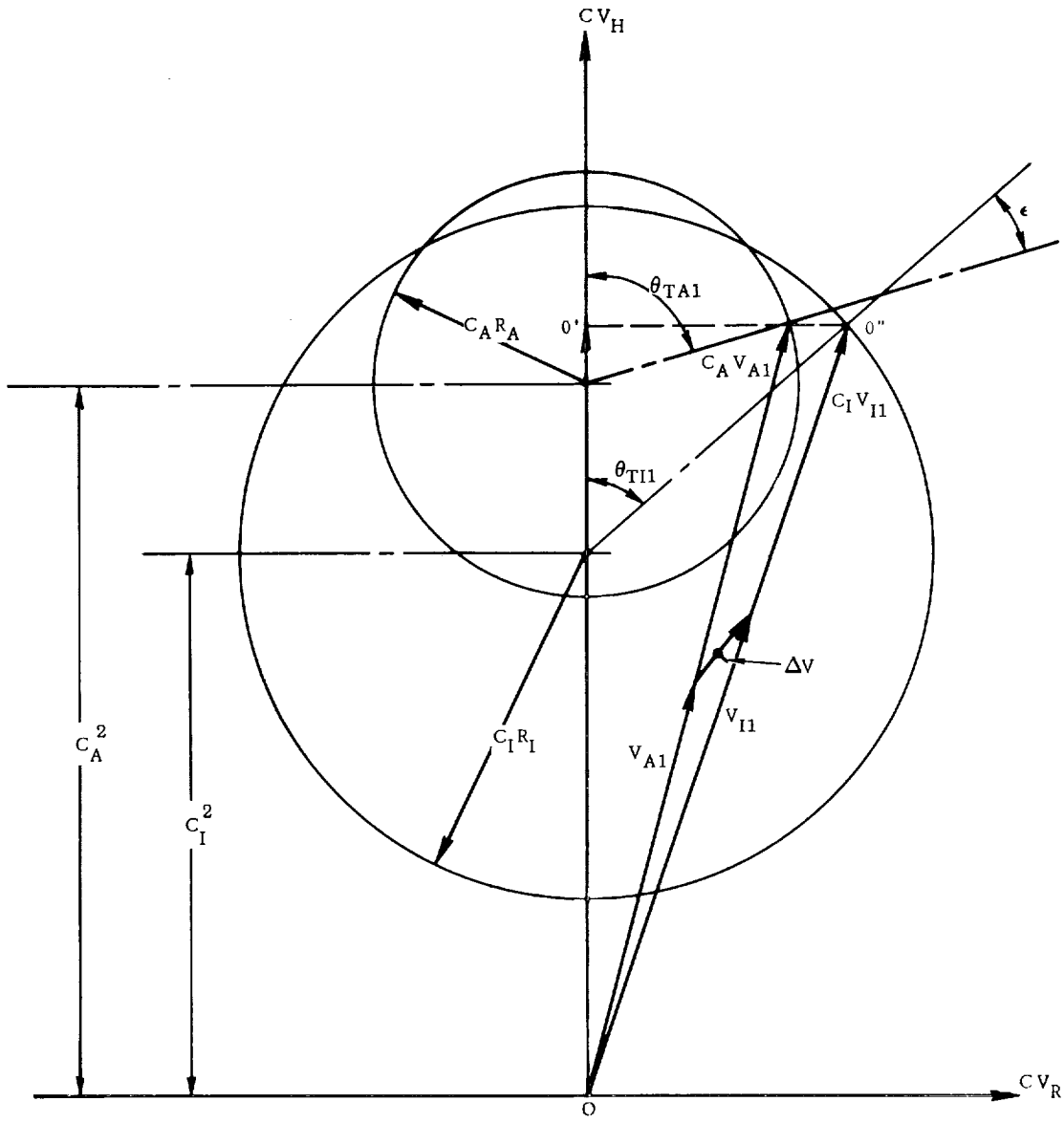

Figure B-11. Modified Hodograph for Elliptic Orbits of Figure B-10

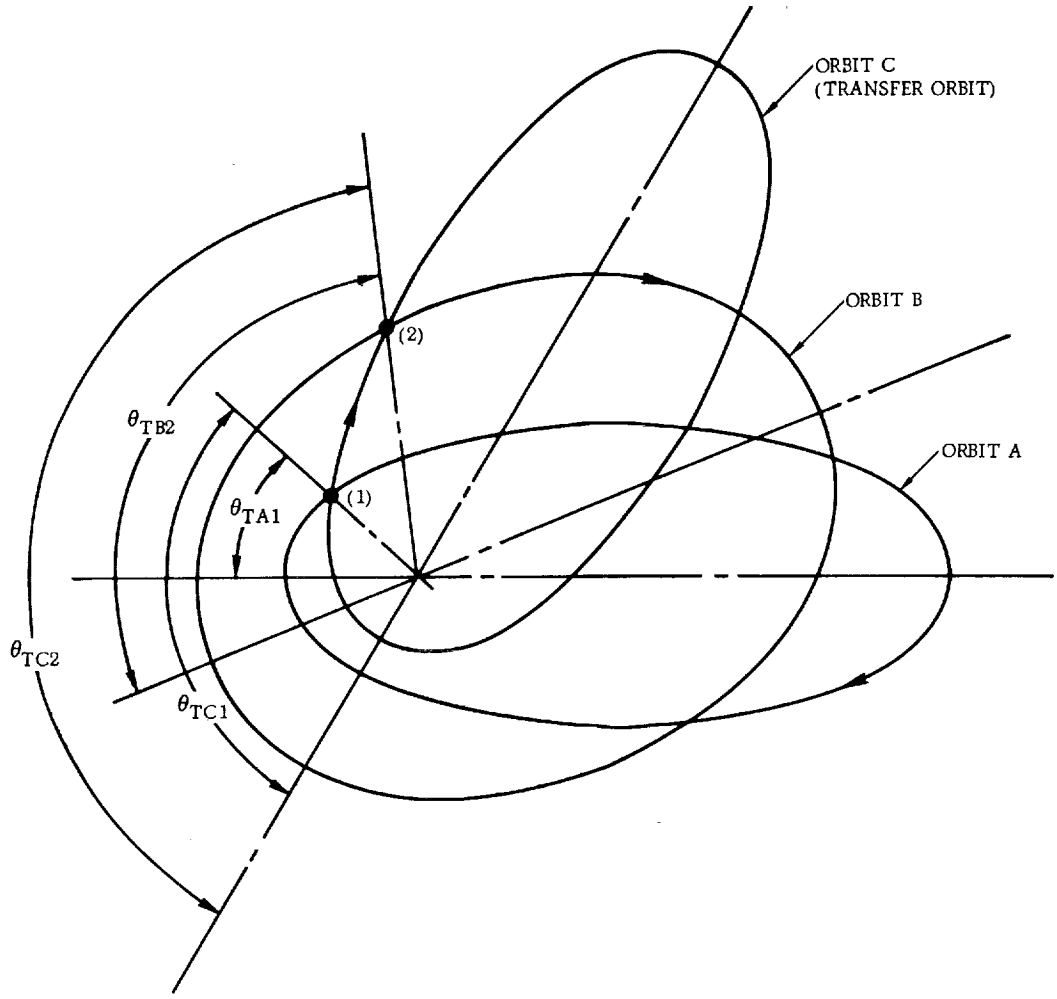

Figure B-12. Orbital Transfer via an Intermediate Transfer Orbit

$$e = \left[1 + \frac{2EH^2}{\mu^2}\right]^{1/2} \tag{B48}$$

$$r = \frac{\ell}{1 + e \cos \theta_T} \tag{B49}$$

$$\ell = r_p (1 + e) \tag{B50}$$

$$r_p = a (e - 1) \tag{B51}$$

Table B-1. Orbit Parameters

		Orbit A	Orbit B	Orbit C
a	ft $\times 10^{-6}$	200	200	200
r_p	ft $\times 10^{-6}$	80	135	40
e	N.D.	0.6	0.325	0.8
ℓ	ft $\times 10^{-6}$	128	178.9	72
H	$ft^2/sec \times 10^{-11}$	13.42	15.87	10.07
E	$ft^2/sec^2 \times 10^{-6}$	-35.19	-35.19	-35.19
C	ft/sec $\times 10^{-3}$	10.49	8.87	13.98
R	ft/sec $\times 10^{-3}$	6.30	2.88	11.18
C^2	$ft^2/sec^2 \times 10^{-6}$	110.0	78.68	195.4
CR	$ft^2/sec^2 \times 10^{-6}$	66.07	25.55	156.3

$$\ell = \frac{H^2}{\mu} \tag{B52}$$

$$b = a\,(e^2 - 1)^{1/2} \tag{B53}$$

$$V = \left[\mu\left(\frac{2}{r} + \frac{1}{a}\right)\right]^{1/2} \tag{B54}$$

$$\cos\gamma = \frac{1 + e\cos\theta_T}{\left[1 + 2\,e\cos\theta_T + e^2\right]^{1/2}} \tag{B55}$$

The time required to travel from perigee to any point on the orbit is given by

$$t = \left(\frac{a^3}{\mu}\right)^{1/2}\left[\frac{e\sqrt{e^2-1}\,\sin\theta_T}{1+e\cos\theta_T} - \ln\left(\frac{\sqrt{e+1} + \sqrt{e-1}\,\tan\frac{\theta_T}{2}}{\sqrt{e+1} - \sqrt{e-1}\,\tan\frac{\theta_T}{2}}\right)\right] \tag{B56}$$

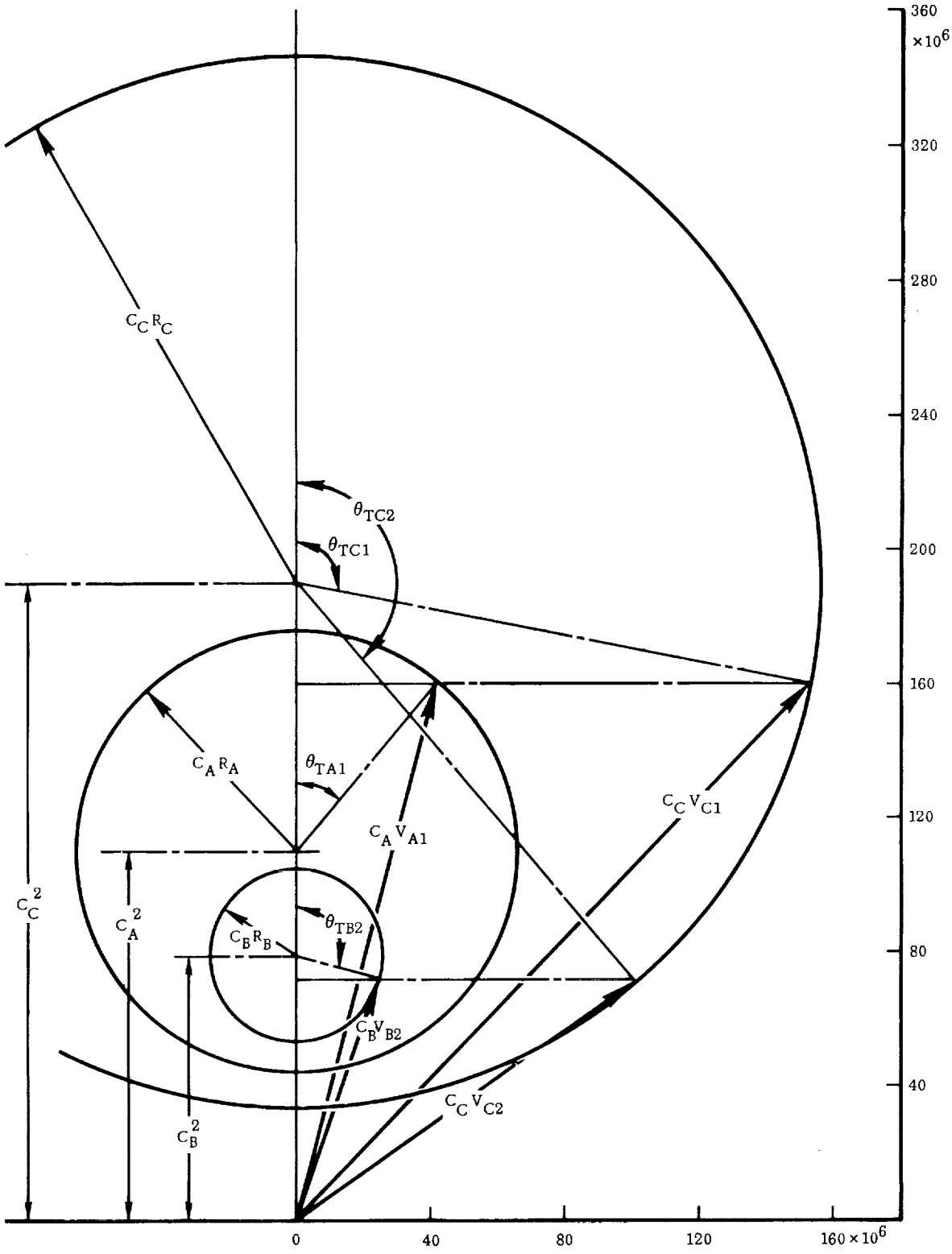

Figure B-13. Hodograph for Orbits of Figure B-12

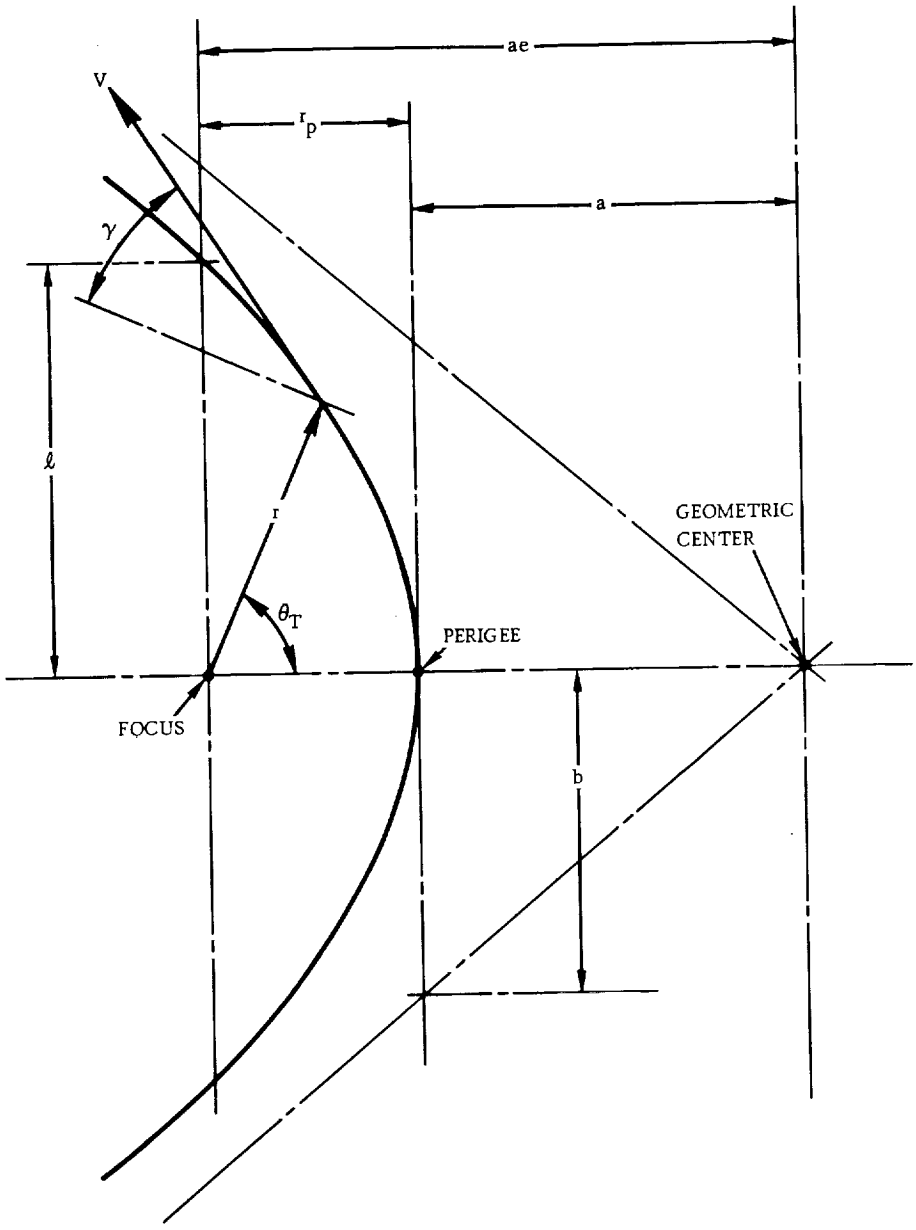

Figure B-14. Geometry of the Hyperbola

Also

$$V_H = r\dot{\theta} \tag{B57}$$

$$V_R = \frac{\mu e}{H} \sin \theta_T \tag{B58}$$

$$\tan \gamma = \frac{er}{\ell} \sin \theta_T \tag{B59}$$

APPENDIX C

ENTRY DYNAMICS

The equations of motion for a vehicle during the entry phase of flight are given by (see Figure C-1).

$$r_o\dot{\varphi} = \frac{Vr_o}{r}\cos\gamma \tag{C1}$$

$$\dot{h} = V\sin\gamma \tag{C2}$$

$$r = r_o + h \tag{C3}$$

$$m\dot{V} = T\cos\delta - D - mg_o\left(\frac{r_o}{r}\right)^2\sin\gamma \tag{C4}$$

$$mV\dot{\gamma} = T\sin\delta + L - mg_o\left(\frac{r_o}{r}\right)^2\cos\gamma + \frac{mV^2}{r}\cos\gamma \tag{C5}$$

These equations are based on planar motion over a spherical, non-rotating planet. For detailed derivations, see Reference 20.

A primary quantity of interest in entry (reentry) studies is the resultant acceleration of the vehicle. This is obtained from Eqs. (C4) and (C5) as follows:

$$A_T = \left[\dot{V}^2 + (V\dot{\gamma})^2\right]^{1/2} \tag{C6}$$

This is a formidable expression in the general case. For preliminary design studies, the following approximations are sometimes valid

$$\frac{r_o}{r} \approx 1$$

$$\frac{V^2}{r} << g_o$$

$$T = 0$$

In this case, Eq. (C6) simplifies to

$$A_T = \left[\left(\frac{L}{m} \cos \gamma - \frac{D}{m} \sin \gamma - g_o \right)^2 + \left(\frac{D}{m} \cos \gamma + \frac{L}{m} \sin \gamma \right)^2 \right]^{1/2} \qquad \text{(C7)}$$

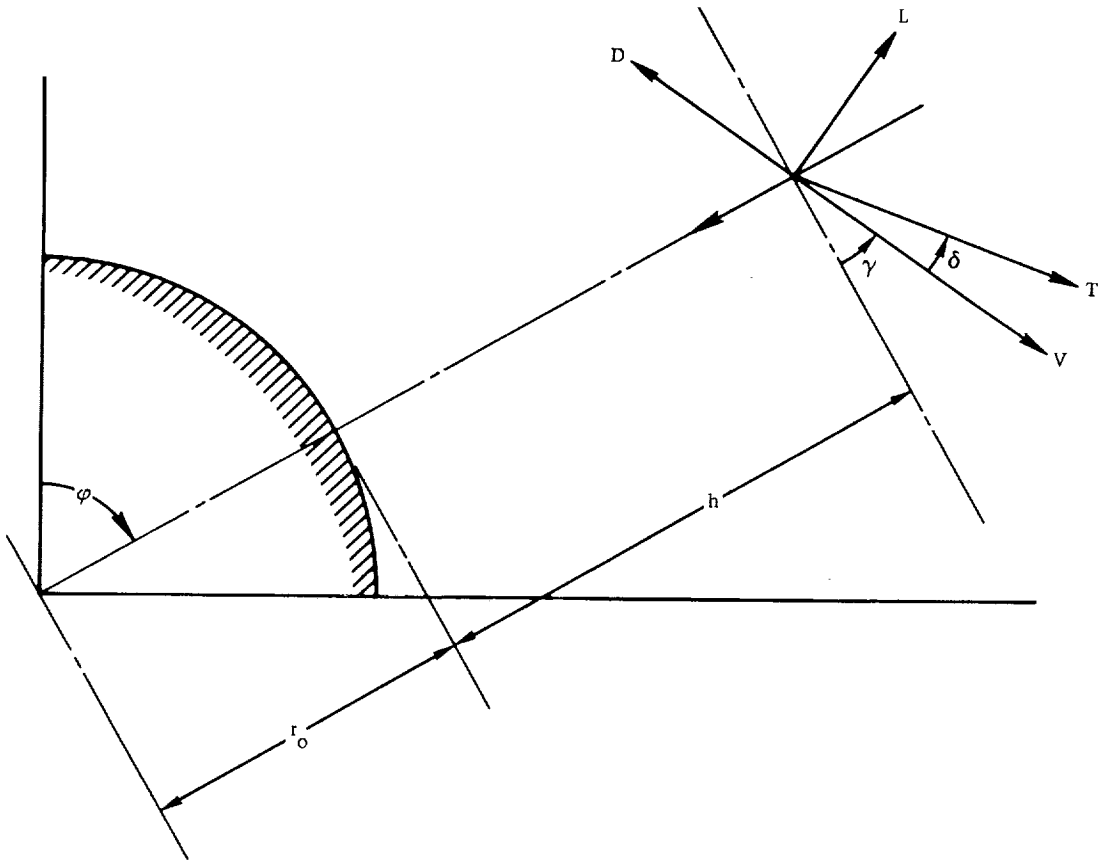

Figure C-1. Planetary Entry Geometry

The acceleration that is sensed by a pilot or instrument is due to the lift and drag forces only; viz.

$$A_S = \left[\left(\frac{L}{m}\cos\gamma - \frac{D}{m}\sin\gamma\right)^2 + \left(\frac{D}{m}\cos\gamma + \frac{L}{m}\sin\gamma\right)^2\right]^{1/2}$$

or

$$A_S = \frac{D\cos\gamma}{m}\left[\left(\frac{L}{D} - \tan\gamma\right)^2 + \left(\frac{L}{D}\tan\gamma + 1\right)^2\right]^{1/2} \tag{C8}$$

For small flight path angles, this reduces to

$$A_S = \frac{D}{m}\left[\left(\frac{L}{D}\right)^2 + 1\right]^{1/2} \tag{C9}$$

The load factor is defined by

$$N = \frac{A_s}{g_o} \tag{C10}$$

In many reentry studies, the vehicle weight is small compared to the drag forces. In this case, $A_S \approx A_T$, and the terms deceleration (in g's) and load factor, are used interchangeably.

APPENDIX D

AERODYNAMIC HEATING

Reentry vehicles entering a planetary atmosphere at high speed encounter severe problems of aerodynamic heating. A detailed investigation of this subject is beyond the scope of the present discussion. Instead, we will focus attention on the simplest way of formulating the basic design criteria from the point of view of heating constraints.

It is usually assumed that for reentry missions of moderatly long duration, the vehicle surface is cooled by reradiation. The reradiation heating rate is given by

$$\dot{Q}_R = K_r K_b T_s^4 \tag{D1}$$

The surface emissivity, K_r, is on the order of 0.80 for high surface temperatures for the materials generally used in reentry vehicles.

The convective heating rate at a stagnation point for a vehicle in hypersonic flow can be expressed as

$$\dot{Q}_c = \frac{K_c}{R_N^{1/2}} \left(\frac{\rho}{\rho_{SL}} \right)^{1/2} \left(\frac{V}{V_S} \right)^3 \tag{D2}$$

In this relation, it is assumed that the gas flow is laminar‡ and that the viscosity of the gas is proportional to the square root of the temperature. Also, the leading edge of the vehicle is assumed to be hemispherical. For the earth's atmosphere, a typical value for K_c is

$$K_c = 17{,}000 \text{ Btu}/(\text{ft}^{3/2} \text{ sec})$$

In an equilibrium condition, such that the heat input due to convective heating is equal to the heat emitted by reradiation, the resulting equilibrium temperature is called the stagnation point temperature. It is obtained by equating (D1) to (D2); viz.

---

‡ During reentry, the Reynolds numbers in the regions important for heat transfer are almost always low enough to ensure laminar flow.

$$T_W = \left[\frac{K_c}{K_r K_b R_N^{1/2}} \right]^{1/4} \left(\frac{\rho}{\rho_{SL}} \right)^{1/8} \left(\frac{V}{V_S} \right)^{3/4} \qquad \text{(D3)}$$

For design purposes, the heating constraint is usually expressed as a maximum allowable value for T_W.

Further details, including extensive references to the open literature are contained in Chapter 7 of Reference 24 and Chapter 14 of Reference 20.

APPENDIX E

GEOPHYSICAL CONSTANTS

Values of the geophysical constants, suitable for preliminary design purposes, are given below. A more complete listing, together with uncertainties in the significant figures, is contained in Reference 24, which also includes an extensive bibliography. An evaluation of the current state of the astrodynamical constants is given in Reference 26.

Mean Radius of Earth

$r_o = 20.89 \times 10^6$ ft

Mean Value of Gravitational Acceleration at Surface of Earth

$g_o = 32.17$ ft/sec^2

Mass of Earth

$M_E = 4.089 \times 10^{23}$ slugs

Universal Gravitational Constant

$G = 3.442 \times 10^{-8}$ ft^3/(slug sec^2)

Gravitational Parameter for Earth

$\mu_E = 1.4076 \times 10^{16}$ ft^3/sec^2

Mass of Moon

$M_M = 5.029 \times 10^{21}$ slugs

Gravitational Parameter for Moon

$\mu_M = 1.731 \times 10^{14}$ ft^3/sec^2

Angular Velocity of Earth

$\Omega_E = 7.292 \times 10^{-5}$ rad/sec

Mean Value of Gravitational Acceleration at Surface of Moon

$g_{Mo} = 5.32 \text{ ft/sec}^2$

Model Atmosphere for Earth

$$\rho = 0.0027 \exp\left(-\frac{h}{23,000}\right) \tag{E1}$$

NASA-Langley, 1968 — 31 CR-835